SINGLE MOLECULE STUDIES OF SYNUCLEIN FAMILY OF PROTEINS AND PEPTIDES WITH NANOPORES

A Thesis Submitted to the College of

Graduate Studies and Research

In Partial Fulfillment of the Requirements

For the Degree of Doctor of Philosophy

In the Department of Biochemistry

University of Saskatchewan

Saskatoon

By

OMID TAVASSOLY

© Copyright Omid Tavassoly, September, 2014. All rights reserved.

Permission to Use

In presenting this thesis in partial fulfilment of the requirements for a Postgraduate degree from the University of Saskatchewan, I agree that the Libraries of this University may make it freely available for inspection. I further agree that permission for copying of this thesis in any manner, in whole or in part, for scholarly purposes may be granted by the professor or professors who supervised my thesis work or, in their absence, by the Head of the Department or the Dean of the College in which my thesis work was done. It is understood that any copying or publication or use of this thesis or parts thereof for financial gain shall not be allowed without my written permission. It is also understood that due recognition shall be given to me and to the University of Saskatchewan in any scholarly use which may be made of any material in my thesis.

Requests for permission to copy or to make other use of material in this thesis in whole or part should be addressed to:

Head of the Department of Biochemistry
University of Saskatchewan
Saskatoon, Saskatchewan S7N 5E5

ABSTRACT

Alpha-synuclein (AS) is a natively unfolded protein whose structure is extremely sensitive to its environment. The hallmark of Parkinson's disease (PD) is aggregation and deposition of AS in inclusion bodies. Formation of misfolded AS monomers which are partially folded is the first and critical stage in fibrillation of AS and is a good target for designing therapeutic strategies. Characterization the biochemical properties of partially folded intermediates induced by fibrillization and anti- fibrillization agents will help to design drugs as new inhibitors of AS misfolding and aggregation. Nanopore analysis is an emerging technique for studying the molecular mechanism of protein misfolding. This technique was used to characterize the conformational change of AS in the presence of two groups of chemicals; anti-parkinsonian small molecules (dopamine and nicotine) and Parkinson's developing toxin (Cu(II) and methamphetamine). Other biophysical techniques such as NMR spectroscopy and isothermal titration calorimetry (ITC) were able to confirm the nanopore analysis results and also to study other biophysical properties of the partially folded intermediates such as the binding constant of the interaction and the secondary structure content. The results from nanopore analysis showed that both groups of ligands shifted the blockade current peak of AS (centered at -86 pA) to lower blockade currents but in a different manner. Anti-parkinsonian drugs shifted the blockade current of AS to intermediate peaks between -40 to -80 pA but Parkinson developing toxins shifted the peak to a lower blockade current centered at -25 pA which suggests a more compact conformation. Thus nanopore analysis distinguished the different conformation induced by different ligands. Furthermore nanopore analysis with AS fragments showed that these ligands bind to different regions of AS. NMR spectroscopy of AS in the presence of dopamine and nicotine isomers was in agreement with the nanopore analysis and showed conformational changes of AS in a concentration dependent manner. CD spectroscopy results showed that the

secondary structure of AS alone and in the presence of ligands was mostly random coil and suggests a loop formation model for the interaction of ligands with AS. The results of this thesis showed the application of nanopore analysis as a real-time and label-free technique to screen a library of ligands for designing misfolding inhibitors for PD treatment. The result of a synergic experiment with nicotine and caffeine showed that combination of these anti-parkinsonian small molecules would be a promising new drug for treatment of PD.

Published Works

Omid Tavassoly, Joe Kakish, Sergiy Norkhrin, Oleg Dmitriev and Jeremy S. Lee (2014). **The use of nanopore analysis for discovering drugs which bind to α-synuclein for treatment of Parkinson's disease**. ***European Journal of Medicinal Chemistry***. doi: 10.1016/j.ejmech.2014.07.090.

Omid Tavassoly, Sergiy Norkhrin, Oleg Dmitriev and Jeremy S. Lee (2014). **Cu(II) and dopamine bind to alpha-Synuclein and cause large conformational changes**. ***FEBS Journal***. 281, 2738-2753.

Omid Tavassoly and Jeremy S. Lee (2012). **Methamphetamine binds to α-Synuclein and causes a conformational change which can be detected by nanopore analysis**. ***FEBS Letters*.** 586, 3222-3228.

Claudia Madampage , **Omid Tavassoly** , Chris Christensen , Meena Kumari and Jeremy S. Lee (2012). **Nanopore analysis: an emerging technique for studying the folding and misfolding of proteins**. ***Prion*** 6, 116-123.

ACKNOWLEDGMENTS

I would like to thank my supervisor Professor Jeremy S. Lee for all his support throughout my PhD program. Thank you for your invaluable advice and support. Your knowledge, brilliant suggestions, innovative ideas and passion for research have made laboratory work so much more motivating and exciting.

A special thank you to my graduate advisory committee: Dr. Bill Roesler, Dr. Stan Moore (Committee Chair), Dr. Oleg Dmitriev, Dr. Edward Krol (Dept. of Pharmacy and Nutrition), and Dr. Scot Leary for all their suggestion and support throughout my program.

I would also like to thank all members of Dr. Lee's lab (past and present): Dr. Radu Stefureac, Dr. Claudia Madampage, Dr. Besnik Krasniqi, Meena Kumari, Chris Christensen, Joe Kakish and Elisabet Jakova.

Special thanks to Dr. Oleg Dmitriev and Dr. Sergiy Nokhrin for help with NMR experiments. I also would like to thank the Protein Characterization and Crystallization Facility (PCCF) of the College of Medicine, University of Saskatchewan and Dr. Michal Boniecki for help with CD and ITC.

Finally, I would like to thank the Parkinson Society Saskatchewan and Parkinson Society Canada for providing financial support and granting me a graduate student award.

Dedication

I DEDICATE THIS THESIS TO MY WIFE (SHAHRZAD), PARENTS (HOMA & JABBAR), SISTERS (ZAHRA & AREZOO), AND BROTHER (IMAN).

TABLE OF CONTENTS

page

LIST OF TABLES

LIST OF FIGURES

LIST OF ABBREVIATIONS

αHL	alpha-hemolysin
Aβ42	β-amyloid-42
AD	Alzheimer disease
AFM	atomic force microscopy
AS	Alpha-synuclein
ATF6	activating transcription factor 6
BBB	blood brain barrier
BCB	blood–CSF barrier
BiP	Binding immunoglobulin protein
CD	circular dichroism
COMT	catechol O-methyltransferase
CR	Congo Red
CSF	cerebral spinal fluid
CSPα	cysteine-string protein α
Ctr1	copper transporter 1
DA	dopaminergic
DAT	dopamine transporter
DMT1	divalent metal transporter-1
DRP1	Dynamin-related protein 1
ER	Endoplasmic Reticulum
ERAD	Endoplasmic-reticulum-associated protein degradation
ETC	electron-transport chain
FTIR	Fourier transform infrared spectroscopy
GRP78	glucose-regulated protein 78
HSQC-NMR	Heteronuclear Single Quantum Correlation-Nuclear Magnetic Resonance
IDP	Intrinsically disorder protein
IMM	inner mitochondrial membrane
IMS	intermembrane space
IRE1	inositol requiring enzyme 1
ITC	Isothermal Titration Calorimetry
L-DOPA	L-3,4-dihydroxyphenylalanine
LRR	leucine-rich repeat
MAO-B	monoamine oxidase-B
MPTP	1-methyl-4-phenyl-1,2,3,6-tetrahydropyridine
MTS	mitochondrial targeting sequence
nt	nucleotide
OMM	outer mitochondrial membrane
PA	phosphatidic acid
PC	phosphatidylcholine
PD	Parkinson’s disease
PE	phosphatidylethanolamine
PERK	PKR-like endoplasmic reticulum kinase
PFFs	preformed fibrils
pI	isoelectric point
PLD2	phospholipase D2

PS	phosphatidylserine
RBC	red blood cell
ROS	reactive oxygen species
SLAS	sodium lauroyl sarcosinate
smFRET	single molecule Forster resonance energy transfer
SMFS	single molecule force spectroscopy
SN	substantia nigra
SOD1	superoxide dismutase 1
SUV	small unilamellar vesicle
TH	tyrosine hydroxylase
UBL	ubiquitin-like
UPR	unfolded protein response
UPS	ubiquitin-proteasome system
VMAT2	vesicular monoamine transporter 2

1 Introduction and Literature Review

1.1 Introduction

Parkinson's disease (PD) is a progressive neurodegenerative disease that permanently impairs movement, with a prevalence of approximately 2% after the age of 65 (Leonard, 2002; Pahwa and Lyons, 2007). The characteristic property of PD is the aggregation and deposition of α-synuclein (AS) in inclusion bodies (Dauer and Przedborski, 2003; Henchcliffe and Beal, 2008; Lotharius and Brundin, 2002b; Moore *et al.*, 2005; Ottolini *et al.*, 2013). Aggregated AS undergoes degradation by the ubiquitin-proteasome system (UPS) to protect cells from the deleterious toxicity of these aggregates. Two of the UPS components are Parkin and Ubiquitin carboxyl-terminal hydrolase L1 (*UCH-L1*) which are important in maintaining the protective function of this system against aggregated proteins (Dauer and Przedborski, 2003; Moore *et al.*, 2005). Loss of function mutations in Parkin and UCH-L1 genes can also cause PD because of the accumulation of AS aggregates in dopaminergic neurons (Dauer and Przedborski, 2003; Ottolini *et al.*, 2013). This accumulation finally leads to the death of dopaminergic neurons and dopamine depletion due to an increase in reactive oxygen species (ROS) production, mitochondrial impairment and the unfolded protein response (UPR) in the Endoplasmic Reticulum (ER) (Cooper *et al.*, 2006; Franssens *et al.*, 2010; Gorbatyuk *et al.*, 2012). Moreover, misfolding and aggregation of AS leads to the loss of function of this unfolded protein which has an important role in dopamine homeostasis and metabolism (Kanaan and Manfredsson, 2012; Lashuel *et al.*, 2013). Aggregates of AS are able to propagate and transfer the PD pathogenicity from cell to cell in a prion-like manner (Angot *et al.*, 2012; Braak *et al.*, 2003; Danzer *et al.*, 2012; Masuda-Suzukake *et al.*, 2013). Thus AS aggregation is a key step in the development of PD pathology and highlights the importance of preventing the aggregation process as a therapeutic strategy for PD treatment. The critical stage of AS aggregation is the conformational changes of intrinsically disordered AS monomers to form partially folded intermediates (Fink, 2006; Uversky and Eliezer, 2009; Uversky *et al.*, 2001a; Uversky *et al.*, 2001c). It is known that there are aggregation promoter and inhibitor agents which interact with AS monomers and favor the conversion into a partially folded intermediate. The partially folded conformations induced by anti-fibrillogenic and fibrillogenic agents are thought to be different due to the many possible modes of interaction with the intrinsically disordered protein (Fink, 2006; Uversky *et al.*, 2001b). Understanding the initial stages of AS aggregation, is therefore important for designing

inhibitors as new therapeutics to prevent the pathogenic process (Trexler and Rhoades, 2010b). The focus of this thesis is the use of nanopore analysis and other biophysical methods to study the folding of AS and its interaction with small molecules. One promising approach in order to develop therapeutics for treatment of PD is to inhibit AS misfolding and aggregation with small molecules identified using high-throughput screening (May et al., 2006; Rochet, 2007). NMR spectroscopy (Lendel et al., 2009; Rao et al., 2008) and single molecule biophysics techniques such as nanopore analysis have been successfully used to characterize the partially folded intermediate or misfolded conformation of AS in the presence of different types of small molecules (Asandei *et al.*, 2013; Wang *et al.*, 2011a; Wang *et al.*, 2013).

1.2 Nanopore analysis

Nanopores are *nm* sized openings that ions and macromolecules can pass through. There are two types of these nano-scale pores; the biological protein pores and synthetic solid state pores. The biological pores are naturally occurring protein complexes such as alpha-hemolysin (αHL) toxin from *Staphylococcus aureus* that interact with lipid bilayers to form a transmembrane pore. Synthetic pores are fabricated in solid-state membranes (Iqbal and Bashir, 2011; Ma and Cockroft, 2010; Wang et al., 2010a).

For the first time in 1996, Kasianowicz *et al.* recruited a biological protein pore as a sensitive biosensor to probe individual single stranded DNA and RNA. In this study αHL was inserted into a lipid bilayer which was painted on a 0.1-mm-diameter hole in a 25-mm thick Teflon partition separating two compartments filled with 1 M KCl, 5mM HEPES buffer (pH 7.5) (Kasianowicz et al., 1996). Each compartment contained an electrode connected to a patch clamp amplifier. Upon applying a voltage across the membrane, ions transport through the pore and create a stable current (I) (Figure 1.1a). They found that by adding single stranded DNA into the compartment with the cathode electrode, the DNA molecules could translocate through the pore electrophoretically and cause blockade of the transient ionic current (I) for a certain duration of time (T) (Figure 1.1b) (Kasianowicz et al., 1996; Ma and Cockroft, 2010).

This was the beginning of nanopore-based single molecule spectroscopy for real-time probing of macromolecular behavior. Since then, this technique has been used to study conformational changes and molecular interactions of biological macromolecules and also has become a candidate for developing the next generation sequencing devices (Branton et al., 2008; Carlsen et al., 2014; Clarke et al., 2009; Derrington et al., 2010; Ku and Roukos, 2013; Maitra et al., 2012;

Scheicher et al., 2012). As shown by Madampage *et al.* nanopore analysis can also be used to study protein conformation (Madampage et al., 2012). Many serious human diseases have been linked to protein misfolding and aggregation (Dawson and Dawson, 2003; Jaikaran and Clark, 2001; Lotharius and Brundin, 2002b; Prusiner, 2001; Selkoe, 2004; Watanabe et al., 2001). Nanopore analysis is an emerging technique for studying the conformational changes of misfolded proteins and designing small molecules to prevent their misfolding and aggregation (see later) (Madampage et al., 2012; Wang et al., 2013; Wang et al., 2011a).

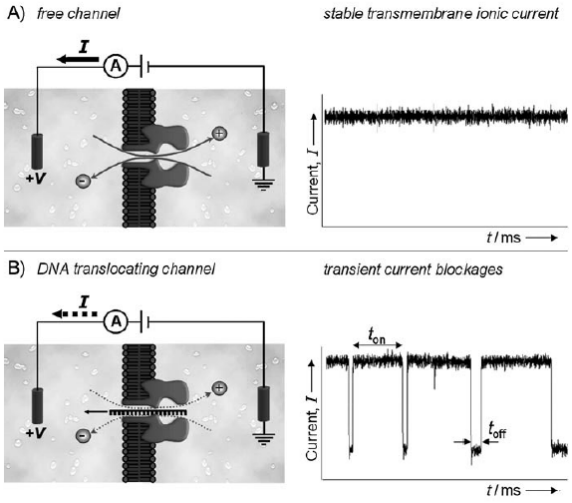

Figure 1.1 Schematic representation of the first nanopore based detection of single stranded DNA translocation through the αHL pore. (A) Shows the free channel state which is the experimental set up before adding DNA. A voltage is applied across the membrane which creates the transmembrane ionic current. (B) Translocation of individual DNA molecules interrupts the transient ionic current and causes blockades of this current which is represented by a drop in current (I) for a duration of time (T). Reprinted with permission from (Ma and Cockroft, 2010). Copyright © 2010 WILEY-VCH Verlag GmbH & Co. KGaA, Weinheim. All rights reserved.

1.2.1 Principles of nanopore analysis

1.2.1.1 Alpha-hemolysin as a model nanopore

Alpha-hemolysin is a toxin secreted by *Staphylococcus aureus* as a water soluble monomer. Each monomer has molecular weight of 33 kDa and is composed of 293 amino acids. The toxicity of αHL is due to its ability to bind and form transmembrane pores in mammalian cells such as erythrocytes and lymphocytes which finally leads to cell lysis and death (Berube and Bubeck Wardenburg, 2013; Ma and Cockroft, 2010; Menestrina et al., 2001). To form a channel, seven monomers assemble in the phospholipid bilayer and form a mushroom-shaped

transmembrane pore (Ma and Cockroft, 2010). The crystal structure of heptameric αHL has been determined to 1.89 Å (Song et al., 1996) and 2.30 Å (Tanaka et al., 2011). Figure 1.2 shows the cross-sectional model of the channel. The channel diameter is not constant and changes along the length. The diameter of the cap opening is 2.6 Å which leads into an inner vestibule with the widest diameter of 3.6 nm. The vestibule narrows into a 1.5 nm limiting aperture which connects the vestibule to the transmembrane stem with an internal diameter of 2.2 nm. The stem consists of 14 antiparallel strands (DeGuzman et al., 2006; Ma and Cockroft, 2010).

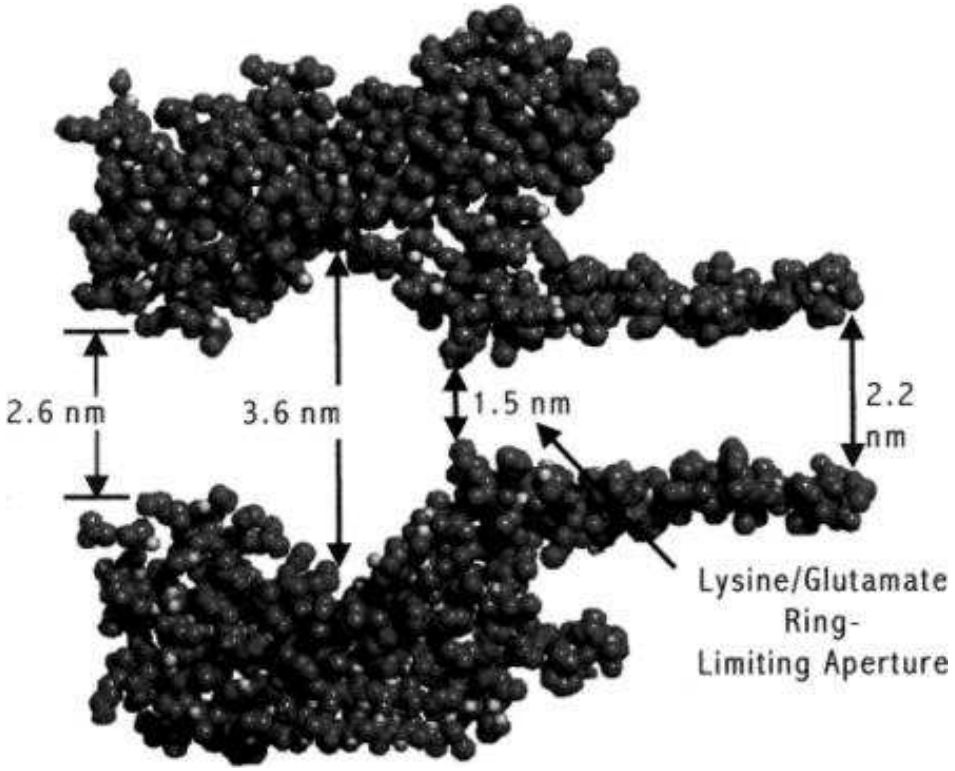

Figure 1.2 Cross-sectional model of the alpha-hemolysin channel demonstrating the dimensions of the channel of pore. Reprinted with permission from (DeGuzman et al., 2006). Copyright © 2006 Oxford University Press. All rights reserved.

The biophysical features of the αHL pore make it ideal for nanopore analysis. Monomers of this toxin self-assemble and insert into the lipid bilayer to form the heptamer channel spontaneously. The lumen of the channel is hydrophilic which facilitates the transport of ions and biological molecules between separated compartments. Furthermore, this pore has thermal stability up to 100°C and a wide range of pH tolerance from 2 to 12 (DeGuzman et al., 2006; Ma and Cockroft, 2010; Song et al., 1996). It also has stability against urea denaturation and the heptamer complex inserted into the lipid bilayer can resist up to 7.8 M urea (Pastoriza-Gallego et

al., 2007). It also has a low-noise characteristic and has been used for probing different types of macromolecules such as proteins, nucleic acids and carbohydrates but its size limitation (1.5 nm) makes it suitable for single stranded nucleic acids and unfolded peptides (Kasianowicz et al., 2008; Madampage et al., 2012; Mulero et al., 2010; Venkatesan and Bashir, 2011; Wanunu et al., 2011).

The interaction of macromolecules with the αHL pore can be categorized into three different events (Figure 1.3). Events with the smallest blockade current represent bumping events which show the interaction of large or compact macromolecule with the outside of the pore. This interaction blocks the ionic flow for a short time (Figure 1.3c). Translocation events occur with the highest blockade current and are due to translocation of macromolecules through the pore (Figure 1.3a). The third type of events is intercalation which has an intermediate blockade current. It is proposed that these events occur when a part of a macromolecule (a loop or a domain) enters the vestibule of the pore and is stuck there before diffusing away (Figure 1.3b). It's difficult to distinguish intercalation and translocation events (Meng et al., 2010a). The blockade current distribution can be fitted with a Gaussian function to obtain event populations in a graph which represents the number of events versus the blockade currents (pA) (Christensen et al., 2011; Krasniqi and Lee, 2012; Krasniqi and Lee, 2014; Madampage et al., 2010; Meng et al., 2010a; Stefureac et al., 2008; Stefureac and Lee, 2008; Stefureac et al., 2010).

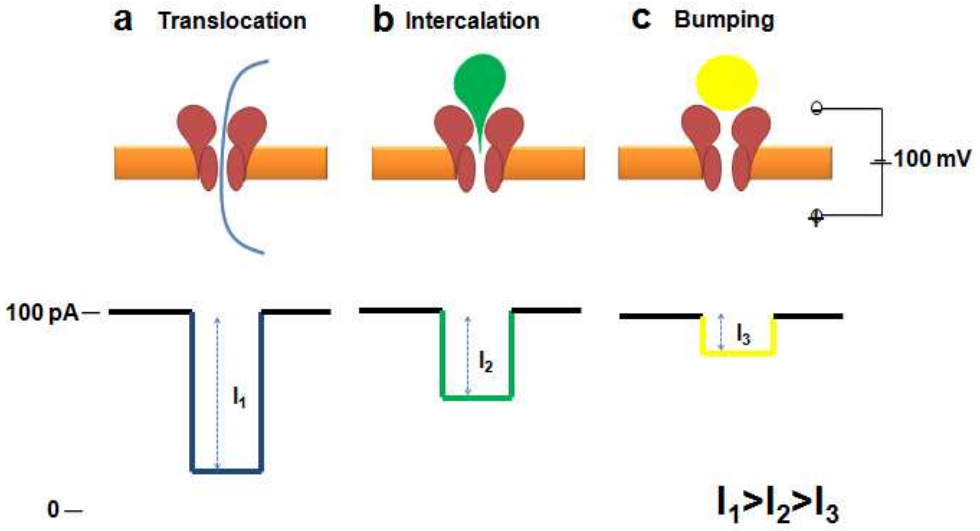

Figure 1.3 Schematic representation of possible interaction of macromolecules with αHL (top) and also the corresponding event profiles (bottom). Idea adapted from (Meng et al., 2010a).
Copyright © 2010 European Peptide Society and John Wiley & Sons, Ltd. All rights reserved.

1.2.1.2 Nanopores as biochemical sensors

In nanopore analysis the parameters, I and T are exquisitely sensitive to the conformation of the protein at the moment it interacts with the pore (Christensen et al., 2011). Therefore, it can be used as a biosensor to detect conformational changes induced by binding of ligands to the individual molecules. Nanopore analysis is a real-time, label-free and sensitive technique which requires very low concentrations of ligand and target molecules (Larkin et al., 2013). These features make it more efficient than other analytical chemistry techniques especially for studying misfolded proteins and short nucleic acids such as aptamers (Arnaut et al.; Madampage et al., 2012; Wang et al., 2013; Wang et al., 2011a; Ying et al., 2011).

1.2.1.2.1 Nanopore sensing of peptides and peptide-metal interactions

The ability of nanopore analysis to detect conformational changes of peptides upon binding to a ligand has been used to study the interaction of metal ions with peptides. Under an applied voltage each peptide has unique event parameters of blockade current (I) or time (T). Binding of a metal ion may cause a conformational change which alters the event parameters (Brucale et al., 2014; Stefureac and Lee, 2008; Stefureac et al., 2010). The ability of nanopore analysis to detect conformational changes of biomacromolecules by monitoring the event parameters has been used to study the interaction of metal ions and peptides. For example, nanopore analysis was used to detect the folding of a zinc-finger molecule (Zif268) which has 28 amino acids. The blockade current histogram of this motif was changed in the presence of Zn(II) with an increase in the magnitude of the bumping peak and a simultaneous decrease in the proportion of translocation events. This demonstrated the compaction and folding of this peptide upon adding Zn(II) which was not observed with Mg(II) (Stefureac and Lee, 2008). In another study (Mereuta *et al.*, 2012), the α-HL pore has been used to investigate the conformational changes of an antimicrobial-derived chimera peptide (CAMA) of 20 amino acids which has a His residue as part of the Cu(II) binding site. Cu(II) alters the event parameters (I and T) of this peptide. The results of nanopore analysis demonstrated an increase in the number of bumping events with short blockade current in the presence of various concentrations of copper (II) (Mereuta et al., 2012). These researchers showed that nanopore analysis can be used as a biosensor to study the interaction of metal ions with other peptides such as misfolded proteins (Brucale et al., 2014). Most of the misfolded proteins which are important in the pathology of neurodegenerative

disease are metal binding peptides. Thus nanopore analysis has the ability to study the conformation of these peptides in the presence of metals (Brucale et al., 2014; Lee, 2014). As these peptides are unfolded, they can translocate through the pore and result in a large blockade current. Binding of metal ions to these peptides changes their conformations and causes local or overall folding and compaction of their structure. The interaction of a more compact conformation with the pore results in blockade currents which are shorter than the blockade current of the natively unfolded conformation (Baran et al., 2010; Lee, 2014; Madampage et al., 2012; Stefureac et al., 2010). An example of a misfolding protein is the β-amyloid (Aβ) peptide. Interaction of Cu(II) with human and rat amyloid fragments Aβ (1−16) was investigated using nanopore analysis. Addition of various concentrations of Cu(II) causes a reduction in the number of events with long blockage and a simultaneous increase in the number of events with short blockage. The results showed that Cu(II) causes folding and compaction of this peptide (Asandei et al., 2013). The prion protein is another example of a misfolded protein which has been studied with nanopore analysis. The prion protein has 220 residues and is found in most tissues including the brain. Prion proteins are metal binding proteins and it has been shown that metal ions change the conformation of this protein by inducing the formation of a local β-sheet conformer. The main metal binding region of the prion protein is four tandem repeats of an octapeptide sequence (Octa) in the N-terminal of the protein which can bind 4-5 Cu(II) ions with K_d in the range of nano to micro molar. Nanopore analysis using α-HL was used to investigate the effect of Cu(II), Zn(II), Mg(II) and Mn(II) on a prion peptide with two tandem repeats of the Octa region (Octa2). The authors found that Cu(II) and Zn(II) change the event parameters of this peptide but no changes were observed with Mg(II) and Mn(II). Octa2 which is a very short peptide translocates through the pore and a single translocation peak with high blockade current centered at -67 pA was found. In the presence of Cu(II), the translocation peak shifted to -77 pA and a bumping peak was found at -24 pA. In addition, the translocation time was increased from 0.16 ms to 0.46 ms. Thus, Cu(II) binds to the peptide and causes conformational changes. The effect of Zn(II) on the Octa2 structure was less than the effect of Cu(II). Zn(II), at a concentration of 320 μM, shifted the translocation peak to -72 pA and made it broaden. A small bumping peak is also found in the presence of Zn(II). So the interaction of Zn(II) with Octa2 is weaker than Cu(II) (Stefureac et al., 2010). This technique also has been used to study the interaction of Cu(II) and Zn(II) with Myelin basic protein (MBP). Blockade current histogram of this intrinsically

disordered protein shows a single translocation peak centered at -65 pA. Upon addition of Cu(II) or Zn(II) to the experiment the proportion of translocation events decreased and a new peak formed at around -25 pA which represents the more compact conformation of MBP bound to the metal ions (Baran et al., 2010; Lee, 2014). These studies together showed the sensitivity of nanopore analysis to detect subtle conformational changes of misfolded peptides in the presence of metal ions and also the potential application to other misfolded peptides such as AS (Lee, 2014). Since metal ions bind proteins and are able to change their conformation even at very low concentrations, it is important to consider any sort of metal contamination in characterizing the structure and function of proteins in *in vitro* experiments. For example Krasniqi *et al.* demonstrated that adding of EDTA as a metal chelator to the nanopore cup containing maltose binding protein in HEPES buffer has a large impact on the blockade current histogram of this protein. Without EDTA this protein mostly adopted a compact conformation as a bumping peak (-25 pA) and also a broader peak with blockade currents higher than -40 pA. In the presence of EDTA the proportion of the intermediate peak increased. This peak represents the conformation of this protein in the absence of metal contamination. Control experiments with EDTA can be helpful to detect any conformational change due to metal contaminations (Krasniqi and Lee, 2012; Lee, 2014).

1.2.1.2.2 Nanopore sensing of macromolecule-ligand interactions

The study of the interaction between biological macromolecules and small molecules is important for drug screening and development. Nanopore analysis has been utilized as a high-throughput tool to investigate the interaction of small molecules and bio-macromolecules such as proteins and nucleic acids (Wang et al., 2013; Wang et al., 2011a).

As a proof of concept, the interaction of A53T-AS with trehalose (Wang et al., 2013) was studied using natural nanopore analysis. In this study a voltage of 100 mV was applied and two baselines were considered to record the current blockades; the open pore current level (at 100 pA) as the primary baseline and a secondary baseline which shows the capture of monomers into the vestibule of α-HL. They showed that the interaction of AS molecules with the pore is a two step process and causes two drops from the first baseline, *i.e.* the open pore current level. They showed that the first drop of current from the primary baseline (L_o) to the secondary baseline (L_c) is due to the capture of AS monomers into the vestibule of the pore followed by a second drop from L_c to a lower level (L_b). For AS-wild type the total drop was about 85 pA consisting of

80 pA for capture events from L_o to L_c and a 5 pA drop from L_c to L_b due to translocation. For A53T the total drop from primary baseline is smaller than that of AS-wild type because of a reduction in the blockade current of the capture events (L_o-L_c). They showed that trehalose causes a significant reduction in the transient blockade events between L_o and L_b. This study showed that nanopore analysis detects the conformational changes of AS monomers upon binding to a small molecule (Wang et al., 2013).

This technique also has been used to study the opposite effects of β-cyclodextrin (β-CD) and Congo Red (CR) in the aggregation transition of β-amyloid-42 (Aβ42). β-CD and CR are aggregation promoter and inhibitor agents, respectively, and their effects on Aβ42 misfolding and aggregation has been detected by monitoring the corresponding blockade current and time. The blockade current histogram for Aβ42 showed two peaks concentrated at 21.5 pA and 96.25 pA. In the presence of CR the peak centered at 96.25 pA dramatically decreases and there is an increase in the events with the characteristic current concentrated at 29 pA and also corresponding long duration times were observed. This profile showed that CR reduces formation of the misfolded or compact conformation of Aβ42. In the presence of β-CD a significant peak at 23.25 pA was detected which was different from free Aβ42 and Aβ42-CR complex (Wang et al., 2011a).

Nanopores have also been used to study the interaction of small molecules and nucleic acids (Arnaut et al.; Larkin et al., 2013; Wanunu et al., 2011; Ying et al., 2011). Most of the nanopore experiments in this field are carried out using nucleic acid aptamers. Aptamers are synthetic single-stranded fragments of DNA or RNA, usually 20-80 nt long, with very high affinity for their targets (Banerjee and Nilsen-Hamilton, 2013; Iliuk et al., 2011; Radom et al., 2013). Nanopore analysis has been used as a real-time electrochemical sensor to probe the interaction of aptamers with AMP, ADP, ATP (Arnaut et al.; Ying et al., 2011), thrombin (Arnaut et al.) and cocaine (Kawano et al., 2011). Ying *et al.* investigated the interaction of a 33-mer ATP-binding DNA aptamer using the αHL nanopore. The aptamer had a folded conformation and was not able to translocate completely through the pore, suggesting that aptamers sit in the vestibule without transiting the pore. That is why the majority of the events (95%) have lower blockage current (46 pA). To keep the aptamer unfolded a 10-mer reporter sequence was pre-hybridized to the aptamer before adding to the *cis* side and then ATP was added to the *cis* compartment. The duplex of aptamer/reporter resulted in a translocation peak of lower blockade current,

concentrated at 30.35 pA, with a shorter duration time relative to the folded aptamer. Adding ATP at equimolar amounts of 0.15 nmol aptamer and 0.15 nmol reporter changes the blockade current profile. The authors showed that adding ATP to the duplex of aptamer/reporter causes the release of reporter from aptamer and formation of an ATP/aptamer complex which has a different conformation (Ying et al., 2011). In another study a modified aptamer was designed to detect the interaction of aptamer and ATP. In this study aptamer and ATP were added to *cis* and *trans* compartments respectively. The general structure of the modified sequence was composed of 5′-stopper-spacer-aptamer-thread-3′. A +120 mV voltage was applied which forces the aptamer to denature and pass through the pore. A stable hairpin sequence at the 5′ end prevented complete translocation of the sequence from *cis* side into the *trans* side. After detecting a capture event by observing a drop in current, the captured sequence was kept inside the pore by reducing the applied voltage to +50 mV. Afterward a reverse voltage of -200 mV was applied to force the aptamer to denature and re-enter the *cis* compartment. Upon reversing and increasing the applied voltage, the observed rise of current was recorded as the unfolding voltage which represents the unfolding and escaping of aptamer from *trans* side to the *cis* side. These unfolding voltages have been used to calculate the binding constant of ATP. This experiment also has been done for other aptamer targets (ADP and AMP) and the results showed that the affinity of aptamer for AMP and ADP is more than ATP (Arnaut et al.). Furthermore, Kawano *et al.* used a cocaine binding aptamer for selective detection of cocaine. Rapid and real time detection of recreational drugs such as cocaine is important. The sensitivity of this detection was 300 ng/mL in a very short time (60 seconds). They designed an ssDNA aptamer with a long tail which facilitated the oligo to easily pass through the αHL pore when a 100 mV voltage was applied. In the presence of cocaine, the complex of cocaine/aptamer was not able to pass through the pore and was captured on the *cis* side of the pore. This capture results in a drop of current which has been recorded as the captured blockade current. The results showed that the cocaine concentration is dependent on the captured-interval time which means that the time was increased as the cocaine concentration decreased (Kawano et al., 2011).

1.3 Parkinson's Disease

Parkinson disease (PD) is a chronic, progressive neurodegenerative disease. James Parkinson described PD as tremor, gait disorder, and bradykinesia for the first time in 1817 (Grosset et al., 2009; Leonard, 2002; Shulman et al., 2011). This observation was based on six cases. PD is the

second most common neurodegenerative disorder with a prevalence of about 1% at age 65. The incidence and prevalence of PD are age dependent and increase with age. The onset of symptoms is approximately 60 years on average and almost 2% of people over 65 years have PD (Leonard, 2002; Pahwa and Lyons, 2007). There is an extensive destruction of dopaminergic neurons in the substantia nigra (SN). The SN is a small area of cells in the midbrain (Uversky, 2007; Uversky and Eliezer, 2009). Defects in energy metabolism, especially a significant reduction in the function of complex I of the mitochondrial electron transport chain, is detected in patients with PD (Seth and Seth, 2009). Gradual degeneration of the SN causes a reduction in the dopamine content (Amer et al., 2006; Uversky, 2007; Uversky and Eliezer, 2009). For extrapyramidal motor activity a balance between the excitatory cholinergic and the inhibitory dopaminergic components is essential. In PD the degradation of dopaminergic neurons in the SN causes the cholinergic component to become dominant. This imbalance between the two components causes movement difficulty in PD (Seth and Seth, 2009). Resting tremor, generalized slowness of movement or difficulty initiating movement, stiffness of limbs and balance problems are all obvious clinical characteristics of PD (Amer et al., 2006; Uversky and Eliezer, 2009). The hallmark of PD is the degeneration of dopaminergic neurons in the SN which leads to the depigmentation of this area and the presence of Lewy bodies which are cytoplasmic inclusions of aggregated AS (Grosset et al., 2009; Shulman et al., 2011).

1.3.1 Cell biology of Parkinson's disease

PD is a multifactorial neurodegenerative disease which finally leads to the death of dopaminergic neurons. Endoplasmic reticulum (ER) stress and mitochondrial dysfunction are the main cellular mechanisms that cause the development of PD (Calì et al., 2011). Mitochondria have a central role in development of PD and many of the PD genetic factors (see below) are involved in the maintenance of mitochondrial integrity. Impairment of mitochondria-related metabolic pathways such as the respiratory pathway, fusion and fission are associated with Parkinson's disease pathology (Calì et al., 2011; Exner et al., 2012).

1.3.1.1 Role of ER stress in Parkinson's disease

The activation of endoplasmic reticulum (ER) stress due to accumulation of unfolded proteins in the ER lumen is a cellular process which is linked to PD. The ER is involved in synthesis, folding and targeting of secretory proteins in eukaryotic cells. Folding of synthesized proteins

into their functional conformation, post-translational modifications and disulfide bond formation are the main biochemical roles of the ER in the secretory protein pathway. Secretory proteins also undergo a quality-control process in the ER which allows the exportation of correctly folded proteins to the Golgi complex whereas proteins with uncompleted folding status either undergo another folding process to assure their native conformation or enter the degradation pathway. Conditions that alter the ER control system on protein folding leads to ER stress and the protective response to overcome this stress is called the unfolded protein response (UPR) (Schröder and Kaufman, 2005).

Under conditions which lead to ER stress, UPR is activated to allow cell survival by inhibition of protein translation and recovery of the normal protein folding process but in the case of extreme stress it results in cell death through apoptosis (Doyle et al., 2011; Ferri and Kroemer, 2001). There are three transmembrane proteins which initiate the major protecting pathways in the response of ER stress. These proteins are inositol requiring enzyme 1(IRE1), PKR-like endoplasmic reticulum kinase (PERK) and activating transcription factor 6 (ATF6). In unstressed cells these proteins are associated with Binding immunoglobulin protein (BiP) also known as glucose-regulated protein 78 (GRP78). Upon initiation of ER stress, interaction of unfolded proteins with GRP78 leads to its dissociation from PERK, IRE1 and ATF6. This dissociation activates these proteins to initiate signalling pathways to relieve the stress and protect cells against the harmful effects of ER stress by inhibiting protein translation, increase of degradation of malfunction proteins, and up-regulation of chaperone expression (Doyle et al., 2011).

In the event of prolonged or unmitigated ER stress, the ER-UPR triggers apoptosis through the PERK, ATF6 and IRE1 signaling pathways. PERK and ATF6 branches of UPR promote apoptosis through activation of CCAAT/-enhancer-binding protein homologous protein (CHOP) which alters the balance between pro-apoptotic and antiapoptotic BCL-2 family members and transits the protective UPR to an apoptotic response. (Bernales et al., 2012; Doyle et al., 2011; Mercado et al., 2013; Schonthal, 2012).

The apoptosis pathway through the IRE1 branch of UPR initiates after activation of tumor-necrosis- factor-receptor-(TNFR-) associated factor 2 (TRAF2) by IRE1 which finally activates the pro-apoptic members of Bcl-2 and inhibits the anti-apoptic members of this protein family

and stimulates the apoptosis response (Bernales et al., 2012; Doyle et al., 2011; Schonthal, 2012).

The ER has a critical role in the folding of synthetic secretory proteins and any disruption of this function leads to accumulation of misfolded proteins and induction of UPR. Misfolded proteins and their aggregation are associated with the pathology of neurodegenerative disease such as PD. Accumulation of misfolded proteins activates UPR which facilitates normal folding by increasing the expression of chaperones. Furthermore, the misfolded proteins undergo degradation by the Endoplasmic-reticulum-associated protein degradation (ERAD) system, a process which involves retro-translocation of unfolded proteins from the ER lumen to the cytosol to be degraded by the polyubiquitination system, which is also activated during UPR (Doyle et al., 2011). Up-regulation of some of the signaling proteins involving in UPR such as Grp78, XBP1, CHOP, and ATF4 have been reported in the brain of AS transgenic mice (Bellucci et al., 2011; Colla et al., 2012a; Colla et al., 2012b; Mercado et al., 2013). Smith *et al.* have shown that expressing of the A53T mutant of AS which is prone to adopt the misfolded conformation, causes the activation of ER stress in differentiated PC12 cells. (Smith et al., 2005). Furthermore, Bellucci *et al.* demonstrated that accumulation of AS in the ER lumen activates the PERK dependent UPR pathway. *In vitro* and *in vivo* experiments demonstrated direct interaction of AS with GRP78 which causes the dissociation of the PERK-GRP78 complex and activation of PERK to initiate the UPR (Bellucci et al., 2011). In another study, wild type AS was over expressed in the substantia nigra pars compacta (SNc) of a mouse model of PD. After four weeks they found elevated levels of phosphorylated eIf2α, ATF4, and ATF6(N) which are UPR markers from PERK and ATF pathways, respectively. Furthermore, the level of CHOP was significantly increased due to activation of ATF4 and PERK pathways. This pro-apoptic protein, *i.e.* CHOP, initiates the apoptosis pathway which finally leads to death of dopaminergic neurons (Gorbatyuk et al., 2012). Gorbatyuk *et al.* also studied the effects of GRP78 overexpression on AS accumulation and toxicity which leads to cell death and apoptosis due to induction of ER stress and activation of UPR. This study showed the attenuation of AS accumulation toxicity by GRP78 overexpression and proposed GRP78 as a new target for treatment of PD (Gorbatyuk et al., 2012). It also has been reported that AS overexpression reduces the degradation of malformed proteins by the ERAD pathway in a yeast model of PD and results in accumulation of

unfolded proteins in ER which initiates the ER stress (Cooper et al., 2006; Franssens et al., 2010).

Other PD proteins which are involved in dealing with unfolded protein stress are Parkin and UCHL-1. These proteins are part of the ubiquitin and proteasome system (UPS) which is an important element of the ERAD pathway during UPR. Mutation of the genes encoding Parkin and UCHL-1 results in loss of their activity in the ERAD pathway which leads to accumulation of proteins (Shimura et al., 2000; Tan et al., 2008; Trempe et al., 2013; Tsai et al., 2003; Wauer and Komander, 2013) and activation of ER stress (Imai et al., 2000; Ledesma et al., 2002; Tan et al., 2008).

1.3.1.2 Role of mitochondria in Parkinson's disease

Mitochondria are eukaryotic intracellular organelles with key functions in metabolism and generation of energy. This organelle is surrounded by two membranes, the outer mitochondrial membrane (OMM) and the inner mitochondrial membrane (IMM). This compartmentalization creates two spaces between the OMM and the IMM, *i.e.* the intermembrane space (IMS) and the space inside the IMM, *i.e.* matrix. The most important role of this organelle is production of energy by the respiratory chain or electron-transport chain (ETC) and the oxidative-phosphorylation system located in the highly folded regions of IMM. Five protein complexes and two electron carriers are responsible for generating energy as ATP through the ETC (DiMauro and Schon, 2003; Perier and Vila, 2012). The first complex of the respiratory chain, *i.e.* complex I, is crucial for the maintenance of the mitochondrial role in ATP synthesis and any defect of this complex impairs the respiratory chain and the generation of ATP and finally causes disorders of the respiratory chain. This multimer complex is composed of 45 subunits encoded by mtDNA and the nuclear genome. Mitochondrial DNA encodes seven subunits of this complex (ND1–ND6 and ND4L) and the other subunits are encoded by nuclear DNA. The catalytic site of this complex consists of 14 subunits encoded by both mitochondrial and nuclear genes including NDUFV1, NDUFV2, NDUFS1, NDUFS2, NDUFS3, NDUFS7, NDUFS8, ND1, ND2, ND3, ND4, ND5, ND6 and ND4L (Bridges et al., 2011; Dieteren et al., 2008). Dysfunction of the respiratory chain especially at the level of complex I has been reported as one of the pathological features of PD (Blake et al., 1997; Keane et al., 2011; Keeney et al., 2006; Parker and Swerdlow, 1998; Perier and Vila, 2012).

Using post-mortem human brain samples, Keenay *et al.* have shown that the dysfunction of mitochondrial complex I in PD is due to oxidation of its catalytic subunit (Keeney et al., 2006). This study showed up-regulation and oxidation of catalytic subunits of mitochondrial complex I of PD samples in comparison with the controls. This might be the reason for the reduced activity of this complex in PD patients (Keeney et al., 2006; Perier and Vila, 2012). The consequences of complex I dysfunction are the depletion of ATP levels in brain (Chan et al., 1991; Perier and Vila, 2012; Scotcher et al., 1990) and increase in ROS production (Perier et al., 2005; Perier and Vila, 2012; Ramsay et al., 1987).

Several studies have found an association between some of the genes involved in familial PD, including PINKI and AS, and deficits of the mitochondrial complex I (Abramov et al., 2011; Banerjee et al., 2010; Chinta et al., 2010; Devi et al., 2008; Gautier et al., 2008; Hsu et al., 2000; Liu et al., 2009; Loeb et al., 2010; Martin et al., 2006; Matsuda et al., 2013; Morais et al., 2014; Morais et al., 2009; Plun-Favreau and Hardy, 2008). Morais *et al.* have shown that PINK1 loss of function reduces the normal activity of mitochondrial complex I and finally leads to the mitochondrial depolarization and sensitivity to apoptotic stress in fruit fly and mouse models of PD. Loss of PINK1 causes a reduction in the mitochondrial membrane potential which is required for ATP synthesis in both PD models (Morais et al., 2009). Dysfunction of mitochondria also has been reported in $PINK1^{-/-}$ mice which is due to the impaired mitochondrial respiration in the striatum and elevated oxidative stress associated with dopamine metabolism (Gautier et al., 2008). It also has been shown that the mitochondrial membrane potential is decreased in the presence of PINK1 mutations in human fibroblasts (Abramov et al., 2011). It has been shown that PINK1 regulates the phosphorylation of NdufA10 subunit of complex I which is required for its activity and maintenance of the respiratory chain (Morais et al., 2014).

AS is another protein involved in PD and has been shown to be associated with mitochondrial function (Chinta et al., 2010; Devi et al., 2008; Hsu et al., 2000). It has been reported that overexpression of AS causes mitochondrial dysfunction, oxidative stress and cell death (Banerjee et al., 2010; Hsu et al., 2000; Martin et al., 2006). Several research groups have reported that the overexpression of AS inhibits mitochondrial complex I activity (Liu et al., 2009; Loeb et al., 2010). Devi et al. (Devi et al., 2008) have identified that AS has a cryptic mitochondrial targeting sequence located at the N-terminus of the peptide. They also have found that the transportation and accumulation of AS in mitochondria impairs mitochondrial complex I. Direct interaction of

AS and mitochondrial complex I also has been reported in the striatum of PD brain samples, normal brain samples and dopaminergic primary neuronal (DAN) cells expressing AS using blue native electrophoresis (Devi et al., 2008). Another research group has reported that the monomers and oligomers of AS are imported and localized in the mitochondria of dopaminergic neurons from transgenic mice overexpressing the A53T mutant AS (Chinta et al., 2010). These results together showed the association of overexpressed AS and mitochondria dysfunction in the pathology of PD. Constitutive expression of AS is important in maintaining the integrity of mitochondria especially for the activity of complex I. Pathological conditions such as up-regulation or mutation of AS gene which cause accumulation of AS inside the mitochondria result in impairment of mitochondrial function (Chinta et al., 2010; Devi et al., 2008; Hsu et al., 2000; Ottolini et al., 2013).

It also has been reported that genetics and environmental factors involved in PD participate in maintenance of mitochondrial dynamics through control of mitochondrial fission, fusion and mitophagy (Arduino et al., 2011; Barsoum et al., 2006; Cagalinec et al., 2013; Gomez-Lazaro et al., 2008; Meuer et al., 2007; van der Bliek et al., 2013; Youle and van der Bliek, 2012). Mitochondria have a dynamic structure and undergo frequent cycles of fission and fusion to maintain the quantity and quality of their biological functions such as cellular biogenesis and respiratory function (Arduino et al., 2011; Perier and Vila, 2012; van der Bliek et al., 2013). During mitochondrial fusion two mitochondria are fused into a single organelle (Figure 1.4b) and mitochondrial fission defines the separation of a large mitochondrion into two or more smaller organelles (Figure 1.4a). Mitophagy is the selective elimination of mitochondria through the autophagic degradation process which is important in removal of damaged mitochondria and maintenance of mitochondrion numbers (Figure 1.4c). During the mitophagy process damaged mitochondria are sequestrated into an autophagosome which is a double membrane bounded structure which is then fused with the lysosome to degrade the targeted mitochondria. Mitophagy is associated with the fission and fusion process by involving elimination of the damaged and hypopolarized mitochondria resulting from fission processes (Figure 1.4c) (Cagalinec et al., 2013; Chan, 2012; Imai and Lu, 2011; Youle and van der Bliek, 2012).

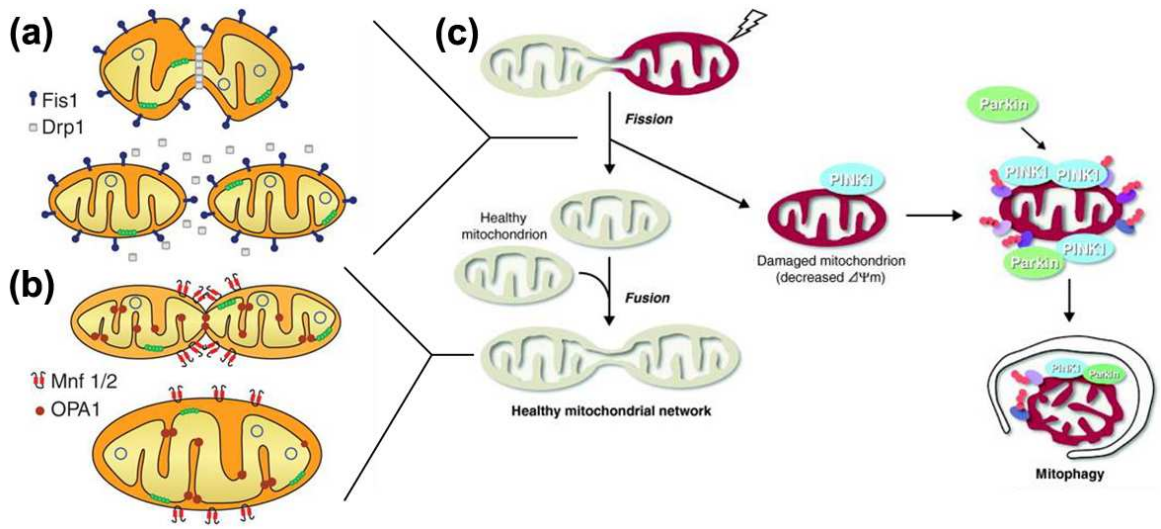

Figure 1.4 Schematic representation of mitochondrial fission-fusion processes associated with mitophagy. (a) The fission or separation of a large mitochondrion into two daughter mitochondria (b) The fusion of two mitochondria to form a single mitochondrion (c) The elimination of damaged mitochondrion through mitophagy. Parkin and pink1 are involved in this process. Reprinted and adopted with permission from (Imai and Lu, 2011; Perier and Vila, 2012). Copyright © 2011 Elsevier and Copyright © 2012 Cold Spring Harbor Laboratory Press. All rights reserved.

Accumulation of PINK1 on the OMM serves as a signal for initiating mitophagy in damaged mitochondria. PINK1 accumulates on the OMM and phosphorylates Mfn2 by its kinase activity. Phosphorylated mfn2 serves as a Parkin receptor on damaged mitochondria (Chen and Dorn, 2013). Parkin then mediates the ubiquitination of a variety of OMM proteins such as Mfn1 and Mfn2 and induces autophagic elimination of the damaged mitochondrion. Ubiquitination of Mfn1 and Mfn2 prevents the fusion of damaged mitochondria with healthy mitochondria (Deas et al., 2011; Grenier et al., 2013; Ivatt and Whitworth, 2014; Jin and Youle, 2012; Springer and Kahle, 2011; Vincow et al., 2013).

Mitochondrial fission and fusion is mediated by a group of GTPases whose function causes division and fusion of mitochondrial membranes (Figure 1.4a). Fusion of OMM and IMM mediated by mitofusins (Mfn1, Mfn2) and optic atrophy 1 (OPA1), respectively. Dynamin-related protein 1 (Drp1) is required for the fission process (Figure 1.4b) (Chan, 2012; Ottolini et al., 2013; Perier and Vila, 2012; Youle and van der Bliek, 2012).

In the case of PD, it has been shown that toxins like 6-hydroxydopamine (6-OHDA), rotenone, and MPP^+ which induce Parkinson disease pathology also cause the fragmentation of mitochondria (Barsoum et al., 2006; Gomez-Lazaro et al., 2008; Meuer et al., 2007). Barsoum *et*

al. have shown that treatment of cortical neuronal cultures, derived from embryonic rats, with rotenone causes mitochondrial fission in a dose dependent manner, causing up to 80% of fragmentation at 100nM. Further investigations revealed that overexpression of Mfn1 and the dominant-negative mutant Drp1 prevent mitochondrial fission induced by 100 nM rotenone and inhibits cell death (Barsoum et al., 2006). The MPP^+ induced fission also has been reduced in rat primary midbrain neurons expressing a dominant-negative mutant of Drp1 (Meuer et al., 2007). It also has been shown that silencing of Drp1 inhibits mitochondrial fragmentation induced by 6-OHDA which is another complex I inhibitor (Gomez-Lazaro et al., 2008). These results showed the role of Drp1 function in mitochondrial fission and cell death induced by these neurotoxins (Barsoum et al., 2006; Gomez-Lazaro et al., 2008; Meuer et al., 2007).

Besides the effects of PD environmental factors on mitochondrial fission and fusion, it has been shown that genetics factors causing familial PD (PINK1 and Parkin) regulate the fission and fusion processes in mitochondria. Deng *et al.* have shown the role of the Pink1-Parkin pathway in regulation of mitochondrial fission and fusion in Drosophila. The Pink1/Parkin pathway promotes and inhibits the fission and fusion processes respectively. The controlling effect of pink1 and parkin on mitochondrial dynamics is through the activation of the fission protein Drp1 and inactivation of fusion proteins mfn and opa1 (Deng et al., 2008). Furthermore the regulatory role of the pink1-parkin pathway in mitochondrial dynamics also has been demonstrated in rat midbrain dopaminergic neurons (Yu et al., 2011).

1.3.2 Pathophysiology of Parkinson's disease

The hallmarks of PD pathology are the loss of dopaminergic (DA) neurons of the substantia nigra (or nigrostriatal neurons) which lie at the pars compacta (SNpc) and the presence of Lewy body inclusions in the substantia nigra. The cell bodies of nigrostriatal neurons are in the SNpc, and they lead out to the putamen. As the normal cells contain noticeable amounts of neuromelanin, their loss produces the common neuropathology feature of PD which is the depigmentation of the SNpc (Dauer and Przedborski, 2003; Henchcliffe and Beal, 2008; Lotharius and Brundin, 2002b; Moore et al., 2005; Ottolini et al., 2013; Zigmond and Burke, 2002). Cytoplasmic inclusions or Lewy bodies are found in some of the dopaminergic neurons in the substantia nigra of PD patients. Electron microscopic imaging showed that compartments of Lewy bodies are densely aggregated filaments. Biochemical studies have demonstrated that Lewy bodies are composed of a mixture of proteins with aggregated AS as the most significant

component. Immunostaining with an antibody against AS is the method that can be used to label Lewy bodies. In this immunostained method, a Lewy body is revealed as a strongly immunoreactive central zone which is surrounded by a weakly immunoreactive marginal zone (Figure 1.5) (Pahwa and Lyons, 2007).

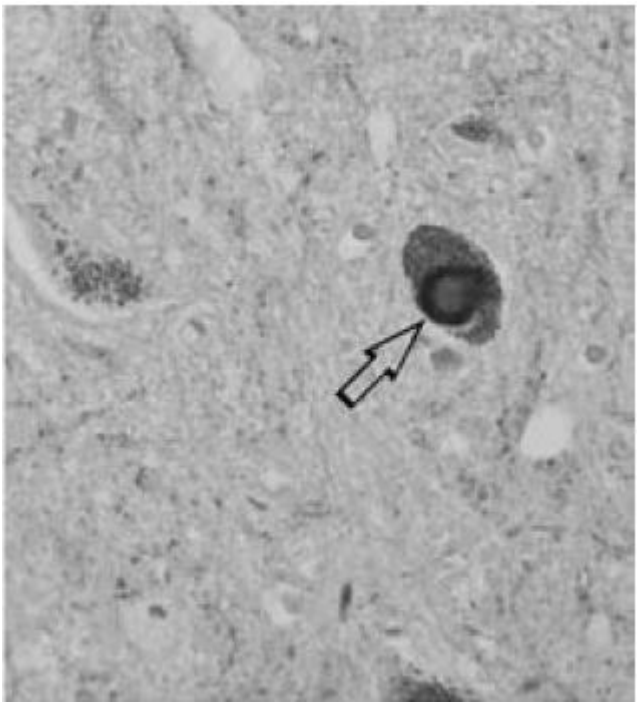

Figure 1.5 Substantia nigra of Parkinson's disease brain. Arrow shows the Lewy body immunostained with AS antibody. Reprinted with permission from (Pahwa and Lyons, 2007). Copyright © 2008 Wolters Kluwer Health. All rights reserved.

1.3.2.1 Genetic factors

Although the detailed etiology of this condition is still unknown, several genetic and environmental risk factors have been identified. The second major risk factor after increasing age for developing PD is a family history of PD. Although familial PD is less common than the sporadic form of PD, having a family history of PD doubles the risk of PD development compared to the background population. Eleven monogenetic PARK loci have been identified in the development of PD. Some of these genes (PARK 1, 3, 4, 8 and 11) are autosomal dominant (AD) and others are autosomal recessive (AR). Mutations in these genes have been reported to be associated with PD (Bekris et al., 2010; Grosset et al., 2009; Pahwa and Lyons, 2007).

Among the genes involving in PD pathology, just one of them (*PARK6*) is a mitochondrial gene but in the disease condition, the other genes are associated with mitochondrial function. The

PARK6 gene which encodes PINK1 is located on chromosome 1p35–p36. Mutations in this gene have been identified in early-onset familial cases of PD. PINK1 is synthesized as a 66 KD protein with 581 amino acids which contains a mitochondrial targeting sequence (MTS) at the N-terminal and a serine/threonine protein kinase domain at the C-terminal which faces the cytosol. The MTS is a transmembrane domain which spans the mitochondrial membranes (Moore et al., 2005; Ottolini et al., 2013).

PARK2 which encodes the parkin protein is located on chromosome 6q25.2–q27. Loss of activity mutations in this gene are common in recessively inherited PD. Parkin gene encodes a protein with 465 amino acids which contains three distinct domains including an ubiquitin-like (UBL) domain at the N terminus, a RING domain at the C-terminus which is composed of two RING finger motifs separated by an in-between RING (IBR) finger domain. As parkin is a RING finger–containing protein, it acts as an E3 ubiquitin protein ligase which is a part of the ubiquitin-proteasome system. Thus parkin function is to identify targeted proteins and label them with ubiquitin for degradation (Dauer and Przedborski, 2003; Moore et al., 2005). It has been shown that Synphilin-1 is the link between parkin and Lewy body formation in PD. This protein interacts with AS and coexpression of both of them in cultured cells causes the formation of intracellular inclusion bodies. Parkin is able to interact with ubiquitinated α-synuclein/synphilin-1 inclusions and transfers them to be digested by the proteasomal complex. Thus, parkin activity has an important role in survival of neuronal cells against the toxicity of α-synuclein/synphilin-1 Lewy body like inclusions (Moore et al., 2005).

Ubiquitin carboxyl-terminal hydrolase L1 (*UCH-L1*) or *PARK5* is another gene which is involved in PD pathogenicity. Mutant forms of this protein have been identified in familial PD cases. UCK-L1 is one of the components of the ubiquitin-proteasome system and is responsible for recycling of poly-Ub chains by hydrolysis of Ub monomers after degradation of the targeted protein. One of the mutant forms of UCH-L1 which has been identified in familial PD (I93M) reduces the hydrolysis activity of UCH-L1 *in vivo* (Dauer and Przedborski, 2003; Moore et al., 2005).

DJ-1 which is encoded by *PARK7* is located on chromosome 1p36 and the mutated forms of this gene have been identified in familial PD. DJ-1 is a 189 amino acid-protein with a DJ-1/PfpI domain that belongs to the DJ-1/PfpI superfamily of proteins. It has been reported that DJ-1 might have protease activity and further studies found an active site involving Cys106 and

His126 which is similar to the active site of cysteine proteases (Moore et al., 2005). Another function for DJ-1 is its protective activity against oxidative stress (Dauer and Przedborski, 2003; Moore et al., 2005; Ottolini et al., 2013). This protective function is based on the findings that showed this protein acts as a peroxiredoxin-like peroxidase (Andres-Mateos et al., 2007).

Another gene which has been identified in PD pathology is *LRRK2*. This gene possesses 51 exons and encodes LRRK2 or dardarin protein with 2527 amino acids. Mutations in the *LRRK2* gene have been identified in autosomal-dominant and also in idiopathic PD (Smith et al., 2006). This protein has GTPase and kinase activities and is composed of several domains such as a leucine-rich repeat domain (LRR), a Ras of complex (ROC) domain which belongs to Ras-like/small GTPase superfamily and a tyrosine kinase-like domain (Lin et al., 2011; Mata et al., 2006). The most important functions of LRRK2 are its GTPase and kinase activities and mutations that impair these functions are associated with PD (Lin et al., 2011).

1.3.2.1.1 Role of alpha-synuclein in Parkinson's disease

Loss of AS function has been proposed to be involved in the development of PD pathology. AS loss of function can be due to aggregation, reduced expression or overexpression (Kanaan and Manfredsson, 2012; Lashuel et al., 2013). Under normal conditions AS acts as a regulator of dopamine homeostasis and is involved in almost all of the dopamine metabolism pathways including dopamine biosynthesis, storage of dopamine in synaptic vesicles, dopamine release in the response to an action potential and re-uptake of released dopamine from the presynaptic space (Lotharius and Brundin, 2002a; Stefanis, 2012; Yu et al., 2005). The normal function of AS is important for clearance of dopamine from the cytoplasm of the presynaptic terminal and storage in synaptic vesicles. AS also regulates the re-uptake of released dopamine molecules from presynaptic space into the synaptic terminal. This homeostasis protects cells from deleterious effects of dopamine oxidation in the cytoplasm and also helps the replenishment of synaptic dopamine. Loss of normal AS function promotes the accumulation of dopamine in the cytoplasm of the presynaptic terminal which leads to oxidative stress (Lotharius and Brundin, 2002a, b; Yu et al., 2005).

There are three possibilities causing the AS loss of function. The first one is mutations in the AS gene associated with familial forms of PD. The main mutants of AS affecting its structure and function are A30P, A53T and E46K. Loss of function can also occur due to misfolding and aggregation (Yu et al., 2005) of AS which might be a result of *SNCA* multiplication, associated

with some familial forms of parkinsonism (Lashuel et al., 2013), or *SNCA* overexpression (Spinelli et al., 2014). Formation of AS oligomers or aggregates results in the reduction of available functional AS (Kanaan and Manfredsson, 2012). It has been shown that AS exists in three forms in presynaptic terminals. The first two forms of AS are the functional protein and exists as monomers which are unbound or bound to synaptic vesicles. The third form of AS is characterized by microaggregates of the protein. Furthermore it has been demonstrated that in animal models with moderate overexpression of the *SNCA* gene, a condition which is similar to multiplication mutations linked to PD, the microaggregates are found in presynaptic terminals and ultimately lead to dysfunction of the presynaptic terminals (Spinelli et al., 2014). In the moderate overexpression condition, the pathology of AS microaggregates is similar to the AS aggregates in Lewy bodies including proteinase K-resistance, phosphorylation at serine-129 and oxidation damage (Spinelli et al., 2014).

Dopamine is synthesized in the cytoplasm of presynaptic terminals but cannot be stored at the normal pH of the cytoplasm as it undergoes auto-oxidation or enzymatic oxidation by MAO and forms reactive oxygen species (ROS) which contribute to the pathogenesis of PD. The cytoplasmic dopamine which has been synthesized from L-DOPA or transported into the cell is isolated into monoaminergic vesicles by the vesicular monoamine transporter 2 (VMAT2) (Lotharius and Brundin, 2002a). Monoaminergic vesicles provide a low pH environment lacking MOA to protect cytosolic dopamine from oxidation. Efficient dopamine sequestration which requires formation of synaptic vesicles from early endosomes is a protective process against the toxic effects of dopamine oxidation. It has been shown that AS is involved in the formation of synaptic vesicles from early endosomes (Lotharius and Brundin, 2002a, b). As well, the normal structure of AS is required for its function in regulating oxidative stress and the pathology of AS mutants might be related to their reduced capability in the scavenging of reactive oxygen species (Kanda et al., 2000).

The function of AS in dopamine presynaptic vesicle formation and release depends on its ability to bind with membrane phospholipid. Any change in AS structure which causes the loss of this ability disrupts synaptic plasticity and dopamine metabolism which finally leads to oxidative stress and cell death. It has been reported that the A30P and A53T mutants of AS which are associated with familial PD lose the phospholipid binding activity partially (A30P) or

completely (A53T). This shows another link between AS loss of function and PD pathology (Perrin et al., 2000).

Besides AS loss of function, another hypothesis to explain the role of AS in PD is the cytotoxicity of AS oligomers (Wan and Chung, 2012; Winner et al., 2011). Aggregation of AS is a two stage process which starts from monomers. The first stage is the oligomerization of misfolded monomers follow by aggregation of oligomers to form fibrils. It has been shown that AS oligomers are more toxic than the fibrils and formation of fibrils is a protective mechanism to reduce the cytotoxicity of oligomers and increase cell survival (Colla et al., 2012b; Wan and Chung, 2012; Winner et al., 2011).

Recent studies have shown that AS can transfer neuron to neuron and spread the hallmark of PD, *i.e.* Lewy pathology, throughout the brain in a prion-like manner as the disease progresses (Angot et al., 2012; Braak et al., 2003; Danzer et al., 2012; Desplats et al., 2009; Hansen et al., 2011; Hansen and Li, 2012; Kordower et al., 2008; Kurowska et al., 2011; Li et al., 2008; Luk et al., 2012; Masuda-Suzukake et al., 2013; Steiner et al., 2011; Volpicelli-Daley et al., 2011). Support for the AS propagation hypothesis comes from reports which showed the development of Lewy body pathology in grafted neurons which were transplanted to PD patients many years before (Kordower et al., 2008; Kurowska et al., 2011; Li et al., 2008). These observations provide evidence for the prion like transmission of misfolded AS from the host cells to the normal grafted cells with spread of PD pathology (Hansen and Li, 2012; Kordower et al., 2008; Kurowska et al., 2011; Li et al., 2008; Volpicelli-Daley et al., 2011). *In vitro* experiments using pure WT AS preformed fibrils (PFFs) showed the entrance of the PFFs into primary neuronal cultures, prepared from E16-E18 C57BL/6 mouse brains, and conversion of normal and soluble endogenous AS into Lewy bodies (Volpicelli-Daley et al., 2011). The uptake of AS by neuronal cells has been shown *in vitro*, *i.e.* in cell culture, (Desplats et al., 2009; Hansen et al., 2011) and *in vivo*, *i.e.* in mouse brain (Hansen et al., 2011; Luk et al., 2012; Masuda-Suzukake et al., 2013).

1.3.2.2 Environmental factors

Development of PD is not just due to mutation and impairment of genes, as environmental factors can also cause PD. Environmental factors such as heavy metals, 1-methyl-4-phenyl-1,2,3,6-tetrahydropyridine (MPTP), pesticides, solvent and head injury increase the incidence of PD (Grosset et al., 2009; Pahwa and Lyons, 2007). MPTP which is an analog for narcotic

meperidine that inhibits the activity of complex I and leads to the reduction of oxidative phosphorylation in mitochondria. (Exner et al., 2012; Perier and Vila, 2012).

6-hydroxydopamine (6-OHDA) has been widely used as a neurotoxin to create animal models for PD research. Because of its polarity, 6-OHDA does not cross the blood brain barrier (BBB) easily. The 6-OHDA structure is similar to dopamine and can bind to the dopamine transporter (DAT) to be transferred from the extracellular space to dopaminergic neurons (Bové et al., 2005). Inside the cells 6-OHDA reacts with O_2 and generates reactive oxygen species (ROS) such as hydrogen peroxide and semiquinone (Tirmenstein et al., 2005).

Pesticides which are widely used to control different types of organisms have been identified as significant risk factors for PD. Several studies have reported that exposure to rotenone and paraquat increases the incidence of PD (Berry et al., 2010; Franco et al., 2010). Paraquat (1,1′-dimethyl-4,4′-bipyridinium dichloride) is a quarternary nitrogen herbicide (Douna et al., 2012; Franco et al., 2010; Olanow and Tatton, 1999). It has been shown that paraquat enters into the dopaminergic cells by a Na-dependent transporter (Shimizu et al., 2001). Inside the neuronal cells paraquat induces oxidative stress and leads to the loss of dopaminergic neurons and also formation of AS containing inclusions (Franco et al., 2010). Another pesticide with potential risk for developing PD is rotenone. Rotenone is used as an insecticide and is a lipophilic compound which can easily cross the BBB. Several reports demonstrated that rotenone cytotoxicity is due to its ability to bind and inhibit mitochondrial complex I. It has been proposed that this inhibition could be due to the elevation of mitochondrial ROS level as ROS has an important role in apoptosis through inhibition of the respiratory chain (Li et al., 2003; Xiong et al., 2012).

1.3.2.3 Current Treatments of Parkinson's disease

Despite significant progress in the understanding of the molecular mechanism of PD, there is no definitive treatment. The current strategy is based on the control of symptoms by restoring the loss of dopamine. The most efficient treatment is L-3,4-dihydroxyphenylalanine (L-DOPA) which is a precursor of dopamine. To increase the lifetime of dopamine, levodopa is administrated with other drugs to slow the metabolism of dopamine. These adjunctive medications of levodopa include catechol O-methyltransferase (COMT) inhibitors, monoamine oxidase-B (MAO-B) inhibitors, and peripheral dopamine decarboxylase inhibitors (Grosset et al., 2009; Olivares et al., 2009; Pahwa and Lyons, 2007).

L-DOPA is an aromatic amino acid and naturally is found in seedlings, pods, and broad beans. It crosses the blood–brain barrier (BBB) to maintain the level of dopamine (Grosset et al., 2009; Olivares et al., 2009; Pahwa and Lyons, 2007). Metabolism of L-DOPA occurs peripherally (outside of the BBB) and centrally (inside of the BBB) (Figure 1.6). L-DOPA is co-administrated with dopamine decarboxylase inhibitors such as carbidopa to prevent the peripheral conversion of levodopa to dopamine. These inhibitors lead to an increase of the half life of L-DOPA in peripheral cells and promote the transport across BBB. Dopamine decarboxylase inhibitors can not cross through the BBB and do not affect the conversion of L-DOPA to dopamine in brain. L-DOPA in brain is converted to dopamine. L-DOPA is also converted to 3-O-methyldopa (3-OMD) by peripheral catechol-O-methyltransferase (COMT). To prevent the peripheral metabolism of levodopa to 3-OMD, peripheral catechol-O-methyltransferase (COMT) inhibitor such as entacapone or tolcapone are added to increases the half-life. For example Stalevo® is a combination medication that contains carbidopa, levodopa, and entacapone for the treatment of Parkinson's disease. L-DOPA entering the BBB undergoes central metabolism. In the brain central dopamine decarboxylase converts levodopa to dopamine.

Dopamine is the substrate of two enzymes in the brain (Di Giovanni et al., 2010; Grosset et al., 2009; Pahwa and Lyons, 2007). Monoamine oxidase-B (MAO-B) converts dopamine to 3,4-dioxyphenylacetic acid (3,4-DPA) (Figure 1.6). MAO B inhibitors such as selegiline are administrated to maintain the level of dopamine in brain. Furthermore, central catechol-O-methyltransferase (COMT) converts dopamine to 3-methoxytyramine (3-MT) which is a substrate of MAO-B. 3-MT is converted to homovanillic acid (HVA) but MAO-B inhibitors prevent this conversion (Di Giovanni et al., 2010; Grosset et al., 2009; Pahwa and Lyons, 2007).

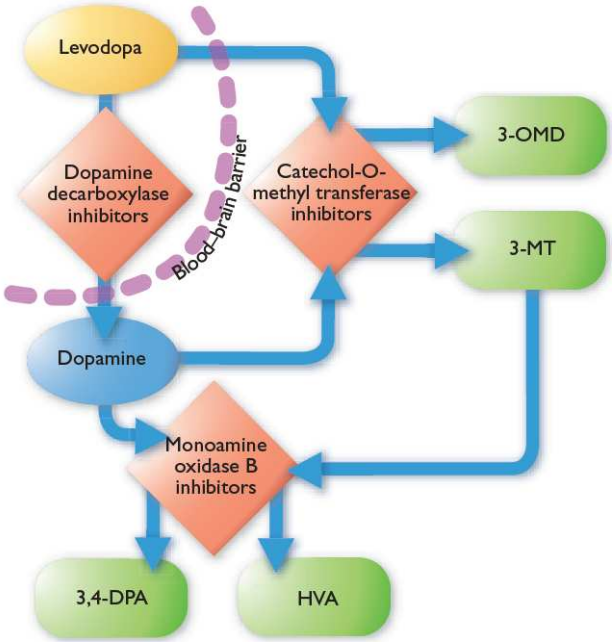

Figure 1.6 Metabolism of L-DOPA and enzyme inhibitors. This pathway shows metabolism of L-DOPA to dopamine. Side products (green) and sites of enzyme inhibitors are shown as green and orange respectively. Abbreviations: 3-OMD, 3-O-methyldopa; 3,4-DPA, 3,4-dioxyphenylacetic acid; HVA, homovanillic acid; 3-MT, 3-methoxytyramine. Reprinted with permission from (Grosset et al., 2009). Copyright © 2010 Oxford University Press. All rights reserved.

1.4 Intrinsically disordered proteins

Intrinsically disordered proteins (IDPs) are a group of proteins which share an unusual biophysical characteristic. The native form of these proteins lacks the secondary and tertiary structures observed in ordered proteins. Thus these proteins are also called natively unfolded proteins to be distinguished from folded or structured proteins with regular three dimensional structures (Theillet et al., 2013; Tompa, 2012; Uversky, 2011). Biophysical studies of these proteins revealed that their NMR spectrum is not as well resolved with some line-broadening and peak overlap which is typical for a random-coil conformation. Furthermore CD and FTIR spectroscopy experiments also show a random coil conformation of these proteins (Brucale et al., 2014; Chiti and Dobson, 2006; Dyson and Wright, 2005; Uversky, 2013a, b; Uversky et al., 2008). Natively unstructured proteins are very sensitive to their environment. Genetic mutations and environmental modification such as exposure to toxins or drugs folds these proteins into a non-functional state, a process which is called misfolding. The non-functional or misfolded conformations are prone to oligomerization and aggregation through β-sheet formation (Babu et

al., 2011; Oldfield and Dunker, 2014; Theillet et al., 2013; Tompa, 2012; Uversky, 2013a; Uversky et al., 2008).

A broad range of human diseases arise from the misfolding of IDPs which are referred to as protein conformational or protein misfolding diseases. Although the size of the protein and the primary location of the affected organs are variable, all protein misfolding diseases are characterized by the presence of fibrillar aggregates or amyloid plaques which are linked to cell toxicity and death (Chiti and Dobson, 2006). For example, in Type 2 diabetes amylin (37 residues), also known as Islet Amyloid Polypeptide is the culprit whereas in Alzheimer's Disease (AD) the peptide Aβ42 (40 or 42 residues) is clearly implicated (Jackson et al., 2013; Janson et al., 2004). AD is just one example of a neurodegenerative disease caused by protein misfolding; others include Amyotrophic Lateral Sclerosis (ALS) involving superoxide dismutase 1 (SOD1) (153 residues) (Valentine et al., 2005), and the prion protein (253 residues) which causes diseases such as Creutzfeldt - Jacob disease (CJD) and Fatal Familial Insomnia (FFI) (Prusiner, 2001).

1.4.1 Alpha-Synuclein

AS has 140 amino acids and lacks cysteine and tryptophan residues. The molecular weight and isoelectric point (pI) of this protein are 14460 D and 4.67, respectively. The total numbers of negatively charged and positively charged residues are 24 and 15, respectively, so that the net charge of the protein is -9 (Fink, 2006; McClendon et al., 2009; Vigneswara et al., 2013). The structure of AS can be divided into three regions including N-terminal, non amyloid-β component (NAC) and C-terminal (Figure 1.7). AS is a natively unfolded protein which in aqueous environments does not achieve any secondary structure. Binding of the protein with lipid molecules or phospholipid membranes induces the formation of an α-helix in the N-terminal region. Three missense mutations in this region are associated with familial PD (Figure 1.7). The NAC region of the protein is able to undergo conformational changes from random coil to β-sheet. The acidic C-terminal is always unfolded, probably because of its highly acidic nature.(Ulmer et al., 2005a; Uversky, 2007; Uversky and Eliezer, 2009).

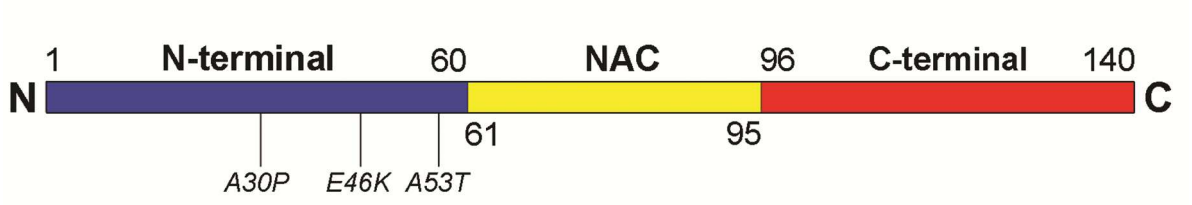

Figure 1.7 Schematic of the structure of AS, showing the N-terminal segment, the NAC segment, and the C-terminal segment. The positions of missense mutations in the N-terminus are also indicated.

1.4.1.1 Physiology and biological function of alpha-Synuclein

Whereas the biological function of AS is not fully characterized, it has been demonstrated that this protein is involved in the homeostasis of dopamine metabolism including dopamine biosynthesis, vesicle recycling, dopamine storage, and release, vesicle transportation, dopamine transporter activity and dopamine uptake (Yu et al., 2005). The major function of AS is synaptic vesicle recycling, dopamine storage, and release. It has been reported that AS is involved in dopamine storage by promoting the formation of synaptic vesicles from early endosomes (Figure 1.8) (Lotharius and Brundin, 2002b). It is also involved in synaptic vesicle fusion with the presynaptic plasma membrane which leads to release of dopamine in the presynaptic space and also participates in vesicle recycling from the presynaptic plasma membrane (Lashuel et al., 2013).

AS involvement in synaptic vesicle recycling is important for dopamine homeostasis in the dopaminergic nigrostriatal terminal. As illustrated in Figure 1.8, despite dopamine being synthesized in the cytoplasm of the presynaptic terminal it cannot be stored in the normal pH of the cytoplasm as it undergoes auto-oxidation or enzymatic oxidation by MAO and forms reactive oxygen species (ROS) which contribute to the pathogenesis of PD (Lashuel et al., 2013; Lotharius and Brundin, 2002a, b). The cytoplasmic dopamine which has been synthesized from L-DOPA or transported into the cell is isolated into monoaminergic vesicles by the vesicular monoamine transporter 2 (VMAT2) (Lotharius and Brundin, 2002a). Monoaminergic vesicles provide a low pH environment lacking MOA to protect cytosolic dopamine from oxidation processes. Efficient dopamine sequestration which requires formation of synaptic vesicles from early endosomes is a protective process against the toxic effects of dopamine oxidation. It has been shown that AS is involved in the formation of synaptic vesicles through interactions with phospholipase D2 (PLD2) (Figure 1.8) (Lotharius and Brundin, 2002a, b).

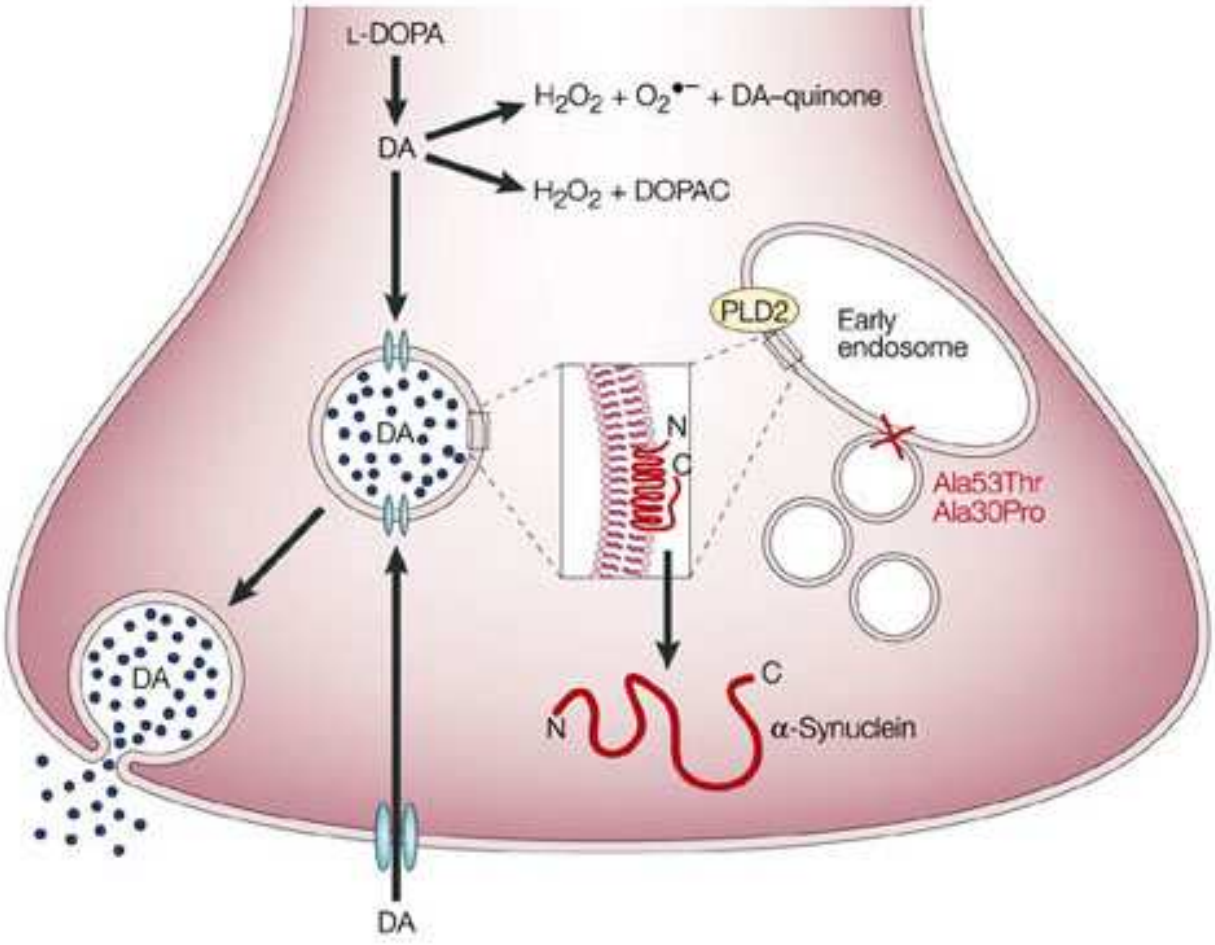

Figure 1.8 The role of AS in the formation of synaptic vesicles. Phosphorylation of AS by G-protein receptor kinases stops its inhibitory effect on phospholipase D2 activity and triggers the vesicle formation from the early endosome. Reprinted with permission from (Lotharius and Brundin, 2002b). Copyright © 2002 Nature Publishing Group. All rights reserved.

There are two isoforms of PLD enzymes; PLD1 and PLD2. The membrane-bound enzymes catalyse the formation of phosphatidic acid (PA) from phosphatidylcholine (PC) in response to chemical signals such as neurotransmitters and hormones. They are involved in regulation of synaptic vesicle recycling and neurotransmitter release. The catalytic product of PLD, PA, acts as an intracellular messenger to activate coatomer or clathrin coat proteins and finally facilitates budding of vesicles from the plasma membrane, early endosomes and Golgi network. It has been shown that in the absence of stimuli, the activity of PLD enzymes is masked by AS. It has been

demonstrated that the N-terminal of AS interacts with PLDs and inhibits their function. The activation pathway occurs after a high-frequency stimulation which increases the intracellular concentration of Ca^{2+} and activates calcium-sensor proteins follow by the activation of G-protein receptor kinases. Finally phosphorylation of AS by the activated G-protein receptor kinases, stops the inhibitory effect of AS on PLD activity and leads to budding of vesicles from the early endosomes (Lotharius and Brundin, 2002a). Binding of AS through its N-terminus with membrane phospholipids is the critical stage in the formation of synaptic vesicles and dopamine storage as a protection against cytosolic oxidation of dopamine. Two mutations in the N-terminal, *i.e.* A30P and A53T, which are associated with a familial form of PD have lower phospholipid binding ability. Thus these mutations impair the storage of dopamine in synaptic vesicles and increase the cytosolic concentrations of dopamine which can then undergo oxidation (Lotharius and Brundin, 2002a, b).

AS also has a role in the fusion of synaptic vesicles with the presynaptic plasma membrane for releasing dopamine into the presynaptic space and then recycling of the fused vesicle from the presynaptic plasma membrane. For these functions, AS along with cysteine-string protein α (CSPα) act as a chaperone and changes the conformation of SNARE (Soluble NSF (N-ethylmaleimide-sensitive factor) attachment protein (SNAP) receptor) proteins which are involved in synaptic vesicle fusion and recycling (Bonini and Giasson, 2005; Sharma et al., 2011). In normal cells CSPα acts as a chaperone to stabilize the functional conformation of the SNAP-25 protein which is required for SNARE complex formation and membrane fusion. AS acts as an auxiliary molecular chaperone and assists CSPα to complete this step. Membrane fusion and neurotransmitter release occurs in response to an action potential which stimulates opening of Ca^{2+} channels and increases the intracellular concentration of Ca^{2+} and finally leads to SNARE complex formation and fusion of synaptic vesicles with the plasma membrane. The cooperation of CSPα and AS facilitates the priming stage in membrane fusion which is the interaction of vesicle-associated SNARE (v-SNARE) and target membrane-associated SNARE (t-SNARE). Upon membrane fusion and neurotransmitter release the SNARE complex dissociates and the synaptic vesicle is recycled (Bonini and Giasson, 2005; Chandra et al., 2005; Sudhof, 2013).

Regulation of dopamine homeostasis by AS is not limited to dopamine storage and release. AS also is involved in regulation of dopamine transporter activity, dopamine reuptake and

dopamine biosynthesis (Yu et al., 2005). The effect of AS on dopamine biosynthesis occurs by regulating the expression and activity of a tyrosine hydroxylase enzyme which is the key enzyme in dopamine biosynthesis (Kanaan and Manfredsson, 2012; Yu et al., 2005). It also has been reported that AS has ferrireductase activity and provides Fe (II) required for tyrosine hydroxylase function (Brown, 2013; Davies et al., 2011). Baptista *et al.* have reported that overexpression of the wild type AS gene in human neuroblastoma cell lines causes downregulation of tyrosine hydroxylase (TH) (Baptista et al., 2003).

After release of dopamine into the presynaptic space in response to an action potential, the released dopamine must be re-uptaken into the presynaptic terminal in order to terminate dopamine signaling and also replenish the synaptic dopamine. The dopamine transporter (DAT) is responsible for dopamine reuptake, a process which is regulated by AS. Uptake of positively charged dopamine molecules by DAT depends on co-transportation of Na^+ and Cl^- ions (Butler et al., 2012). Lee *et al.* have demonstrated a direct interaction between AS and DAT using a yeast model, neuronal cell culture and also a co-immunoprecipitation assay (Lee et al., 2001). This association involves interaction of the AS-NAC region with the C-terminal tail of DAT consisting of its last 22 amino acids (Glu598-Val620) (Butler et al., 2012; Lee et al., 2001). Overall AS binds to DAT and alters its activity in the uptake of dopamine from the presynaptic space (Butler et al., 2012).

1.4.1.2 Structure of alpha-Synuclein

In this thesis structural biology methods were used to characterize the structure and conformation of AS. In this section the structure of this protein will be reviewed. The AS protein is divided into three regions: the N-terminal region covering amino acids 1-60, the middle region residues 61-95 which is the NAC region; and the C-terminal residues 96-140 (Alderson and Markley, 2013; Uversky, 2007). The secondary structure content of AS has been previously measured with CD spectroscopy and Fourier-transform infrared spectroscopy (FTIR) (Weinreb et al., 1996). The CD spectra of AS is characteristic of a random coil or denatured protein and shows a maximum ellipticity at 200 nm and lacks the α-helical and β-sheet characteristic bands in the 210–230 nm region (Figure 1.9) (Serpell et al., 2000; Uversky et al., 2001b; Weinreb et al., 1996; Zheng et al., 2013).

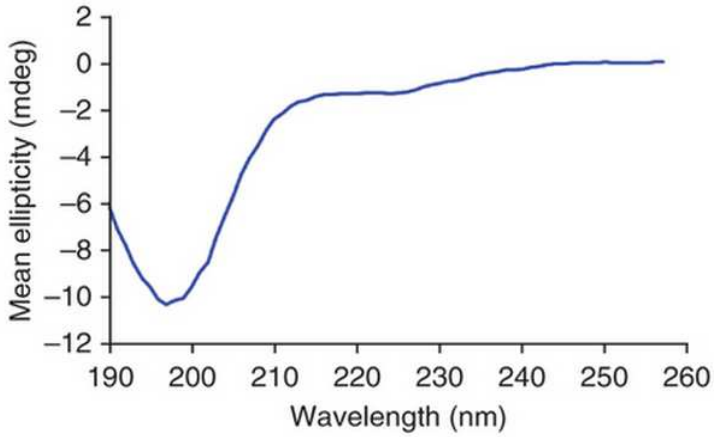

Figure 1.9 CD spectrum of AS which is typical for a random coil conformation and shows an ellipticity at around 200 nm. Reprinted with permission from (Zheng et al., 2013). Copyright © 2013 Nature Publishing Group. All rights reserved.

The random coil conformation of AS is independent of AS concentration (up to 600 μM), buffer properties such as pH (~5.5 to ~9) and the ionic strength. The conformation of AS does not change with increasing concentration which indicates that this protein normally exists as a monomer rather than oligomers or aggregates. At lower pH (pH<5), the negative intensity around 222 nm increases as a function of pH reduction. This shows that a very acidic environment leads to the formation of secondary structures in AS (Uversky et al., 2001b). The plot of ellipticity at 222 nm ($[\theta]_{222}$) versus pH changes is sigmoidal and has an isosbestic point at pH 5 which represents the transition point from natively unfolded state (pH>5) to partially folded intermediate (pH<5) (Uversky et al., 2001b). Furthermore it has been shown that the conformational changes of AS induced by reduction in pH are reversible and also independent of AS concentration which indicates that this conformational change is due to folding of monomers, not intermolecular interaction or aggregation (Uversky et al., 2001b). There is also no conformational change in the presence of 2 mM NaCl, 2 mM $MgCl_2$, 10 mM $CaCl_2$ and 0.1 mM ATP. Thus ionic interactions are not involved in stabilizing the AS native conformation (Weinreb et al., 1996). The conformational change of AS at different temperatures was also studied using CD spectroscopy, which demonstrated that by increasing the temperature from 3°C to 50°C, the magnitude of $[\theta]_{222}$ increased. Therefore, at low temperatures AS has a random coil conformation which is typical for unstructured proteins, while high temperature causes secondary structure formation and induces the transition from unfolded conformation to a

partially folded intermediate similar to the conformation induced by low pH (Uversky et al., 2001b).

FTIR spectroscopy which is more sensitive for β-sheet detection also showed that AS has a natively unfolded structure (Meng et al., 2010b; Sandal et al., 2008; Silva et al., 2013; Uversky et al., 2001b; Weinreb et al., 1996). The attenuated total reflectance FTIR spectrum of AS at pH 7.5 shows a broad amide I absorption band centered at 1642 cm^{-1} which is typical for the random coil conformation of unstructured proteins (Weinreb et al., 1996) but at pH 3 a new band appeared at around 1626 cm^{-1} which is characteristic for the β-sheet conformer. This result indicates that acidic pH causes a transition from natively unfolded AS to a partially folded intermediate with β-sheet structure (Uversky et al., 2001b). The natively unfolded structure of AS has also been characterized by ^{1}H-^{15}N-HSQC NMR (Chandra et al., 2003; Wu et al., 2008). The ^{1}H-^{15}N spectrum of AS is characteristic of unfolded proteins because it is not as well resolved with some line-broadening and peak overlap (Chandra et al., 2003; Wu et al., 2008).

One of the biological roles of AS is the regulation of vesicular fusion and there are many reports which demonstrated the co-localization of AS with synaptic vesicles. These facts reveal that AS is a lipid binding protein and further studies showed that interaction of AS with lipids and membrane change the secondary structure content of protein. The 1-87 region of AS consists of seven imperfect repeats of an 11-amino acid sequence which is classified as an amphipathic α-helical domain. The domains contain a six-amino acid core with the consensus KTKEGV and have homology with A2-type amphipathic α-helices in apolipoproteins and other lipid-binding proteins (Auluck et al., 2010; Dikiy and Eliezer, 2012; Jo et al., 2000). AS binds to membranes through the amphipathic α-helical domains. This binding causes the formation of either two α-helices connected by a flexible linker or a single extended α-helix in the region of AS covering the seven repeats (Burré et al., 2012).

To characterize the binding specificity of AS, small unilamellar vesicles (SUVs) were prepared from 1:1 (w/w) ratios of synthetic phospholipids. The results showed that AS does not bind to the SUVs containing phosphatidylcholine (PC) only, or a mixture of PC and phosphatidylethanolamine (PE) at a 1:1 ratio. However, AS binds with mixed SUVs containing acidic phospholipids such as phosphatidylinositol (PI), phosphatidylserine (PS) and phosphatidic acid (PA) (Davidson et al., 1998). Furthermore, CD spectroscopy has been used to investigate the secondary structure of AS in the presence of negatively charged phospholipids and revealed

that the AS conformation undergoes a transition from random coil to α-helical conformation upon binding to phospholipids (Davidson et al., 1998; Jo et al., 2000). It also has been shown with CD spectroscopy that acidic detergents such as lysosphatidylserine, lysophosphatidic acid and SDS change the CD spectra of natively unfolded AS in the same way as the acidic SUVs.

The conformational change of AS in the presence of PS-SUVs and SDS was further investigated by NMR spectroscopy. The ^{1}H-^{15}N HSQC spectrum of AS (0.1 mM) was typical of an unfolded protein with a dense cluster of cross-peaks over a narrow range but in the presence of saturating concentrations of PS-SUVs and SDS most of the cross-peaks disappeared and their intensity reduced significantly. The residues which disappeared are involved in the folding of AS due to binding with large size SUVs which leads to broadening of the resonances of the corresponding amide groups of AS and are consistent with the formation of α-helical structure upon micelle binding. The position and intensity of some other cross-peaks remained unchanged and demonstrated that these residues do not bind to lipid and stay unfolded even in the presence of SUVs (Chandra et al., 2003). Diagnosis of the secondary structure properties of the AS:SDS complex was performed by analysis of short range Nuclear Overhauser Effect (NOE). The results showed that the first 100 residues of AS adopted a α-helical structure with a break at residues 43 and 44. In 2005 the detailed structure and dynamic of SDS-micelles:AS complex was characterized with NMR spectroscopy (Ulmer et al., 2005a). This study also showed a broken helix in the N-terminal of AS in the presence of SDS. Residues Val3-Val37 forms the first helix and residues from Lys45 to Thr92, are involved in the second helix. An extended linker which has an anti-parallel arrangement connected the two helixes. Subsequently there is a short extended sequence from Gly93 to Lys97 followed by the C-terminal flexible tail (Asp98-Ala140) (Ulmer et al., 2005a).

The broken helix model for micelle-bound AS has been also demonstrated with site-directed spin labeling-electron paramagnetic resonance (SDSL-EPR) using 1-palmitoyl-2-oleoylsn-glycero-3-[phospho-L-serine] PS-SUV or SDS micelles. The helix formation was also modeled by molecular dynamic simulations (Bortolus et al., 2008). Another proof of the broken helix model for AS structure in the presence of negatively charged detergents was demonstrated in 2010 using a combination of NMR and EPR (Rao et al., 2010). In this study the partially folded intermediate conformation of AS in the presence of micelles of the detergent sodium lauroyl sarcosinate (SLAS) was characterized. It was found that SLAS-bound AS shows two antiparallel

α-helixes encompassing residues Asp2-Lys32 and Ser42-Thr92 which are connected by a linker (Rao et al., 2010). These results were consistent with SDS- and PS-SUV-bond AS and all of them showed the formation of a broken helix covering the first 100 residues of AS in the presence of negatively charged detergents (Bortolus et al., 2008; Rao et al., 2010; Ulmer et al., 2005b). After these reports, another model was proposed for micelle-bond AS which implied that in the presence of micelles the AS conformation is not just a broken helix but another conformation, the elongated helix also exists (Georgieva et al., 2010; Lokappa and Ulmer, 2011). AS exists in both elongated and broken states and the population ratio of 7.6:1 has been reported (Lokappa and Ulmer, 2011). An ESR study of the structural changes of AS in the presence of SDS micelles revealed that inter-conversion between broken and extended helix conformations depends on the micelles shape, *i.e.* spheroidal or rod-like, which depends on the SDS and AS concentrations. Spheroidal micelles form at low concentrations of SDS (5-60 mM) but the critical concentration for rod-like micelles formation is 430 mM (Georgieva et al., 2010). A model has been proposed based on the AS physiological role in facilitating synaptic vesicle fusion with the plasma membrane by making a bridge between vesicle and the plasma membrane (Figure 1.10). In this model spheroidal and rod-like micelles represented the vesicular and plasma membranes. The natively unfolded AS binds to the synaptic vesicle and forms an extended helix which converted to membrane-spanning broken helix when the vesicle reaches the plasma membrane. The membrane-spanning broken helix facilitates the fusion of dopamine containing vesicles with the plasma membrane (Figure 1.10) (Georgieva et al., 2010).

The natively unfolded conformation of AS monomer arises from expression of the AS gene in bacteria and purification of overexpressed protein using protocols requiring heating and denaturing of sample (Bartels et al., 2011). In 2011 a tetramer structure was reported for AS and defined as a four helix bundle (Bartels et al., 2011; Burre et al., 2013; Wang et al., 2011b). Wang *et al*. used a non-denaturing protocol to purify AS from *E.coli*. Size-exclusion chromatography demonstrated a peak with a molecular weight (MW) of 56 kDa which is almost 3.6 times an AS monomer. Subsequently, glutaraldehyde was added to the protein solution to cross-link AS monomers. Loading of the cross-linked AS on a 12% SDS-PAGE showed four bands which suggested that AS monomers are prone to form a tetramer structure (Wang et al., 2011b). Further analysis of the isolated cross-linked band also confirmed the existence of AS oligomers. The

oligomer structure has been detected on a Blue Native-PAGE (BN-PAGE) gel, a non-denaturing electrophoresis method, as a band with molecular weight of 48 kDa (Wang et al., 2011b).

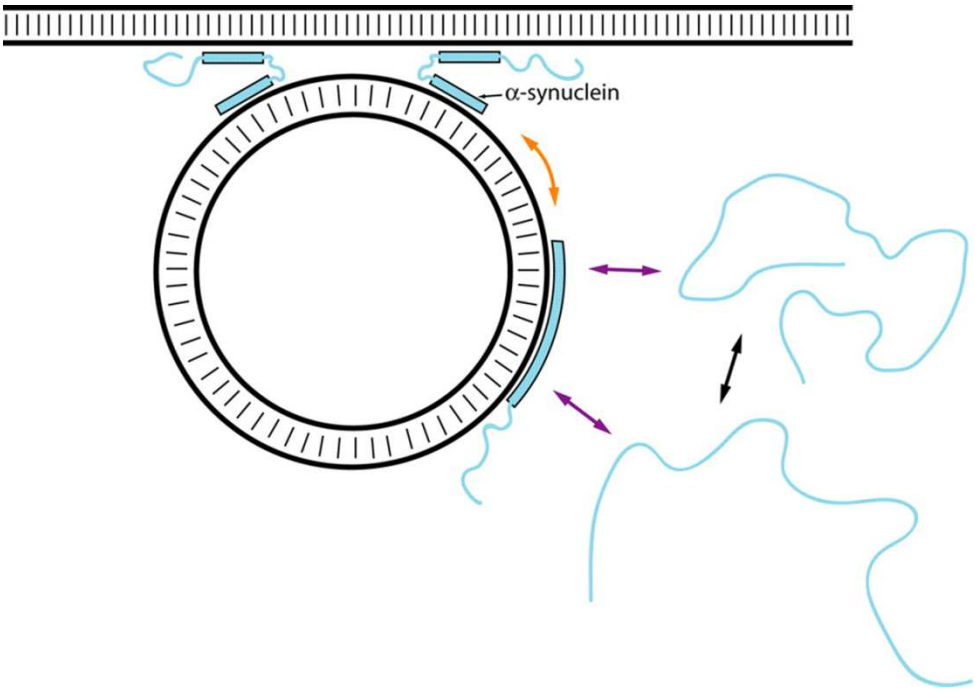

Figure 1.10 Proposed model for the role of AS in synaptic vesicle fusion with the plasma membrane. Binding of the natively unfolded AS to the synaptic vesicle (purple arrow) causes the transition from random coil to an extended helix. The extended helix converts to a broken helix (orange arrow) when vesicle reaches the plasma membrane. Reprinted with permission from (Georgieva et al., 2010). Copyright © 2010 American Society for Biochemistry and Molecular Biology. All rights reserved.

In another study, Western blot analysis was performed on lysates of M17D cells (the dopaminergic human neuroblastoma line), HEK293, HeLa, COS-7, red blood cell (RBC) lysate and cells from the frontal cortex of mouse brain (mouse cort.). The AS from all of the lysates showed a 45–50 kDa band in BN-PAGE. The clear native–PAGE (CN–PAGE) gel system which lacks the coomassie-dye also has been used to clarify the native AS species from lysates. AS molecules from all lysates migrated as an apparent tetramer species with a MW of 55-60kDa on CN-PAGE (Bartels et al., 2011).

The secondary structure of *E. coli* and RBS derived AS oligomers has been characterized using CD spectroscopy and showed a negative ellipticity at 222nm and 208nm with a positive ellipticity at 193nm which is typical for the α-helical conformation (Figure 1.11a) (Bartels et al., 2011; Wang et al., 2011b). By comparison, the CD spectrum of recombinant AS monomer was typical for an unfolded protein with a mostly random coil conformation (Figure 1.11b).

Furthermore no conformational change has been detected for tetrameric AS in the presence of negatively charged SUVs (Figure 1.11a) but the recombinant monomer AS undergoes an α-helical transition upon binding to negatively charged SUVs (Figure 1.11b) (Bartels et al., 2011). Further structural characterization of tetramer AS was performed by *in vivo* ^{1}H-^{15}N HSQC NMR of labeled AS in *E. coli* cells and showed two α-helical regions encompassing residues Phe4-Thr43 (α1) and His50-Asn103 (α2). The predicted structure for the C-terminal (104-140) was random coil (Wang et al., 2011b).

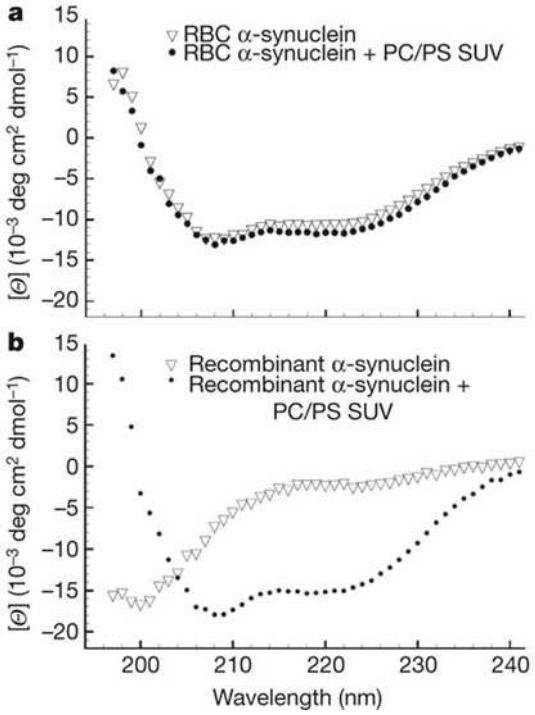

Figure 1.11 CD spectra of monomeric and tetrameric AS in the presence and absence of lipids. (a) CD spectra of tetrameric AS in the absence and presence of negatively charged SUVs (PC/PS 4:1; protein:lipid 1:500) (b) CD spectra of monomeric AS in the absence and presence of negatively charged SUVs (PC/PS 4:1; protein:lipid 1:500). Reprinted with permission from (Bartels et al., 2011). Copyright © 2011 Nature Publishing Group. All rights reserved.

1.4.1.3 Misfolding and Aggregation

As detailed above, the AS monomer is sufficiently stable to allow detailed structural studies. However, under some conditions it can rapidly aggregate. AS aggregation is a process which starts from the natively unfolded monomers which are finally converted to oligomers or fibrils of AS. The intermediate stage is the conformational change of monomers to form partially folded intermediates, a process which is called misfolding (Fink, 2006; Uversky et al., 2001a).

Mutations and environmental factors favor the conversion of the unfolded monomers into a partially folded conformation (Lee and Trojanowski, 2006). In these intermediates nonpolar side chains of residues form a hydrophobic surface which triggers the intra-molecular hydrophobic interaction and leads to the second stage which is the oligomerization and fibrillization of AS. The natively unfolded monomer lacks the hydrophobic surface. Thus factors shifting the equilibrium in favor of the partially folded intermediate can form soluble oligomers or insoluble fibrils depending on the conditions. (Figure 1.12) (Fink, 2006; Uversky and Eliezer, 2009; Uversky et al., 2001a; Uversky et al., 2001c).

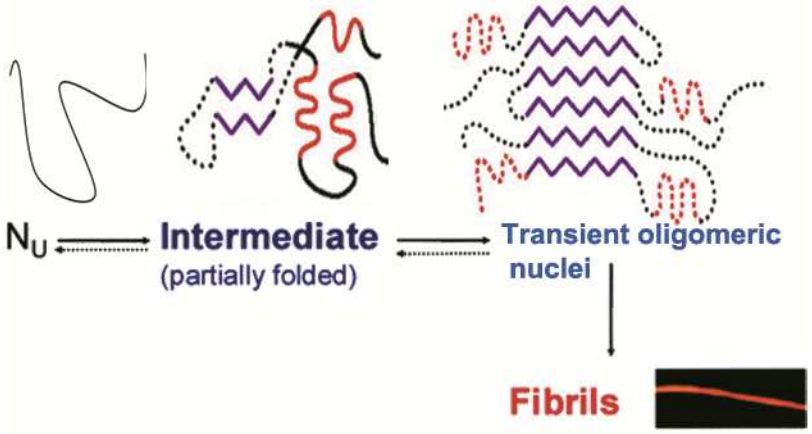

Figure 1.12 Schematic representation which shows the fibrillization process of natively unfolded monomers of AS (Nu). It shows misfolding of AS into partially folded intermediate and their assembly to form oligomers and fibrils. Reprinted and adopted with permission from (Fink, 2006). Copyright © 2006 American Chemical Society. All rights reserved.

The native AS monomer has predominantly a random coil conformation (Serpell et al., 2000; Uversky et al., 2001b; Weinreb et al., 1996; Zheng et al., 2013) but the partially folded intermediates usually contain α-helical or β-sheet conformations which can be detected by CD and FTIR spectroscopies. For example acidic pH causes a transition from natively unfolded AS to a partially folded intermediate with β-sheet structure (Uversky et al., 2001b) whereas it converts from random coil to an α-helical conformation upon binding to trifluoroethanol (TFE) and negatively charged phospholipids (Anderson et al., 2010; Davidson et al., 1998; Jo et al., 2000). The conformational change of AS at low pH is due to a reduction in intramolecular charge-charge repulsion that favours intramolecular hydrophobic interactions (Uversky, 2008). Binding of TFE with AS induces a helical partially folded intermediate which has been detected in the UV CD spectrum absorbance at 208 and 222 nm. Furthermore, the TFE-induced AS

aggregates have been characterized by atomic force microscopy (AFM) and the thioflavin-T assay (Anderson et al., 2010). The conformational changes induced by some factors such as small molecules cannot be differentiated from the natively unfolded monomers by CD spectroscopy because the induced partially folded intermediate contains predominantly random coil conformers. For example, the CD spectra of the mutants of AS (Li et al., 2001) and AS in the presence of dopamine (Cappai et al., 2005; Outeiro et al., 2009), chlorazole black E (Rao et al., 2008), a copper complex of phthalocyanine tetrasulfonate (PcTS-Cu^{2+}) (Rao et al., 2008), polycations (polylysine, polyarginine, and polyethyleneimine) (Goers et al., 2003), putrescine, spermine (Antony et al., 2003), congo red (Lendel et al., 2009; Rao et al., 2008), trehalose (Yu et al., 2012) and lacmoid (Lendel et al., 2009; Rao et al., 2008) were typical of a random coil conformation, demonstrating that mutation and complex formation with small molecules do not necessarily cause significant changes in the secondary structure of AS.

Understanding the initiation stage of AS aggregation, *i.e.* formation of partially folded intermediates, will help in the design of inhibitors as new therapeutics to prevent this pathogenic process (Trexler and Rhoades, 2010a). NMR spectroscopy (Lendel et al., 2009; Rao et al., 2008) and single molecule biophysics techniques have been used to characterize the partially folded intermediate or misfolded conformation of AS. Sandal *et al.* have used single molecule force spectroscopy (SMFS) to characterize the conformation of AS under three very different conditions known to accelerate aggregation of AS including Cu^{2+} (1μM), the A30P mutant and high ionic strength (500 mM Tris/HCl). The results showed an increase in β-like structure in the conformation of AS and demonstrated that the partially folded intermediate for AS aggregation under these conditions predominantly contains β-like conformers (Sandal et al., 2008). This single molecule technique also has been used to characterize the conformation of pathological AS mutants A30P, A53T, and E46K and have found that the mutants gain more compact conformations as compared with native wild type AS. It already has been reported that the aggregation rate of AS mutants is significantly higher than wild type AS under the same conditions (Li et al., 2001; Pandey et al., 2006). So these compact conformations with high amount of β-like structure contents demonstrating the partially folded intermediates of AS (Brucale et al., 2009). Furthermore Trexler *et al.* have used single molecule Forster resonance energy transfer (smFRET) to characterize the conformation of AS at low pH or after addition of spermine and heparin. The results demonstrated that low pH (=3) induces the folding of the AS

C-terminus. Binding of spermine and heparin also causes folding of AS (Trexler and Rhoades, 2010a). Another example of AS conformational characterization using smFRET is the effect of trimethylamine-N-oxide (TMAO), a protecting osmolyte, and urea, a denaturing osmolyte, on AS structure. This technique revealed that TMAO and urea change the average dimensions of the AS normal conformation into more compact and expanded conformations respectively (Ferreon et al., 2012). Folded intermediate conformations of AS induced by binding of congo red, PcTS-Cu^{2+}, chlorazole black E and lacmoid has been characterized using ^{1}H-^{15}N HSQC NMR (Lendel et al., 2009; Rao et al., 2008). The spectra of AS in the presence of these ligands showed a decrease in intensity of most peaks and the NMR resonances of AS residues involved in the interaction were severely broadened which is due to exchange on a slow to intermediate time scale (Lendel et al., 2009; Rao et al., 2008).

AS fibril formation is a nucleation-dependent polymerization. This process involves assembly of the partially folded intermediates to form a transient soluble oligomeric species which serves as a nucleus for further polymerization to form the fibrils. Monitoring of fibrillization kinetics using the thioflavin T assay is based on a fluorescence enhancement of the bound dye to the amyloid fibrils. A sigmoidal curve results which is characterized by three phases: an initial lag phase, a consequent exponential growth phase, and a final equilibrium phase (Figure 1.13). The lag phase involves the misfolding of AS monomers to form partially folded intermediates which are aggregation prone and assembly of these intermediates to form the soluble oligomeric nuclei. Further association of misfolded monomers to the oligomeric nuclei in the exponential growth phase leads to the formation of proto-filaments with a diameter of 3.8±0.5 nm and the assembly of the proto-filaments forms the proto-fibrils with a diameter of 6.5±0.6 nm. Association of proto-fibrils in the exponential phase causes the formation of the mature insoluble fibrils with a diameter of 9.8±1.1 nm which represents the saturated aggregation form of AS and leads to the equilibrium phase (Conway et al., 2000; Fink, 2006; Khurana et al., 2003; Uversky et al., 2001c).

In vitro fibrillization of AS depends on the concentration of AS, temperature and the duration and agitation of the sample. For example, agitation accelerates the fibrillization of 70μM AS from months to 3 days at 37°C (Fink, 2006; Uversky et al., 2001c). It has been shown that increasing the AS concentration causes the reduction of the lag time and an increase in the rate of fibrillization (Fink, 2006; Uversky et al., 2001c). Formation of transient soluble oligomeric

species has been characterized for A30P and A53T mutants of AS (Conway et al., 2000; Kaylor et al., 2005; Lashuel et al., 2002; Volles and Lansbury, 2002; Volles et al., 2001).

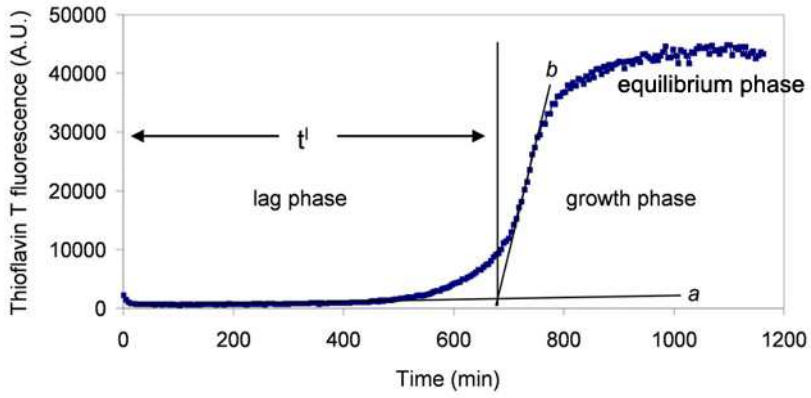

Figure 1.13 Monitoring of the aggregation process using the thioflavin T assay which shows the lag, growth and equilibrium phases. Reprinted and adopted with permission from (Brorsson et al., 2010). Copyright © 2010 Frontiers in Bioscience. All rights reserved.

It has been shown that fibrillization of AS wild type and the mutants under the same conditions occur with different lag times.The lag times for 200μM of A53T, A30P and wild type are 35–42 days, 45–49 days and 52–63 days, respectively. Addition of AS preformed fibrils to the incubation samples causes a significant reduction in the lag phase and accelerates fibril formation. Thus, formation of oligomeric nuclei in the lag phase is the rate-limiting step in the aggregation process and preformed fibrils serve as the nuclei which can induce significant fibrillization within 15–30 days. The fibrillization of the A53T mutant is faster than A30P and wild type (Conway et al., 2000). Furthermore, monitoring of AS aggregation by collecting CD spectra at several time points showed the transition from random coil conformation to the β-sheet structure for all AS types but the transition time for A53T was faster (Conway et al., 2000). The β-sheet structure of the transient soluble oligomeric species also has been characterized by Raman microscopy. The results showed the progressive increase in the Raman amide I band to 1667 cm^{-1} which represents an increase in β-sheet structure occurring with the formation of more ordered aggregates (Apetri et al., 2006). The transient soluble oligomeric species of AS have been isolated after sedimentation of fibrils from incubated samples. Then gel-filtration chromatography of supernatant was used to separate oligomers as ≥600 kDa species. AFM analysis of the concentrated eluate showed spherical species as the transient soluble oligomeric nuclei of the AS fibrillization process (Conway et al., 2000). Monitoring of the aggregation

process of AS WT and mutants using electron microscopy revealed pore-like oligomer species. It has been shown that A30P and WT form annular and pore-like oligomers and A53T forms annular and tubular oligomers (Lashuel et al., 2002). The annular oligomers, not the monomeric and the fibrillar forms, are able to permeabilize and destroy vesicles via a detergent-like mechanism (Lashuel et al., 2002; Volles and Lansbury, 2002; Volles et al., 2001). This ability of AS oligomers is associated with their cellular toxicity. It has been shown that AS oligomers are more toxic than the fibrils and formation of fibrils is a protective mechanism to reduce the cytotoxicity of oligomers and increase cell survival (Colla et al., 2012b; Wan and Chung, 2012; Winner et al., 2011). AS fibrillization is a sensitive process which depends on environmental factors. Fibrillization-promoting factors include agitation (Fink, 2006; Uversky et al., 2001c), low pH (Trexler and Rhoades, 2010a; Uversky et al., 2001b), metals (like copper, lead, iron, mercury, zinc, and aluminum) (Bisaglia et al., 2009; Uversky et al., 2001c), pesticides (Silva et al., 2013; Uversky et al., 2002; Uversky et al., 2001d) and temperatures above 40 °C (Uversky et al., 2001b). There are some chemicals which prevent the fibrillization of AS such as nicotine (Hong et al., 2009; Ono et al., 2007b), selegiline (Braga et al., 2011; Ono et al., 2007a), entacapone, tolcapone (Di Giovanni et al., 2010), dopamine and its analogs (Leong et al., 2009; Li et al., 2005).

1.4.1.4 Metals and drugs that influence alpha-synuclein misfolding and aggregation

1.4.1.4.1 Metals

Comparison of Parkinsonian and age-matched control brain tissue shows an elevation in total Fe (Dexter et al., 1989; Gorell et al., 1995; Griffiths et al., 1999; Mann et al., 1994; Minati et al., 2007; Riederer et al., 1989) and a reduction in the Cu (II) contents in the substantia nigra (SN) (Davies et al., 2014; Dexter et al., 1989; Riederer et al., 1989). The zinc content of PD brain didn’t show any change as compared with normal brain (Davies et al., 2014). It also has been shown that there was a 50% reduction of copper transporter 1 (Ctr1) in PD brains in comparison with controls. Moreover the level of superoxide dismutase 1 (SOD1) was increased in the SN of PD brains (Davies et al., 2014). Furthermore the copper concentrations in cerebral spinal fluid (CSF) samples of PD patients (18.8 ng/ml) are higher than in control samples (10.2 ng/ml) (Boll et al., 2008; Hozumi et al., 2011; Pall et al., 1987). Under normal conditions, the blood–CSF barrier (BCB) is responsible for homeostasis of copper in the CSF a process with is regulated by

ctr1 and a divalent metal transporter-1 (DMT1) (Skjørringe et al., 2012; Zheng et al., 2012). Leaking of copper from brain tissues into CSF is due to the impairment of copper transportation (Dexter et al., 1989; Loeffler et al., 1996; Skjørringe et al., 2012; Zheng et al., 2012) and also damage of brain tissues in PD pathology (Dexter et al., 1989; Loeffler et al., 1996; Zheng et al., 2012). It has been shown that there is an association between low concentrations of copper in PD tissues and impairment of copper binding proteins such as AS and copper- and zinc-containing superoxide dismutase (Cu/Zn-SOD). Cu/Zn-SOD protects cells against ROS by catalysing the conversion of superoxide to hydrogen peroxide using copper as a cofactor. So reduction of copper concentrations and elevation of SOD levels in SN of PD patients increases free radical production and cell death (Davies et al., 2014; Montes et al., 2014). It has been shown that chelation of copper in SH-SY5Y neuroblastoma cell cultures resulted in a decrease in SOD activity and also elevation of ROS (Lombardo et al., 2003). Another copper binding protein is AS which has ferrireductase activity. It binds to copper (II) and NADH in order to reduce Fe (III) to Fe (II) required for tyrosine hydroxylase function (Brown, 2013; Davies et al., 2011). Reduction of copper in PD reduces dopamine biosynthesis and might be involved in the pathology of PD (Montes et al., 2014).

In vitro studies showed that di- and trivalent metal ions such as Al(III), Cd(II), Cu(II), Fe(III), Co(III), and Mn(II) interact with AS and cause conformational changes and form partially folded intermediates which have a high tendency for aggregation (Bisaglia et al., 2009; Uversky et al., 2001c). Among the divalent metals which can induce conformational changes in AS structure, Cu(II) appears to have the highest affinity. AS has two binding sites with different affinities for Cu(II). The high affinity site (K_d~0.1) is located at ^{1}MDVFMKGLS^{9} and ^{48}VAHGV^{52}. The anchoring residue for the binding site at the N-terminal is His50 (Figure 1.14). NMR studies show that Cu(II) binds to His50 and N-terminal residues (1-9) and forms a loop. The complex of Cu(II) and AS serves as a nucleation point for β-strand formation (Binolfi et al., 2012; Rose et al., 2011). Cu (II) at micromolar range (<100μM) binds to this site. There is a common, low affinity (K_d~1mM) binding site at the C-terminal located at ^{119}DPDNEA^{124} for some divalent metals including: Zn(II), Fe(II), Mn(II), Co(II) and Ni(II) (Binolfi et al., 2012; Binolfi et al., 2006; Rasia et al., 2005) (Figure 1.14). These metals and also Cu (II) at high concentrations bind to this site (Binolfi et al., 2012; Davies et al., 2014; Rasia et al., 2005).

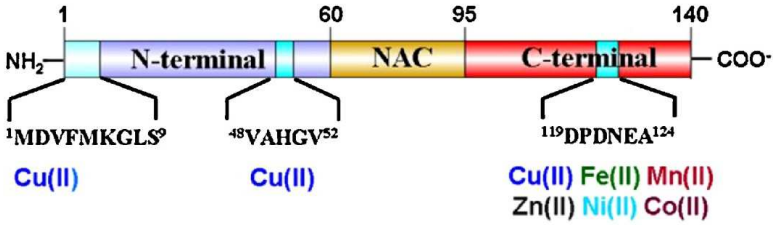

Figure 1.14 Schematic representation showing Cu(II) binding sites in the N-terminus and a general metal binding site at the C-terminus of AS. Reprinted with permission from (Binolfi et al., 2012). Copyright © 2012 Elsevier All rights reserved.

1.4.1.4.2 Methamphetamine

Methamphetamine has a chiral center, and two optical isomers: (+)-methamphetamine (d-methamphetamine) (Figure 1.15a) and (-)-methamphetamine (l-methamphetamine) (Figure 1.15b) (Anglin et al., 2000; Mendelson et al., 2006).

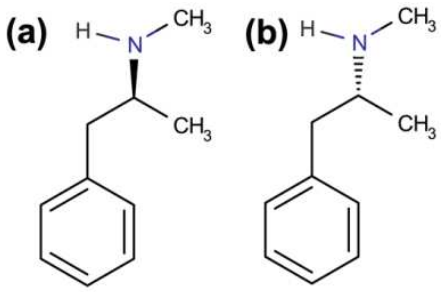

Figure 1.15 Structure of (+)-methamphetamine (d-methamphetamine) (a) and (-)-methamphetamine (l-methamphetamine) (b).

The drugs may be abused as single isomers or a mixture, depending on the drug product or source. The d-isomer is most of the "illicit methamphetamine" in the United States (Mendelson et al., 2006). The pharmacological properties of (+)-methamphetamine are known and it is revealed that this drug promotes release of dopamine from the nerve endings into the synapse and increases the extracellular levels of the monoamine neurotransmitters. It has been shown that the striatum of the brain is the target area of d-methamphetamine. At the molecular level d-methamphetamine stimulates the reverse transportation of dopamine from synaptic vesicles to the cytoplasm of nerve endings by the vesicular monoamine transporter 2 (VMAT2) and then release of dopamine into the synapse by dopamine transporters (Granado et al., 2013; Kish, 2008). The increase of synaptic levels of dopamine causes desired effects for abusers such as wellbeing, ecstasy, wakefulness, alertness, increased physical activity and energy. It also has

many adverse effects such as increased blood pressure and heart rate, damage of brain vessels, suppression of appetite and cerebrovascular accident (Granado et al., 2013; Kish, 2008; Mendelson et al., 2006).

The effects of racemic and l-methamphetamine in humans are relatively unknown. The l-isomer of methamphetamine is present in the Vicks Vapor Inhaler (containing 50 mg l-methamphetamine but called levmetamfetamine by the manufacturer). The dextrorotatory isomer of methamphetamine is marketed as Desoxyn for the treatment of attention deficit disorder and narcolepsy. In general, the d-isomer is more effective than the l-isomer in producing central nervous system (CNS) stimulation. Furthermore, human studies showed that d-methamphetamine produces more cardiovascular effects than equivalent doses of l-methamphetamine. L-methamphetamine intoxication is similar to that of the d-isomer at high doses, but the psychodynamic effects are shorter-lived and less desired by abusers (Mendelson et al., 2006).

As methamphetamine induces dopamine deficiency in animals, there was a concern that use of methamphetamine might damage dopamine neurons in humans and thereby increase the risk of developing PD (Callaghan et al., 2010; Granado et al., 2013). Positron emission tomography of d-methamphetamine abusers showed a significant loss of DA transporters in the striatum (Callaghan et al., 2010; Thrash et al., 2009; Volkow et al., 2001a; Volkow et al., 2001b). Drug abusers also have a low level of brain dopamine which might be due to brain damage (Granado et al., 2013; Kish, 2008). Recently it has been reported that methamphetamine addicts have a higher incidence of PD (Callaghan et al., 2010; Callaghan et al., 2012; Granado et al., 2013; Moszczynska et al., 2004). In this study competing risks analysis was used to determine whether the methamphetamine users group had elevated risk of developing PD in comparison to a matched population-proxy appendicitis group and a matched cocaine drug control group. The results demonstrated that the methamphetamine user group showed an increased risk of PD compared to the other groups (Callaghan et al., 2012). Further investigation showed the association between d-methamphetamine neurotoxicity and AS expression (Ajjimaporn et al., 2007; Chen et al., 2013; Fornai et al., 2005; Mauceli et al., 2006). Fornai *et al.* showed that treatment of mice at a dose of 5mg/kg×3 with 2 hours intervals results in a significant decrease in dopamine levels of the striatum. Furthermore immunostaining of AS in the substantia nigra showed the enhancement of AS immunofluorescence in the treated mice and also demonstrated

that AS was assembled in compact spots within dopaminergic neurons. These findings suggested that d-methamphetamine causes the overexpression of AS which finally accumulates and aggregates in the brain (Fornai et al., 2005). Overexpression of AS after treatment with d-methamphetamine has been demonstrated in human SK-N-SH neuroblastoma cells used as a model for dopaminergic cells. The results showed that treatment of cells with different concentrations of methamphetamine increased the AS levels up to about 50% in comparison with control cells and also reduces the cell viability (Ajjimaporn et al., 2007). Moreover it has been demonstrated that silencing of AS expression in methamphetamine treated SH-SY5Ycells, increases the viability of these cells (Chen et al., 2013). These results together showed the involvement of AS in methamphetamine induced pathology and suggested that the high incidence of PD pathology among methamphetamine abuser is due to the overexpression and aggregation of AS (Ajjimaporn et al., 2007; Chen et al., 2013; Fornai et al., 2005; Mauceli et al., 2006).

1.4.1.4.3 Nicotine

Epidemiological studies reveal that tobacco smoking significantly decreases the risk of PD (Checkoway et al., 2002; Hernán et al., 2002; Kessler and Diamond, 1971; Ono et al., 2007b; Quik, 2004; Ross and Petrovitch, 2001). More than a thousand compounds have been identified in cigarette smoke and some of them may have therapeutic effects which may provide protection. It has been shown that the nicotine of tobacco smoke has a neuroprotective effect against PD symptoms (Alves et al., 2004; Hernán et al., 2002; Hong et al., 2009; Quik, 2004). The nicotine brain concentration after consumption of one cigarette has been calculated to be 50 ng/ml (Rose et al., 1999) based on the reported nicotine blood concentrations in smokers (Benowitz et al., 1982; Brody et al., 2006; Gritz et al., 1981; Rose et al., 1999; Rose et al., 2010; Russell et al., 1980). The average number of cigarettes consumed by smokers in a day is 30 to 36 (Benowitz et al., 1982; Russell et al., 1980) which would result in a maximum concentration 1500 to 1800 ng/ml if the breakdown is slow.

Tobacco is prepared from a plant which belongs to the *Solanaceae* family. Examples of edible products derive from the *Solanaceae* family are peppers, tomatoes, potatoes, and eggplants. The results of a study on 490 idiopathic PD patients and 644 normal controls revealed that a diet including *Solanaceae* family products such as peppers, tomatoes, tomato juice, and potatoes (baked or mashed) reduced the risk of PD (Nielsen et al., 2013). Nicotine is an optically active

compound (Moore et al., 2003; Welter et al., 2005) and the naturally occurring form of nicotine is (-)-nicotine or l-nicotine (Figure 1.16a). The dextrorotatory form, (+)-nicotine or d-nicotine (Figure 1.16b) is physiologically less active than (-)-nicotine (Moore et al., 2003; Rapier et al., 1988) and (-)-nicotine is more toxic than (+)-nicotine (Moore et al., 2003).

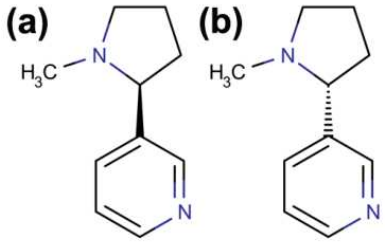

Figure 1.16 Structure of (-)-nicotine or l-nicotine (a) and (+)-nicotine or d-nicotine (b).

The neuroprotective effect of nicotine in PD is through stimulation of the nicotinic acetylcholine receptors (nAChRs). It has been shown that nicotine evoked the release of dopamine from striatal synaptosome in rats with an EC_{50} of 3.8 μM. This ability was stereospecific and it has been shown that the action of (-)-nicotine was 100 times stronger than (+)-nicotine (Fujita et al., 2006; Rapier et al., 1988). It also has been shown that chronic nicotine exposure changes the expression of genes in the substantia nigra pars compacta (SNc). In this study mice received 2 mg/kg/h (-)-nicotine for 14 days. Twenty dopaminergic neurons were isolated from mice brains and were subjected to single cell transcriptomics using Illumina Sequencing. The results revealed that the expression of 129 genes were changed after nicotine exposure (67 upregulated, 62 downregulated) including genes involve in the ubiquitin–proteasome pathway which has an important role in the pathogenicity of PD (Henley et al., 2013). *In vivo* studies in a monkey model of PD, caused by chronic exposure to MPTP, has demonstrated the synergistic effect of levodopa and SIB-l508Y, a nAChR agonist, in relieving motor symptoms (Schneider et al., 1998). In another study using the monkey model of PD, both levodopa and nicotine therapies were administrated simultaneously. These monkeys received 20 mg/kg daily doses of nicotine and levdopa for up to 6 months. The results showed a reduction in the levodopa-induced dyskinesias in animals treated with both nicotine and levodopa in comparison with those receiving just levodopa (Quik et al., 2013). Furthermore, (-)-nicotine administered orally by gum or transdermally by the patch has been shown to improve symptoms of PD (Hong et al., 2009; Quik, 2004; Quik et al., 2009). A clinical trial in six males suffering

from idiopathic PD received increasing doses of nicotine, 5–105 mg/day, within 14 weeks using nicotine patches. The results showed an improvement of motor symptoms in all subjects and also patients were less dependent on levodopa treatment (Villafane et al., 2007).

Another mechanism proposed for the neuroprotective effects of (-)-nicotine in PD is anti-fibrillogenic and fibril-destabilizing activity (Hong et al., 2009; Ono et al., 2007b). In one study the effect of (-)-nicotine and related compounds on AS fibrillization was investigated. Hydroquinone was used as a control in this study because it has a different structure from the other smoke compounds and also is a known inhibitor of AS fibrillization. Thioflavin T (ThT) assays, SDS-PAGE, Size-Exclusion HPLC (SEC-HPLC) and atomic force microscopy (AFM) were used to investigate the inhibitory effects. The results reveal that (-)-nicotine and hydroquinone inhibit AS fibril formation in a concentration-dependent manner. Hong *et al.* used the ThT fluorescence assay to study the inhibitory effect of different ratios of AS to (-)-nicotine ([1:1.5], [1:3] and [1:6]). They showed that as the (-)-nicotine concentration increases, the ThT fluorescence signal decreases, suggesting the effective inhibition of AS fibrillization. Furthermore, the AFM studies showed that at a ratio of AS to (-)-nicotine of 1:6, AS fibrillization is inhibited almost completely (Hong et al., 2009).

In another study a fragmentation approach was used to examine the effects of (-)-nicotine and two components of (-)-nicotine (pyridine and N-methylpyrrolidine) on the formation and destabilization of AS fibrils from wild-type AS and the A53T mutant. Fluorescence spectroscopy with thioflavin S (ThS), electron microscopy (EM) and atomic force microscopy (AFM) were the techniques used. The results show that (-)-nicotine inhibited the formation of AS fibrils and destabilized the fibrils from both wild-type AS and the A53T mutant. The inhibitory effect of (-)-nicotine was concentration-dependent. Furthermore, the N-methylpyrrolidine moiety of (-)-nicotine was identified as the functional fragment for the anti-fibrillogenic and fibril-destabilizing activity of (-)-nicotine (Ono et al., 2007b).

1.4.1.4.4 Dopamine

Dopamine is a member of the catecholamine family of compounds which acts as a neurotransmitter. Dopamine consists of an amine group (NH2) linked to a catechol structure (Figure 1.17). There are five known types of dopamine receptors; D1, D2, D3, D4, and D5 in the brain. Dopamine is produced in several areas of the brain, including the substantia nigra and the ventral tegmental area (Seth and Seth, 2009; Waller *et al.*, 2001). Anden *et al.* have reported that

the dopamine concentration within striatal nerve terminals is as high as 50 mM (Andén et al., 1966; Spencer et al., 1996). This concentration is an estimation of dopamine contents of the whole neuron and doesn't reflect the cytoplasmic concentration of dopamine. The cytoplasmic dopamine which has been synthesized from L-DOPA or transported into the cell is isolated into monoaminergic vesicles to protect them from auto-oxidation processes promoted by the cytoplasmic high pH environment (Lotharius and Brundin, 2002a). The cytoplasmic concentration of dopamine has been measured in the μM range (0.5-2.2) in pheochromocytoma cells and a single neuron of the pond snail (Olefirowicz and Ewing, 1990; Perlman and Sheard, 1982). This reveals the importance of efficient dopamine sequestration into monoaminergic vesicles (Lotharius and Brundin, 2002a, b). AS has an important role in the formation of synaptic vesicles and dopamine storage as a protection against cytosolic oxidation of dopamine (Lotharius and Brundin, 2002a; Sudhof, 2013).

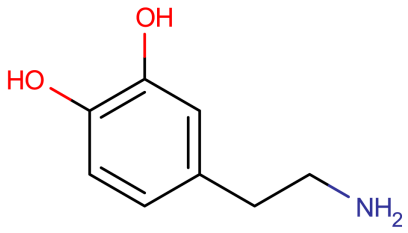

Figure 1.17 Structure of dopamine.

Degeneration of the basal ganglia in the brains of PD patients primarily affects dopaminergic neurons in the substantia nigra which results in dopamine deficiency. Exogenous L-dopa can replace the endogenous deficient neurotransmitter. L-DOPA is taken up by the remaining dopaminergic neurons where it undergoes decarboxylation in the presynaptic terminal to form dopamine (Grosset *et al.*, 2009; Pahwa and Lyons, 2007).

There have been conflicting reports concerning the effect of dopamine on the aggregation/fibrillization of AS (Cappai et al., 2005; Conway et al., 2001; Follmer et al., 2006; Jethva et al., 2011; Lee et al., 2011; Leong et al., 2009; Li et al., 2005; Li et al., 2004; Norris et al., 2005; Ono et al., 2007a). It would appear that dopamine stabilizes the formation of oligomeric AS by inducing AS monomer oligomerization or destabilization of preformed AS fibrils. Figure 1.18 demonstrated the multiple effects of dopamine in the AS fibrillization process. Route 1 shows the AS fibril formation from AS monomers. In this process monomers are aggregated to form transient oligomers and assembly of these oligomers leads to the

formation of fibrils (Figure 1.18). It has been reported that dopamine destabilized preformed AS fibrils and dissolved them into soluble oligomers (Route 2) (Leong et al., 2009; Li et al., 2004; Ono et al., 2007a). It has been demonstrated that incubation of dopamine with monomeric AS causes the formation of stabilized oligomers which are SDS resistant and no significant fibrillization occurs from assembly of these oligomers (Route 3a) (Figure 1.18) (Cappai et al., 2005; Fink, 2006; Lee et al., 2011; Leong et al., 2009; Norris et al., 2005). Further investigations revealed that these stabilized oligomers resulted from adduct formation between oxidized dopamine and AS monomers (Conway et al., 2001; Li et al., 2005; Li et al., 2004). Dopamine and AS were incubated with or without shaking at 37°C for a long time (1-30 days) (Cappai et al., 2005; Conway et al., 2001; Norris et al., 2005). This condition promoted the oxidative ligation of dopamine to AS, since addition of antioxidants eliminated adduct formation (Conway et al., 2001). The stabilized oligomers can be converted to fibrils slowly after prolonged incubation and with a very low rate (Route 3b) (Figure 1.18) (Follmer et al., 2006; Leong et al., 2009).

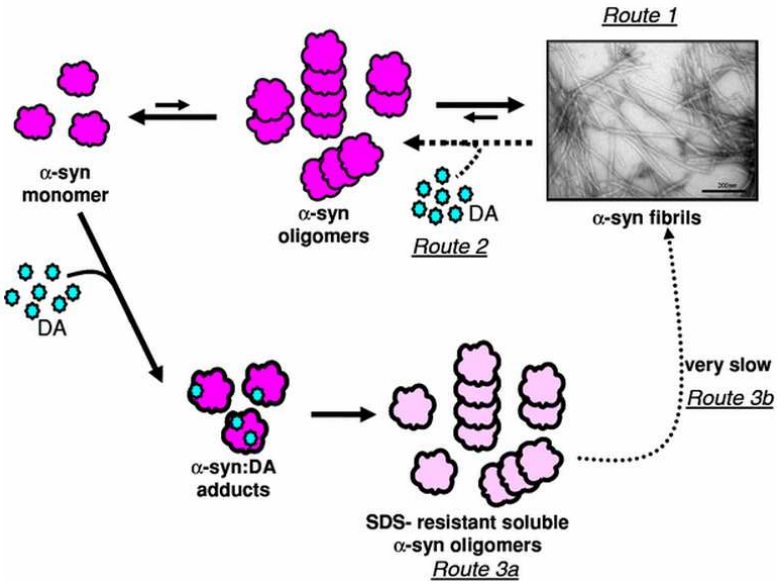

Figure 1.18 Schematic representation of the effect of dopamine in AS misfolding and aggregation. (Route 1) fibrillization of AS from monomers (Route 2) destabilization of AS fibrils by dopamine (Route 3a) Formation of stabilized oligomers of AS due to adduct formation between oxidized dopamine and AS monomers (Route 3b) conversion of stabilized oligomers to fibrils is a very slow process. Reprinted with permission from (Leong et al., 2009). Copyright © 2009 Springer. All rights reserved.

1.4.1.4.5 Other small molecules

Epidemiologic studies demonstrated an inverse association between caffeine use and PD (Altman et al., 2011; Ascherio and Chen, 2003; Postuma et al., 2012; Rivera-Oliver and Díaz-Ríos, 2014; Ross et al., 2000; Schapira et al., 2006). Caffeine (Figure 1.19a) is a nonselective adenosine antagonist which possesses neuroprotective properties (Chen et al., 2001; Schapira et al., 2006). *In vivo* studies using rat models of PD have demonstrated the neuro-protective effects of caffeine to prevent the degeneration of dopaminergic neurons (Chen et al., 2001; Machado-Filho et al., 2014; Mpofana et al., 2014; Schwarzschild et al., 2003). Chen *et al.* have shown that treatment of the MPTP rat model of PD with caffeine (10 mg/kg) before intraperitoneal injections of MPTP (20 mg/kg ×4) reduced the MPTP induced biochemical lesions of the dopaminergic nigrostriatal system including recovery of dopamine depletion and a significant increase in brain levels of the dopamine transporter, dopamine and its metabolite dihydroxyphenylacetic acid (DOPAC) (Chen et al., 2001). The neuro-protective effect of caffeine also has been demonstrated in a 6-hydroxydopamine (6-OHDA) rat model of PD. It has been shown that treatment of rats with 20 mg/kg caffeine results in improvement of locomotor activity, increased dopamine and tyrosine hydroxylase activity in the striatum and the attenuation of the 6-OHDA induced brain lesions (Machado-Filho et al., 2014; Mpofana et al., 2014).

Curcumin (Figure 1.19b) is another natural compound with neuroprotective properties for PD (Ahmad and Lapidus, 2012; Darvesh et al., 2012; Jiang et al., 2013; Liu et al., 2011; Mythri and Bharath, 2012; Pandey et al., 2008; Qualls et al., 2014; Siddique et al., 2014; Singh et al., 2012; Wang et al., 2010b; Yang et al., 2014). Curcumin (diferuloylmethane) is a polyphenolic compound found in turmeric which has blood brain barrier crossing ability. This natural compound has a potential therapeutic role in neurological disorders including Alzheimer's, Parkinson's, and Huntington's disease (Mythri and Bharath, 2012; Singh et al., 2012). *In vivo* and *in vitro* studies have shown the neuroprotective effects of curcumin against PD pathogenicity (Qualls et al., 2014; Siddique et al., 2014; Yang et al., 2014). Yang *et al.* have shown that curcumin improved the behavioral and pathological symptoms in a 6-OHDA-induced PD rat in a concentration dependent manner. Treatment of rat models of PD with 5-20 mg/kg/day of curcumin resulted in significant elevation in body weight and improvement in neurobehavior. Furthermore curcumin increased the level of monoamine neurotransmitters in hippocampus and

also prevented 6-OHDA-induced cell lesions and stimulated regeneration of neurons in the hippocampus (Yang et al., 2014). In another study it was demonstrated that pre-treatment of SH-SY5Y cells with curcumin protects them against the neurotoxicity effect of rotenone and also increased the cell viability (Qualls et al., 2014). Curcumin also attenuated PD symptoms in a fly model of PD in a dose dependent manner. Treatment of transgenic *Drosophila* expressing human AS with 25-100 μM curcumin resulted in postponed loss of activity patterns, reduction in the oxidative stress and apoptosis, and an increase in the survival rate (Siddique et al., 2014). Other studies revealed a link between the neuroprotective effect of cucumin and AS pathogenicity in PD (Ahmad and Lapidus, 2012; Jiang et al., 2013; Liu et al., 2011; Pandey et al., 2008; Wang et al., 2010b). It has been shown that curcumin attenuates the cytotoxicity induced by overexpression of wild type and A53T mutant of AS by reducing apoptosis and ROS production in SH-SY5Y and PC12 cells (Jiang et al., 2013; Liu et al., 2011; Wang et al., 2010b). Curcumin also interacts with AS directly and inhibits its aggregation *in vitro* (Ahmad and Lapidus, 2012; Pandey et al., 2008). Pandey *et al.* showed that that curcumin (0.01-100 μM) modulated the fibrillization of 5μM AS in the presence of 1mM $FeCl_3$, as an aggregation promoting agent, and increased the SDS-soluble AS monomers (14 kDa) in a dose-dependent manner. The fibril destabilizing effect of curcumin against AS aggregates also has been demonstrated in SH-SY5Y and dopaminergic MN9D cells transfected with the A53T mutant AS (Pandey et al., 2008). Ahmad *et al.* have shown that curcumin binds to the monomers of AS and the dissociation constant for this interaction has been measured as 10^{-5} M. Mutants of AS, Y39W/A69C and A69C/F94W, have been used to study the binding of curcumin by measuring Trp fluorescence. Furthermore monitoring fibrillization and oligomerization of AS in the presence of curcumine by ThT fluorescence and far-UV CD at 217 nm revealed the inhibitory effect of curcumin against AS fibril and oligomer formation. The results showed no increase in ThT fluorescence and β-sheet structured (Ahmad and Lapidus, 2012).

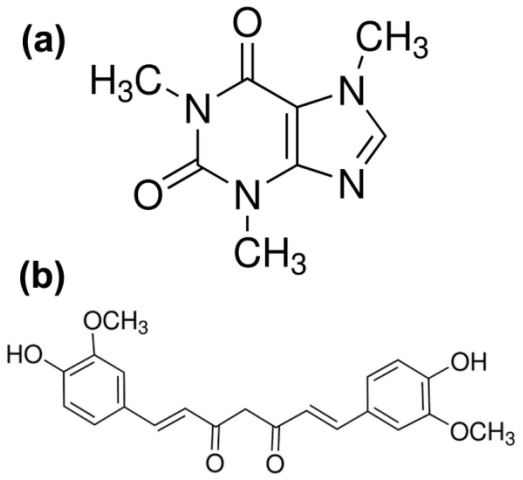

Figure 1.19 Structure of caffeine (a) and curcumin (b).

1.5 HSQC-NMR

1.5.1 Principles

Many serious human diseases have been linked to protein misfolding and aggregation. NMR has appeared as an important tool for studying the protein folding and misfolding process because of the unique structural insights it can provide into the events of the protein folding process (Dyson and Wright, 2004). The major aim of many studies on protein interactions with large or small molecules is delineation of the site of binding. The most frequently used NMR method for studying protein-ligand interactions is Heteronuclear Single Quantum Correlation (HSQC) spectroscopy which is based on chemical shift changes resulting from complex formation. HSQC-based experiments allow the detection of ligand interaction over a wide range of dissociation constant values. Binding is detected by comparing 2D ^{1}H-^{15}N HSQC spectra of ^{15}N-labeled protein in the absence and presence of ligand to reveal ligand-induced changes in chemical shift and peak intensity. Each residue of the protein (except proline) has an amide proton attached to nitrogen in the peptide bond. The HSQC provides the correlation between the nitrogen and amide proton and each amide yields a peak in the HSQC spectra. The spectrum provides an excellent high-resolution fingerprint of a protein as there is a signal for each covalently bonded ^{1}H-^{15}N group of each peptide bond in HSQC-NMR. In general, each residue should produce an observable peak in the spectrum (Barbar, 1999; Chatterjee et al., 2005; Dyson and Wright, 2004; Hartmann et al., 2008; Konrat, 2014; Kosol et al., 2013; Kwan et al., 2011). Some of the residual side chains also have a proton attached to nitrogen such as tryptophan and

asparagine. These ^{1}H-^{15}N groups also appear in the HSQC-NMR spectrum (Hartmann et al., 2008; Kwan et al., 2011). The nuclei of ^{1}H and ^{15}N possess nuclear spin which generates a magnetic dipole. The NMR spectrometer applies a magnetic field to the solution containing protein samples labeled with ^{15}N. This magnetic field forces the magnetic dipoles to be aligned with the applied field in two different ways; the same orientation (parallel) or the opposite orientation (antiparallel). The energy of antiparallel orientation is higher than the parallel orientation. By applying pulses of electromagnetic energy at the resonance frequencies, some energy is absorbed and permits the nuclei to switch into the high-energy state. The frequency of the absorbed energy depends on the nuclei and chemical environment and nuclei in different environments or different positions of a specific protein resonate at different frequencies. HSQC-NMR is a 2D plot of ^{15}N resonance frequency against ^{1}H resonance frequency and the width of each signal represents the intensity of the absorbed electromagnetic energy. The resonance frequencies are described as chemical shifts in units of p.p.m. (Dyson and Wright, 2004; Hartmann et al., 2008; Kosol et al., 2013; Kwan et al., 2011). ^{15}N labeled samples are recombinant proteins which are produced in bacteria with a medium containing nutrients with ^{15}N labeled isotope such as $^{15}NH_4Cl$ (Kwan et al., 2011).

HSQC-NMR gives information about the structure and dynamics of proteins (Barbar, 1999; Chatterjee et al., 2005; Dyson and Wright, 2004; Hartmann et al., 2008; Konrat, 2014; Kosol et al., 2013; Kwan et al., 2011). The HSQC spectra for random coil and α-helix-rich proteins are less well dispersed than proteins with high β-sheet contents. The spectra for unfolded proteins show that all amide protons are exposed to solvent and exist in the same chemical environment. Structured proteins and natively unfolded ones have high quality spectra with sharp lines but the spectra for partially folded intermediates have a poorer quality with broader lines. This line broadening is a result of structural flexibility of molten globule intermediates which allows them to shift between different possible ensembles on the μs-ms timescale. Thus there is signal decay for nuclei of partially folded intermediates which results in line broadening (Chatterjee et al., 2005; Dyson and Wright, 2004; Hartmann et al., 2008; Kosol et al., 2013; Kwan et al., 2011). This technique also can be used to characterize the stability of a protein over time if the sample undergoes aggregation or dimerization (Barbar, 1999; Dyson and Wright, 2004; Hartmann et al., 2008; Kosol et al., 2013; Kwan et al., 2011).

1.5.2 Application in alpha-synuclein structure and function determination

The natively unfolded structure of AS has been characterized by ^{1}H-^{15}N-HSQC NMR (Chandra et al., 2003; Sung and Eliezer, 2007; Wu et al., 2008). NMR spectroscopy has been used to characterize the partially folded intermediate or misfolded conformation of AS resulting from its interaction with small molecules and lipids (Lendel et al., 2009; Rao et al., 2008). The folded intermediate conformations of AS induced by binding of vitamin K (da Silva et al., 2013), congo red (Lendel et al., 2009; Maltsev et al., 2011; Rao et al., 2008), PcTS-Cu^{2+} (Rao et al., 2008), exifone (Yamaguchi et al., 2010), chlorazole black E (Rao et al., 2008) and lacmoid (Lendel et al., 2009; Rao et al., 2008) have been characterized using ^{1}H-^{15}N HSQC NMR (FM19,20,NMR8). The spectra of AS in the presence of these ligands showed a decrease in intensity of most peaks and NMR resonances of AS residues involved in the interaction were severely broadened which is due to a slow to intermediate time scale as the main reason for the reduced residual peak intensity. In some cases a few peaks also shifted (Lendel et al., 2009; Maltsev et al., 2011; Rao et al., 2008).

The conformational change of AS in the presence of phosphatidylserine-small unilamellar vesicles (PS-SUVs) and SDS was further investigated by NMR spectroscopy. The ^{1}H-^{15}N HSQC spectrum of AS (0.1 mM) was typical of an unfolded protein with a dense cluster of cross-peaks over a narrow range but in the presence of saturating concentrations of PS-SUVs and SDS most of the cross-peaks disappeared and their intensity reduced significantly. The disappeared residues are involved in the folding of AS due to binding with large size SUVs which leads to broadening of the resonances of the corresponding amide groups of AS and are consistent with the formation of α-helical structure upon micelle binding revealed by CD spectroscopy. The position and intensity of some other cross-peaks remained unchanged and demonstrated that these residues do not bind to lipid and stay unfolded even in the presence of SUVs (Chandra et al., 2003). Furthermore it has been demonstrated that in the presence of negatively charged lipids the first 100 residues of AS interact with the surface of SUVs or detergents and adopt α-helical conformation. This conformational change causes them to broaden and therefore they did not show up in the HSQC spectra (Chandra et al., 2003; Davidson et al., 1998; Georgieva et al., 2008; Jao et al., 2008; Ulmer et al., 2005a).

1.6 Objectives

The purpose of this thesis is to characterize the conformational changes of AS in the presence of Cu(II) as a fibrillization agent, caffeine as an anti-parkinsonian small molecule, methamphetamine as a Parkinson's developing toxin and anti-fibrillization agents such as dopamine, nicotine and curcumin. Nanopore analysis will be used as the main technique for studying conformational changes induced by the binding of copper and small molecules to AS. Further details of the interaction have been elucidated by CD spectroscopy, ITC and NMR spectroscopy.

The Objectives of the project are as follow:

1- Characterize the conformational changes of AS peptides in the presence of ligands using nanopore analysis, CD spectroscopy and NMR spectroscopy.

2- Characterize the binding site(s) of the ligands by NMR spectroscopy and mapping of the binding site(s) using nanopore analysis of AS peptide fragments.

3- Measure the dissociation constants of interactions using isothermal titration calorimetry.

1.7 Hypothesis

The central hypothesis of this thesis is that nanopore analysis is a useful technique to detect and differentiate conformational changes of AS in the presence of different ligands.

2 MATERIALS AND METHODS

2.1 Reagents, supplies, and equipment

The reagents, supplies, and equipment used in this thesis are listed in Table 2.1. Table 2.2 lists the names and addresses of supplier companies.

Table 2.1 List of chemical reagents and equipments with their suppliers.

Item	Supplier
Chemical and biological reagents	
1,2-diphytanoyl-*sn*-glycero-3-phosphocholine in chloroform	Avanti Polar Lipids
^{15}N-Alpha-Synuclein (Uniform Label)	rPeptide
2,2-dimethyl-2-silapentane-5-sulfonic acid	Sigma-Aldrich
4-(2-Hydroxyethyl)piperazine-1-ethanesulfonic acid (HEPES)	BDH
Acetic acid, glacial ($C_2H_4O_2$)	BDH
Alpha-hemolysin	Sigma-Aldrich
Alpha-Synuclein	rPeptide
Alpha-Synuclein, 1-60	rPeptide
Alpha-Synuclein, 61-140	rPeptide
Alpha-Synuclein, 96-140	rPeptide
Alpha-Synuclein, A30P mutant	rPeptide
Alpha-Synuclein, A53T mutant	rPeptide
Alpha-Synuclein, E46K mutant	rPeptide
Alpha-Synuclein, Delta NAC	rPeptide
Anabasine	Sigma-Aldrich
Caffeine solution (analytical standard)	Sigma-Aldrich
Copper sulfate ($Cu_2SO_4 \cdot 5H_2O$)	Sigma-Aldrich
Curcumin	Sigma-Aldrich
Decane (anhydrous)	Sigma-Aldrich
Deuterium oxide (D_2O)	Sigma-Aldrich
Disodium ethylenediaminetetraacetate dehydrate (EDTA-Na_2)	Sigma-Aldrich
Dopamine hydrochloride	Sigma-Aldrich
Ethanol	EMD
Glycerol	Thermo Fisher Scientific
Hydrochloric acid (HCl)	BDH
Magnesium chloride ($MgCl_2$)	BDH
(-)-Methamphetamine	TRC
(+)-Methamphetamine hydrochloride solution	Sigma-Aldrich
(+)-Nicotine	TRC
(-)-Nicotine solution (analytical standard)	Sigma-Aldrich
Nitrogen (gaseous)	Praxair
Nuclease-free Water	Life Technologies

Octyl β-D-glucopyranoside	Sigma-Aldrich
palmitoyl-2-hydroxy-sn-glycero-3-[phospho-rac-(1-glycerol)]	Avanti Polar Lipids
Phosphate buffered saline	Sigma-Aldrich
Potassium chloride (KCl)	EMD
Pur-A-Lyzer™ Mini Dialysis Kit	Sigma-Aldrich
Sodium Acetate (CH_3COONa)	Sigma-Aldrich
Sodium bicarbonate ($NaHCO_3$)	Sigma-Aldrich
Sodium carbonate, Na_2CO_3	Sigma-Aldrich
Sodium hydroxide (NaOH), pellets	EMD
Sodium phosphate dibasic (Na_2HPO_4)	Thermo Fisher Scientific
Sodium phosphate monobasic (NaH_2PO_4)	Thermo Fisher Scientific
Sulfuric acid (H_2SO_4)	EMD

Equipment and supplies

Amplifier, Axopatch 200B	Axon Instruments
Bruker Avance NMR spectrometer (600 MHz)	Bruker
CHIRASCAN PLUS CD spectrophotometer	AppliedPhotophysics
Digitzer, DigiData 1440A	Axon Instruments
Faraday cage	Warner Instruments
Glass vials with caps	Kimble Chase & VWR
Headstage, CV203BU	Axon Instruments
Microcentrifuge, Hettich Mikro 20	Hettich Zentrifugen
Microcentrifuge tubes, non-stick	Life Technologies
Molecular Operating Environment (MOE) software package	Chemical Computing Group
NanoAnalyze software	TA Instruments
Nano-ITC	TA Instruments
Nano ITC Run Software	TA Instruments
NMRPipe	Dr. Bax Group, NIH
NMRViewJ	One Moon Scientific
Origin 7 graphing software	OriginLab
Paintbrushes, size 000	Island Blue
Parafilm	VWR
Pasteur pipettes	VWR
pClamp 9.0 and 10.1 software suite	Axon Instruments
PCR microcetrifuge tubes	VWR
Perfusion bilayer chamber and cup	Warner Instruments
pH meter	Thermo Fisher Scientific
Pipettes	Eppendorf
Power supply, ONEAC PC750A	Oneac
Pro-Data™ Software Suite	AppliedPhotophysics
Silver wire	Alfa Aesar
Syringe filters, 0.2 μm	Thermo Fisher Scientific
Syringe needles	Becton Dickinson
Syringes, microliter	Hamilton

Syringes, milliliter	Becton Dickinson

Table 2.2 List of companies with addresses.

Company	Address
Alfa Aesar	Alfa Aesar, Ward Hill, MA, USA
AppliedPhotophysics	Surrey, United Kingdom
Avanti Polar Lipids	Avanti Polar Lipids, Alabaster, AL, USA
Axon Instruments	Molecular Devices,Sunnyvale, CA, USA
BDH	VWR International, Edmonton, AB, Canada
Becton Dickinson	Becton Dickinson Canada, Mississauga, ON, Canada
Bruker	Milton, Ontario, Canada
Chemical Computing Group	Montreal, Quebec, Canada
EMD	EMD Millipore, Gibbstown, NJ, USA
Eppendorf	Eppendorf Canada, Mississauga, Ontario, Canada
Hamilton	Hamilton Company, Reno, NV, USA
Island Blue	Island Blue Print, Victoria, BC, Canada
Life Technologies	Life Technologies, Burlington, ON, Canada
OriginLab	OriginLab, Northampton, MA, USA
Praxair	Praxair, Saskatoon, SK, Canada
rPeptide	Bogart, GA, USA
Sigma-Aldrich	Sigma-Aldrich Canada, Oakville, ON, Canada
TA Instruments	New Castle, PA, USA
Thermo Fisher Scientific	Fisher Scientific Company, Ottawa, ON, Canada
TRC	Toronto Research Chemicals, Toronto, Ontario, Canada
VWR	VWR International, Edmonton, AB, Canada
Warner Instruments	Warner Instruments, Hamden, CT, USA

2.2 Nanopore sensing and patch-clamp experimental setup

The nanopore experiments with 0.35 mg of 1,2-diphytanoyl-sn-glycero-3-phosphocholine (DPhPC) micelles and wild type AS were performed by David Boyle. The nanopore experiments with caffeine and curcumin were performed by Joe Kakish.

In general the nanopore analysis was performed in a buffer containing 1 M KCl, 10 mM HEPES-KOH, pH 7.8 and EDTA was added to the *cis* chamber to a final concentration of 1 mM. Figure 2.1 shows a schematic representation of the nanopore experimental set up using the αHL pore. With a small brush a lipid bilayer of 1,2-diphytanoyl-sn-glycero-3-phosphocholine (DPhPC), was painted onto a 150 μm opening in a Teflon ® perfusion cup (Figure 2.2b,c) which separated two buffer compartments, the *cis* and *trans* chambers, of 1.5 mL volume each.

Experiments were set up in a Faraday cage. Chambers were filled with the buffer and Ag/AgCl electrodes were placed into each chamber. The cathode was put into the *cis* chamber to allow the negatively charged AS proteins and peptides to move towards the *trans* chamber. Electrodes were connected to a current amplifier and a digitizer (Figure 2.1, Figure 2.2a). The experiments were carried out at 22 ± 1°C with an applied potential of -100 mV at a band width of 10 KHz using an Axopatch 200B amplifier (Axon Instruments) under voltage clamp conditions. To study the effect of voltage in the event time, a series of experiments were performed at three voltages usually -75 mV, -100 mV and -125 mV.

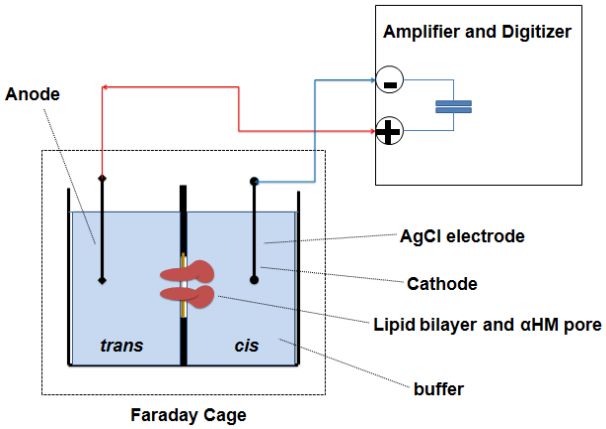

Figure 2.1 Schematic representation of a nanopore experiment showing the αHL inserted in a lipid bilayer, chambers with AgCl electrodes and their connection with amplifier and digitizer. Idea adapted from (Merstorf *et al.*, 2012). Copyright © 2012 Springer. All rights reserved.

2.2.1 The patch-clamp hardware

Nanopore experiments were performed using patch-clamp hardware which consists of three major components including the Faraday cage, patch clamp amplifier (Axopatch 200B, Molecular Devices) and digitizer (Digidata 1332A) (Figure 2.2a). Experiments were set up in the Faraday cage as shown in Figure 2.2b. All nanopore experiments were carried out in the perfusion unit (Figure 2.2b,c) consisting of two pieces; the black part which is the holder of the white part or cup (Figure 2.2c). The cup has a 150 µM aperture which is the place of lipid bilayer formation (Figure 2.2c). After painting the lipid bilayer onto the opening of the cup, it was installed into the holder to form *cis* and *trans* chambers (Figure 2.2b). Then the chambers were filled with buffer and the anode and cathode electrodes were placed into the *trans* and *cis* chambers (Figure 2.2b). To control the thickness of the membrane a syringe was connected to

the *cis* chamber through a hole on the holder. The thickness of the membrane was reduced using a painting brush.

In some cases after formation of the lipid bilayer the capacitive spike disappeared which is due to the temporary removal of the painted lipid from the aperture. In this case pulling and pushing of some buffer from the *cis* side using the connected syringe mediate the reforming of the lipid bilayer on the aperture and a capacitive spike reappeared on the system.

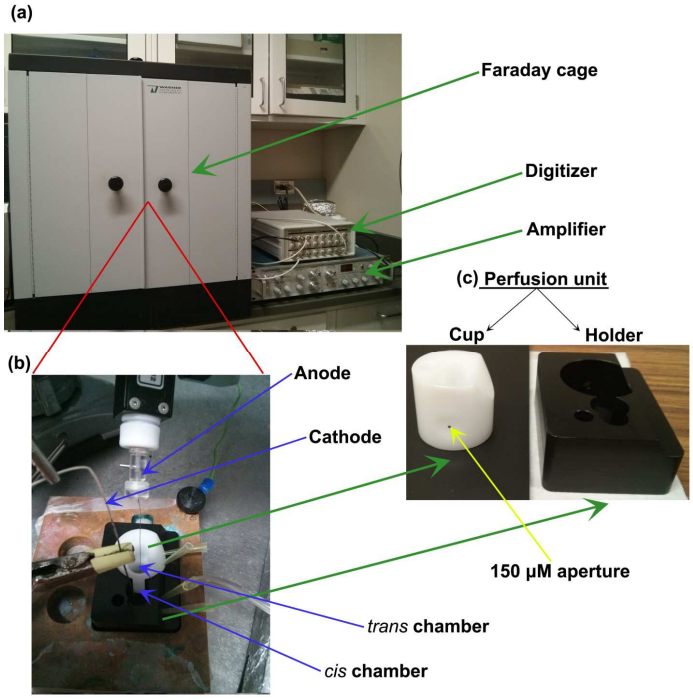

Figure 2.2 The patch-clamp hardware and a typical experimental setup. (a) The patch-clamp hardware compartments including Faraday cage, amplifier and digitizer. (b) The experimental setup inside the Faraday cage using the perfusion unit and the electrodes in the *cis* and *trans* chambers (c) The compartments of the perfusion unit including the cup and holder.

2.2.2 Lipid bilayer formation and pore insertion

After the set up of the experiment, a voltage of -100 mV was applied. Formation of the lipid bilayer is detected as a membrane resistance (Figure 2.3a). The membrane thickness was measured by the patch-clamp hardware Clampex software as the capacitance of the formed membrane. The thickness was monitored until it reached about 10 pF. The α-HL solution was made by diluting stock solution (1 mg/ml) in a buffer to a final concentration of 1 µg/mL. Then 5 µL of this solution was added to one side of the membrane and the current was monitored until stable pore insertion was achieved. A successful pore insertion is determined by the sudden

appearance of a current (Figure 2.3b). For example in an experiment with 1 M KCl and an applied potential of -100 mV, formation of a single pore causes a current of 100±5 pA. Insertion of α-hemolysin into the membrane to make a pore is a spontaneous event and can take anything from a few seconds to several minutes to occur. A pore produces a current in the pA range due to ionic conductance (Figure 2.3b). Then an aliquot of the peptide to be studied was added to the chamber. The final concentration of protein on the *cis*-side was 1 μM.

2.2.3 Data recording and processing

Interaction of a molecule with the pore blocks the ionic flow and causes a blockade current, I, for a blockade time, T. Values of I and T depend on the biophysical properties of molecules such as net charge, molecular weight, charge distribution and structure. As shown in Figure 2.3c negatively charged unfolded peptides are able to translocate through the pore and cause a large drop in current. Peptides with compact conformation interact with the outside of the pore and block the ionic flow for a short time. This results in a smaller drop in the current as compared with the translocation events (Figure 2.3d). In some cases intercalation events can be recorded. An intercalation event occurs when a part of a peptide, for example a loop or a domain, enters the vestibule of the pore but the whole molecule cannot pass through the pore and is stuck there before diffusing away. Intercalation and translocation events can be distinguished by doing a voltage study experiment and monitoring the event time by increasing the applied voltage. For translocation events, the blockade time decreases with increasing applied voltage. The events were monitored real-time and captured on a PC connected to the patch-clamp hardware (Figure 2.3e) using the "fixed-length events" mode of Clampex 9 software. Figure 2.3e shows an example of the snapshot of the events profile. The blockade current events were characterized and analyzed using Clampfit software to remove noise and then the blockade current populations were obtained by fitting the blockade current distribution with the Gaussian function using Origin software (Figure 2.3f).

The recorded raw data were imported to Clampfit software for choosing well-defined events and removing the multiple or overranging events. At first the data was converted to concatenated traces, then a single-channel search was applied to detect and characterize the events. This involved specifying a region of data using cursors and then adjusting the thresholds to be screened by the software for detected events. Then the detected events on the event viewer were corrected by rejecting the events which were mostly out of the range of applied voltage or have

very small current values. The properties of the selected events including blockade time and current have been were output as an ".rlt" file and were imported to Origin7 for further processing and fitting. The detected events underwent further screening based on the blockade time and current. Blockade current correction involved removal of events with blockade current less than 10 pA and more than 100 pA. Blockade time correction involved removal of events with blockade times less than 0.05 ms and more than 50 ms. The blockade current profile was plotted versus the number of events and the peaks were fitted with the Gaussian function. The corresponding time values for each peak were extracted from the data and the blockade time profile was plotted versus the number of events. The blockade time distribution was fitted using an exponential (ExpDecay1) function.

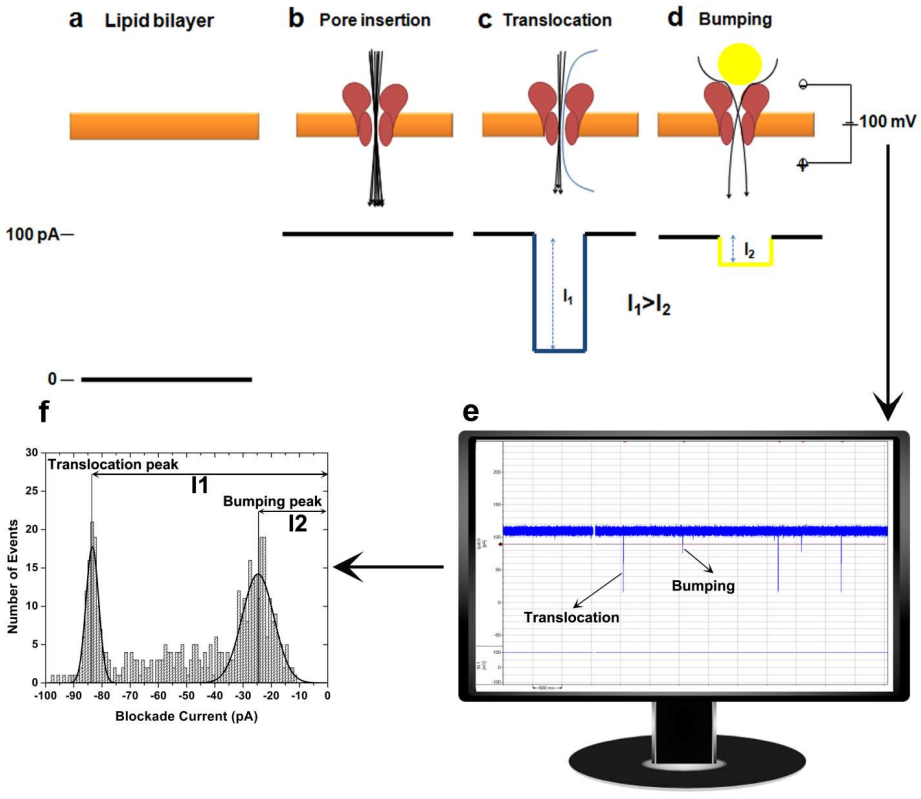

Figure 2.3 Schematic of data recording and processing in nanopore experiment. (a,b,c,d) The schematic representation of lipid bilayer formation, pore insertion, translocation and bumping events when a voltage of -100mV was applied. The drop in current for translocation and bumping events is also shown as I1 and I2 (e) A snapshot of the events profile (f) The blockade current histogram with bumping and translocation peaks. The idea behind the design of parts "a","b","c" and "d" were adopted from Oxford Nanopore Technologies Ltd. webpage. Image URL:https://www.nanoporetech.com/uploads/Technology_New/Nanopore_Sensing/filemanager-1.jpg?mw=720.

2.3 HSQC-NMR

All NMR experiments were performed in collaboration with Dr.Sergiy Nokhrin and Dr. Oleg Dmitriev. NMR spectra were collected at 15 °C using a 600 MHz Bruker Avance spectrometer equipped with 5 mm TXI Inverse Triple (1H,{15N,13C}) Resonance Cold Probe, located at the Saskatchewan Structural Science Centre, University of Saskatchewan. I prepared the ^{15}N-AS and ligands samples. NMR sample preparation, experiments and data processing performed by Dr.Sergiy Nokhrin. I participated in NMR peak labeling.

2.3.1 Sample preparation and experimental set up

The ^{15}N-AS sample was prepared in 0.5×PBS (69 mM NaCl, 1.35 mM KCl, 5 mM Na_2HPO_4, and 1 mM KH_2PO_4) at a concentration of 50µM and dialyzed overnight in 250 ml of 0.5x PBS with 5% glycerol. Initially, the dialysis buffer also contained 0.05% of the detergent β-octyl glucoside (BOG). In the presence of this detergent, spectra were well resolved and there were no significant changes upon addition of ligand (dopamine). Thus, BOG interferes with binding of ligands and all dialysis was then performed in a buffer without BOG to get a typical spectrum for an unfolded protein which were not as well resolved with some line-broadening and peak overlap. The NMR sample was prepared with 5% D2O (v/v) and 2 mM DSS (2,2-dimethyl-2-silapentane-5-sulfonic acid) as a proton reference standard. Ligands were added directly in the NMR tube at different ratios. All ^{1}H,^{15}N- HSQC spectra were collected with 50 µM AS. For the dopamine titration, ligand was added directly in the NMR tube to final concentrations of 250 µM, 500 µM and 1250 µM. For (-)- and (+)-nicotine titration, the ligand was added directly to the NMR tube to final concentrations of 100 µM, 250 µM and 500 µM. NMR spectra were also recorded in the presence of 0.02% of the lysolipid palmitoyl-2-hydroxy-sn-glycero-3-[phospho-rac-(1-glycerol)] (LPPG), which was above its critical micellar concentration (CMC) and dopamine was added in the NMR tube to a final concentration of 500 µM.

2.3.2 Data recording and processing

The ^{15}N – HSQC spectra were collected using 64 x 1024 complex incremental data points in the F1 (15N) and the F2 (1H) dimensions, with 8 or 16 scans per increment and a 1 s relaxation delay. Spectral widths of 40 ppm (centred at 115.7 ppm) and 16 ppm (centred at 4.7 ppm) were used for the ^{15}N and the ^{1}H dimension, respectively.

NMR spectra were processed using NMRPipe (Delaglio *et al.*, 1995) and analyzed using NMRPipe and NMRViewJ (Johnson and Blevins, 1994). The peak positions were labeled using the previously reported sequential chemical shift assignments (Maltsev *et al.*, 2012). The first stage in data processing was the conversion of Bruker formatted files as input data to the NMRpipe formatted file using NMRpipe. Then the NMRpipe formatted output file underwent zero-filling, fourier transformation and phase correction. After processing, data were output as matrix in NMRPipe format and also these matrices were converted into NMRView format for visualization with NMRViewJ.

For chemical shift assignments a script has been used for "pick picking" which picks all real peaks and discriminate them from the noise peaks. After mapping a clean 2D peak list, resonance signals were compared with their counterparts in the previously reported sequential chemical shift (Maltsev *et al.*, 2012). In this process the resultant proton and ^{15}N shifts were compared with the reference to find the matched residue for each detected peak. Then the chemical shifts and relative peak intensities, I/I_0 (I_{bound}/I_{free}), of the HSQC cross peaks in the AS/ligand complex and free AS were plotted versus the amino acid sequence of AS.

2.4 Isothermal Titration Calorimetry

Isothermal titration calorimetry (ITC) analysis was performed on a Nano-ITC (TA Instruments, New Castle, PA, USA), located at the Protein Characterization and Crystallization Facility (PCCF) of the College of Medicine, University of Saskatchewan. The experiment conditions were set up on the PC connected to the machine using the Nano ITC Run Software (TA Instruments).

2.4.1 Sample preparation and experimental set up

Peptide and ligand samples were dissolved in the buffer used for nanopore experiments, containing 1 M KCl and 10 mM HEPES-KOH, pH 7.8. For dopamine the experiments were also performed in the NMR buffer (0.5×PBS). Samples were degassed in a vacuum at 22 °C for 30 minutes. Reference cell and sample cell were filled with 250 µl of degassed buffer solution and the peptide solution, respectively, using a long-needle syringe. The calorimeter syringe was filled with ligand solution. The ligand solution was injected into a sample cell containing 250 µl of 5 µM AS at 22 °C. Other experimental settings were as follow: stirring rate (250 RPM), start delay (250 s) and injection intervals (200 s). The concentrations of ligands in the syringe, the number

of injections and the injection volume for the studied ligands were as follow: (-)-Nicotine (100 µM- 10 injections- 5µl), (+)-Nicotine (150 µM- 10 injections- 5µl), (-)-Methamphetamine (150 µM- 10 injections- 5µl), (+)-Methamphetamine (90 µM- 10 injections- 5µl) and dopamine (1 mM- 8 injections- 6.25µl). The ITC set up for dopamine in the NMR buffer involved 14 injections (3.5 µL each) of 2 mM dopamine. Blank experiments were performed by titrating ligands into the sample cell containing 250 µl of the buffer.

2.4.2 Data recording and processing

The background titration signal for the buffer was subtracted from that of the sample spectra. NanoAnalyze (TA Instruments) was used to fit the raw data. To find the binding model the data were fitted with different reaction models such as independent, multiple sites, competitive and cooperative to find the best model that fits with the data points. Then the best reaction model was used to fit the titration data. The fitting process involves a series of attempts to optimize the output fit. Each model is an equation with thermodynamic variables which correlates entropy (ΔS) as a function of enthalpy (ΔH), number of binding sites (n) and association constant (K_a). So the theoretical models used to explain stages of binding process and give rise to valuable thermodynamic information of the experimental data curve. All the ITC experiments performed in this thesis were fitted with the independent model with one binding site because this equation followed the resulted data points most closely. Finally the values of dissociation constant (K_d) have been reported to compare the affinity of ligands with AS.

2.5 CD Spectroscopy

Experiments were performed on an AppliedPhotophysics CHIRASCAN PLUS CD spectrophotometer equipped with a Quantum Northwest TC125 temperature controller, located at the Protein Characterization and Crystallization Facility (PCCF) of the College of Medicine, University of Saskatchewan. The experiment conditions were set up on the PC connected to the machine using the Pro-Data™ Software Suite (AppliedPhotophysics).

2.5.1 Sample preparation and experimental set up

The spectrophotometer was started up by purging the instrument with nitrogen for 15 minutes before switching on the light source. It took about 30 minutes for the light source to achieve stability. Experiments were performed at 22°C using a cell with a 0.05 cm path length. Samples consisted of 5 µM of AS in 10 mM sodium phosphate buffer (pH 7.4) with or without ligands.

Circular dichroism (CD) spectra were recorded over the range 185-360 nm in millidegrees. For each sample three scans were recorded. For each protein sample the background spectra were recorded as the spectrum of the solvent.

For dopamine experiments, samples consisted of 5 μM of wild type-AS or the A30P mutant AS with or without 50 μM and 125 μM of dopamine. Methamphetamine experiments were performed with samples of 5 μM of wild type-AS with or without 25 μM, 50 μM and 100 μM (+)- or (-)-methamphetamine. For the nicotine experiments samples were composed of 5 μM of wild type-AS with or without 10 μM, 25 μM and 50 μM (+)- or (-)-nicotine.

2.5.2 Data recording and processing

Pro-Data™ Software Suite was used to process the raw data. The average of three scans was calculated by the software. The spectra of the samples were corrected by subtracting the spectrum of the corresponding solvent. The resulting spectra were smoothed 10 times and the units were converted from millidegrees to MRE (mean residue ellipticity) in deg x cm^2 x $dmol^{-1}$.

2.6 Docking simulation of methamphetamine and alpha-synuclein interaction

The 3D structure of AS(PDB ID: 1XQ8) together with the protonated form of the 3D conformer of (+)-methamphetamine (PubChem CID: 10836) were used for the docking simulation. The C-terminal of AS, residues 61 to 140, was removed from the structure to obtain the target binding peptide, *i.e.* residues 1 to 60.

2.6.1 Software and docking set up

The docking simulation was performed using the molecular operating environment (MOE) from the Chemical Computing Group, Inc. as described previously (Abe *et al.*, 2007). Briefly, the target peptide, AS(1–60), was subjected to an MMFF94 energy minimization protocol until the root mean square of the conjugate gradient reached <0.05 kcal mol−1 Å−1. The MOE-Dock default parameters were used for the docking simulation. The MMFF94s was selected as the force field (Abe *et al.*, 2007). Refinement and Rescoring 2 were set up to the Forcefield and Alpha HB, respectively. A global docking was performed with the target peptide. The docking was carried out for 30 iterations and the docking interaction with the lowest energy (−50 kcal/mol) was reported.

3 RESULTS

3.1 Nanopore analysis of AS in the presence of 1,2-diphytanoyl-sn-glycero-3-phosphocholine and EDTA

Nanopore experiments were used as the primary method to study AS/small molecule interactions. Two important controls are described first. To ensure that there was no metal contamination, a control experiment was performed with the standard HEPES buffer in the presence of 1 mM EDTA which chelates any unwanted divalent metals (Krasniqi and Lee, 2012). The event profile of AS in the presence (Figure 3.1b) and absence (Figure 3.1a) of EDTA showed a translocation peak (see later) at -85 pA and a small bumping peak (see later) at -25 pA. This shows that the small bumping peak centered at -25 pA is not due to metal contamination and represents a very small proportion of the AS conformation (Figure 3.1). Furthermore it has been demonstrated previously that AS does not bind to phosphatidylcholine (PC) but has the ability to bind acidic phospholipids such as phosphatidylinositol (PI), phosphatidylserine (PS) and phosphatidic acid (PA) (Davidson *et al.*, 1998; Jo *et al.*, 2000). To ensure that AS does not bind to the 1,2-diphytanoyl-sn-glycero-3-phosphocholine (DPhPC) the following control was performed. AS was incubated with 0.35 mg of DPhPC micelles and the sample was added to the *cis* side of the cup. The event profile of AS (Figure 3.1b) in the presence of 0.35 mg of DPhPC was unchanged (Figure 3.1c).

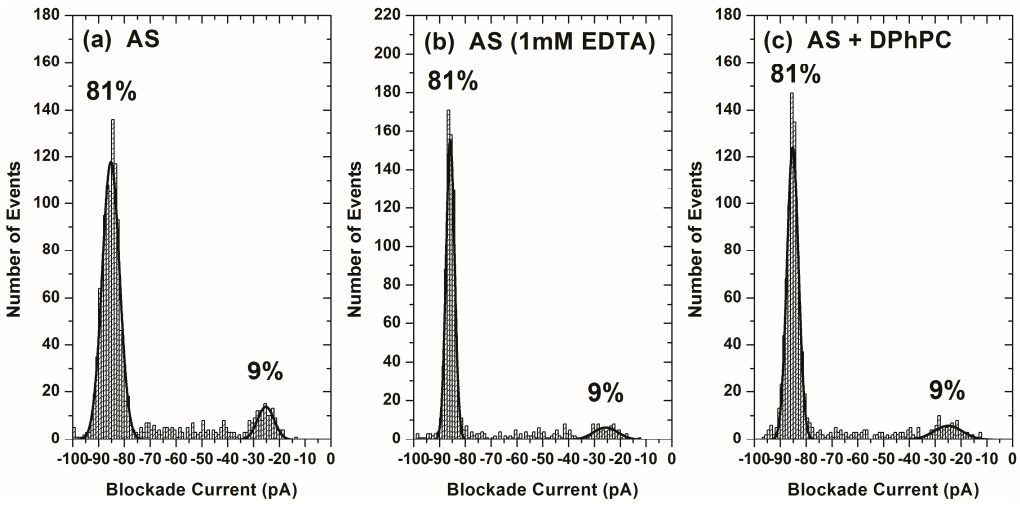

Figure 3.1 Blockade current histogram of AS in different buffers. Blockade current profile of AS in standard HEPES buffer (a) AS in standard HEPES buffer-1 mM EDTA (b) and AS in standard HEPES buffer-1mM EDTA and in the presence of 0.35 mg of DPhPC micelles (c) [Part "c" performed by David Boyle]

3.2 Nanopore analysis of wild type and mutants of AS

The wild type and three major mutants of AS were analyzed using the patch clamp technique and a buffer of 1 M KCl, 10 mM HEPES–KOH (pH 7.8) containing 1 mM EDTA on the *cis* side. Figure 3.2 shows current blockade histograms of the wild type (a) and pathological AS mutants: A30P (b), E46K (c) and A53T (d). These results clearly demonstrate the conformational heterogeneity among the wild type and mutants. For the wild-type, (Figure 3.2a) the major peak was centered at -86 pA and represents the natively unfolded structure. There was also a very small bumping peak at -25 pA. The blockade current histogram for the E46K mutant (Figure 3.2c) was similar to wild type and there were two peaks which are centered at -85 pA and -24 pA. The difference between these two AS types is the proportion of bumping and translocation peaks. The proportion of translocation events for E46K (Figure 3.2c) is about 67% which is less than for the wild type (Figure 3.2a). For the mutants A30P (Figure 3.2b) and A53T, there are three peaks including a bumping peak with lower blockade current, a translocation peak with high blockade current and a peak with intermediate blockade current. For the A30P mutant these peaks are centered at -85 pA, -41 pA and -25 pA. The Mutant A53T (Figure 3.2d) has three peaks at -86 pA, -42 pA and -23 pA. Mutants A30P and A53T show similar conformational properties but for mutant A53T the bumping peak is larger than the mutant A30P. Furthermore, the peak centered at around -85 pA which represents the translocation events shows that the mutant A30P has more translocation events than A53T. The event parameters including blockade current (I) and time (T) for the bumping (I_b and T_b) and translocation (I_t and T_t) peaks are summarized in Table 3.1. As the net charge of the mutant E46K is -7 it has the longest translocation time at 100mV. The other two mutants (A53T, A30P) and the wild type have a larger overall negative charge (-9) and their average translocation time is less than E46K.

To show that the peak which is placed at around -85 pA is due to translocation events a voltage study was done at 75 mV and 100 mV. The calculated event parameters are summarized in Table 3.2. The results show that by increasing the voltage the average time decreases which means that the protein is being electrophoretically driven through the pore. Figure 3.3 shows blockade time graphs for the translocation peaks of the wild type (a) and pathological AS mutants: A30P (b), E46K (c) and A53T (d) at 100 mV.

Table 3.1 Event parameters for the translocation and bumping peaks of AS and mutants at 100 mV.

AS	I_b (pA)	I_t (pA)	T_b (ms)	T_t (ms)
Wild type	-25	-85	0.12	0.49
A30P	-25	-87	0.02	0.34
E46K	-24	-86	0.03	0.71
A53T	-23	-87	0.23	0.28

I and T represent the intensity and duration of the current blockade. The subscripts b and t refer to bumping and translocation event populations.
(The error is estimated to be ±1 pA for I and ±10% for T)

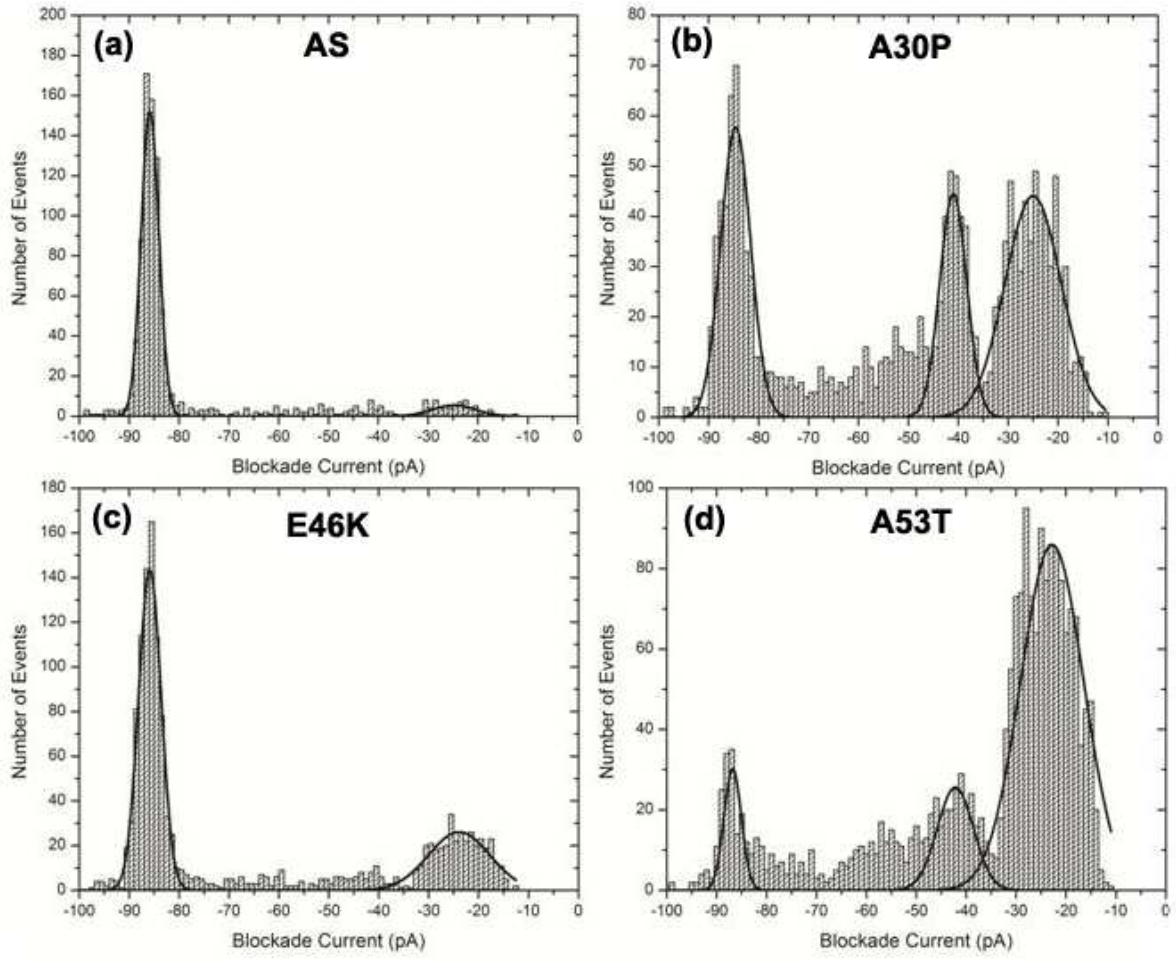

Figure 3.2 Blockade current histograms for AS. (A) wild type, (B) mutant A30P, (C) mutant E46K and (D) mutant A53T. The applied voltage was 100 mV.

Table 3.2 Event parameters for the translocation peak of the AS peptides at two different voltages

	I_{75} (pA)	I_{100} (pA)	T_{75} (ms)	T_{100} (ms)
AS	-63	-85	0.61	0.49
A30P	-62	-87	0.82	0.34
E46K	-63	-86	1.17	0.71
A53T	-66	-87	0.75	0.28

I and T represent the intensity and duration of the current blockade. The subscripts 75 and 100 refer to translocation peak when 75 mV and 100 mV of voltage are applied respectively. (The error is estimated to be <±1 pA for I and <±10% for T)

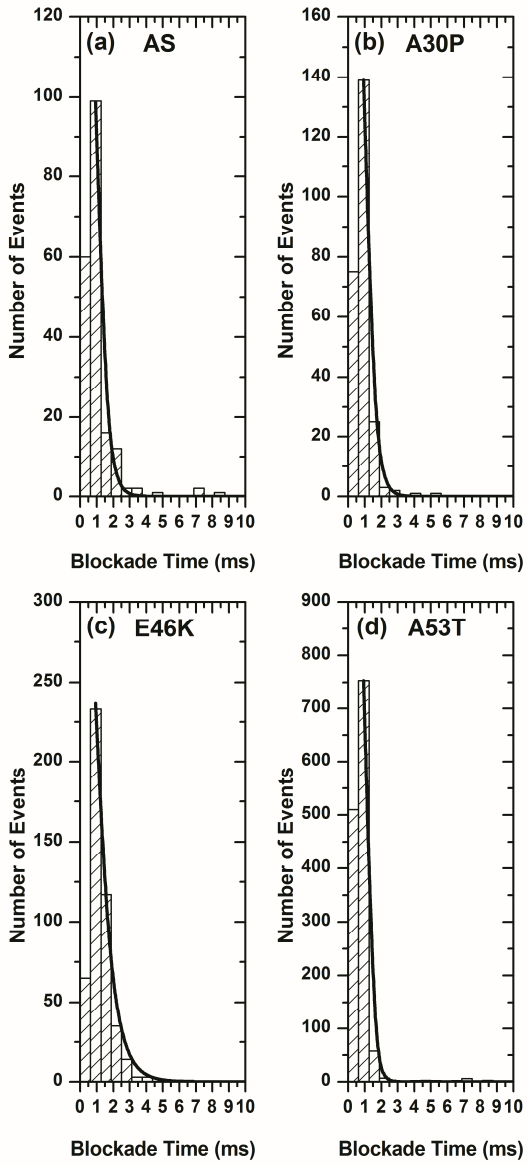

Figure 3.3 Blockade time profiles for AS. (A) wild type, (B) mutant A30P, (C) mutant E46K and (D) mutant A53T. The applied voltage was 100 mV.

3.3 Alpha-synuclein and methamphetamine isomers interaction

3.3.1 Introduction

It has been shown previously that the incidence of PD is increased among methamphetamine users (Callaghan *et al.*, 2010; Callaghan *et al.*, 2012). Therefore the interaction of methamphetamine isomers with AS was studied using nanopore analysis, CD spectroscopy and ITC. In order to delineate the binding site of (+)- and (-)-methamphetamine, three segments of AS were analyzed.

3.3.2 Nanopore discrimination of the interaction of methamphetamine isomers with alpha-synuclein

Figure 3.4a,f show snapshots of the typical current trace for (a) AS and (f) AS in the presence of 20µM (+)-methamphetamine. For AS the majority of events have large current blockades at around -85pA (Figure 3.4a) while in the presence of (+)-methamphetamine most of the events have a short current blockade at around -25pA (Figure 3.4f).

Figure 3.4b,c,d,f shows the current blockade histogram for AS and AS in the presence of increasing concentrations of (+)-methamphetamine, *i.e.* 5µM, 10µM and 20µM. As described above, for AS there are two peaks centered at -85pA and -25pA which are due to translocation and bumping. The majority of the events (81%) are translocation and only a small proportion of events (9%) are bumping (Figure 3.4b). Upon addition of increasing concentrations of (+)-methamphetamine to AS the proportion of bumping events increased in a concentration dependent manner with a simultaneous decrease in the proportion of translocation events (Figure 3.4c,d,f). The percentage of bumping events in the presence of 5 µM, 10 µM and 20 µM (+)-methamphetamine was increased from 9% to 34% (Figure 3.4c), 43% (Figure 3.4d) and 50% (Figure 3.4e). This proportional change caused a decrease in the percentage of the translocation peak centered at -85pA as follow: 40% (Figure 3.4c), 35% (Figure 3.4d) and 31% (Figure 3.4e) in the presence of 5µM, 10µM and 20µM drug respectively. There are also a large number of events with intermediate current blockades between -40pA to -75pA which are difficult to characterize because they do not yield a clear Gaussian distribution. The other isomer, (-)-methamphetamine, was also studied. Figure 3.5 shows the blockade current histogram of AS alone (a) AS to (-)-methamphetamine ratio 1:5 (b), 1:10 (c) and 1:20 (d). Considering the blockade current histograms for (+)-methamphetamine (Figure 3.4c,d,e), the results together

show that both (+)- and (-)-methamphetamine change the conformation of AS by changing the proportion of translocation and bumping peaks towards an increase in bumping events.

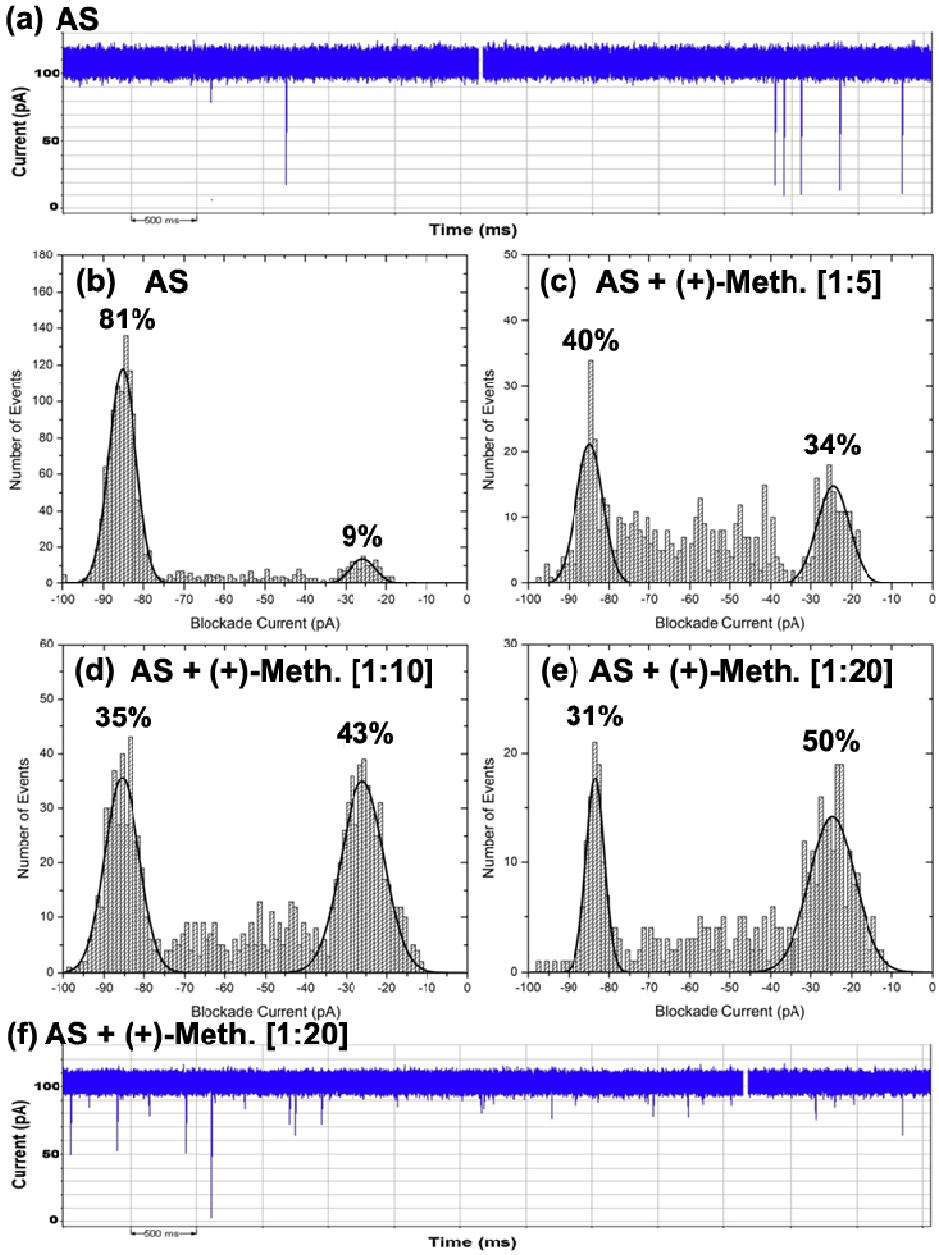

Figure 3.4 Nanopore analysis of the interaction of (+)-methamphetamine with full length AS. (a, f) Typical current traces for AS and AS with 20 μM methamphetamine. (b–e) Blockade current histograms for AS with 0, 5, 10, 20 μM methamphetamine, respectively.

They change the AS conformation in a different manner and at the same concentrations of drugs the changes in the proportion of translocation and bumping peaks are different. For example the proportion of translocation (35%) and bumping (43%) peaks in the presence of 20

μM of (-)-methamphetamine (Figure 3.5d) is similar to the blockade current profile of AS in the presence of 10 μM (+)-methamphetamine (Figure 3.4d).

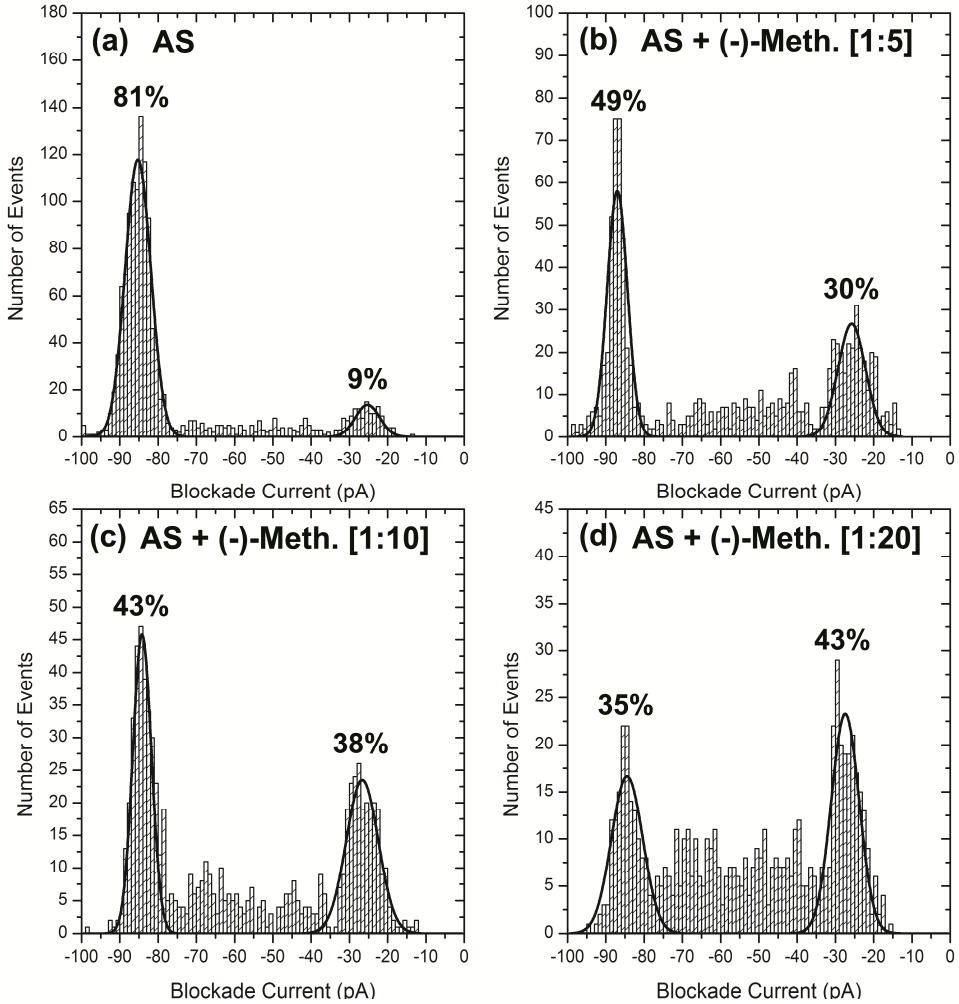

Figure 3.5 Blockade current profiles showing the interaction of (-)-methamphetamine with AS. AS (a), AS to (-)- methamphetamine ratio: (b) 1:5, (c) 1:10 and (d) 1:20.

3.3.2.1 Mapping of the (+)-Methamphetamine binding site using nanopore analysis and a docking simulation

Three segments of the AS protein have been used to map the (+)-methamphetamine binding. These segments include AS(1-60), AS(61-140) and ΔNAC which lacks the middle segment of AS (61-95). Figure 3.6 shows the current blockade histograms for AS(1-60) (a) and in the presence of 5 μM (b), 10 μM (c) and 20 μM (d) (+)-methamphetamine. The AS(1-60) peptide

itself shows a single bumping peak centered at -25pA due to its positive net-charge (+4). The interaction of this positively charged peptide with the pore is diffusion controlled rather than electrophoretically driven and gives rise to a major bumping peak with a proportion of 73% (Figure 3.6a). Addition of increasing concentrations of the drug to this peptide causes a concentration dependent decrease of the proportion of bumping events from 73% to 51% (Figure 3.6b), 30% (Figure 3.6c) and 23% (Figure 3.6d) at the concentrations of 5 µM, 10 µM and 20 µM respectively. These results suggest an N-terminal binding site for (+)-methamphetamine.

As expected (+)-methamphetamine (10 µM) didn't change the current blockade current profile for AS(61-140) (Figure 3.7c,d), and the N-terminal binding site for this drug was confirmed by investigating AS(ΔNAC) (Figure 3.7a,b). In the absence of drug the current blockade histogram for AS(ΔNAC) shows a major translocation peak at -88 pA with a proportion of 61% and a bumping peak centered at -25 pA (Figure 3.7a). Upon addition of 10 µM of drug, the proportion of translocation events underwent an almost 50% decrease and the bumping events were increased from 28% to 44% (Figure 3.7b).

Docking simulations of interactions between (+)-methamphetamine and AS(1-60) were performed using molecular operating environment (MOE) from the Chemical Computing Group, Inc.. A possible binding site encompassing residues 35–44 (Figure 3.8) was identified. The interaction was stabilized in part by polar interactions between Glu35, Gly36, Tyr39 and Thr44, and the amine of the drug as well van der Waals interactions between Leu38, Val40 and Lys43 and the benzene ring of the drug. This interaction causes folding of the peptide around the drug to form a loop which is locked by ionic interaction between Glu35 and Lys43 (Figure 3.8).

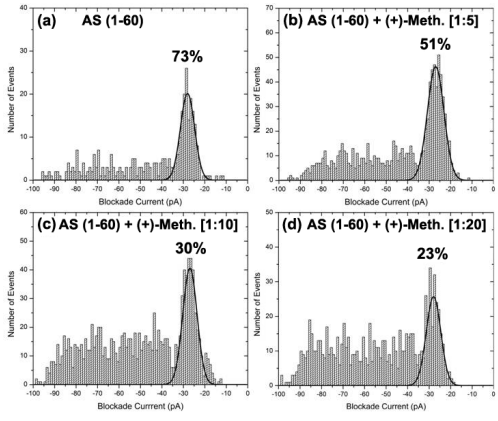

Figure 3.6 Blockade current histograms for N-terminal AS(1–60) in the presence of (+)-methamphetamine. (a-d) Blockade current histograms for N-terminal AS(1–60), with 0, 5, 10, 20 µM (+)-methamphetamine, respectively.

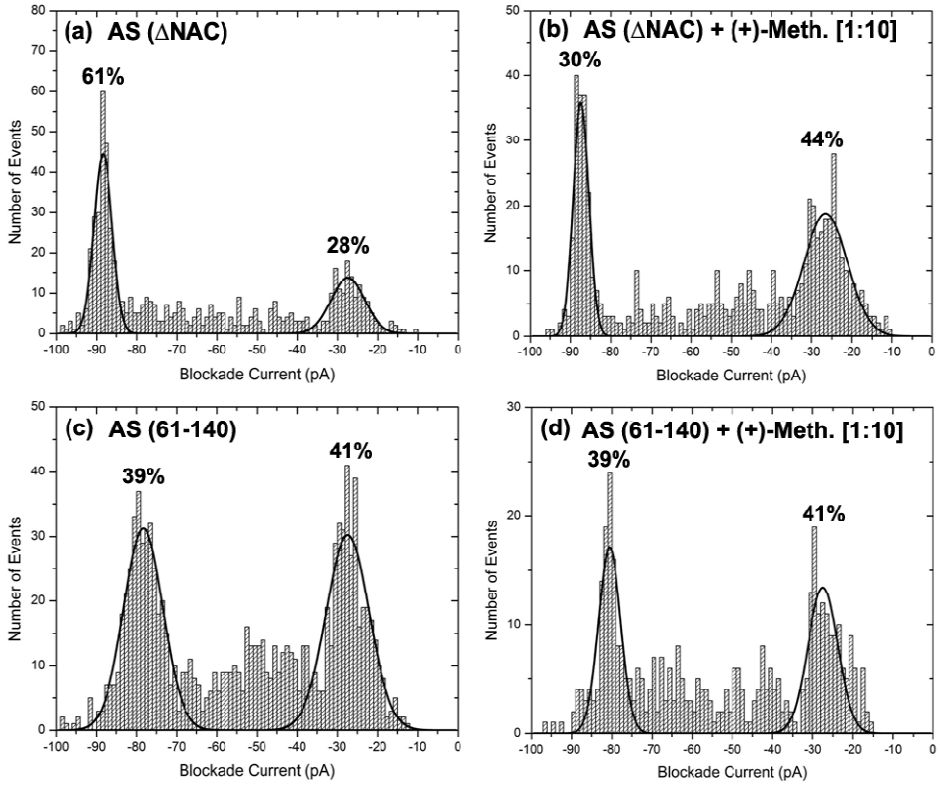

Figure 3.7 Blockade current histograms for AS(ΔNAC) and AS(ΔNAC) in the presence and absence of (+)-methamphetamine. (a, b) Blockade current histograms for AS(ΔNAC) with 0 μM and 10 μM (+)-methamphetamine. (c, d) Blockade current histograms for AS(61–140) with 0 μM and 10 μM (+)-methamphetamine.

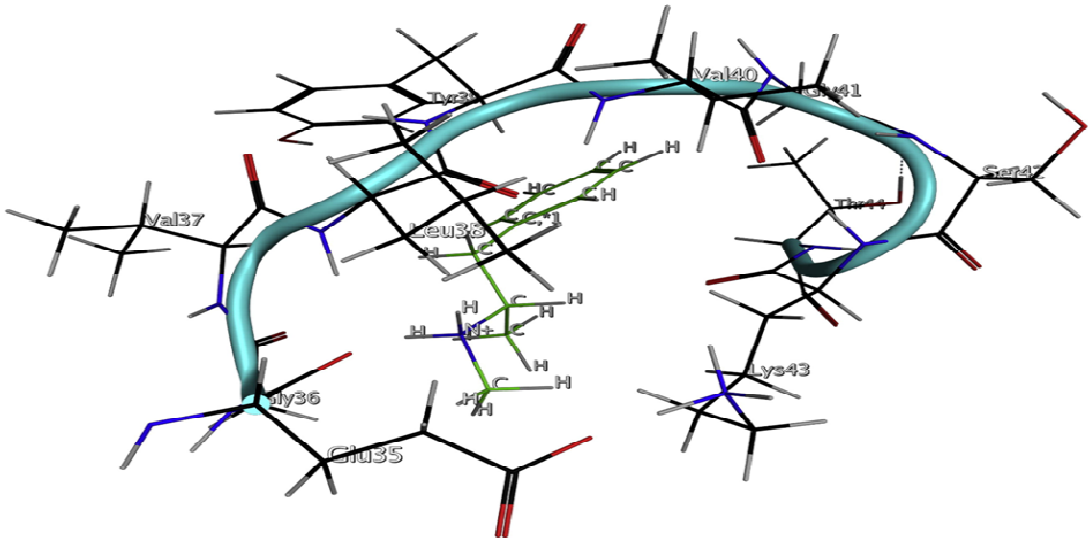

Figure 3.8 Results from docking simulations showing the proposed binding site for (+)-methamphetamine in the N-terminal region of AS.

3.3.2.2 Mapping of the (-)-Methamphetamine binding site using nanopore analysis

The interaction of the (-)-isomer with the same peptides was also studied. Figure 3.9 shows the nanopore analysis of (-)-methamphetamine and AS (61-140) (b), AS (1-60) (d) and AS (ΔNAC) (f). The results showed a conformational change of the C-terminus (Figure 3.9b) and ΔNAC (Figure 3.9f) in the presence of 10 μM of the ligand and suggests a C-terminal binding site for (-)-methamphetamine. The current blockade profile of AS(1-60) in the absence (Figure 3.9c) and presence of (-)-methamphetamine (Figure 3.9d) was the same.

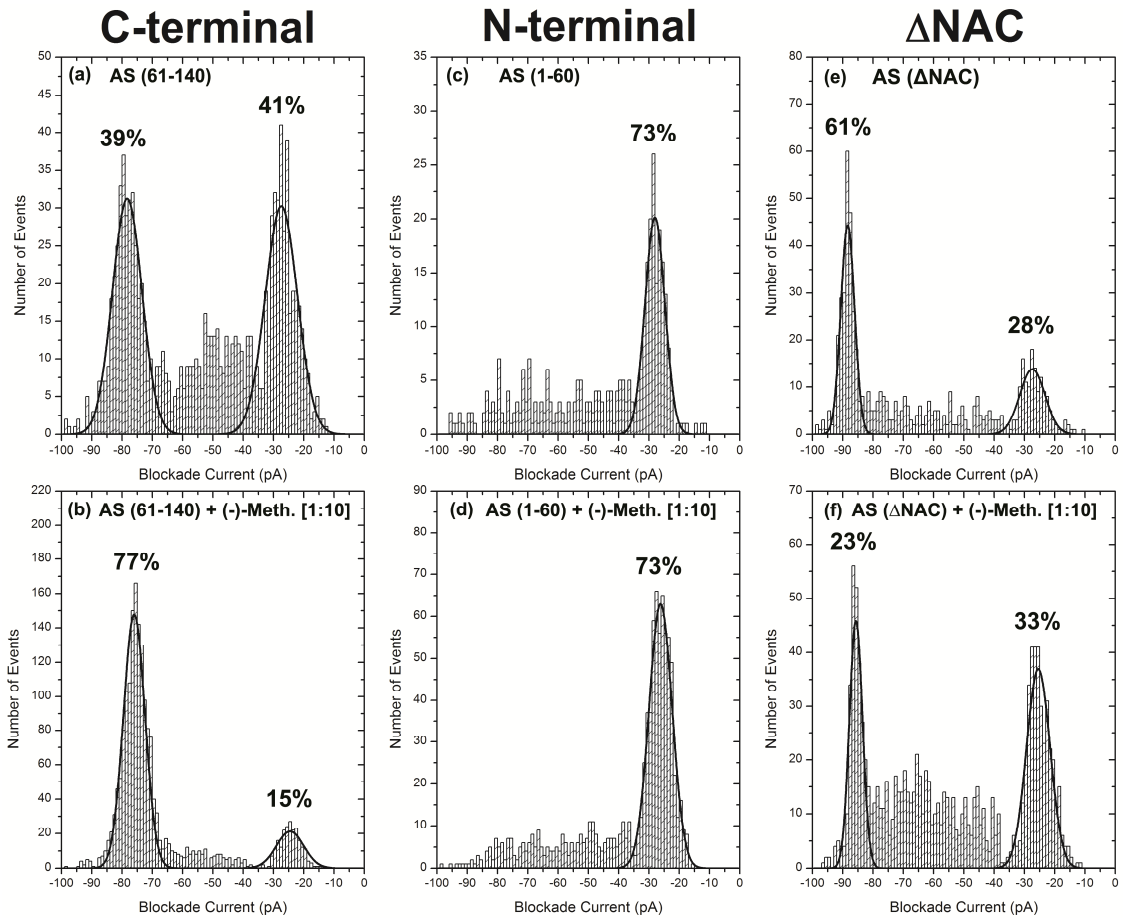

Figure 3.9 Blockade current profiles showing the interaction of (-)-methamphetamine with AS peptides (96-140, 1-60 and ΔNAC). AS (61-140) (a), AS (61-140) to (-)-methamphetamine ratio: (b) 1:10, AS (1-60) (c), AS (1-60) to (-)-methamphetamine ratio: (d) 1:10, AS (ΔNAC) (e), AS (ΔNAC) to (-)-methamphetamine ratio: (f) 1:10.

3.3.3 CD spectroscopy of the AS-methamphetamine interaction

The CD spectrum of AS is typical of an intrinsically disordered protein and is mostly random coil (Serpell *et al.*, 2000; Uversky *et al.*, 2001b; Weinreb *et al.*, 1996; Zheng *et al.*, 2013) (Figure

3.10, black line). Figure 3.10 also shows the CD spectra for AS in the presence of different concentrations of (+)- and (-)-methamphetamine. The addition of increasing amounts of (-)-methamphetamine (25 µM, 50 µM and 100 µM) causes a change in mean residue ellipticity (MRE) at 196 and 220 nm. In contrast (+)-methamphetamine causes no significant change in the magnitude of MRE. Addition of (+)- and (-)-methamphetamine did not cause a significant change in the secondary structure content of AS which implies that the drug is not inducing an α-helical or β-sheet conformation. This might be due to formation of a simple loop or binding pocket which would not be expected to alter the CD spectrum.

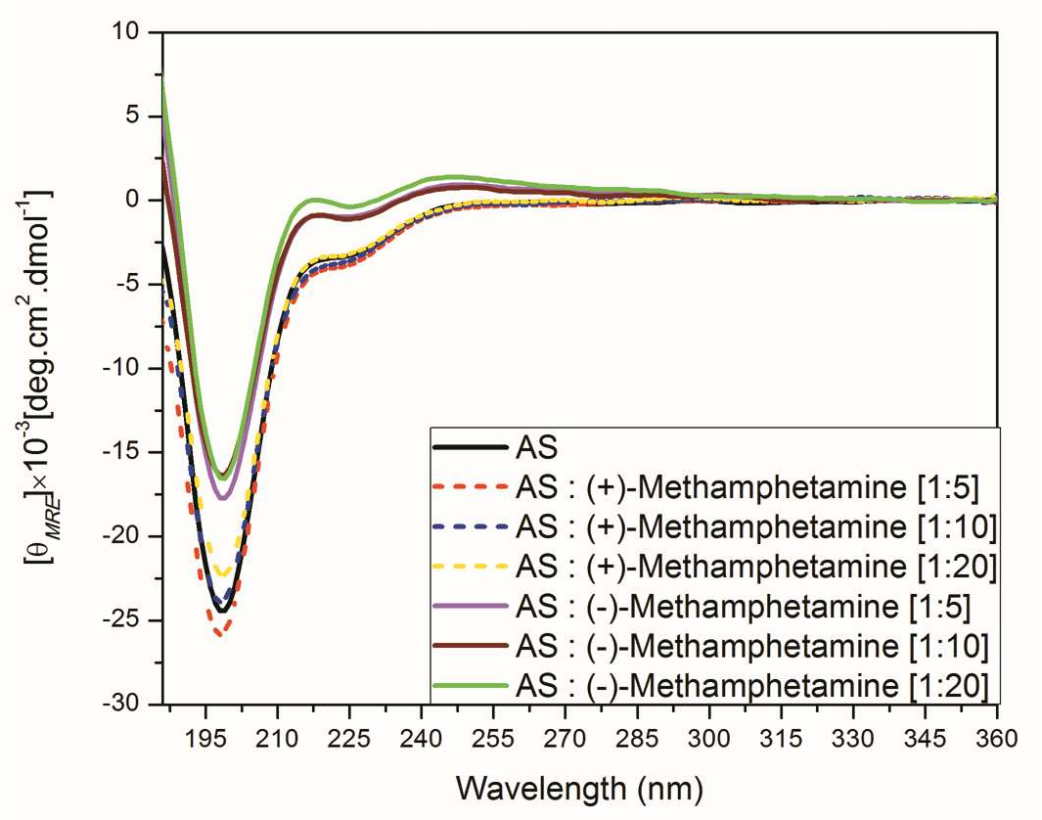

Figure 3.10 CD spectra for full length AS in the presence of (+)- and (-)-methamphetamine. CD spectra for full length AS (black) and in the presence of 25 µM (red-dotted line), 50 µM (blue-dotted line), 100 µM (yellow-dotted line) of (+)-methamphetamine and 25 µM (purple-solid line), 50 µM (brown-solid line), 100 µM (green-solid line) of (-)-methamphetamine.

3.3.4 Isothermal Titration Calorimetry of AS-methamphetamine interaction

ITC experiments have been done to measure the K_d of methamphetamine isomers with AS. Figure 3.11 shows the calorimetric characterization of the interactions between AS and (+)-methamphetamine (a,b) and (-)-methamphetamine (c,d). Titrations of 90 µM (+)-

Methamphetamine (Figure 3.11a,b) and 150 µM (-)-Methamphetamine (Figure 3.11c,d) into 5 µM AS solution indicated a one-site interaction mechanism with K_ds of (5.00 ± 0.02) × 10^{-7} M and (1.95 ± 0.03) × 10^{-6} M (averages of two experiments) respectively. This is in agreement with the nanopore results which showed that (+)-methamphetamine binds tighter than (-)-methamphetamine.

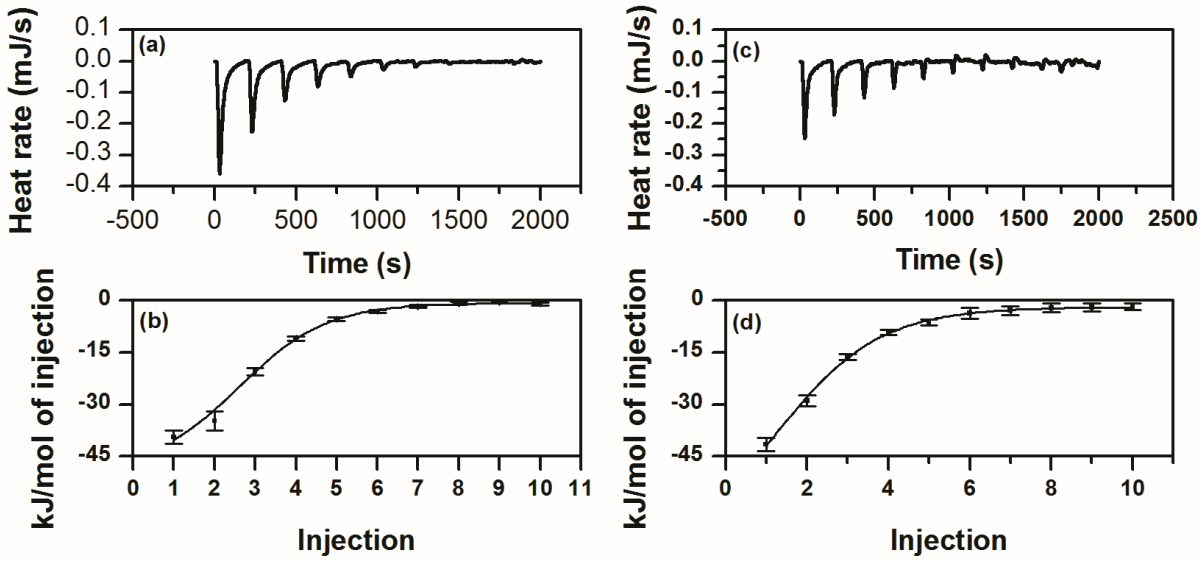

Figure 3.11 Calorimetric characterization of the interactions between AS and (+)-methamphetamine (a), (b) and (-)-methamphetamine (c), (d) in a buffer containing 1 M KCl and 10 mM HEPES-KOH, pH 7.8. Data is fitted with the one-site model which corresponds to "n=1" & "K_d= 0.5 µM" (a) and "K_d= 2 µM".

3.4 Alpha-synuclein and nicotine isomers interaction

3.4.1 Introduction

Nicotine is another commonly used drug. In contrast to methamphetamine, smokers have a lower incidence of PD (Checkoway *et al.*, 2002; Hernán *et al.*, 2002; Kessler and Diamond, 1971; Ono *et al.*, 2007b; Quik, 2004; Ross and Petrovitch, 2001). Therefore the interaction of nicotine isomers with AS was studied using nanopore analysis, CD spectroscopy, ITC and NMR spectroscopy. In order to delineate the binding site of (+)- and (-)-methamphetamine, three segments of AS were analyzed.

3.4.2 Nanopore discrimination of the interaction of nicotine isomers with alpha-synuclein

Nanopore experiments were performed in the presence of 2 μM, 5 μM and 10μM of both (-)- and (+)-nicotine (Figure 3.12). Anabasine was used as the control, because anabasine is another component of cigarette smoke and has the same molecular weight as nicotine. Current histograms for AS alone and anabasine are shown in Figure 3.12a,e. Figure 3.12b-d shows current blockade histograms of AS in the presence of 2 μM (Figure 3.12b), 5 μM (Figure 3.12c) and 10 μM (Figure 3.12d) of (-)-nicotine. In contrast, the corresponding current profiles for the (+)-nicotine are shown in Figure 3.12f-h. In the absence of ligand, (Figure 3.12a) AS blockade current profile shows a sharp translocation peak at -86 pA. The control experiment in the presence of 10 μM anabasine (Figure 3.12e) shows little change in the blockade current profile. After adding 2 μM of (-)-nicotine to the cup, the translocation peak shifted to -81 and also an intermediate peak developed at -40 pA (Figure 3.12b). In contrast, for (+)-nicotine there was just the shift of the translocation peak to -80 pA and an increase in the bumping peak intensity (Figure 3.12f). In the presence of 5 μM of (-)-nicotine the proportion of the intermediate peak increased to 40% and some events with intermediate current blockade appeared between -40 pA to -80 pA (Figure 3.12c). For (+)-nicotine at 5 μM the intensity of the intermediate peak at -40 pA is 70% because the events between -40 pA to -80 pA are not present in the histogram and the profile is much simpler than the (-)-nicotine profile (Figure 3.12g). By increasing the concentration of ligands to 10 μM the intermediate peak became the most significant conformation. At this concentration both ligands show an intermediate peak but at different blockade currents (Figure 3.12d,h); at -62 pA and -42 pA for (-)- and (+)-nicotine respectively. Furthermore, a bumping peak exists at -25 pA. The (-)-nicotine bumping peak is larger than that of the (+)-nicotine. These results show that (-)- and (+)-nicotine change the conformation of AS in two different ways. This might explain why at the concentration of 5 μM (+)-nicotine the profile is much simpler than (-)-nicotine and also why different intermediate peaks are found at the concentration of 10 μM.

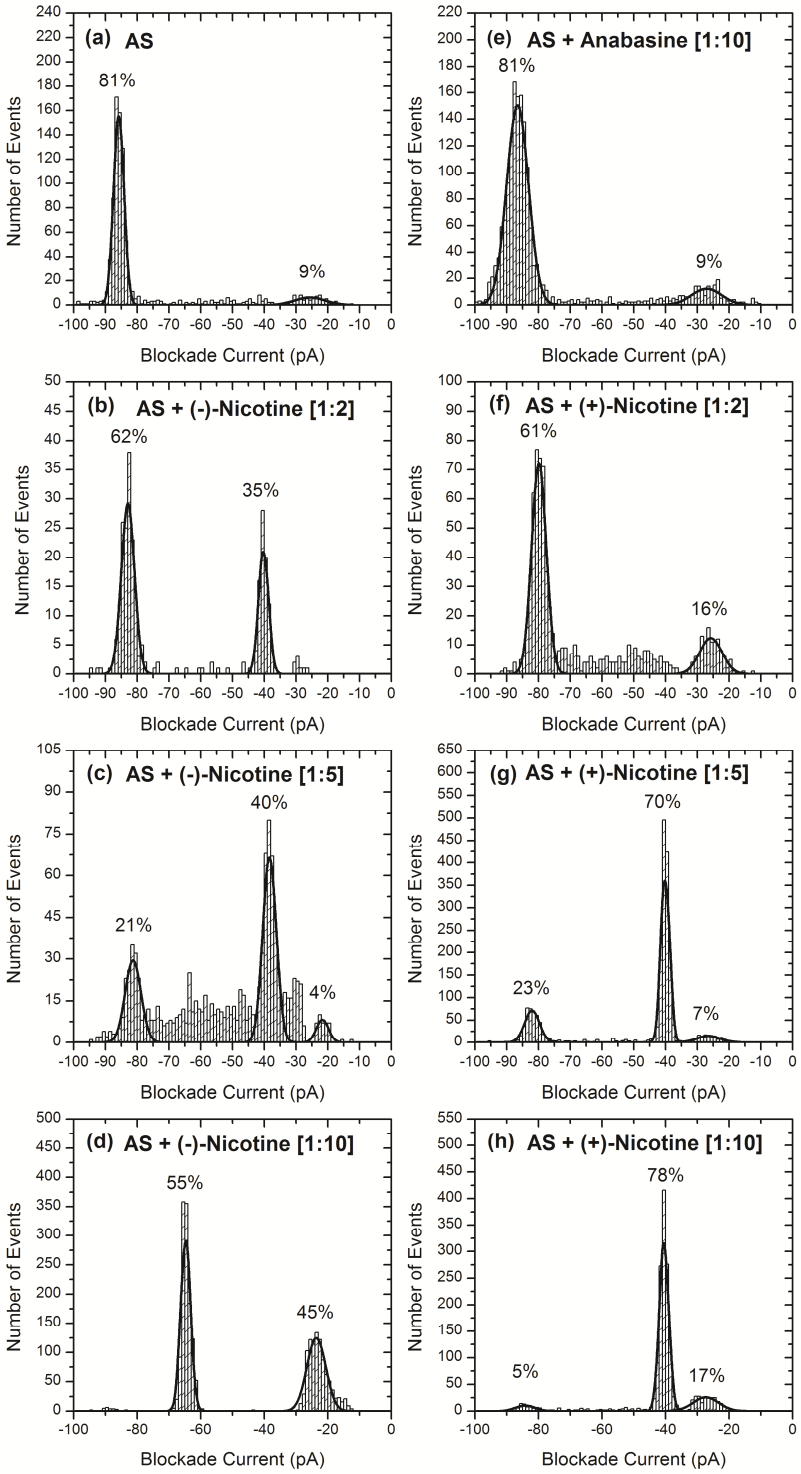

Figure 3.12 Blockade current profiles showing the interaction of anabasine, (+)- and (-)-nicotine with AS (1 µM). AS (a), AS to (-)-nicotine ratio: (b) 1:2, (c) 1:5, (d) 1:10, AS + 10 µM anabasine (e), AS to (+)-nicotine ratio (f) 1:2, (g) 1:5, (h) 1:10. [Anabasine experiment performed by Joe Kakish]

3.4.2.1 Mapping of (-)- and (+)-nicotine binding sites using nanopore analysis

In order to delineate the binding site of (+)- and (-)-nicotine, several AS fragments were studied. Figure 3.13a,b,c show the blockade current histograms for the C-terminal peptide AS(96-140). In the absence of ligand (Figure 3.13a) there are two peaks; one with a blockade current more than -40 pA (91%) and a bumping peak at -25 pA (9%). AS(96-140) underwent a conformational change in the presence of 10 μM (-)-nicotine (Figure 3.13b). Addition of (-)-nicotine to this peptide causes a reduction in the intensity of the translocation peak to 77% and an increase in the bumping peak simultaneously. An intermediate peak was also found at -40 pA (Figure 3.13b). In contrast, the current profile of this peptide showed only a minor change after adding the same concentration of (+)-nicotine with the proportion of the translocation peak decreasing to 86% (Figure 3.13c). Figure 3.13d,e,f shows the blockade current histograms for the N-terminal peptide AS(1-60). In the absence of drug (Figure 3.13d) there was no clear translocation peak and about 52% of the events are bumping. Upon addition of 10μM of (-)- and (+)-nicotine the proportion of bumping events decreases to 25% and 21% respectively (Figure 3.13e,f). Furthermore, there is an intermediate peak at -41 pA in the presence of (-)-nicotine (Figure 3.13e). Figure 3.13g,h,i shows the current profile for ΔNAC in the absence and presence of 10uM (-) and (+)-nicotine respectively. The current profile of this peptide underwent conformational changes in the presence of both isomers of nicotine. For (-)-nicotine an intermediate peak is found at -41 pA and in the presence of (+)-nicotine the translocation peak shifted from -90 pA to -80 pA and the proportion of the bumping peak increased. These nanopore results demonstrate that (-)-nicotine has a binding site consisting of both N- and C-terminal residues of AS but (+)-nicotine has a binding site which mostly involves residues from the N-terminus.

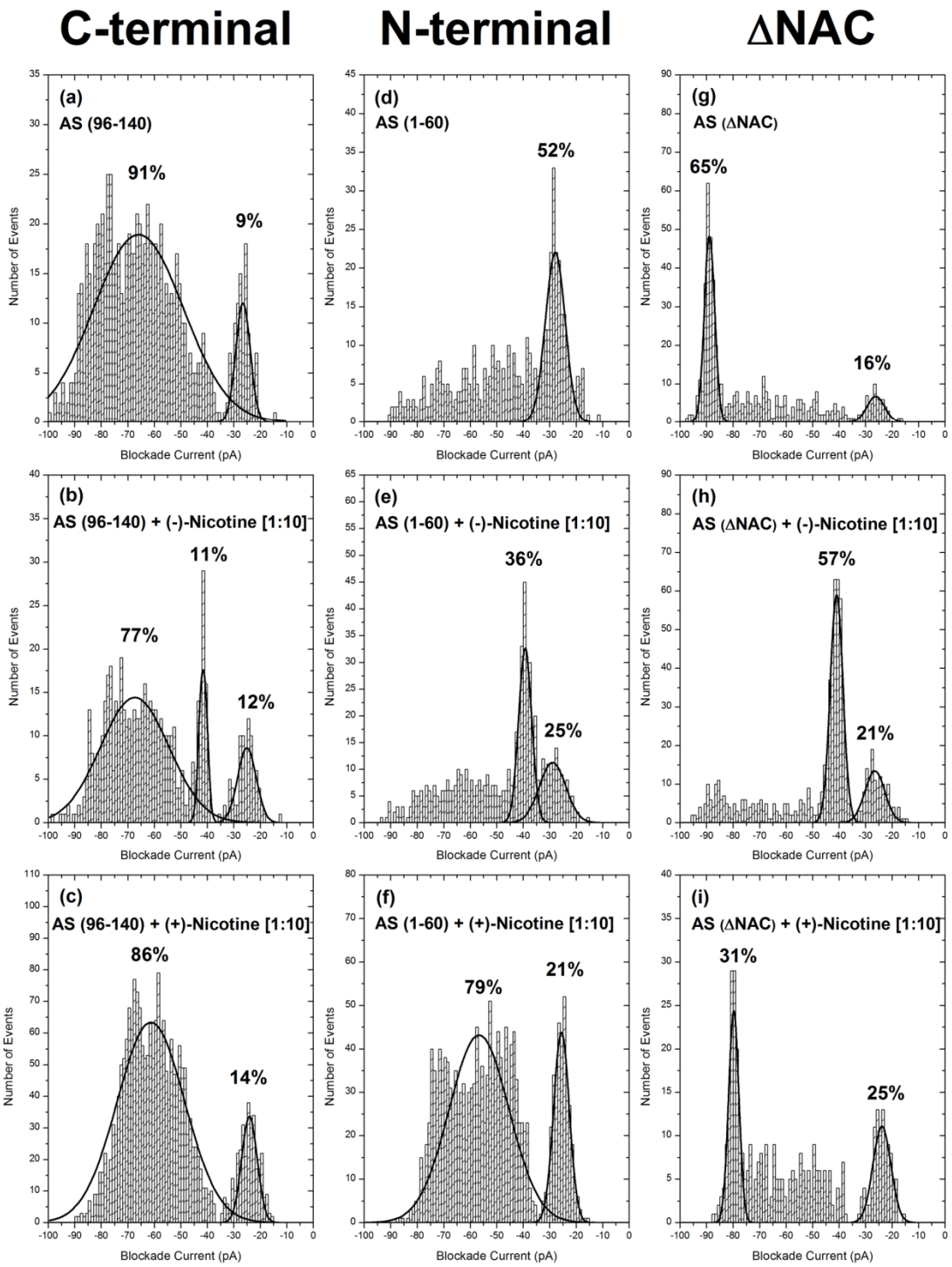

Figure 3.13 Blockade current profiles showing the interaction of nicotine isomers with AS peptides (96-140, 1-60 and ΔNAC). AS (96-140) (a), AS (96-140) to (-)-nicotine ratio: (b) 1:10, AS (96-140) to (+)-nicotine ratio: (c) 1:10, AS (1-60) (d), AS (1-60) to (-)-nicotine ratio: (e) 1:10, AS (1-60) to (+)-nicotine ratio: (f) 1:10, AS (ΔNAC) (g), AS (ΔNAC) to (-)-nicotine ratio: (h) 1:10 and AS (ΔNAC) to (+)-nicotine ratio: (i) 1:10.

3.4.3 Circular dichroism spectroscopy of the alpha-synuclein-nicotine interaction

The interaction of AS with (-)- and (+)-nicotine has been investigated with CD-spectroscopy. Figure 3.14 shows the CD spectra for AS itself and AS to ligand ratios 1:2, 1:5 and 1:10. As above, the spectrum for AS is typical of a random coil and is in agreement with a largely unstructured protein (Hoyer *et al.*, 2004; Lendel *et al.*, 2009; Rao *et al.*, 2008; Uversky *et al.*, 2001b) The addition of increasing amounts of (+)- and (-)-nicotine results in mean residue ellipticity (MRE) changes at 196 and 220 nm but there is no significant increase in α-helix or β-sheet content. By increasing the concentration of (+)- and (-)-nicotine there is an increase in the magnitude of MRE in 196-200 nm region due to the binding of ligand to AS as reported previously for other small molecules such as congo red (Lendel *et al.*, 2009; Rao *et al.*, 2008).

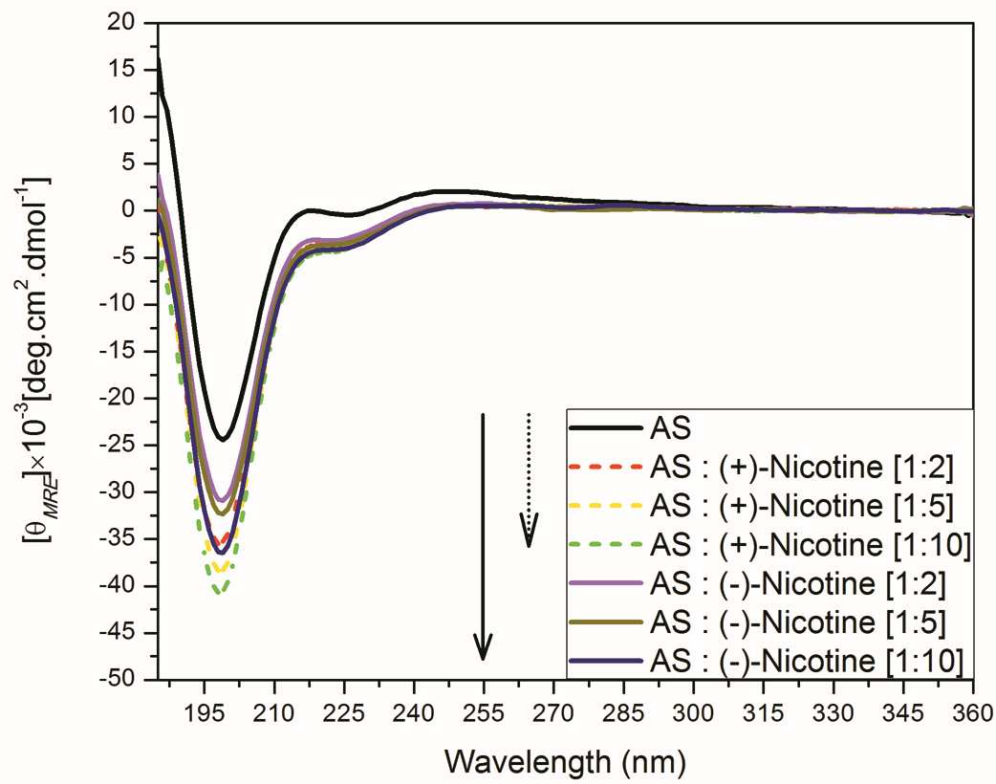

Figure 3.14 CD spectra for full length AS in the presence of (+)- and (-)-nicotine. (a) CD spectra for full length AS (black) and in the presence of 10 μM (red-dotted line), 25 μM (yellow-dotted line), 50 μM (green-dotted line) of (+)-nicotine and 10 μM (purple-solid line), 25 μM (brown-solid line), 50 μM (blue-solid line) of (-)-nicotine.

3.4.4 ITC of the alpha-synuclein-nicotine interaction

Titrations of 100 μM (-)-nicotine (Figure 3.15a,b) and 150 μM (+)-nicotine (Figure 3.15c,d) into a 5 μM AS solution indicated a one-site interaction mechanism with K_ds of (7.40 ± 0.2) × 10^{-7} M and (2.50 ± 0.2) × 10^{-6} M (averages of two experiments))respectively. Thus (+)-nicotine has a lower affinity compared to (-)-nicotine.

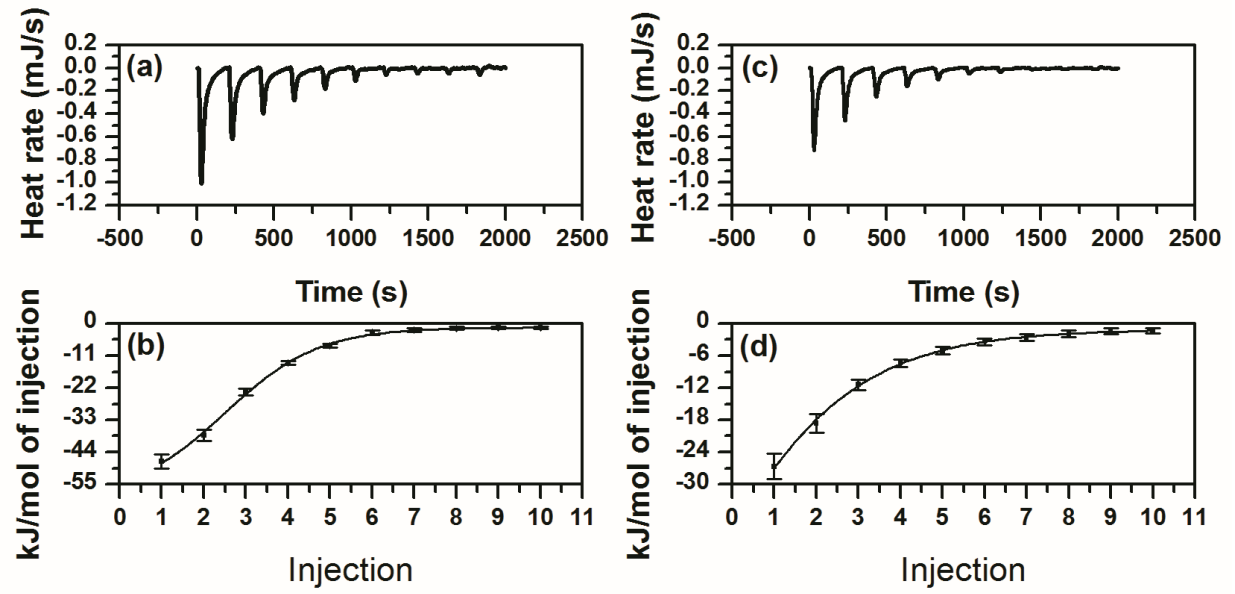

Figure 3.15 Calorimetric characterization of the interactions between AS and (-)-nicotine (a,b) and (+)-nicotine (c,d) in a buffer containing 1 M KCl and 10 mM HEPES-KOH, pH 7.8. Data is fitted with the one-site model which corresponds to "n=1" & "K_d= 0.74 μM" (b) and "K_d= 2.5 μM" (d).

3.4.5 HSQC-NMR

To investigate the conformational changes of AS with time during the NMR spectroscopy, a control sample of AS was kept in an incubator at 15° C during the titration of the AS sample with nicotine (~5 hours) and the spectrum of the control sample was collected immediately after the titration experiments (Figure 3.16). The control experiment showed that AS is stable during the NMR experiment and any changes in conformation are induced by adding ligand to the AS sample. For (-)-nicotine and (+)-nicotine, ^{1}H-^{15}N- HSQC spectra were collected with 50 μM AS , and ligands were added directly in the NMR tube to the ratios of 1:2, 1:5 and 1:10 (AS to ligands). Figure 3.16 shows the ^{1}H-^{15}N HSQC spectra for the ratios of (a) 1:10 AS to (-)-nicotine and (b)1:10 AS to (+)-nicotine. The changes in intensity at the ratio of 1:10 AS to nicotine are

summarized in Figure 3.16c ((-)-nicotine) and Figure 3.16d ((+)-nicotine). The ^{1}H-^{15}N HSQC spectra show that AS underwent a significant conformational change in the presence of (-)-nicotine (Figure 3.17a) and the intensity of most of the peaks are decreased at this concentration of (-)-nicotine (Figure 3.17a). In contrast at the same ratio of (+)-nicotine, the ^{1}H-^{15}N HSQC spectra shows only a few changes in intensity (Figure 3.17b). The changes in the intensity ratio as a function of drug concentration are described in Figure 3.18 for well-resolved residues. In general (+)-nicotine effects few residues from the N-terminal and NAC residues (T33, T44, G67, G68, T81, S87 and G93) but (-)-nicotine causes an overall change in AS conformation involving residues from N-terminal (G7, G41 and K60), NAC (G67, T81 and T92) and C-terminal (E130). Furthermore, the relative signal intensities (Figure 3.18) show that titration of AS with increasing concentrations of (+)- or (-)-nicotine causes a gradual decrease of residue intensity. Therefore, conformational change of AS in the presence of nicotine isomers is concentration dependent and is in agreement with the nanopore analysis which shows different conformational changes induced by each isomer.

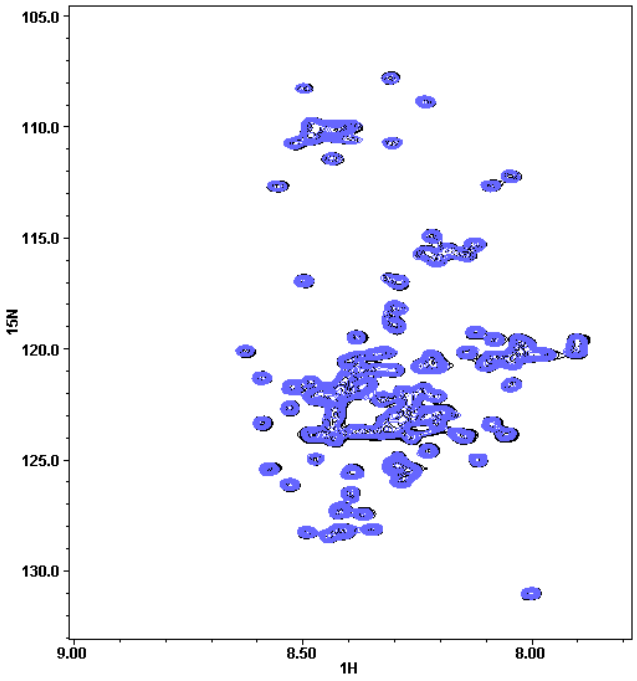

Figure 3.16 ^{1}H-^{15}N HSQC NMR spectrum of a control sample of AS. ^{1}H-^{15}N HSQC NMR spectrum of AS alone (black), control sample of AS which was kept in incubator for ~5 hours (purple) [Experiments performed by Dr. Sergiy Nokhrin].

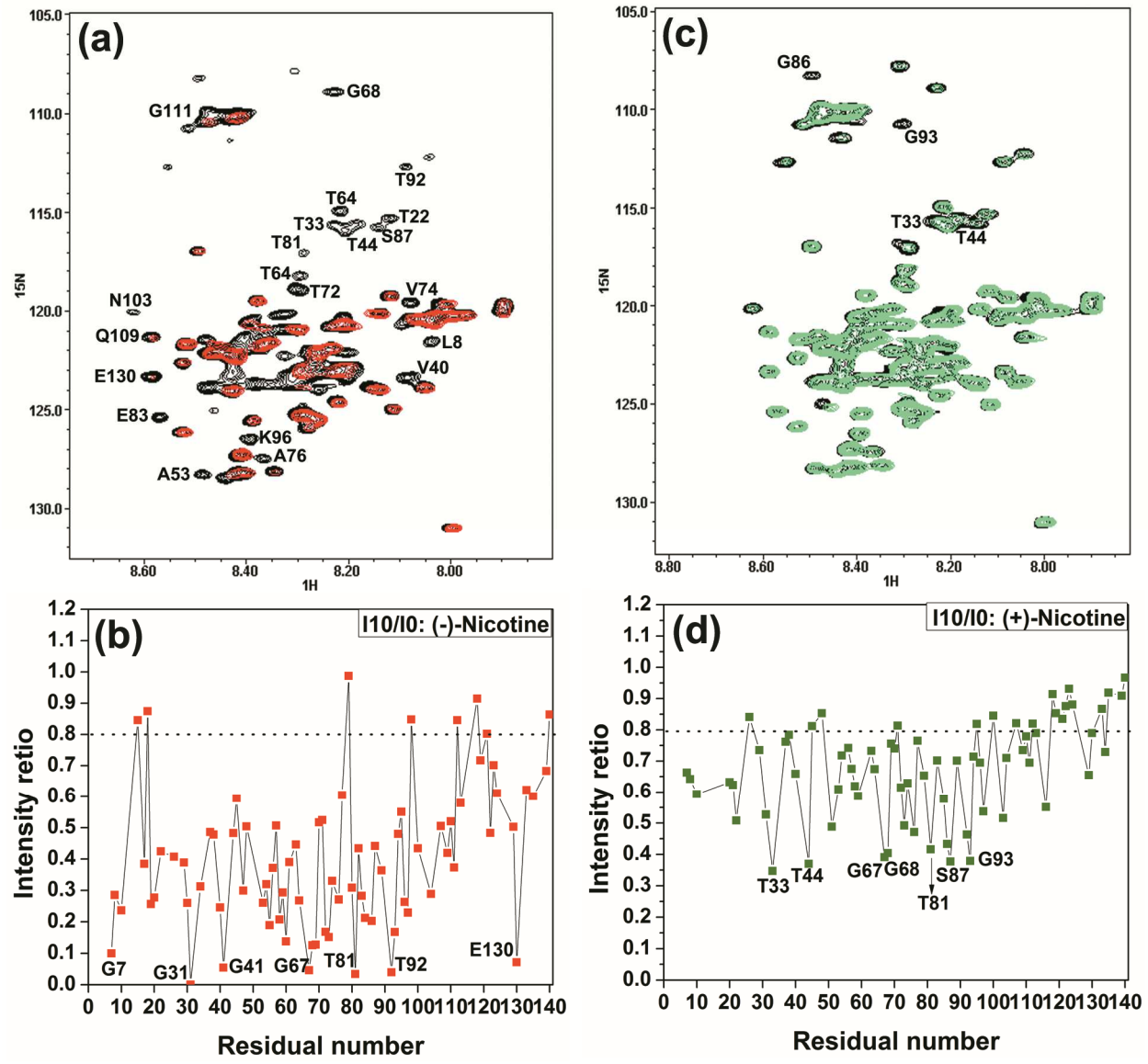

Figure 3.17 ^{1}H-^{15}N HSQC NMR spectra and relative peak intensities graph of AS in the presence of nicotine isomers. ^{1}H-^{15}N HSQC NMR spectrum of AS alone (black) (a,c) and in presence of the ratio of 1:10 (AS to (-)-nicotine) (red) (b) and the ratio of 1:10 (AS to (+)-nicotine) (c). Plot of the relative peak intensities of the HSQC cross peaks in the AS/(-)-nicotine (b) and AS/(-)-nicotine (d) complexes and free AS versus the amino acid sequence of AS. The baseline intensity ratio is 0.8 due to dilution upon addition of dopamine [Experiments performed by Dr. Sergiy Nokhrin].

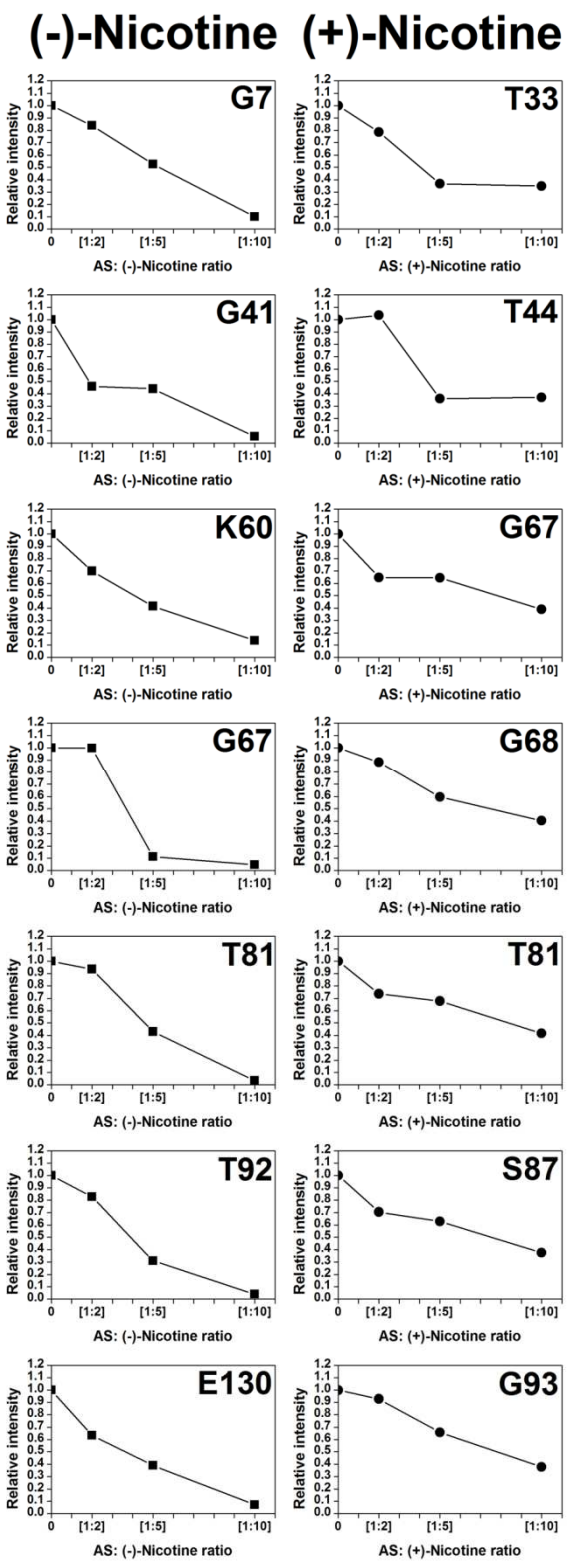

Figure 3.18 Relative signal intensities at three concentrations of (-)- and (+)-nicotine for selected residues as a function of the AS:nicotine ratio.

3.5 Interaction of copper and dopamine with alpha-synuclein

3.5.1 Introduction

Cu(II) and dopamine have an important role in PD. As a proof of concept, a comparison of Parkinsonian and age-matched control brain tissue showed a reduction in the Cu (II) content in the substantia nigra (SN) (Davies *et al.*, 2014; Dexter *et al.*, 1989; Riederer *et al.*, 1989). AS has an important role in dopamine homeostasis and is involved in almost all of the dopamine metabolism pathways including dopamine biosynthesis, storage of dopamine in synaptic vesicles, dopamine release in the response to an action potential and re-uptake of released dopamine from the presynaptic space (Lotharius and Brundin, 2002a; Stefanis, 2012; Yu *et al.*, 2005). Furthermore, the main feature of PD is aggregation of AS which results in AS malfunction and dopamine depletion. Thus dopamine replacement therapy is the main treatment for PD (Grosset *et al.*, 2009; Lotharius and Brundin, 2002a, b; Pahwa and Lyons, 2007; Yu *et al.*, 2005). Therefore the interaction of Cu(II) and dopamine with AS was studied using nanopore analysis, CD spectroscopy, ITC and NMR spectroscopy. In order to delineate the binding site of Cu(II) and dopamine, three segments of AS were analyzed.

3.5.2 Nanopore sensing of copper binding to AS

Figure 3.19 shows the current blockade histograms for wild type AS in the presence of 10 µM and 25 µM of Cu (II) and Mg (II) and also E46K in the presence of 10 µM and 25 µM of Cu (II). Mg(II) was used as the control, because AS has a specific binding site for Cu(II) at N-terminal and a general binding site at C-terminal which binds to Cu(II), Fe(II), Mn(II), Zn(II), Ni(II) and Co(II). Furthermore, no specific interaction between Mg (II) and AS has been reported (Binolfi *et al.*, 2012). Cu(II) alters the proportion of translocation and bumping events by increasing the percentage of the bumping peak in a concentration dependent manner (Figure 3.19b,c). At the concentration of 10 µM (Figure 3.19b) and 25 µM (Figure 3.19c) Cu(II) increases the bumping proportion to 45% and 65%, respectively. In contrast Mg(II) at the same concentrations (Figure 3.19d,e) causes a much smaller change in the peak intensities. This shows that the interaction of Cu(II) is specific and causes folding and compaction of AS. The E46K mutant was selected to be investigated by nanopore analysis as this mutation is close to the His50 residue which acts as an anchoring residue in the interaction of Cu(II) with AS (Binolfi *et al.*, 2012; Rose *et al.*, 2011). Adding Cu(II) to E46K causes a significant change in the peak intensities and at the concentration of 10 µM and 25 µM the majority of events are bumping and few translocation

events are observed (Figure 3.19g,h). This shows that the conformation of E46K is more sensitive to Cu(II) binding as compared to the AS wild type.

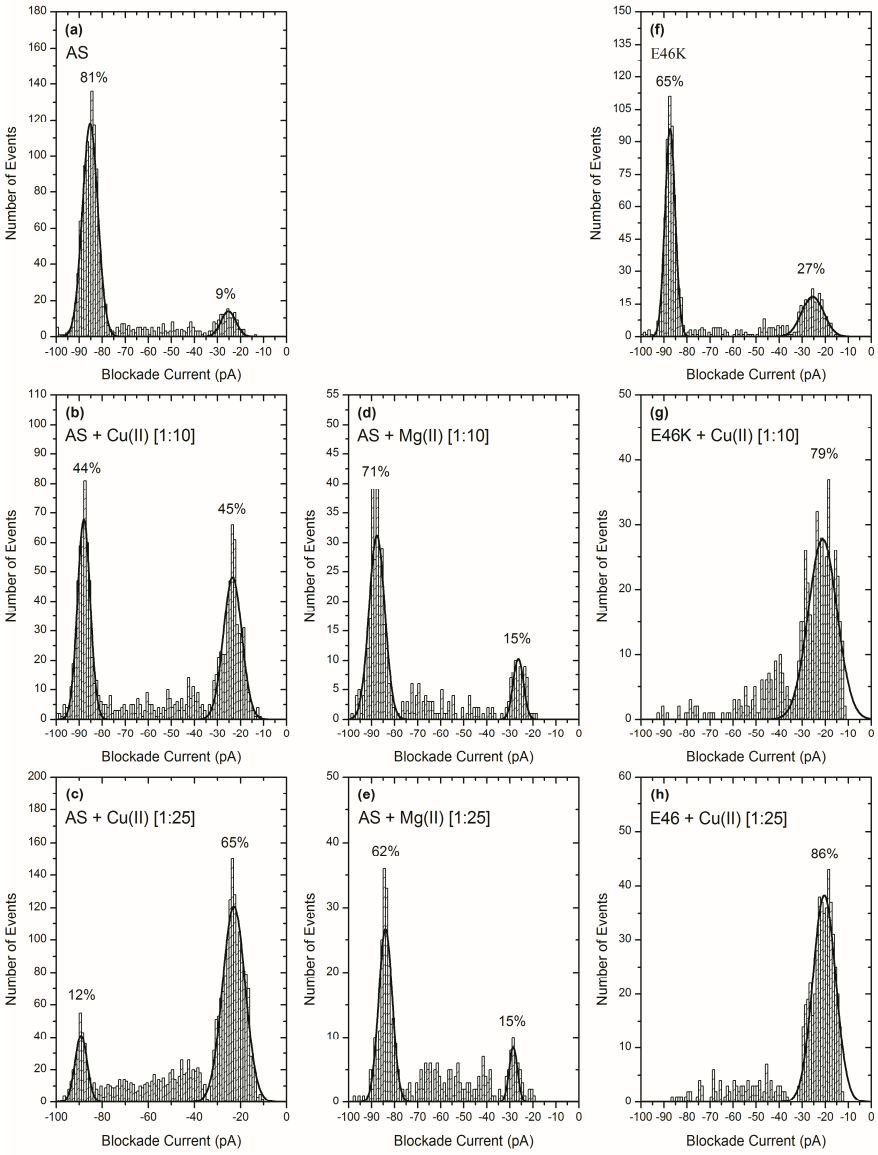

Figure 3.19 Blockade current histogram showing the interaction of Cu(II) and Mg(II) with AS and E46K mutant. (a, b, c) Blockade current histograms for AS with 0 μM, 10 μM and 25 μM Cu(II). (d, e) Blockade current histograms for AS with 10 μM and 25 μM Mg(II) (f,g, h) Blockade current histograms for E46K with 0 μM, 10 μM and 25 μM Cu(II).

3.5.2.1 Mapping of copper binding sites using nanopore analysis

Three peptides, the N-terminal (1-60), C-terminal (96-140) and ΔNAC have been used to map the Cu(II) binding site. For each peptide, nanopore experiments were performed at 10 μM and 25 μM Cu(II) (Figure 3.20). As shown in Figure 3.20a,b,c Cu(II) did not change the current

blockade profiles of AS(96-140) at 25 µM but it reduced the proportion of the bumping peak of the AS(1-60) peptide to 52% (Figure 3.20e) and 30% (Figure 3.20f) at 10 µM and 25 µM respectively. These results together show that AS(1-60) is the region of Cu(II) binding. Because the AS(1-95) lacks the C-terminal acidic tail of AS, was not electrophoretically driven through the pore and caused frequent blockage, the N-terminal binding site for Cu(II) was confirmed by doing nanopore experiments with ΔNAC. Cu(II) changes the intensity of the bumping and translocation peaks by increasing the proportion of bumping events in a concentration dependent manner (Figure 3.20h,i). There are also increases in the number of events with intermediate blockade currents which do not form a clear Gaussian peak but have been considered in the calculation of the peak magnitudes.

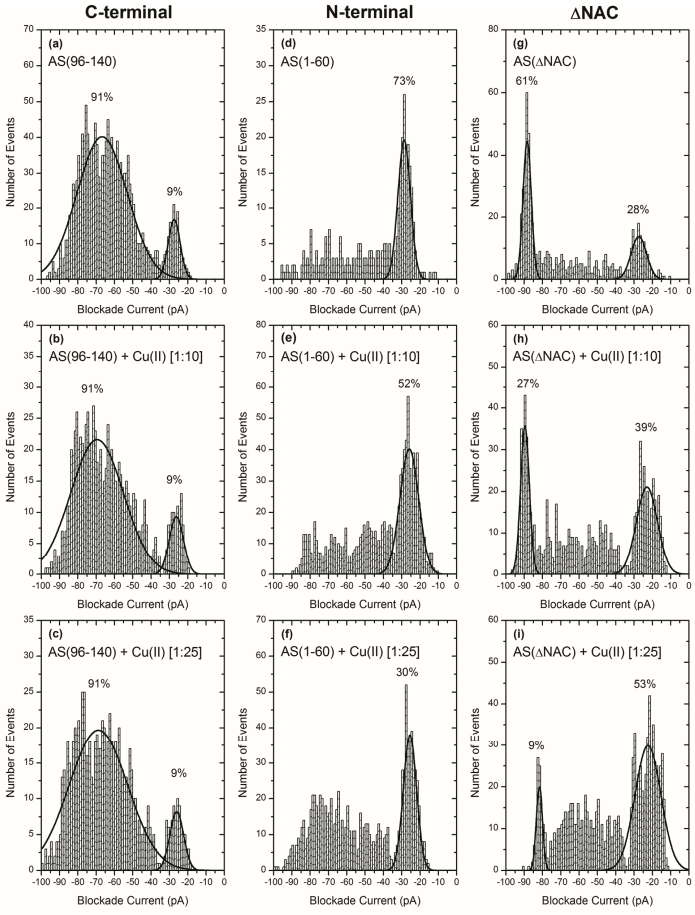

Figure 3.20 Blockade current profiles showing the interaction of Cu(II) with AS peptides (96-140, 1-60 and ΔNAC) (a, b, c) Blockade current histograms for AS (96-140) with 0 µM, 10 µM and 25 µM Cu(II). (d, e, f) Blockade current histograms for AS (1-60) with 0 µM, 10 µM and 25 µM Cu(II) (g, h, i) Blockade current histograms for AS ΔNAC with 0 µM, 10 µM and 25 µM Cu(II).

3.5.3 Nanopore sensing of dopamine binding to alpha-synuclein

In the presence of dopamine the translocation peak of AS which is centered at -85 pA (Figure 3.21a) shifts to lower blockade current (-80 pA) and also there is an increase in the intensity of the bumping peak (Figure 3.21b). For the A30P mutant in the absence of drug the majority of events (72%) are bumping (Figure 3.21c) and upon addition of 25 µM dopamine a new peak forms at -80 pA which includes the majority of the events (Figure 3.21d). The peaks at -80 pA represent a new conformation of AS and A30P induced by dopamine. To investigate if these peaks are still due to translocation of peptides through the pore, a voltage study was performed and the event parameters are summarized in Table 3.3. For both AS and A30P, increasing the applied voltage from 75 mV to 100 mV caused the average time for the peak centered at -80 pA to decrease which shows that these peaks are due to translocation. Figure 3.22 shows the blockade time profiles for the peak centered at -80 pA of AS at 75 mV (a) and 100mV (b) with average event times of 1.25 ms and 0.56 ms respectively (Table 3.3).

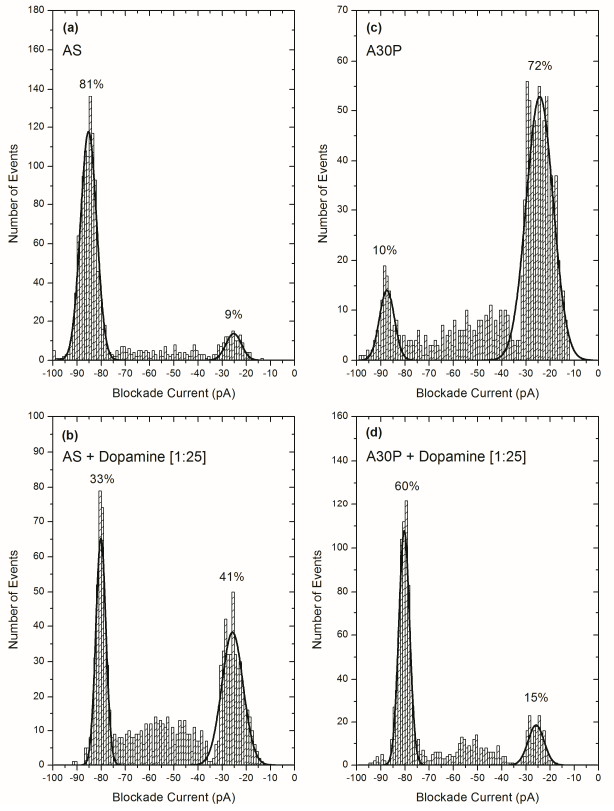

Figure 3.21 Blockade current profiles showing the interaction of dopamine with 1µM AS or A30P mutant. (a, b) Blockade current histograms for AS with 0 µM and 25 µM dopamine (c, d) Blockade current histograms for A30P with 0 µM and 25 µM dopamine.

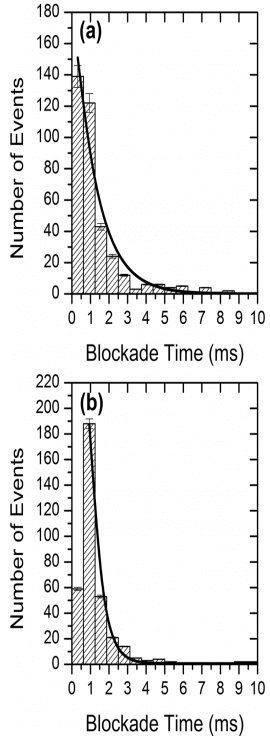

Figure 3.22 Blockade time profiles for AS in the presence of 25 μM dopamine. Profiles show the blockade times for the events at -80 pA at 75 mV (a) and 100 mV (b)

Table 3.3 Event parameters for the AS peptides (Wild type and A30P)

	I_{75} (pA)	I_{100} (pA)	T_{75} (ms)	T_{100} (ms)
AS	-63	-85	0.61	0.49
A30P	-62	-87	0.82	0.34
AS + Dopamine [1:25]	-59	-80	1.25	0.56
A30P + Dopamine [1:25]	-59	-80	0.63	0.54

I and T represent the intensity and duration of the current blockade. The subscripts 75 and 100 refer to translocation peak when 75 mV and 100 mV of voltage are applied respectively. (The error is estimated to be <±1 pA for I and <±10% for T)

3.5.3.1 Mapping of dopamine binding sites using nanopore analysis

Figure 3.23 shows the blockade current histograms of AS(96-140), AS(1-60) and AS(ΔNAC) in the absence and presence of 10 μM and 25 μM dopamine. For AS(96-140) dopamine changes the event profiles by increasing the proportion of bumping events and a simultaneous decrease of the proportion of translocation events (Figure 3.23b,c). In the case of AS(1-60), dopamine reduces the intensity of bumping peak centered at -25 pA in a concentration dependent manner

(Figure 3.23e,f). At the concentration of 10 µM a sharp intermediate peak also occurs at -45 pA (Figure 3.23e). The conformational change of AS(ΔNAC) in the presence of dopamine involves an increase in the proportion of bumping events. Events with intermediate current blockades were also found between -40 pA and -80 pA. These events did not show a Gaussian distribution and therefore were not fitted in the graphs (Figure 3.23h,i).

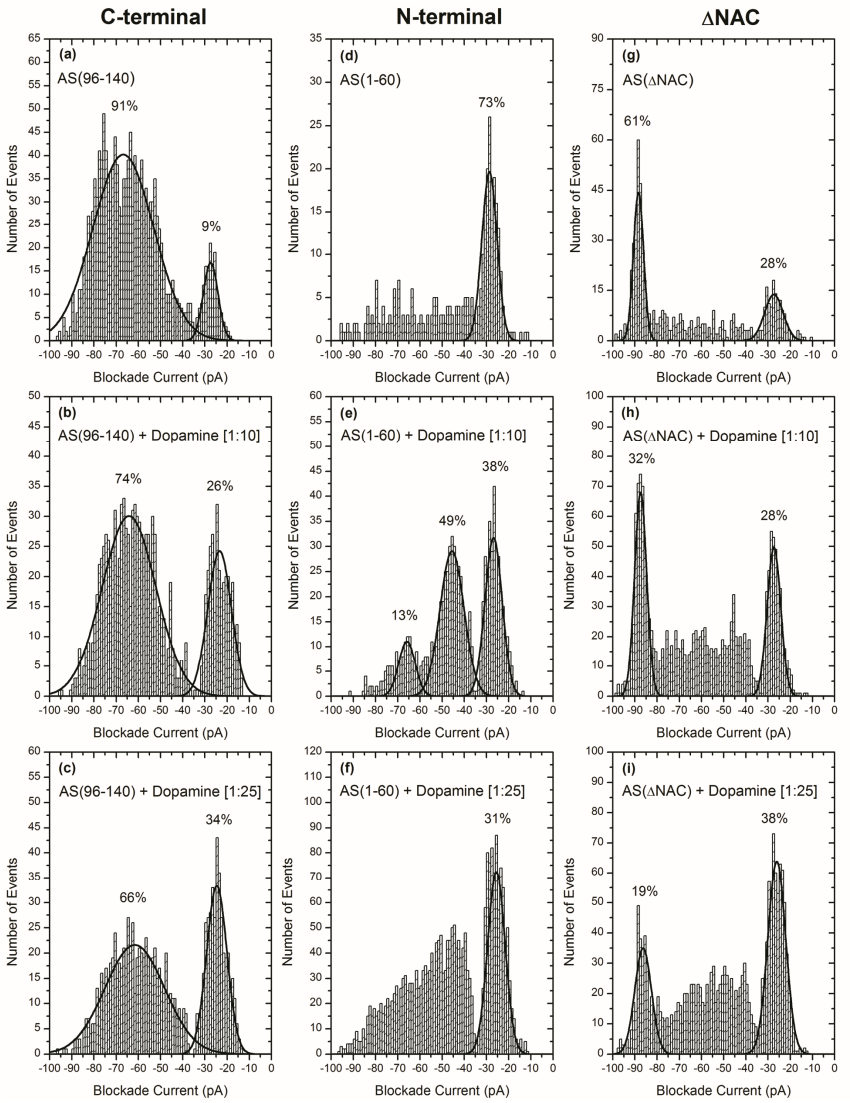

Figure 3.23 Blockade current profiles showing the interaction of dopamine with AS peptides (96-140, 1-60 and ΔNAC). (a, b, c) Blockade current histograms for AS (96-140) with 0 µM, 10 µM and 25 µM dopamine. (d, e, f) Blockade current histograms for AS (1-60) with 0 µM, 10 µM and 25 µM dopamine. (g, h, i) Blockade current histograms for AS ΔNAC with 0 µM, 10 µM and 25 µM dopamine.

3.5.4 Study of the interaction of Cu(II) and dopamine with AS

Nanopore experiments were also performed in the presence of both ligands to investigate whether the binding sites for Cu(II) and dopamine are independent. Figure 3.24 shows the nanopore analysis of AS in the presence of different ratios of Cu(II) and dopamine. The current blockade histogram of AS in the presence of 10 µM Cu(II) and 25 µM dopamine (Figure 3.24e) shows three peaks centered at -25 pA, -47 pA and -80 pA. The peak at -47 pA was not observed in the presence of 10 µM Cu(II) (Figure 3.19b,3.24c) or 25 µM dopamine (Figure 3.21b,3.24b) and is a new peak of events with intermediate current blockade that suggests a new conformation of AS upon binding to both Cu(II) and dopamine. Upon adding 25 µM of Cu(II) and dopamine, two intermediate peak found between -35pA and -80 pA and the proportion of the bumping peak increased from 26% to 39% with a simultaneous reduction in the intensities of the intermediate and translocation peaks.

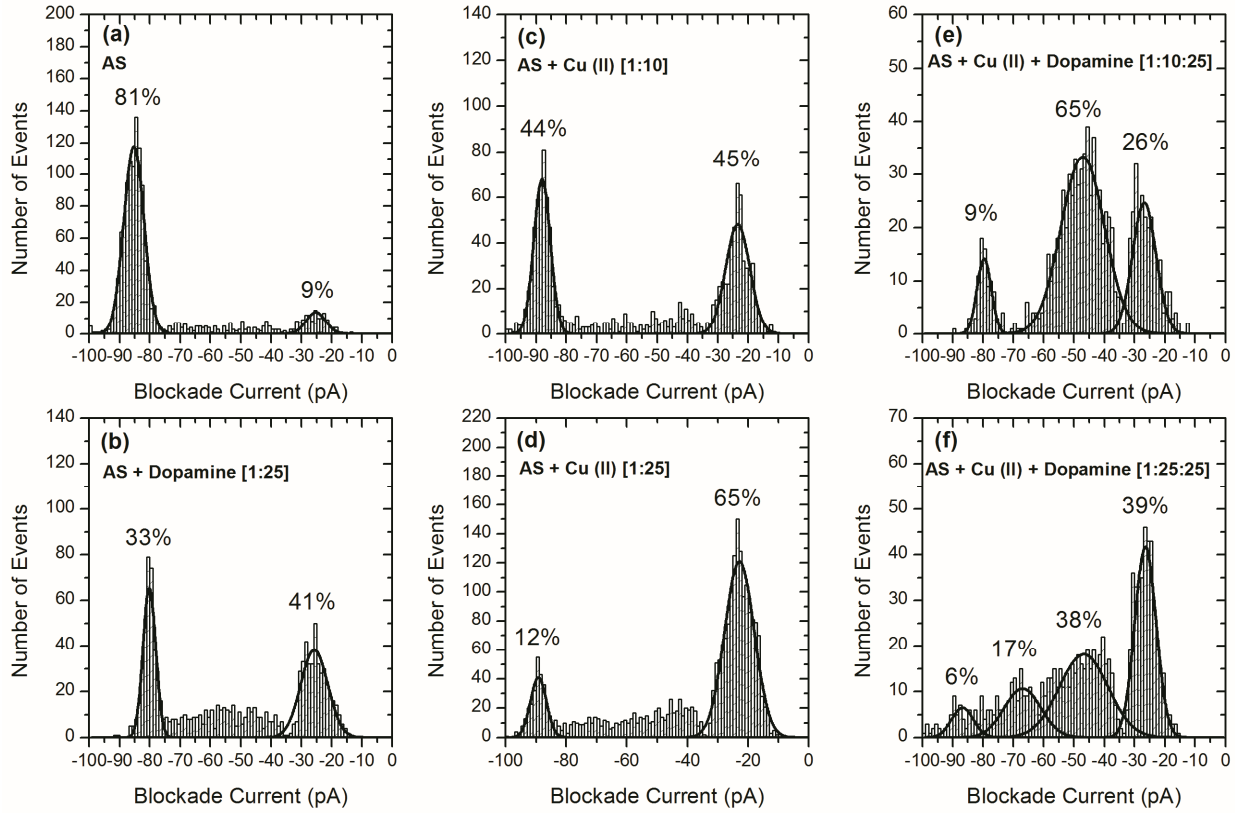

Figure 3.24 Blockade current profiles showing the interaction of Cu(II) and dopamine with AS. Blockade current histogram for AS (a) and AS with; 25 µM dopamine (b), 10 µM Cu(II) (c), 25 µM Cu(II) (d), 10 µM Cu(II) and 25 µM dopamine (e) and 25 µM Cu(II) and 25 µM dopamine.

3.5.5 Circular dichroism of the alpha-synuclein-dopamine interaction

The binding of dopamine to AS wild type and A30P mutant was investigated by CD. As shown in Figure 3.25 the CD spectra of both wild type (Figure 3.25a-black line) and A30P mutant (Figure 3.25b-black line) is typical for random coil conformation with a maximum ellipticity at 200 nm and lacks the α-helical and β-sheet characteristic bands in the 210–230 nm region (Serpell *et al.*, 2000; Uversky *et al.*, 2001b; Weinreb *et al.*, 1996; Zheng *et al.*, 2013). Dopamine at the concentrations of 10 µM and 25 µM didn't change the secondary structure content of AS and the resulted spectra (Figure 3.25a,b) are still mostly random coil conformation.

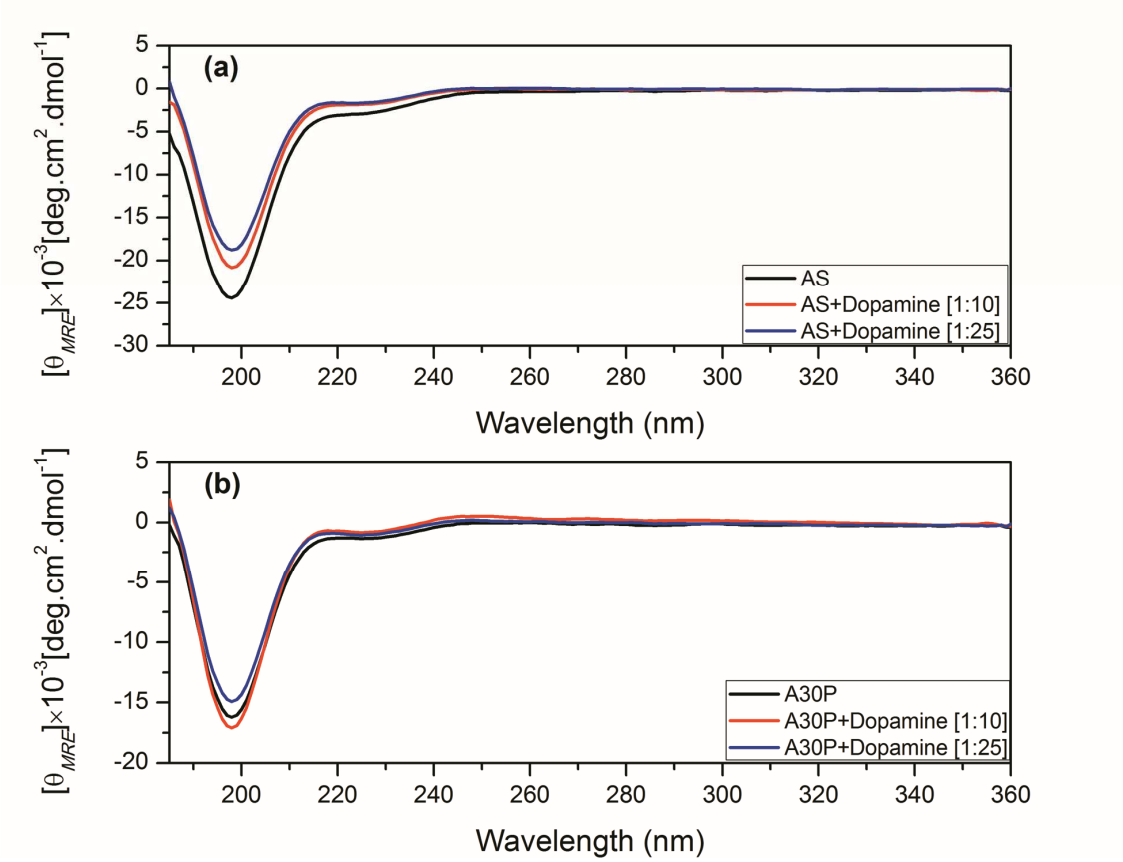

Figure 3.25 CD spectra for AS and A30P mutant in the presence of dopamine. (a) CD spectra for full length AS (black) and in the presence of 50 µM (red) and 125 µM (blue) of dopamine. (b) CD spectra for full length mutant A30P (black) and in the presence of 50 µM (red) and 125 µM (blue) of dopamine.

3.5.6 ITC of alpha-synuclein-dopamine interaction

ITC has been used to measure the K_d of AS and dopamine interaction in both nanopore (1 M KCl, 10 mM HEPES-KOH, pH 7.8) and NMR (0.5x PBS) buffers. The best fit to the experimental points was obtained with a single binding site model (i.e. n=1) and a K_d of (2.85 ±0.01) × 10^{-4}M was measured under ionic conditions used for performing both nanopore analysis (Figure 3.26a,b) and NMR spectroscopy (Figure 3.26c,d).

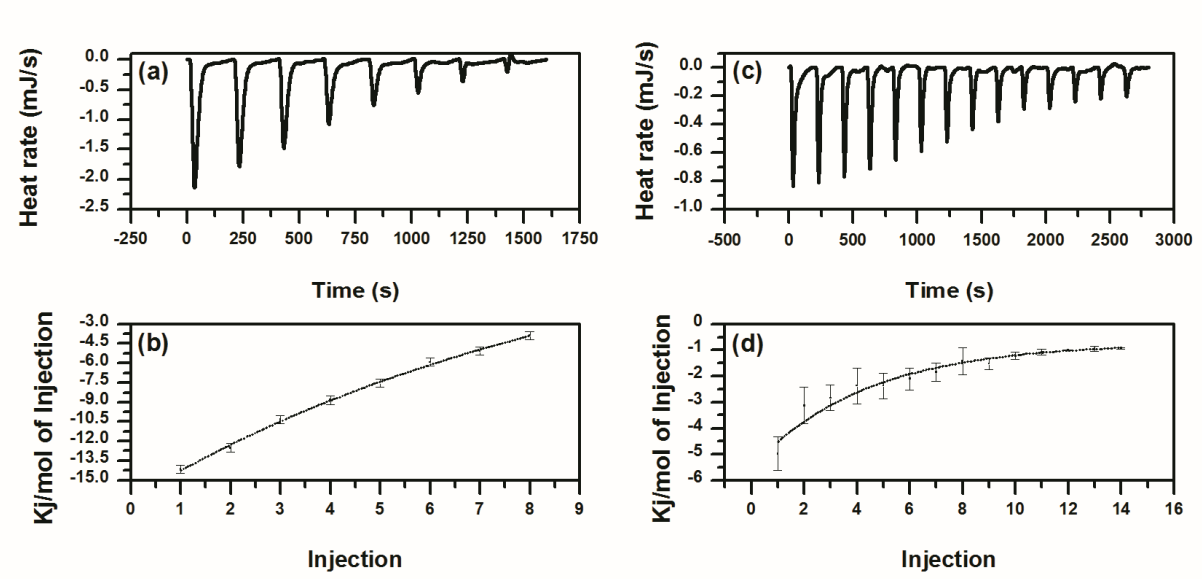

Figure 3.26 (a,b) Calorimetric characterization of the interactions between dopamine and AS in a buffer containing 1 M KCl and 10 mM HEPES-KOH, pH 7.8. Data is fitted with the one-site model which corresponds to "n=1" and $K_d = 2.85\times10^{-4}$ M. (c,d) Calorimetric characterization of the interactions between dopamine and AS in 0.5xPBS. Data is fitted with the one-site model which corresponds to "n=1" and $K_d = 2.85\times10^{-4}$ M.

3.5.7 HSQC-NMR of alpha-synuclein-dopamine interaction

Primary NMR spectroscopy experiments were performed in a buffer containing 5% glycerol and 0.05% BOG. The resulting $^{1}H,^{15}N$-HSQC NMR spectra were well dispersed but no significant change was observed upon addition of dopamine which showed that BOG interferes with the binding of dopamine. Therefore NMR experiments were performed without adding BOG to the buffer. As show in Figure 3.27a the ^{1}H-^{15}N HSQC NMR spectrum of AS alone (black) is characteristic of unfolded proteins because it is not as well resolved with some line-

broadening and peak overlap. At a ratio of 1:25 (AS to dopamine) (red) most of the peaks such as L8, T22, T33, G41, V63, G67, G68,T92, G106, M116, D135 and E137 underwent a reduction in their intensities. The changes in residue intensities are summarized in Figure 3.27b which is a plot of the relative peak intensities, I/I_0 (I_{bound}/I_{free}), of the HSQC cross peaks in the AS/dopamine complex and free AS versus the amino acid sequence of AS. Furthermore a few peaks (L8, G106 and E137) shifted in the presence of dopamine and their chemical shift perturbations are shown in Figure 3.27c,d,e. The changes in the intensity ratio as a function of drug concentration are described in Figure 3.28 for well-resolved residues (G41, G67, G68 and G106) and show that titration of AS with increasing concentrations of dopamine causes a gradually decrease of residue intensity. This shows that this interaction is concentration dependent.

Previously it has been demonstrated that in the presence of negatively charged lipids, the first 100 residues of AS interact with the surface of micelles and adopt an α-helical conformation. However because of the size of the micelles, these residues disappeared from the spectrum (Chandra *et al.*, 2003; Davidson *et al.*, 1998; Georgieva *et al.*, 2008; Jao *et al.*, 2008; Ulmer *et al.*, 2005a). Figure 3.29a shows the ^{1}H-^{15}N HSQC NMR spectrum of AS alone (black) and in presence of 0.02% LPPG (green) (a). The peaks of the first 100 residues of AS became "invisible" by NMR and the visible peaks are from the last 40 residues of AS. Adding dopamine at the ratio of 1:10 (AS to dopamine) to the experiment (red) (Figure 3.29b) didn't change the spectrum and shows that LPPG interferes with binding of dopamine to AS. The chemical shifts plot of the HSQC cross peaks in the AS/dopamine/LPPG complex and free AS is shown in Figure 3.29c. This graph shows that E110, E114, and E137 are significantly shifted compared to the AS alone.

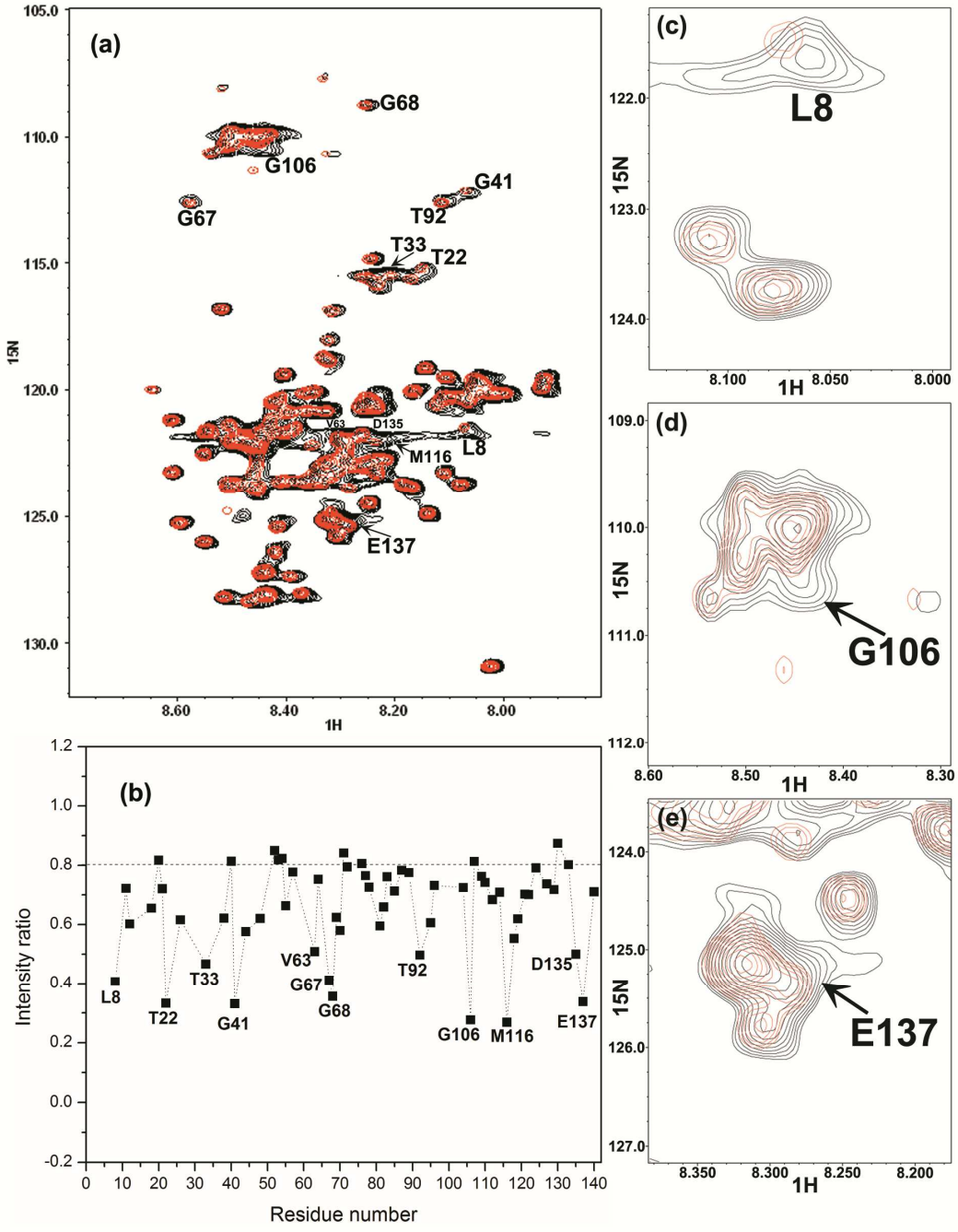

Figure 3.27 ^{1}H-^{15}N HSQC NMR spectrum and relative peak intensities graph of AS in the presence of dopamine. (a) ^{1}H-^{15}N HSQC NMR spectrum of AS alone (black) and in presence of the ratio of 1:25 (AS to dopamine) (red) (b) Plot of the relative peak intensities of the HSQC cross peaks in the AS/dopamine complex and free AS versus the amino acid sequence of AS. The baseline intensity ratio is 0.8 due to dilution upon addition of dopamine. (c, d, e) Expanded view of the chemical shifts for residues L8, G106 and E137 [Experiments performed by Dr. Sergiy Nokhrin].

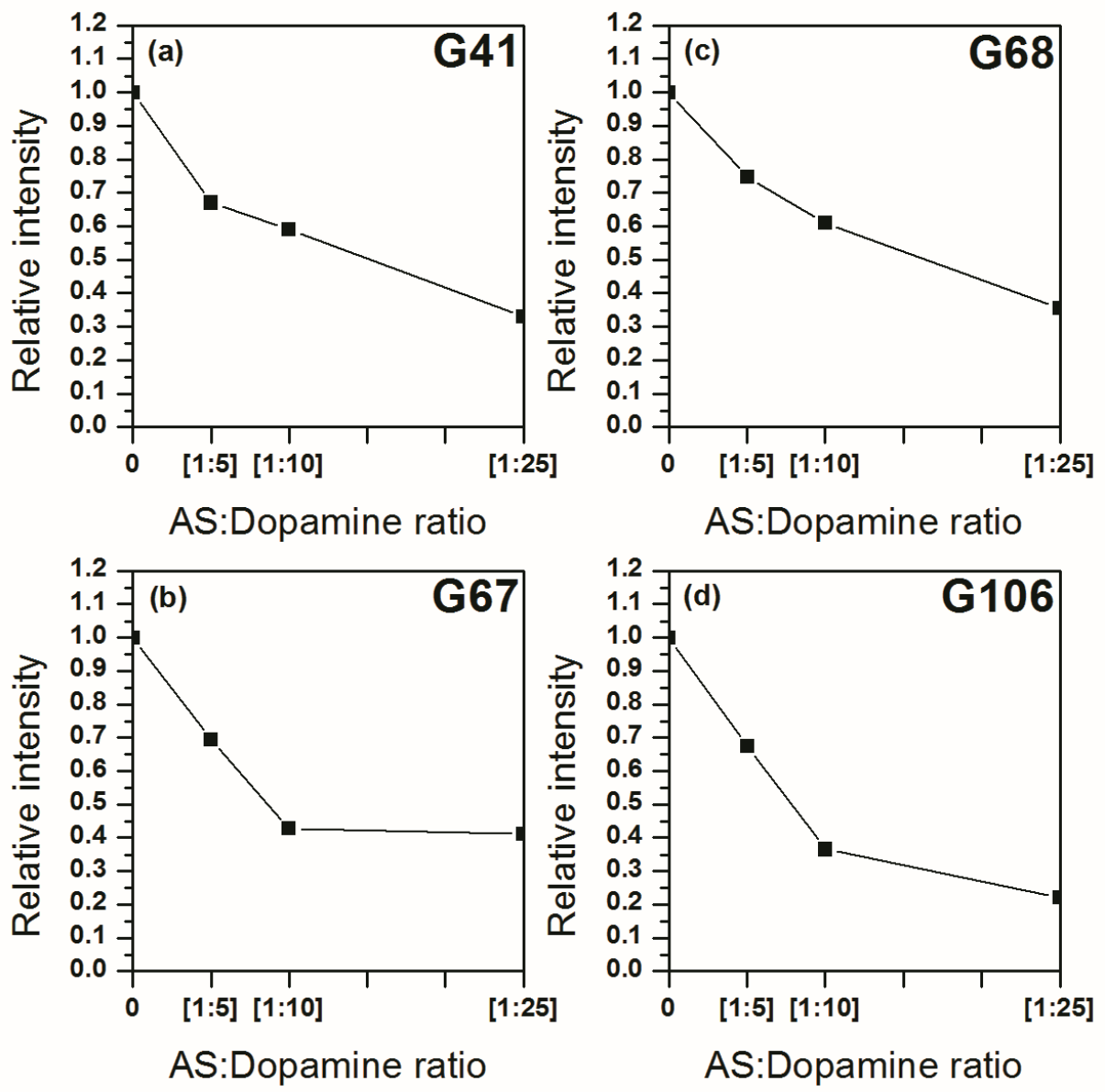

Figure 3.28 Relative signal intensities at three concentrations of dopamine for selected residues as a function of the AS:dopamine ratio. (a) G41 (b) G67 (c) G68 (d) G106.

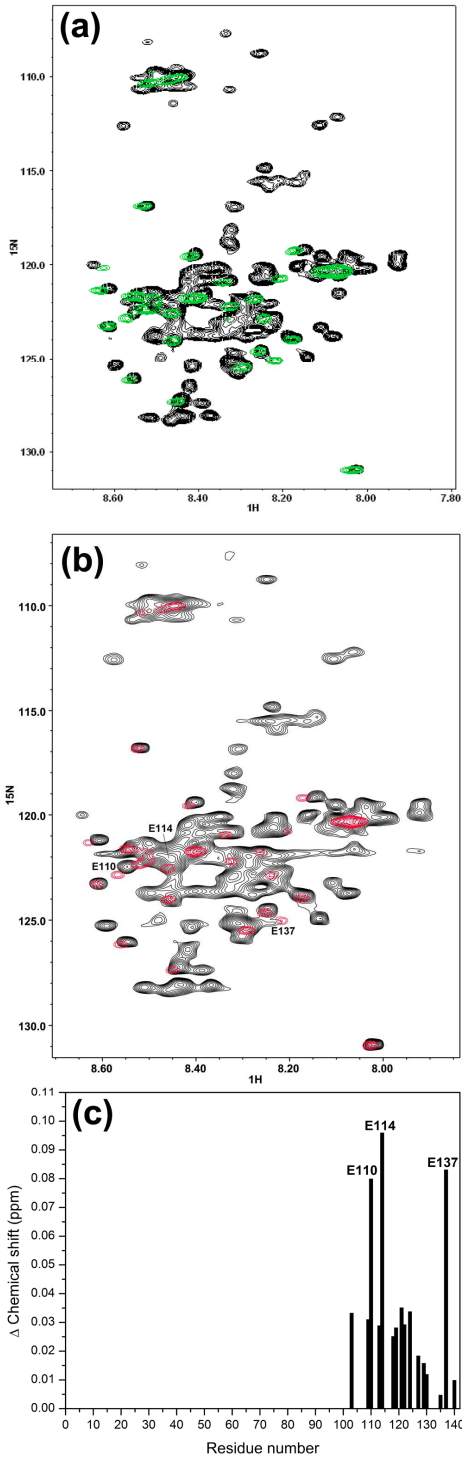

Figure 3.29 ^{1}H-^{15}N HSQC NMR spectrum and chemical shift graph of AS in the presence of LPPG and dopamine. (a) ^{1}H-^{15}N HSQC NMR spectrum of AS alone (black) and in presence of 0.02%LPPG (green) (b) ^{1}H-^{15}N HSQC NMR spectrum of AS alone (black) and in presence of 0.02%LPPG and at the ratio of 1:10 (AS to dopamine) (red) (c) Plot of the chemical shifts of the HSQC cross peaks in the AS/dopamine/LPPG complex and free AS versus the amino acid sequence of AS [Experiments performed by Dr. Sergiy Nokhrin].

3.6 Other drugs and natural small molecules

The nanopore analysis, NMR spectroscopy and ITC showed that nicotine has high affinity for AS and caused a significant change in AS conformation. In order to find another effective chemical, the interactions of other natural products, caffeine and curcumin, with AS have been studied using nanopore analysis. Epidemiological studies suggested that both caffeine and nicotine intake is associated with lower incidence of PD (Altman *et al.*, 2011; Ascherio and Chen, 2003; Darvesh *et al.*, 2012; Mythri and Bharath, 2012; Postuma *et al.*, 2012; Ross *et al.*, 2000).

3.6.1 Caffeine and Curcumin

Figure 3.30 shows the blockade current histograms of AS in the presence of 5 µM and 10 µM of caffeine and curcumin. Both caffeine and curcumin cause a shift in the AS translocation peak from -86 to lower blockade currents between -70 to -80 pA and also change the intensity of bumping and translocation peaks (Figure 3.30). In the presence of 5 µM caffeine there are two peaks centered at -78 pA and -35 pA with intensities of 44% and 38% respectively (Figure 3.30b). By increasing the concentration of caffeine to 10 µM, 93% of events formed a peak at -76 pA and a few events observed with lower current blockades (Figure 3.30d). Adding 5µM curcumin to AS results in two peaks centered at -70 pA and -29 pA with intensities of 38% and 57% (Figure 3.30c). In the presence of 10µM of curcumin there are two peaks centered at -79 pA and -31 pA with intensities of 53% and 37% (Figure 3.30e).

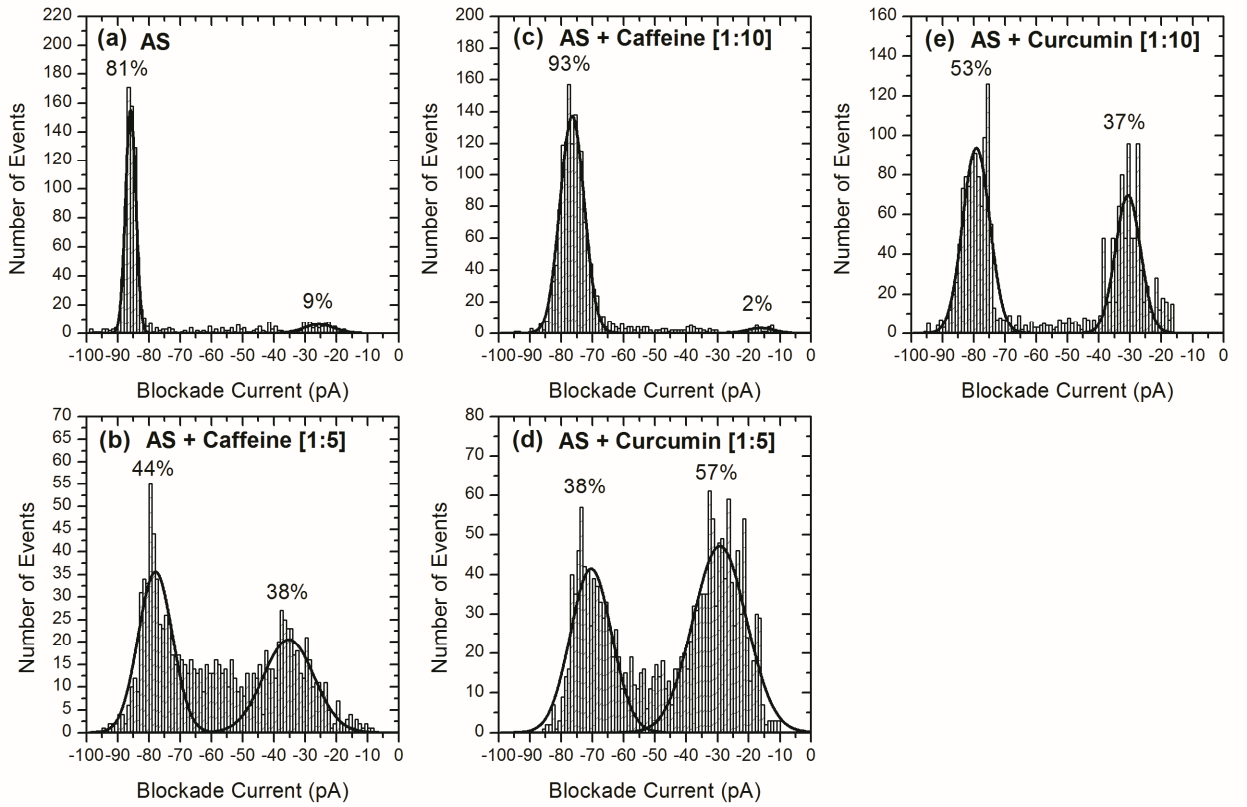

Figure 3.30 Blockade current profiles showing the interaction of caffeine and curcumin with AS. AS (a) and AS to caffeine ratio: (b) 1:5, (c) 1:10 and AS to curcumin ratio: (d) 1:5, (e) 1:10. [Experiments performed by Joe Kakish]

3.6.2 Binding of caffeine and (-)-nicotine simultaneously

Our results showed that (-)-nicotine (Figure 3.31b) and caffeine (Figure 3.31c) at the concentration of 10 μM shifted the AS translocation peak (Figure 3.31.a) from -86 pA to -60 pA and -80 pA respectively. To investigate the effect of these small molecules on the AS conformation a nanopore experiment has been done in the presence of 5 μM of each molecule (Figure 3.31d). The blockade current histogram showed an increase in the intensity of the peak centered at -25 pA when both drugs are present (Figure 3.31d) in comparison with (-)-nicotine (Figure 3.31b) and caffeine experiments (Figure 3.31c) and also the intermediate peaks in the presence of nicotine and caffeine were disappeared (Figure 3.31b,c).

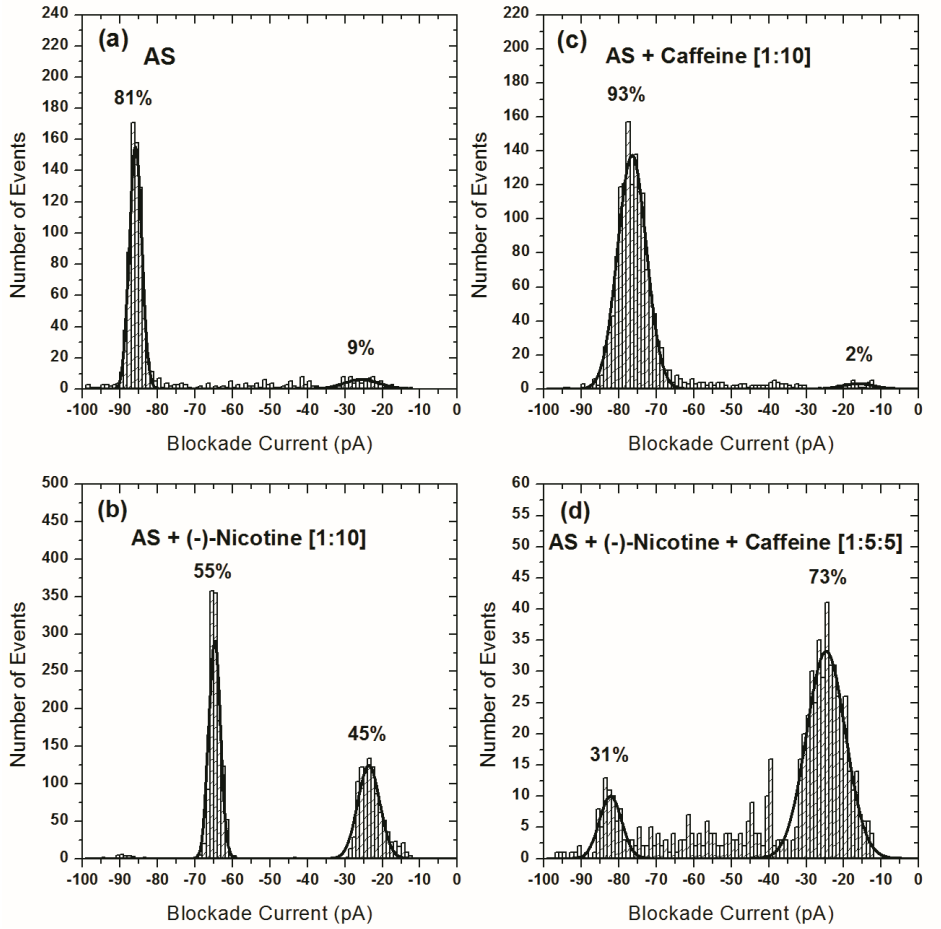

Figure 3.31 Blockade current profiles showing the interaction of (-)-nicotine, caffeine and their synergic effect with AS. AS (a) and AS to (-)-nicotine ratio: (b) 1:10, AS to caffeine ratio: (c) 1:10, synergic experiment with AS to (-)-nicotine to caffeine ratio: (d) 1:5:5. [Caffeine experiment (Part b) performed by Joe Kakish]

4 DISCUSSION

4.1 Biophysical study of AS-ligand interaction

4.1.1 Introduction

Nanopore analysis was the primary technique used in this thesis to characterize the partially folded intermediate conformations of AS. The concentration of AS used to perform the nanopore experiments was 1 µM whereas classical techniques such as NMR spectroscopy require at least 50 µM of AS (Maltsev *et al.*, 2012). Working with low concentrations of AS reduces the chance of AS oligomerization and aggregation which occur at high concentrations of AS (Fink, 2006; Wood *et al.*, 1999). Interestingly, the total concentration of AS in dopaminergic neurons has been measured to be 6 µM (Cremades *et al.*, 2012; Iwai *et al.*, 1995) which is the same order of magnitude as the concentrations used in nanopore experiments. Thus the nanopore analysis results have more relevance to the physiological conditions as compared with the classical methods. Nanopore analysis is a single molecule technique which has been successfully used to study the conformational changes of unfolded proteins such as prion peptides (Madampage *et al.*, 2010; Madampage *et al.*, 2013a; Madampage *et al.*, 2013b; Stefureac *et al.*, 2010), β-amyloid (Asandei *et al.*, 2013; Wang *et al.*, 2011a) and AS (Wang *et al.*, 2013). Other examples of single molecule techniques which have been successfully used in studying the conformation of unfolded proteins are single-molecule force spectroscopy (SMFS) and Single-Molecule Förster Resonance Energy Transfer (FRET) (Brucale *et al.*, 2014; Hoffmann *et al.*, 2013). As single molecule techniques overcome the limitations of classical methods, *i.e.* averaging of time and ensemble signals, they have been widely used to study unfolded proteins (Hoffmann *et al.*, 2013). The main advantage of these techniques is their ability to study single monomers in a real-time scale and avoid the averaging of ensembles (Brucale *et al.*, 2014; Hoffmann *et al.*, 2013). The ability to individually recognize molecules within a population at the maximum possible temporal resolution makes them a useful tool to study the early stages of the aggregation process (Hoffmann *et al.*, 2013). Although single molecule techniques have the ability of monitoring individual molecules one at a time, nanopore analysis has features which make it more feasible for studying protein misfolding (Hoffmann *et al.*, 2013; Madampage *et al.*, 2011). The main advantage of nanopore analysis is that this technique does not require any labeling or chemical modification of proteins whereas FRET and SMFS do require chemical modifications

(Brucale *et al.*, 2009; Brucale *et al.*, 2014; Ferreon *et al.*, 2012; Hoffmann *et al.*, 2013; Sandal *et al.*, 2008; Trexler and Rhoades, 2010a). For example, FRET requires a donor–acceptor dye pair attached to the unfolded proteins and SMFS samples must have an atomic force microscopy (AFM) tip and surface or bead and surface attachments (Brucale *et al.*, 2014; Hoffmann *et al.*, 2013). Thus the ability of nanopore analysis in detecting unmodified proteins makes this technique a faster and lower cost technique as compared to FRET and SMFS. Another benefit of nanopore analysis is the possibility of studying oligomers and aggregates by using artificial pores with different diameters (Hoffmann *et al.*, 2013; Yusko *et al.*, 2011).

One challenge that has been discussed by Hoffmann *et al.* in a review is the possibility of undesired interaction between the protein sample and lipid surfaces (Hoffmann *et al.*, 2013). To eliminate any noise arising from the undesired interaction between AS and the lipid used to set up the nanopore experiments, a control was set up with 0.35 mg of 1,2-diphytanoyl-sn-glycero-3-phosphocholine (DPhPC) micelles and wild type AS (Figure 3.1c). Our control experiment was in agreement with previous work (Wang *et al.*, 2013) and showed no interaction between DPhPC and AS. Further control experiments were performed by adding the drugs into the nanopore cup to investigate any noise arising from the interaction of the drugs with αHL pore. After making sure that the drug does not alter the event profile, AS was added to the cup. Also to eliminate any metal contaminations (Krasniqi and Lee, 2012), experiments were performed in the presence of 1 mM EDTA which chelates any unwanted divalent metals (Figure 3.1b).

Another challenge which has been discussed by Hoffmann *et al.* is that "*it can be difficult to relate blockade currents to structures, especially when the possible structures are themselves unknown*" (Hoffmann *et al.*, 2013). First, it can be argued that this is also true for the other single molecule techniques. Second, structural information is available for nanopore analysis. Nanopore analysis signals or events arise from the interaction of the analyte with the αHL pore leading to a reduction of the baseline ionic current due to partial or complete occupation of the pore which is called the current blockade (Figure 2.3) (Brucale *et al.*, 2014; Christensen *et al.*, 2011; Iqbal and Bashir, 2011; Ma and Cockroft, 2010; Meng *et al.*, 2010a; Mulero *et al.*, 2010; Sutherland *et al.*, 2004; Wang *et al.*, 2010a). Quantitative parameters of the blockade, such as its duration (T) and amplitude (I) depend on the structure of the analyte and are signatures for each analyte (Figure 2.3) (Brucale *et al.*, 2014; Christensen *et al.*, 2011; Meng *et al.*, 2010a; Stefureac *et al.*, 2008; Stefureac and Lee, 2008; Stefureac *et al.*, 2010; Sutherland *et al.*, 2004; Wang *et al.*,

2010a). In the nanopore experiments performed for AS, the T and I values have been measured for translocation and bumping peaks to investigate the conformational changes of AS under different conditions. Furthermore, the changes of the intensity of bumping and translocation peaks have been measured to compare the conformational changes in different conditions. CD and NMR spectra of AS have shown the random coil or unstructured conformation for AS (Figure 3.10, 3.14, 3.17a,c, 3.25a, 3.27a and 3.28a) which were in agreement with previous work (Antony *et al.*, 2003; Cappai *et al.*, 2005; Chandra *et al.*, 2003; Goers *et al.*, 2003; Lendel *et al.*, 2009; Maltsev *et al.*, 2011; Outeiro *et al.*, 2009; Rao *et al.*, 2008; Serpell *et al.*, 2000; Sung and Eliezer, 2007; Uversky *et al.*, 2001b; Weinreb *et al.*, 1996; Wu *et al.*, 2008; Yu *et al.*, 2012; Zheng *et al.*, 2013). As this protein has a random coil conformation, the blockade current histogram of AS wild type showed a significant peak at -85 pA (Figure 3.2a). Furthermore voltage studies were performed at two voltages and showed that this peak is due to translocation of the AS monomers through the αHL pore. Mutants of AS (A30P, E46K and A53T) also were studied (Figure 3.2) and the quantitative parameters of the peaks centered at -25 pA and -85 pA were measured (Table 3.1). For all peptides the T values for the peak centered at -25 pA were less than the T values for the peak at -85 pA. As the bumping events are due to the blockage of the ionic flow by compact conformations for a short time (Christensen *et al.*, 2011; Meng *et al.*, 2010a; Stefureac and Lee, 2008; Stefureac *et al.*, 2010), the peak centered at -25 pA represent the bumping peak. However, voltage studies of the peak at -85 pA showed that by increasing the voltage the average time decreases which means that the protein is being electrophoretically driven through the pore as has been shown for other proteins (Jetha *et al.*, 2013; Krasniqi and Lee, 2014; Madampage *et al.*, 2011; Wang *et al.*, 2013). Thus, the peaks centered at -85 pA in the blockade histograms of the AS mutants are also due to the translocation of these peptides through the pore. As the net charge of the mutant E46K is -7 it has the longest translocation time at 100mV. The other two mutants (A53T A30P) and the wild type have a strong overall negative charge (-9) and their average translocation time is less than E46K (Table 3.2). The blockade current histograms of AS wild type and mutants were different and clearly demonstrate the conformational heterogeneity among the wild type and mutants (Figure 3.2). Previous work with SMFS also showed that the wild type and mutants of AS have different conformations (Brucale *et al.*, 2009; Sandal *et al.*, 2008). They have found that the conformation of the AS mutants are more compact as compared to the AS-wild type. This is in agreement with our nanopore results

which showed that the blockade current histograms of AS mutants contain significantly more bumping events than the AS wild type. Moreover, mutants A30P and A53T show similar conformational properties with some differences in the proportion of bumping and translocation events (Figure 3.2). As a proof of concept, the SMFS results also showed that A30P and A53T have a similar conformation that is significantly different from that of wild type and the E46K (Brucale *et al.*, 2009; Sandal *et al.*, 2008). Thus Hoffmann *et al.* may be correct but detailed conformation information also cannot be extracted from other single molecule techniques.

Wang *et al.* (2013) used the αHL pore to investigate AS fibrillization. Their experimental set up was the same as our nanopore experiments; a voltage of 100 mV was applied and both the αHL and the AS were added to the *cis* side (Wang *et al.*, 2013). Although they recorded the typical translocation events with a magnitude of 85 pA, the way that they processed and interpreted the collected data was different from our methods. Normally the open pore current level is considered as the baseline (in our experiments at 100 pA) (Figure 2.3a,b,c,d) (Christensen *et al.*, 2011; Krasniqi and Lee, 2012; Krasniqi and Lee, 2014; Krasniqi *et al.*, 2012; Madampage *et al.*, 2013a; Madampage *et al.*, 2013b; Meng *et al.*, 2010a; Stefureac *et al.*, 2008; Stefureac *et al.*, 2010) but in this paper a second baseline also was recognized at 20 pA. They believed that the interaction of AS with the pore is a two step process and causes two drops in the first baseline, *i.e.* the open pore current level. They showed that the first drop of current from the primary baseline (100 pA) to the secondary baseline (20 pA) is due to the capture of AS into the vestibule of the pore. The next drop occurs from the second baseline (20 pA) to 15 pA due to translocation of AS monomers from vestibule to the trans side (Wang *et al.*, 2013). The overall interaction of AS wild type with αHL causes a total blockade with the magnitude of 85 pA due to translocation of AS which is in agreement with our experiments. In our data processing, we measured the total current blockade from the open pore current level to 15 pA which is consistent with their reports.

Recently Gurnev *et al.* (2014) used nanopore analysis to study the AS conformation but indicated that they were not able to detect any blockages upon addition of the AS into the *cis*-side, even at voltages up to 100 mV of both polarities (Gurnev *et al.*, 2014). Wang *et al.* (2013) and our nanopore experiments showed that AS is electrophoretically driven through the αHL pore due to its negative net charge (-9). The main problem of this paper is that their αHL stock solution contained 8 M urea (Gurnev *et al.*, 2014) which results in structural change to the αHL

(Pastoriza-Gallego *et al.*, 2007). Thus αHL which was added to the *cis* side was already denatured and this might be the reason for the unsuccessful detection of an AS blockade from the *cis* side. The poor interaction of AS with the *cis* side of the pore might be due to contamination or low purity of the sample. They also suggest that AS binds to the membrane but our control shows that this is wrong. To ensure that AS does not bind to the 1,2-diphytanoyl-sn-glycero-3-phosphocholine (DPhPC) the following control was performed (Figure 3.1c). AS was incubated with 0.35 mg of DPhPC micelles and the sample was added to the *cis* side of the cup. The event profile of AS (Figure 3.1b) in the presence of 0.35 mg of DPhPC was unchanged (Figure 3.1c). Furthermore it has been demonstrated previously that AS does not bind to phosphatidylcholine (PC) but has the ability to bind acidic phospholipids such as phosphatidylinositol (PI), phosphatidylserine (PS) and phosphatidic acid (PA) (Davidson *et al.*, 1998; Jo *et al.*, 2000).

Natively unstructured proteins such as AS and β-amyliod (Aβ) are very sensitive to their environment. Environmental modification such as exposure to toxins or drugs folds these proteins into partially folded intermediates, a process which is called misfolding (Fink, 2006; Uversky *et al.*, 2001a). These intermediates can oligomerize and eventually form aggregates which are associated with the pathology of neurodegenerative diseases such as PD and Alzheimer disease (Finder and Glockshuber, 2007; Fink, 2006; Nasica-Labouze and Mousseau, 2012; Rijal Upadhaya *et al.*, 2014; Uversky and Eliezer, 2009; Uversky *et al.*, 2001a; Uversky *et al.*, 2001c). Thus, characterization of these intermediates are important for the development of small molecules as misfolding inhibitors. Previous work has used nanopore analysis to study the interaction of unfolded proteins with different ligands and characterized the partially folded intermediates (Asandei *et al.*, 2013; Baran *et al.*, 2010; Stefureac *et al.*, 2010; Wang *et al.*, 2013; Wang *et al.*, 2011a). For example, Baran *et al.* studied the interaction of the recombinant murine myelin basic protein (MBP) with Cu(II) and Zn(II) using nanopore analysis. Monitoring of the proportion of translocation and bumping events showed that both Cu(II) and Zn(II) cause a reduction in the number of translocation events. Binding of metals with MBP induces folding or compaction of this protein into one or more conformations that are too large to pass through the pore and results in an increase in the number of bumping events (Baran *et al.*, 2010). Similar folding and compaction also occurred for AS in the presence of Cu(II) (see below). Another example of conformational change due to binding of metals with unfolded proteins is the interaction of human and rat amyloid fragments Aβ (1−16) with copper (II) (Asandei *et al.*,

2013). Addition of various concentrations of Cu(II) causes a reduction in the number of events with long blockage and a simultaneous increase in the number of events with short blockage. The results showed that Cu(II) causes folding and compaction of this peptide (Asandei *et al.*, 2013). Another example is the interaction of a zinc-finger molecule (Zif268) with Zn(II). The event profile of this motif was changed in the presence of Zn(II) and showed an increase in the intensity of the bumping peak and a simultaneous decrease in the proportion of the translocation peak (Stefureac and Lee, 2008).

The partially folded intermediates induced by interaction of AS and small molecules such as dopamine, nicotine and methamphetamine, were characterized in this thesis (see below). Previous work showed that nanopore analysis can detect the opposite effects of β-cyclodextrin (β-CD) and Congo Red (CR) in aggregation transition of β-amyloid-42 (Aβ42). β-CD and CR are aggregation promoter and inhibitor agents, respectively, and their effects on Aβ42 misfolding and aggregation has been detected by monitoring the corresponding blockade current and time. The blockade current histogram for Aβ42 showed two peaks representing translocation events, and bumping events. In the presence of CR the bumping peak dramatically decreases and there is an increase in translocation events. This profile showed that CR reduces formation of the misfolded or compact conformation of Aβ42. In the presence of β-CD a significant peak at 23.25 pA has been detected which was different from free Aβ42 and Aβ42-CR complex (Wang *et al.*, 2011a).

Nanopore analysis was used in this thesis to characterize the conformational change of AS in the presence of anti-parkinsonian small molecules (dopamine, nicotine, curcumin and caffeine) and methamphetamine as a Parkinson's inducing toxin. Other biophysical techniques such as NMR spectroscopy assisted to verify the nanopore analysis results and also to study other biophysical properties of the partially folded intermediates such as binding constant of the interaction and the secondary structure content.

4.1.2 Interaction of methamphetamine isomers with alpha-synuclein

Several studies showed that methamphetamine addicts have a higher incidence for developing PD (Callaghan *et al.*, 2010; Callaghan *et al.*, 2012; Granado *et al.*, 2013; Moszczynska *et al.*, 2004). Thus, we studied the interaction of methamphetamine with AS to investigate a possible mechanism for the psychoactivity of methamphetamine as well as an increased incidence of Parkinson's disease amongst users of the drug. Addition of both optical isomers of

methamphetamine to AS changed the blockade current profile of AS by increasing the number of events with current blockades lower than -80pA (Figure 3.4, 3.5).

For both (+)- and (-)-methamphetamine the current blockade histograms showed a concentration dependent increase in the intensity of bumping peak centered at -25 pA as compared with the current blockade profile of AS alone (Figure 3.4, 3.5). An increasing in the proportion of bumping events suggests that the protein folds and gets a more compact conformation which cannot translocate through the pore. The effect is similar to adding Zn(II) to the zinc-finger peptide causing folding into a compact conformation which cannot translocate (Stefureac and Lee, 2008).

The CD spectra of AS alone and in the presence of increasing concentrations of (+)- and (-)-methamphetamine showed a maximum ellipticity at 200 nm which is characteristic for random coil or denatured proteins. The CD spectrum showed no indication in the 210–230 nm region of an increase in either α-helix or β-sheet (Figure 3.10). This implies that binding of these ligands to AS does not cause a significant change in the secondary structure content of this peptide. Based on the nanopore and CD spectroscopy results, we proposed a "loop formation" model for the interaction of both optical isomers of methamphetamine with AS (Figure 4.1). This model suggests that AS folds around the ligand and forms a loop or an induced binding pocket. As illustrated in Figure 4.1b for (+)-methamphetamine, this partially folded conformation can be detected by nanopore analysis because this induced conformation cannot translocate the pore and results in an increase in the proportion of bumping events. However, formation of a loop does not alter the secondary structure content of the peptide and cannot be detected with CD spectroscopy. Previous studies also showed that the conformational changes induced by small molecules cannot be differentiated from the natively unfolded monomers using CD spectroscopy. For example, CD spectra for the mutants of AS (Li *et al.*, 2001) and the AS in the presence of dopamine (Cappai *et al.*, 2005; Outeiro *et al.*, 2009), chlorazole black E, copper complex of phthalocyanine tetrasulfonate (PcTS-Cu^{2+}) (Rao *et al.*, 2008), polycations (polylysine, polyarginine, and polyethyleneimine) (Goers *et al.*, 2003), putrescine, spermine (Antony *et al.*, 2003), congo red (Lendel *et al.*, 2009; Rao *et al.*, 2008), trehalose (Yu *et al.*, 2012) and lacmoid (Lendel *et al.*, 2009; Rao *et al.*, 2008) were typical for random coil conformation and demonstrated that mutation and complex formation with small molecules do not cause significant

change in the secondary structure of AS. On the other hand, nanopore analysis as a single molecule biophysics technique has the ability to detect subtle conformational changes.

Further comparison of the blockade current histograms for (+)- and (-)-methamphetamine (Figure 3.4, 3.5) showed that they change the AS conformation in a different manner and at the same concentrations the proportion of bumping events induced by (+)-methamphetamine is more than that induced by the (-)-isomer. Thus, the interaction of AS with methamphetamine is stereospecific and further characterization of these interactions using AS deletion mutants confirmed these specific interactions and showed the N- and C-terminal binding sites for the (+)- and (-)-isomer respectively (Figure 3.6, 3.7, 3.9).

The measured K_d for the interaction of (+)- and (-)-methamphetamine indicated one binding site for each ligand with different K_ds. The affinity of interaction for (+)-methamphetamine ($2x10^6$ M^{-1}) is greater than (-)-methamphetamine ($5x10^5$ M^{-1}) (Figure 3.11). These isomers also have different physiological effects. In general, the (+)-isomer is more effective than the (-)-isomer in producing central nervous system (CNS) stimulation. Furthermore, human studies showed that (+)-methamphetamine produces more cardiovascular effects than equivalent doses of (-)-methamphetamine. (-)-Methamphetamine intoxication is similar to that of the (+)-isomer at high doses, but the psychodynamic effects are shorter-lived and less desired by abusers (Mendelson *et al.*, 2006).

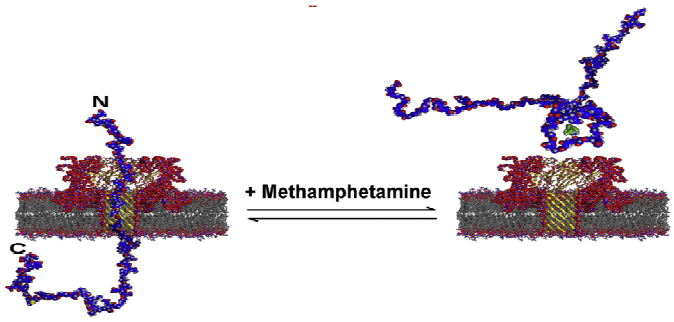

Figure 4.1 Proposed model for binding of (+)-methamphetamine to the N-terminal region of AS. Full length AS can readily translocate the α-hemolysin pore from the C-terminal end which carries a net negative charge. In the presence of methamphetamine, a loop is formed which causes bumping events to be more likely.

4.1.3 Interaction of nicotine isomers with alpha-synuclein

Epidemiological studies showed that PD is less prevalent in smokers (Checkoway *et al.*, 2002; Hernán *et al.*, 2002; Kessler and Diamond, 1971; Ono *et al.*, 2007b; Quik, 2004; Ross and

Petrovitch, 2001). It has been shown that the nicotine of tobacco smoke has a neuroprotective effect against PD symptoms (Alves *et al.*, 2004; Hernán *et al.*, 2002; Hong *et al.*, 2009; Quik, 2004). Tobacco is prepared from a plant which belongs to the *Solanaceae* family. Examples of edible products derive from the *Solanaceae* family are peppers, tomatoes, potatoes, and eggplants. Furthermore the results of a study on 490 idiopathic PD patients and 644 normal controls revealed that a diet including *Solanaceae* family products such as peppers, tomatoes, tomato juice, and potatoes reduces the risk of PD (Nielsen *et al.*, 2013). Nicotine is an optically active compound (Moore *et al.*, 2003; Welter *et al.*, 2005) and the naturally occurring form of nicotine is (-)-nicotine or l-nicotine (Figure 1.16a). The dextrorotatory form, (+)-nicotine or d-nicotine (Figure 1.16b) is physiologically less active than (-)-nicotine (Moore *et al.*, 2003; Rapier *et al.*, 1988) and (-)-nicotine is more toxic than (+)-nicotine (Moore *et al.*, 2003). The neuroprotective effect of nicotine in PD is through stimulation of the nicotinic acetylcholine receptors (nAChRs). It has been shown that nicotine evoked the release of dopamine from striatal synaptosomes in rats with an EC_{50} of 3.8 μM. This ability was stereospecific and it has been shown that the action of (-)-nicotine was 100 times stronger than (+)-nicotine (Fujita *et al.*, 2006; Rapier *et al.*, 1988). Another possible mechanism for the neuroprotective effect of nicotine in PD is modulation of AS aggregation (Hong *et al.*, 2009; Ono *et al.*, 2007b) and the study of the interaction of nicotine with AS may be useful in designing new small molecules as antifibrillization agents. The nanopore studies showed that (-)- and (+)-nicotine change the conformation of AS in a concentration dependent manner and by increasing the ligand concentration, the protein conformation changed differently (Figure 3.12) (see below). Previously thioflavin S (ThS) assays have been used to study the effect of (-)-nicotine on AS fibrillation which requires high concentrations of AS (70 μM). The results showed that (-)-nicotine inhibits the fibrillation of AS and the ThT fluorescence signal decreases as a function of nicotine concentration. In the absence of nicotine, AS monomers are misfolded and aggregated to form transient oligomers and assembly of these oligomers leads to the formation of fibrils but incubation of nicotine with monomeric AS causes the formation of stabilized oligomers which will not fibrillize anymore (Hong *et al.*, 2009). Our nanopore results were performed at a very low concentration of AS (1 μM) to characterize the early stages of AS aggregation, the formation of partially folded intermediates, in the presence of nicotine. The conformations detected by

nanopore analysis (Figure 3.12) might represent the misfolded conformations of AS which are able to oligomerize and form the stabilized oligomers at high concentrations.

Furthermore the conformational changes induced by (-)- and (+)-nicotine at the same concentrations were different (Figure 3.12). Thus the interaction of AS with nicotine is stereospecific and at a concentration of 5 μM (+)-nicotine (Figure 3.12g) the profile is much simpler than (-)-nicotine (Figure 3.12c) and also different intermediate peaks are found at a concentration of 10 μM (Figure 3.12d,h). At this concentration for (-)- and (+)-isomers the intermediate peaks were centered at -62 pA (Figure 3.12d) and -42 pA (Figure 3.12h) respectively. The CD spectra of AS demonstrated no significant increase in ordered secondary structure content in the presence of nicotine even at the highest AS:nicotine ratio of 1:10, the spectra remain dominated by random coil (Figure 3.14). Upon addition of increasing concentrations of (+)- and (-)-nicotine the magnitude of MRE, in the 196-200 nm region, increased in a concentration dependent manner similar to those reported for other small molecules such as such as chlorazole black E , copper complex of phthalocyanine tetrasulfonate (PcTS-Cu^{2+}) (Rao *et al.*, 2008), congo red (Lendel *et al.*, 2009; Rao *et al.*, 2008), trehalose (Yu *et al.*, 2012) and lacmoid (Lendel *et al.*, 2009; Rao *et al.*, 2008).

Nanopore analysis with AS fragments demonstrated that (-)-nicotine has a binding site consisting of both N- and C-terminal residues of AS but (+)-nicotine has a binding site which involves mostly residues from the N-terminus (Figure 3.13). This difference in the binding sites shows the interaction of AS with nicotine optical isomers is specific. Another proof of these specific interactions is the difference in K_as measured by ITC (Figure 3.15) which shows (+)-nicotine has a lower affinity ($4x10^5$ M^{-1}) compared to (-)-nicotine ($1.35x10^6$ M^{-1}). Physiological activity measurments of nicotine have shown that (+)-nicotine is physiologically less active than (-)-nicotine (Moore *et al.*, 2003; Rapier *et al.*, 1988) and (-)-nicotine is more toxic than (+)-nicotine (Moore *et al.*, 2003).

The interaction of AS with (-)- and (+)-nicotine was investigated by HSQC NMR spectroscopy (Figure 3.17). Titrations of the protein with increasing amounts of each isomer showed concentration dependent changes in the intensities of several peaks in the ^{1}H-^{15}N spectrum as compared with AS alone which represents a change in conformation. Furthermore the observed changes in intensities were more significant for (-)-nicotine (Figure 3.17a,b) than for (+)-nicotine (Figure 3.17a,b), in agreement with the higher K_a for the (-)-isomer (Figure

3.15). This is similar to the previous NMR spectroscopy spectra for the interaction of Congo Red and Lacmoid with AS which showed that the interaction of Congo Red with AS is stronger than Lacmoid and causes more changes in the intensity of the NMR signals (Lendel *et al.*, 2009).

The changes in peak intensity observed in the ^{1}H-^{15}N spectra which make them invisible in the spectra is due to broadening of the AS NMR signals as a result of chemical exchange on the µs-ms time scale upon binding to the ligands. This has been previously observed for the interaction of Congo Red, Lacmoid (Lendel *et al.*, 2009; Rao *et al.*, 2008), chlorazole black E, PcTS-Cu^{2+} and rosmarinic acid (Rao *et al.*, 2008).

Moreover the NMR spectroscopy results (Figure 3.17b,d) are in agreement with the mapped binding sites detected by nanopore analysis (Figure 3.13) which demonstrated N- and C-termini binding site for (-)-nicotine and a N-terminal binding site for (+)-nicotine. NMR spectroscopy demonstrated that (+)-nicotine effects few residues from the N-terminal and NAC residues (Figure 3.17c,d) but (-)-nicotine causes an overall change in AS conformation involving residues from the N-terminal, NAC and C-terminal (Figure 3.17a,b). Based on these results, models can be proposed for the binding of nicotine to AS (Figure 4.2b,c). (+)-Nicotine has an N-terminus binding site and its binding might induce a loop formation in the first 100 residues of AS (Figure 4.2c). (-)-Nicotine has a binding site involving residues from both N- and C-terminal and its binding to AS might cause a large conformational change involving the folding and compaction of the whole sequence which leads to the broad change of intensities in the ^{1}H-^{15}N HSQC spectra (Figure 4.2b).

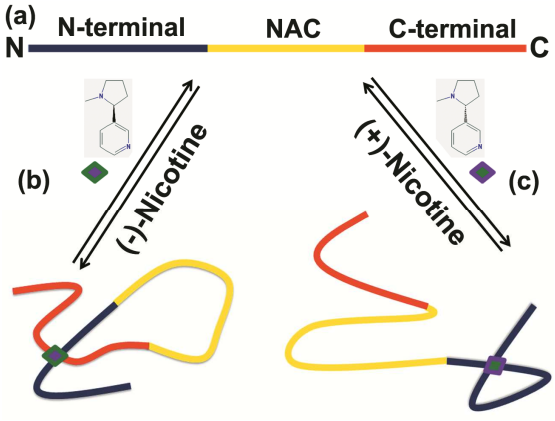

Figure 4.2 Schematic of the structure of AS protein, showing (a) the N-terminal segment, the NAC segment, and the C-terminal segment. (b) The proposed model for interaction of (-)-nicotine and (c) (+)-nicotine with AS. (-)-Nicotine mediates the interaction between the N- and C-termini of AS (b) whereas (+)-nicotine binds to the N-terminus of AS.

4.1.4 Interaction of dopamine and copper with alpha-synuclein

Cu(II) has an important role in the development of PD. In support of this, comparison of Parkinsonian and age-matched control brain tissue showed a reduction in the Cu (II) contents in the substantia nigra (SN) (Davies *et al.*, 2014; Dexter *et al.*, 1989; Riederer *et al.*, 1989). Previous work using NMR spectroscopy have shown that AS has two binding sites for Cu(II) with different affinities (see below). Thus we studied the interaction of Cu(II) and AS to characterize the AS folded conformation induced by Cu(II). The nanopore analysis of the interaction of Cu(II) with the AS wild type and E46K mutant (Figure 3.19) showed that adding increasing concentrations of Cu(II) leads to a concentration dependent increase in the intensity of the bumping peak and a simultaneous decrease in the proportion of the translocation peak and suggested a binding constant of ~$10^5 M^{-1}$, because there is an approximately 50% reduction in the translocation peak at 10 µM Cu(II) (Figure 3.19b). The bumping events represent the folded conformation of AS which is more compact as compared with the native conformation of AS and cannot pass through the pore. Previous work has shown that Zn(II) and Cu(II) increase the number of bumping events due to folding and compaction of zinc finger peptide (Stefureac and Lee, 2008), prion protein (Stefureac *et al.*, 2010) and myelin basic protein (Baran *et al.*, 2010).

Cu(II) at micromolar range (<100µM) binds tightly to the N-terminal site with high affinity (K_d~0.1 µM) located at ^{1}MDVFMKGLS^{9} and ^{48}VAHGV^{52}. M1, D2 and H50 are the residues which are directly involved in the interaction with Cu(II) and result in the formation of a loop in the structure. The complex of Cu(II) and AS serves as a nucleation point for β-strand formation (Figure 4.3) (Rose *et al.*, 2011). The nanopore experiments were performed at concentrations of Cu(II) in the affinity range of the N-terminal binding site and even at the highest Cu(II) concentration (25 µM) (Figure 3.19c,i), Cu(II) binds to the N-terminal and induced loop formation (Rose *et al.*, 2011). Nanopore experiments with the AS segments (Figure 3.20) showed that Cu(II) changes the blockade current profile of the N-terminal and ΔNAC but no conformational change were observed for the C-terminal.

Residues encompassing ^{48}VAHGV^{52} have an important role in the interaction of Cu(II) with AS and especially H50 acts as an anchoring residue for loop formation (Binolfi *et al.*, 2012; Binolfi *et al.*, 2006; Rasia *et al.*, 2005). Nanopore analysis of the E46K mutant (Figure 3.19g,h,i) which is close to this region showed that the conformation of E46K is more sensitive to Cu(II) binding as compared to AS wild type.

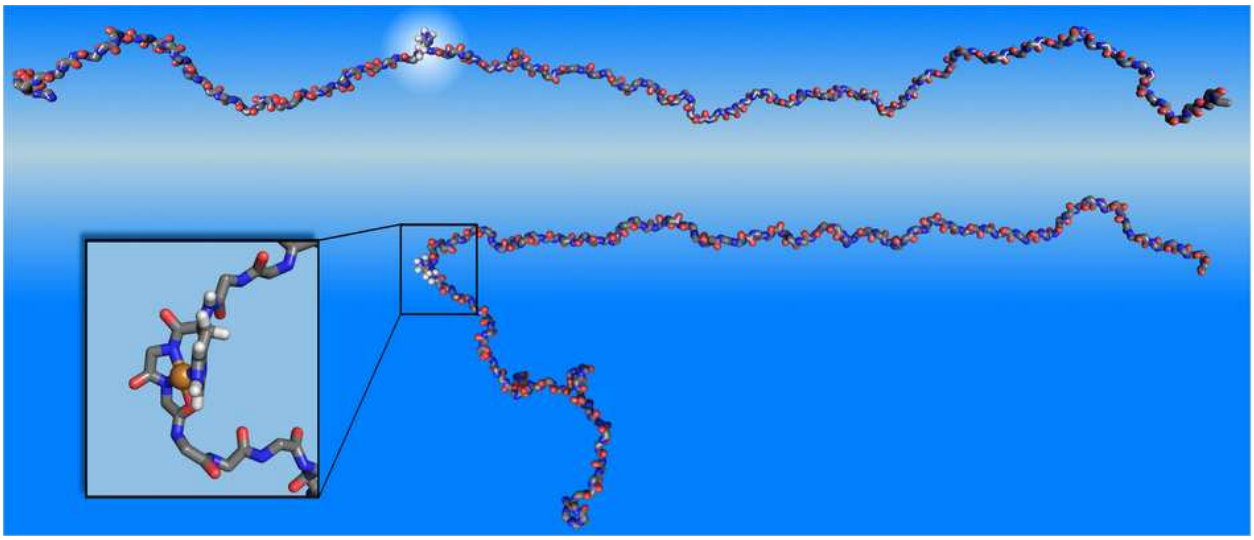

Figure 4.3 Misfolding events in AS due to copper binding. a: Snapshot of the free AS showing the location of His-50 (upper). b: Snapshot of Cu-bound AS with dynamically stable β-sheet. Insets show close-ups at the β-sheet nucleation point (Rose *et al.*, 2011). Copyright © 2011 Rights Managed by Nature Publishing Group. All rights reserved.

Previous work using Thio-T fluorescence assay showed that the aggregation rate of AS mutants (A30P, A53T and E46K) in the presence of Cu(II) is more than that of the wild type AS and among the mutants E46K had the largest rate of fibril formation (Bharathi and Rao, 2008).

There is a low affinity (K_d~1 mM) binding site at the C-terminal of AS located at ^{119}DPDNEA^{124} which serves as a general binding site for divalent metals such as Cu(II), Fe(II), Mn(II), Co(II) and Ni(II) (Binolfi *et al.*, 2012; Binolfi *et al.*, 2006; Rasia *et al.*, 2005). As the nanopore analysis was performed at concentrations below the K_d of the C-terminal binding site, Cu(II) did not bind to the C-terminal peptide and the blockade current profile of this peptide was the same in the absence and presence of Cu(II).

AS has an important role in dopamine homeostasis and is involved in almost all of the dopamine metabolism pathways including dopamine biosynthesis, storage of dopamine in synaptic vesicles, dopamine release in response to an action potential and re-uptake of released dopamine from the presynaptic space (Lotharius and Brundin, 2002a; Stefanis, 2012; Yu *et al.*, 2005). Furthermore the main feature of PD is aggregation of AS which results in AS malfunction and dopamine depletion (Grosset *et al.*, 2009; Lotharius and Brundin, 2002a; Pahwa and Lyons, 2007; Yu *et al.*, 2005). Previous work has shown that dopamine interacts with AS and decreases the fibrillization of AS by stabilizing the oligomers of AS (Cappai *et al.*, 2005; Fink, 2006; Lee *et al.*, 2011; Leong *et al.*, 2009; Norris *et al.*, 2005). Thus there is a possible link between

dopamine depletion, AS misfolding and PD development. Therefore different biophysical techniques were used to characterize the partially folded intermediates of the AS:dopamine complex. Dopamine at a concentration of 25 µM changed the blockade current profile of both Wild type AS (Figure 3.21b) and A30P (Figure 3.21d) to a significant peak centered at -80 pA which was shown to be a translocation peak. The peak at -80 pA might represent a partially folded conformation of AS induced by dopamine which is the precursor for stabilized oligomer formation. The CD spectra of AS showed that dopamine does not change the secondary structure content of AS (Figure 3.25) and was in agreement with previous work (Cappai *et al.*, 2005; Outeiro *et al.*, 2009; Pham and Cappai, 2013). Thus binding of dopamine to AS might cause a simple loop which cannot be detected by CD spectroscopy but is readily detected by nanopore analysis. ITC measurements showed a single binding site for dopamine with a dissociation constant (K_d) of 2.85×10^{-4} M (Figure 3.26). Moreover nanopore analysis of AS segments showed that the binding site included residues from both N- and C-terminal of AS (Figure 3.23). HSQC NMR was performed to characterize which residues were involved in the interaction with dopamine (Figure 3.27). The control experiment (incubation of AS at 15° C for 5 hours) showed that AS is stable during the NMR experiment and any changes in conformation are induced by adding ligand to the AS sample (Figure 3.16). Titrations of AS with increasing amounts of dopamine at three ratios of AS:dopamine (1:5, 1:10 and 1:25) showed concentration dependent changes in the intensities of ^{1}H-^{15}N HSQC signal along the length of the AS sequence which represents a new ensemble of AS structures due to the binding of dopamine (Figure 3.27, 3.28). The intensity changes mostly involve loss of peak intensity rather than chemical shift changes (Figure 3.27a). Such behavior could reflect exchange processes in an intermediate regime caused by drug binding, including conformational transitions and intra-protein interactions as have been observed for the interaction of other small molecules such as congo red, PcTS-Cu^{2+}, chlorazole black E and lacmoid with AS (Lendel *et al.*, 2009; Rao *et al.*, 2008). Conformational changes of AS in the presence of negatively charged lipids was in agreement with previous NMR studies and showed that in the presence of negatively charged lipids (LPPG in our study) (Figure 3.29), the first 100 residues of AS bind to the micelles and become invisible in the NMR spectra (Chandra *et al.*, 2003; Davidson *et al.*, 1998; Georgieva *et al.*, 2008; Jao *et al.*, 2008; Ulmer *et al.*, 2005a). This is another proof of the N- and C-terminal binding sites for dopamine as dopamine did not bind to the last 40 available residues of AS in the presence of LPPG micelles.

The NMR results showed that the dopamine binding site does not overlap with the N-terminal binding site for Cu(II). This is in agreement with the nanopore experiments of AS that showed that a new peak was found in the presence of both dopamine and Cu(II) (Figure 3.24). Residues M1 and D2 are not well resolved in our NMR experiments in the presence of dopamine but for residues F4, M5 and K6 the intensity ratio is at the baseline level. Similarly, H50 is not well resolved but there is little change in the intensity ratio for residues V49, G51 and V52 in the presence of dopamine.

There are two possibilities to explain these results; folding of AS monomers to form a loop or head to tail oligomerization of AS monomers. Since the loss of peak intensity of HSQC NMR peaks does not occur for all residues, our results are not consistent with dopamine-induced oligomerization. Conformational exchange appears to be the explanation most consistent with the nanopore data, which suggests a change in the population distribution of AS conformations in the presence of dopamine. In other words, the peak at -80 pA which appears on addition of dopamine is not consistent with oligomerization. Also, there was no change in the event profile with time.

Taking all the results together, a model is proposed to explain the conformational changes of AS in the presence of dopamine (Figure 4.4). AS folds to form a loop which involves the interaction between the N- and C-termini as shown in Figure 4.4b. Nanopore experiments showed that the NAC region is not directly involved in the interaction with dopamine. As dopamine mediates the interaction between the N- and C-termini, the conformation of NAC is significantly changed due to loop formation which was detected by NMR spectroscopy. Another model would be head to tail dimerization of AS monomers but it seems unlikely that this would cause a significant translocation peak to be observed in the nanopore analysis. Previously a C-terminal binding site was reported for dopamine using molecular dynamic simulations (Herrera *et al.*, 2008) but the structural biology approach used in this thesis to pursue this interaction showed that this interaction is complex and involves residues from both N- and C-terminal regions of AS.

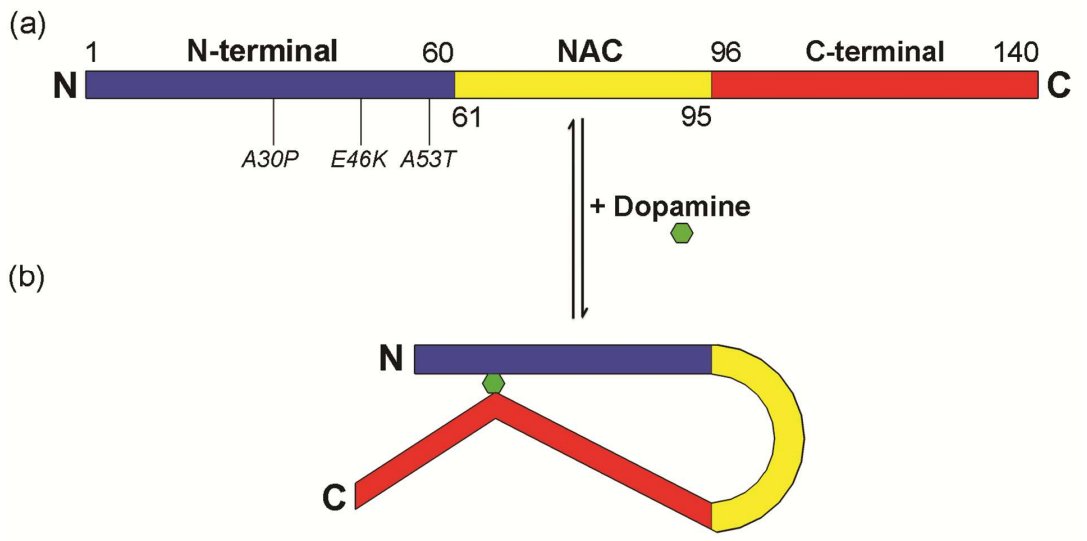

Figure 4.4 . Schematic representation showing the interaction of dopamine with AS. (A) Schematic of the structure of AS, showing the N-terminal segment, the NAC segment, and the C-terminal segment. The positions of missense mutations in the N-terminus are also indicated. (B) The proposed model for interaction of dopamine with AS. Dopamine mediates the interaction between the N-terminus and C-terminus of AS.

4.1.5 Physiological relevance of *in vitro* studies

All of the small molecules and ligands studied in this thesis have been selected based on previous work performed *in vitro* and *in vivo* and the relevance to their effects on AS conformation or PD development (see below). For example, previous work showed that AS has an important role in the control of cytoplasmic dopamine concentrations by promoting the formation of synaptic vesicles from early endosomes and storage of dopamine in these vesicles (Lotharius and Brundin, 2002a, b; Yu *et al.*, 2005). In the cytoplasm of dopaminergic neurons there are two pools of AS molecules, the free AS molecules with unfolded structure and AS bound to the membranes which has a mostly α-helical conformation. Binding of free AS through its N-terminal with membrane phospholipids is the critical stage in the formation of synaptic vesicles and dopamine storage to maintain the cytoplasmic concentration of dopamine in the range of 0.5 µM to 2.2 µM as a protective strategy against cytosolic oxidation of dopamine (Lotharius and Brundin, 2002a, b; Olefirowicz and Ewing, 1990; Perlman and Sheard, 1982). The nanopore experiments performed in this thesis showed that dopamine at the concentration of 25 µM binds to both N- and C-terminal of AS and causes folding of AS molecules into a new ensemble. No conformational change has been observed at dopamine concentrations less than 5

μM (data not shown). ITC results revealed that the affinity of dopamine for AS is 150 to 300 times less than the affinity of methamphetamine and nicotine for AS. The *in vivo* function of AS can be explained using our *in vitro* results. Inside the cells at the safe concentrations of dopamine (0.5-2.2 μM), dopamine cannot change the conformation of free cytoplasmic AS molecules. Upon increasing the cytoplasmic concentration of dopamine, it binds to AS and might serves as a signal to trigger the formation of monoamine vesicles by changing the conformation of unfolded AS into the partially folded intermediate. These intermediate conformations which have been characterized in this thesis might promote vesicle formation by binding to the membrane of early endosomes for storage of the excess of cytoplasmic dopamine into these vesicles. Furthermore, the NMR results demonstrated that dopamine binds to the free unfolded AS molecules and no interaction has been detected in the presence of lipid micelles. Thus it could be concluded that dopamine just binds to the free AS molecules with unfolded structure and causes the formation of partially folded intermediates. Based on the *in vitro* results of this thesis it could be proposed that the unfolded AS in the cytoplasm of dopaminergic neurons might act as a sensor to detect the increase of cytoplasmic dopamine.

Previous work has shown that nicotine from cigarette smoke has protective effects against PD (Alves *et al.*, 2004; Hernán *et al.*, 2002; Hong *et al.*, 2009; Quik, 2004). Furthermore the nicotine brain concentration after consumption of one cigarette has been calculated to be 50 ng/ml (Rose *et al.*, 1999) based on the reported nicotine blood concentrations in smokers (Benowitz *et al.*, 1982; Brody *et al.*, 2006; Gritz *et al.*, 1981; Rose *et al.*, 2010; Russell *et al.*, 1980). Moreover the half life for nicotine elimination from the body has been determined to be 100 to 150 min (Gritz *et al.*, 1981). The average number of cigarettes consumed by smokers in a day is 30 to 36 (Benowitz *et al.*, 1982; Gritz *et al.*, 1981; Russell *et al.*, 1980) which results in a maximum concentration of 1500 to 1800 ng/ml nicotine in the brain. The concentrations of nicotine used in this thesis were in the range of 300 to 1600 ng/ml which is in the same range as the nicotine concentration in the brain of smokers. Thus it is not unreasonable to propose that the protective effect of nicotine is due to binding to AS.

Considering the density of brain (1.081 gr/cm^3) (Barber *et al.*, 1970) the maximum concentration of total Cu(II) in the SN is 11.5 μg/ml (Lutsenko *et al.*, 2010; Rongzhu *et al.*, 2009). Moreover it has been reported that the total copper content of the SN showed a maximum reduction of 45% in PD brain samples as compared with the normal brain (Dexter *et al.*, 1989).

Thus the maximum concentration of total Cu(II) in SN of PD patients would be about 6.3 μg/ml. As the majority of Cu(II) in brain is bound to Cu(II)-binding molecules, the concentration of free Cu(II) would be less than the above values (Bohic *et al.*, 2008; Davies *et al.*, 2014). Based on previous work, Cu (II) at concentrations less than 6.35 μg/ml binds to the N-terminal and at higher concentrations binds to the C-terminal of AS (Binolfi *et al.*, 2012; Binolfi *et al.*, 2006; Rasia *et al.*, 2005). For the nanopore experiments performed in this thesis, the Cu(II) concentrations were 2.5 μg/ml and 6 μg/ml which are consistent with the Cu(II) concentrations in the SN of PD brains. The differences in Cu(II) concentrations in normal and PD brains can be explained from the viewpoint of Cu(II) affinities for AS. In normal brain the concentration of Cu(II) is high and copper has the ability to bind with both binding sites at N- and C-terminals. However, reduction of copper concentration in PD tissues might favour the binding of Cu (II) to the high affinity N-terminal site. Thus the misfolded conformation of AS upon binding of Cu(II) to the N-terminal might be associated with the pathogenicity of PD.

It has been reported that methamphetamine addicts have a higher risk of developing symptoms of PD (Callaghan *et al.*, 2010; Callaghan *et al.*, 2012; Granado *et al.*, 2013; Moszczynska *et al.*, 2004). Pharmacokinetics of methamphetamine in the human brain showed that this toxic drug reaches peak concentrations 9 min after consumption which lasts for more than 75 min. It also has been shown that 9.6% of the consumed dose will be distributed in this organ (Volkow *et al.*, 2010). The total daily amount of drug consumed by addicts is in the range of 0.7 to 1 gram. Chronic abusers smoke this recreational drug every 30 minutes during the day and stop smoking the drug at night to sleep (Cho and Melega, 2002). Consumption of this amount at once results in a brain concentration of 244 μM to 349 μM but gradual consumption results in the concentration of at least 18 μM (Cho and Melega, 2002). Our nanopore experiments suggested that 20 μM of methamphetamine is high enough to cause a significant folding of AS (Figure 3.4e). The high concentration of this recreational drug in the brain of the drug abusers causes a significant change in the normal function of brain cells which finally results in the appearance of PD symptoms (Callaghan *et al.*, 2010; Callaghan *et al.*, 2012; Granado *et al.*, 2013; Thrash *et al.*, 2009). Previous work has shown that methamphetamine alters the cellular levels of AS and dopamine (Ajjimaporn *et al.*, 2007; Chen *et al.*, 2013; Kish, 2008; Mauceli *et al.*, 2006; Volkow *et al.*, 2001a; Volkow *et al.*, 2001b; Volkow *et al.*, 2010). Thus there would be a link between methamphetamine consumption and failure of AS function

in dopamine homeostasis. Treatment of SK-N-SH neuroblastoma cells with methamphetamine causes overexpression of AS (Ajjimaporn *et al.*, 2007). Furthermore (+)-methamphetamine stimulates the reverse transport of dopamine from synaptic vesicles to the cytoplasm of nerve endings by vesicular monoamine transporter 2 (VMAT2) (Granado *et al.*, 2013; Kish, 2008). Although overexpression of AS itself increases the aggregation rate of AS, binding of methamphetamine with AS might prevents its role in dopamine homeostasis. The normal function of AS is important for clearance of dopamine from the cytoplasm of the presynaptic terminal and storage in synaptic vesicles. AS also regulates the re-uptake of released dopamine molecules from presynaptic space into the synaptic terminal. This homeostasis protects cells from the deleterious effects of dopamine oxidation in the cytoplasm and also helps the replenishment of synaptic dopamine. Loss of normal AS function promotes the accumulation of dopamine in the cytoplasm of the presynaptic terminal which leads to oxidative stress (Lotharius and Brundin, 2002a, b; Yu *et al.*, 2005). Thus methamphetamine causes overexpression and aggregation of AS and also results in an increase in the cytoplasmic dopamine levels which finally together are responsible for creating PD pathology in the drug abusers.

4.1.6 Conclusions leading into future directions

Nanopore analysis is an emerging technique for studying protein misfolding. The results of this thesis showed that nanopore analysis differentiates the conformational changes of AS partially folded intermediates in the presence of anti-parkinsonian and Parkinson developing small molecules. The anti-parkinsonian small molecules can be used as candidates for designing inhibitors as new therapeutics for treatment of PD using a fragmentation drug design approach (see below). An important impact of this thesis is that the interaction of AS with D- and L-enantiomers of nicotine and methamphetamine is stereospecific. This shows the importance of chirality in drug design and development for treatment of PD.

4.2 Future directions

4.2.1 Lead compound selection

One promising approach in order to develop therapeutics for treatment of PD is to inhibit AS fibrillization with anti-fibrillization agents identified using high-throughput screening (Acharya *et al.*, 2014; Kritzer *et al.*, 2009; May *et al.*, 2006; Prabhudesai *et al.*, 2012; Rochet, 2007; Shaltiel-Karyo *et al.*, 2010; Toth *et al.*, 2014). Fibril formation is a multistage process which

starts from the monomers of AS. The first stage is misfolding of the protein by formation of partially folded intermediates which are pre-molten globule-like conformers of AS (Fink, 2006; Uversky *et al.*, 2001a). The native AS monomer has predominantly a random coil conformation (R51,R52,R48,R50) but the partially folded intermediates usually contain α-helical or β-sheet conformations (Frid *et al.*, 2007; Serpell *et al.*, 2000; Uversky and Eliezer, 2009; Uversky *et al.*, 2001b; Weinreb *et al.*, 1996; Zheng *et al.*, 2013). Intermolecular interactions of partially folded intermediates lead to the formation of oligomers and the assembly of oligomers forms fibrils (Fink, 2006; Uversky and Eliezer, 2009). Anti-fibrillization agents can be divided into two groups based on their mechanism of action. Some of them stop the fibrillization at the early stage by stabilizing the unfolded conformation of AS (Acharya *et al.*, 2014; Amer *et al.*, 2006; Attar and Bitan, 2014; Attar *et al.*, 2012; Ferreira *et al.*, 2014; Fokkens *et al.*, 2005; Kim *et al.*, 2009; Prabhudesai *et al.*, 2012; Sinha *et al.*, 2012a; Sinha *et al.*, 2011b; Soto, 2003) and others can prevent this pathogenic process at the second step by stabilizing the oligormers of AS (Cappai *et al.*, 2005; Fink, 2006; Hong *et al.*, 2009; Lee *et al.*, 2011; Leong *et al.*, 2009; Norris *et al.*, 2005). The biochemical properties of anti-fibrillization agents determine their mechanism of action. For example molecular tweezers and β-sheet breakers peptides (see below) stabilize the unfolded conformation of AS and prevent the misfolding process but nicotine (Hong *et al.*, 2009) and dopamine (Cappai *et al.*, 2005; Fink, 2006; Lee *et al.*, 2011; Leong *et al.*, 2009; Norris *et al.*, 2005) result in the formation of stabilized oligomers which no longer convert to the fibrils. Although their biochemical mechanisms are different, all of the anti-fibrillization agents result in a reduction of fibril formation which is associated with the pathology of PD (Acharya *et al.*, 2014; Amer *et al.*, 2006; Attar and Bitan, 2014; Fink, 2006; Leong *et al.*, 2009; Sinha *et al.*, 2011a; Soto, 2003).

An important group of chemicals which has been shown to prevent AS fibrillization are catecholamines. Two drug screening studies using different groups of chemicals have shown that catecholamines are the most efficient anti-fibrillization agents with the lowest IC_{50}. In the first screening, a library of 79 compounds belonging to twelve chemical groups were screened to find compounds with inhibitory effects on AS fibril formation (Masuda *et al.*, 2006). Three *in vitro* assays were used to assess the fibril formation. They included electron microscopy, thioflavin S (ThS) fluorescence, and the formation of sarkosyl-insoluble α-synuclein. The IC_{50} values of all 79 compounds for inhibiting AS filament assembly were determined by quantifying the levels of

sarkosyl-insoluble AS. Strong inhibitors of AS filament assembly (IC_{50} values of <10 μM) belong to polyphenols. They include baicalein, delphinidin, dopamine chloride, epigallocatechin gallate, exifone, (-)-gallocatechin, (-)-gallocatechin gallate, gossypetin, hinokiflavone, hypericin, procyanidin B1, procyanidin B2, rosmarinic acid and theaflavine. The common structural feature among them is that they contain adjacent phenolic OH groups. It has been suggested that at least two adjacent phenolic OH groups may be required for the inhibition of AS filament formation via covalent modification. 23 out of the 27 inhibitory polyphenols identified in this study have two adjacent phenolic OH groups. The substitutions of hydroxyl groups on the aromatic benzene are very important to increase their solubility and their tendency for hydrogen bond interaction. For example, exifone (2,3,3',4,4',5'-Hexahydroxybenzophenone) which contains six hydroxyl substitution in both benzene rings has the lowest IC_{50} (2.5 μM) among polyphenols. The IC_{50} of 2,3,4-trihydroxybenzophenone which has three hydroxyl group on just one of its benzene ring is increased to 18.6. In the absence of hydroxyl groups the hydrophobic structure binds to the NAC part of α-synuclein and triggers its misfolding (Masuda *et al.*, 2006).

In another study a library of 127 compounds was screened to identify AS fibrilization inhibitors. Fourteen compounds out of fifteen inhibitors were catecholamines, including dopamine (DA), L-DOPA, norepinephrine, and epinephrine. The common structural feature is that all of them have dopamine as their backbone and contain substituted groups on at least one of the following atoms: amine group, carbon alpha and carbon beta. The results showed that the adjacent phenolic hydroxyl groups of the catechol moiety are critical for the inhibitory function of the compound and modification of them leads to loss of function. Removal of one or both of the adjacent phenolic hydroxyl groups and exchanging one of them with methoxy or hydroxyl-ethyl leads to loss of inhibitory function. Eight out of 15 inhibitors have a hydroxyl group on carbon beta. A hydroxyl group on the beta carbon (Figure 4.5, Figure 4.6) of catecholamines might increase the binding affinity of the ligand to the target molecule (Conway *et al.*, 2001).

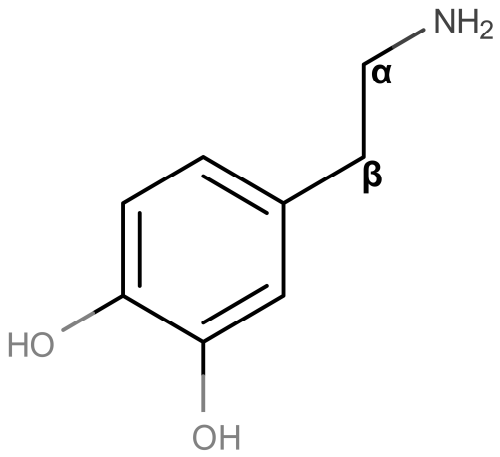

Figure 4.5 Structure of catecholamine which shows the amine group, adjacent phenolic hydroxyl groups, alpha and beta carbon

Furthermore it has been demonstrated that micromolar concentrations of dopamine or L-dopa can significantly inhibit fibril formation or disaggregate existing fibrils of AS *in vitro* (Li *et al.*, 2004). The reason for choosing dopamine as an anti-fibrillization agent in this thesis was that it is an endogenous catecholamine which is synthesized from L-tyrosine and its pharmacokinetics are known. Epinephrine and norepinephrine are other endogenous catecholamines which prevent the aggregation of AS by stabilizing oligomers of AS (Masuda *et al.*, 2006). These catecholamines belong to the adrenergic drug family. As adrenergic drugs produce effects similar to those produced by the sympathetic nervous system, they are also called sympathomimetic drugs. Common functions of catecholamines are stimulation of the nervous system, constriction of the peripheral blood vessels, increase heart rate and dilation of the bronchi (Springhouse, 2008). The advantage of using endogenous chemicals such as dopamine as anti-fibrillization agents is that the molecular function and pharmacokinetics of these chemicals are already established. Because these chemicals have a primary physiological target, AS can be their secondary target. Thus these chemicals can act as dual function agents to maintain the peripheral autonomic system and the central nervous system and also to prevent the AS fibrillization. Their inhibitory effects on AS fibrillization and also their safety for animal studies make catecholamines an important group of chemicals to screen lead compounds for designing new and efficient anti-fibrillization agents.

The results of this thesis showed that dopamine causes folding of AS monomers into a new conformation and previous work demonstrated that dopamine has the ability of preventing

fibrillization by stabilizing oligomers of AS. The limitation of using endogenous catecholamines such as dopamine as therapeutics is that they cannot be taken orally because digestive enzymes can destroy them. As all catecholamines contain hydroxyl and amine groups, they are polar molecules. Thus, at physiological pH they are protonated and will not cross the blood brain barrier easily, so that in effect the catecholamine pools in the brain and in the periphery will not interfere with each other (Golan *et al.*, 2007; Springhouse, 2008). It is possible to modify them chemically in order to overcome their limited absorbance and also increase their half-life in the brain (see below).

Another group of compounds with anti-fibrillization activity are anti-Parkinson's disease drugs such as L-DOPA, entacapone, tolcapone and selegiline (Braga *et al.*, 2011; Di Giovanni *et al.*, 2010). Entacapone and tolcapone block the fibril formation (Di Giovanni *et al.*, 2010) and selegiline lengthens the nucleation phase of fibril formation (Braga *et al.*, 2011). These drugs stabilize the oligomers of AS and lead to formation of nontoxic species (Braga *et al.*, 2011; Di Giovanni *et al.*, 2010). It has been demonstrated that micromolar concentration of L-DOPA can inhibit fibril formation of AS *in vitro* (Li *et al.*, 2004). The advantage of using these drugs as anti-fibrillization agents is that all of them are FDA approved, have known pharmacokinetics and pharmacodynamics, and are administrated for PD patients to control the PD symptoms (Grosset *et al.*, 2009; Seth and Seth, 2009). As dopamine is not able to cross the BBB, Levodopa which is its immediate precursor is admitted. Levodopa is transported across BBB by a large neutral amino acid transporter. In striatal tissue, L-dopa is decarboxylated to dopamine by L-aromatic amino acid decarboxylase. L-dopa is also a precursor of norepinephrine and epinephrine (Seth and Seth, 2009). The half-life of levodopa is short so to prevent its catabolism in peripheral tissues Monoamine oxidase-B (MAO-B) inhibitors such as selegiline and catechol O-methyl transferase (COMT) inhibitors such as tolcapone and entacapone are used as adjuncts to levodopa/carbidopa therapy (Pahwa and Lyons, 2007; Seth and Seth, 2009).

4.2.2 Proposed strategies to prevent AS aggregation

From the above several lead compounds are available. Overall a good lead compound candidate for designing more efficient anti-fibrillization agents is L-DOPA because it is the precursor of dopamine and is administrated to maintain the dopamine depletion in PD patients. Furthermore it does not have the dopamine administration limitations and can be absorbed rapidly and pass the BBB. PD patients take the anti-fibrillization agent such as L-DOPA,

entacapone, tolcapone and selegiline together as their regular treatment for PD. Co-administration of L-DOPA with other drugs increases the half-life of this molecule in the brain. However, the experiments performed in this thesis showed that the K_d of dopamine and AS interaction (285 µM) (Figure 3.26) is higher than the normal cytoplasm dopamine concentration (0.5-2.2 µM) (Olefirowicz and Ewing, 1990; Perlman and Sheard, 1982). This shows that the affinity of dopamine for AS is low and a series of chemical modifications are required to increase this affinity. Thus the structure of dopamine can be considered as the pharmacophore because it contains the minimum functional groups (catechol and amine) which are required for binding to the target sites (Figure 4.6) (Herrera *et al.*, 2008). In Figure 4.6, R1 and R2 groups represent the positions of substituent modifications to increase the affinity of dopamine for AS. As soon as the active inhibitor is designed its prodrug can be proposed by adding a carboxyl group on carbon alpha (Figure 4.6). As the proposed active inhibitor has a positive net charge at physiologic pH adding a carboxyl group makes it neutral and facilitates its absorption by the large neutral amino acid transporter from gut wall and the final transportation by a similar transporter across the BBB (Seth and Seth, 2009). The logP of the prodrug would be less than the active molecule which will facilitate its absorption (Patrick, 2009; Seth and Seth, 2009). In striatal tissue the prodrug undergoes decarboxylation and is converted to the active anti-fibrillization molecule.

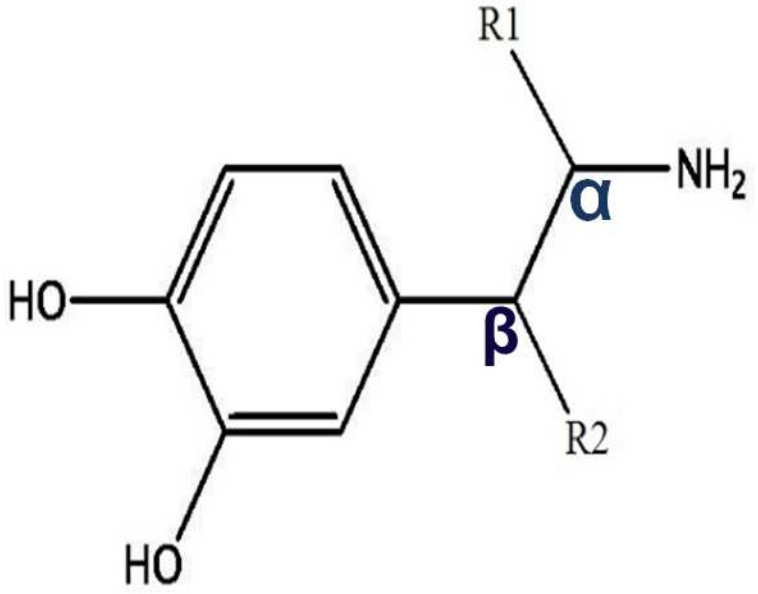

Figure 4.6 The pharmacophore and the substituent groups (R1 and R2) which are considered to improve the binding affinity of the pharmacophore to the target motif.

Another drug design strategy is to find an anti-fibrillization lead compound among the natural compounds found in plants. For example, it has been reported that nicotine, caffeine and curcumin reduce the incidence of PD (Altman *et al.*, 2011; Ascherio and Chen, 2003; Checkoway *et al.*, 2002; Darvesh *et al.*, 2012; Hernán *et al.*, 2002; Kessler and Diamond, 1971; Mythri and Bharath, 2012; Postuma *et al.*, 2012; Quik, 2004; Ross *et al.*, 2000; Ross and Petrovitch, 2001). It also has been reported that nicotine and curcumin inhibit AS fibril formation by stabilizing AS oligomers (Ahmad and Lapidus, 2012; Hong *et al.*, 2009; Singh *et al.*, 2012). As these natural chemicals are parts of the daily diet of most people, their structure can be used as lead compounds to design new anti-fibrillization agents. Our results showed that (-)-nicotine and caffeine at the concentration of 10 μM shifted the AS translocation peak from -86 pA to -60 pA and -80 pA (Figure 3.31a,b). These small molecules can be used as candidates to design a new drug as an AS misfolding inhibitor using a fragmentation drug design approach (Hajduk and Greer, 2007; Joseph-McCarthy *et al.*, 2014). The blockade current histogram showed an increase in the intensity of the peak centered at -25 pA when both drugs are present (Figure 3.31d) in comparison with (-)-nicotine (Figure 3.31b) and caffeine (Figure 3.31c) and also the intermediate peaks in the presence of nicotine and caffeine were disappeared (Figure 3.31b,c). This new peak might represent a new conformation of AS which cannot complete the aggregation process. Thus, these small molecules could be connected together using a linker like the linker of the curcumin molecule (Figure 1.19b). The new drug, caffetine, (Figure 4.7) would possess the features of both caffeine and nicotine and might be used as a new therapeutic to prevent AS misfolding and aggregation. The effect of the new synthesized drug on AS misfolding and aggregation must be evaluated using nanopore analysis, NMR spectroscopy and the ThT assay to characterize the biochemical mechanism. ITC can be used to measure the dissociation constant of the interaction. As the goal in fragment based drug design is to increase the efficacy of the interaction (Hajduk and Greer, 2007; Joseph-McCarthy *et al.*, 2014), the results of *in vitro* experiments with the combined drug must be compared with the individual drugs. Then cell culture assays and animal models can be used to measure the IC_{50} of this drug and also to evaluate its safety.

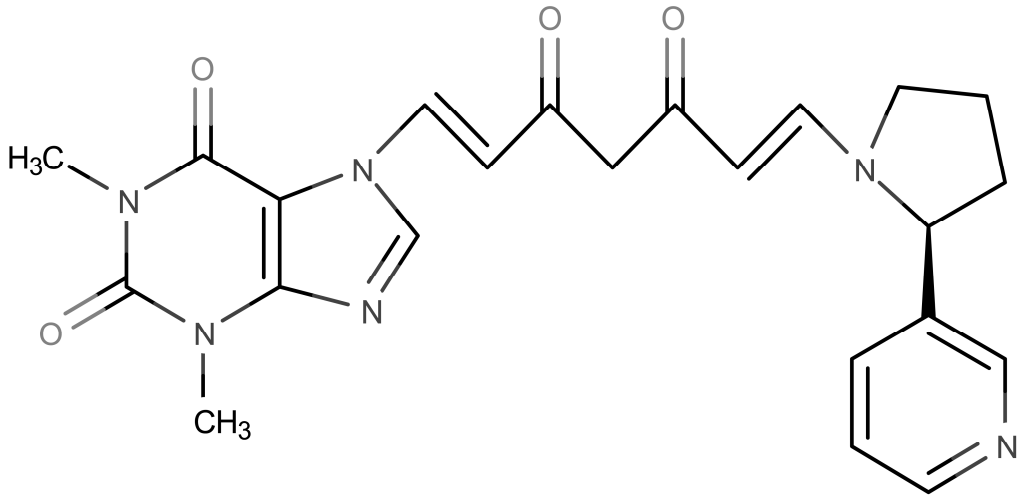

Figure 4.7 Structure of caffetine which results from connection of caffeine and (-)-nicotine using curcumin linker.

Another group of anti-fibrillization agents are β-sheet breaker peptides (Amer *et al.*, 2006; Soto, 2003). Since protein aggregation, which is the result of protein–protein interactions is very specific, preventing these interactions is a feasible strategy to cure and treat PD (Kim *et al.*, 2009). One of the approaches that could attack AS misfolding and aggregation is destabilization of the pathological β-sheet conformation of misfolded proteins, for example by using β-sheet breaker peptides to inhibit and reverse the protein misfolding process (Figure 4.8) (Amer *et al.*, 2006; Soto, 2003). Beta-sheet breakers are modified synthetic peptides based on the native sequences of amyloid peptides or proteins that are able to bind to the native proteins. These short peptides are designed to arrest the folding of the polypeptide chain in a β-sheet structure and to prevent the conversion of native protein or peptide sequences into the β-sheet-rich aggregate (El-Agnaf *et al.*, 2004; Soto, 2003).

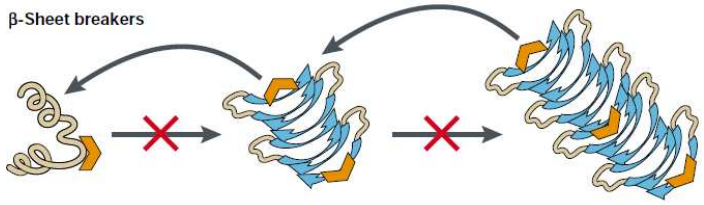

Figure 4.8 Schematic representation of inhibition and reversal of protein misfolding by β-sheet breaker peptides which are shown in brown (Soto, 2003). Copyright © 2003 Nature Publishing Group. All rights reserved.

A part of the hydrophobic region or NAC (amino acids 68–78: "GAVVTGVTAVA") has been determined as the critical binding site for AS. The identified binding region has been used for the design of homologous short peptides which would interact with the same region in the full-length AS molecule, and prevent its misfolding and aggregation by stabilizing the unfolded monomers (Abe *et al.*, 2007; El-Agnaf *et al.*, 2004). Missense mutations which reduce or remove fibril formation of AS are another approach to identify the critical aggregation motifs in AS. Six self fibrillation-defective mutants (V66S, V66P, T72P, V74E, V74G, and T75P) have been identified to block fibrillation of wild-type/PD-linked AS molecules completely. The flanking regions of these mutants can be used as peptide inhibitors to stabilize the unfolded monomers of AS (Choi *et al.*, 2011; Kim *et al.*, 2009; Koo *et al.*, 2009). The disadvantage of these peptides is that they are hydrophobic. A strategy to overcome this limitation is to place hydrophilic residues at one or both termini to increase the solubility of them. For example hydrophilic residues, arginine and glycine, can be placed at the N-terminus and the C-terminus of the synthetic peptides (Amer *et al.*, 2006; El-Agnaf *et al.*, 2004). This strategy which produces positively-charged peptides is an efficient peptide design technique for nanopore studies. As the electrophoretic movement of positively-charged small peptides is away from the pore, they will not produce a significant signal during the experiment. Using this approach a library of β-sheet breaker peptides can be designed and their interaction with AS can be studied using nanopore analysis. The limitation of peptide drugs is that they are substrates for peptidase enzymes and will be degraded before reaching the target. To overcome this limitation, D-amino acids could be used instead of the L-amino acids to synthesize the peptides (Welch *et al.*, 2007).

AS is a natively unfolded protein and lacks any 3D binding pockets which are found in folded proteins with 3D structure. Interaction of a ligand with AS involves binding of the ligand to a group of neighboring or long-distanced residues and causing that region to make a loop around the ligand. The binding region is determined by the ligand biochemical properties such as polarity, hydrophobicity and structure. In 1996 a group of artificial receptors were designed with the ability to bind to specific moieties in a polymer (Klärner *et al.*, 1996). As these horseshoe shaped molecules were able to enfold their specific target groups, they were called "molecular tweezers" (Fokkens *et al.*, 2005; Klärner *et al.*, 1996). Later in 2005 a lysine-specific molecular tweezer (CLR01) was synthesized (Figure 4.9, Figure 4.10a) which specifically binds to lysine residues with a K_d of 20 μM. This molecular tweezer features a rigid horseshoe shaped cavity

with two nonpolar wings and two rotatable peripheral anionic phosphates attached to the joint of the structure (Figure 4.9, Figure 4.10a) (Acharya *et al.*, 2014; Attar *et al.*, 2014; Attar *et al.*, 2012; Ferreira *et al.*, 2014; Fokkens *et al.*, 2005; Prabhudesai *et al.*, 2012; Sinha *et al.*, 2012a; Sinha *et al.*, 2011a; Sinha *et al.*, 2012b; Talbiersky *et al.*, 2008).

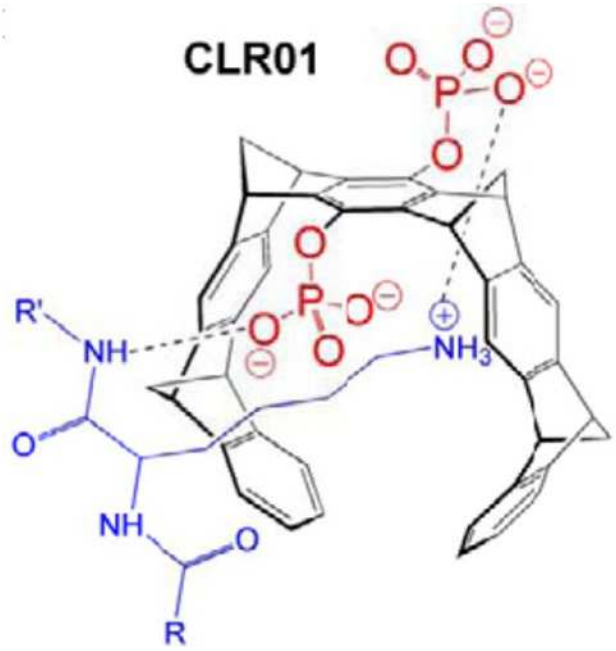

Figure 4.9 Structure of CLR01 bound to a lysine side-chain (blue) (Acharya *et al.*, 2014). Copyright © 2014 American Society for Biochemistry and Molecular Biology. All rights reserved.

Disordered proteins are mostly composed of disorder-promoting residues including polar and charged amino acids (glutamic acid, aspartic acid, lysine, arginine, glycine, glutamine, serine and proline) (Chiti and Dobson, 2006; Oldfield and Dunker, 2014; Theillet *et al.*, 2013; Uversky, 2011, 2013a, b). Among these residues, lysine has an important role in disordered proteins. For example, the "KKLVFF" motif in the central part of the β-amyloid peptide serves as the nucleation site which triggers the misfolding and aggregation (Fokkens *et al.*, 2005; Sinha *et al.*, 2012b). Similarly, AS contains 7 repeats of 11-residue sequence, each containing a variant of the consensus 6-residue sequence "KTKEGV" (Auluck *et al.*, 2010; Dikiy and Eliezer, 2012; Jo *et al.*, 2000). These lysine residues also are involved in hydrophobic and electrostatic interactions which causes the misfolding and self-assembly of unfolded monomers (Sinha *et al.*, 2012b). Targeting of these critical residues with lysine-specific molecular tweezers causes masking of lysine residues and stabilizes the unfolded conformation (Acharya *et al.*, 2014; Attar *et al.*, 2014;

Attar *et al.*, 2012; Ferreira *et al.*, 2014; Fokkens *et al.*, 2005; Prabhudesai *et al.*, 2012; Sinha *et al.*, 2012a; Sinha *et al.*, 2011a; Sinha *et al.*, 2012b). Thus interaction of these groups of small molecules with lysine residues of unfolded proteins, may be an efficient strategy to target specific regions of unfolded proteins which lack regular cavity like binding sites (Acharya *et al.*, 2014; Attar *et al.*, 2014; Attar *et al.*, 2012; Ferreira *et al.*, 2014; Fokkens *et al.*, 2005; Prabhudesai *et al.*, 2012; Sinha *et al.*, 2012a; Sinha *et al.*, 2011a; Sinha *et al.*, 2012b; Talbiersky *et al.*, 2008). These small molecules have been successfully used as anti-fibrillization agents to prevent the fibrillization of AS (Acharya *et al.*, 2014; Attar and Bitan, 2014; Prabhudesai *et al.*, 2012), β2-Microglobulin (Attar and Bitan, 2014), islet Amyloid Polypeptide (IAPP) (Attar and Bitan, 2014), β-amyloid (Attar and Bitan, 2014; Attar *et al.*, 2014; Attar *et al.*, 2012; Sinha *et al.*, 2012a; Sinha *et al.*, 2012b), insulin (Attar and Bitan, 2014), calcitonin (Attar and Bitan, 2014) and transthyretin (Ferreira *et al.*, 2014) in both *in vivo* and *in vitro* systems. AS has 15 lysine residues which are distributed throughout the sequence as follow: 11 residues at the N-terminus, 1 residue at the NAC region and 3 residues at the C-terminus. *In vitro* experiments using thioflavin T fluorescence, electron microscopy and *in vivo* experiments in a zebrafish model of AS have demonstrated that the CLR01 molecular tweezers prevents the misfolding of AS monomers into β-sheet-rich fibrils and also causes the disaggregation of pre-formed fibrils (Acharya *et al.*, 2014; Prabhudesai *et al.*, 2012). Mass-spectrometric analysis has revealed that CLR01 binds two lysine residues at the N-terminus (Lys-10 and/or Lys-12) (Acharya *et al.*, 2014). This molecular tweezers just masks two of the lysine residues at the N-terminus, while there are C-terminal lysine residues which can facilitate long range interaction of C- and N-terminal and cause folding. Thus a possible strategy to increase the efficiency of CLR01 would be chemical modifications which increase its affinity for the C-terminus of AS. Our nanopore experiments with (-)-methamphetamine showed that this molecule binds to the C-terminal of AS (Figure 3.9b). The (l)-N-methyl-propan-2-amine moiety can be attached to the benzyl ring of one side of CLR01 in order to generate a (-)-methamphetamine analogue (Figure 4.10b). The (-)-methamphetamine moiety attached to CLR01 might increase the affinity of the molecule for the C-terminal. Nanopore analysis, NMR spectroscopy, CD spectroscopy and ITC will be useful in assessing the efficacy of these new drugs.

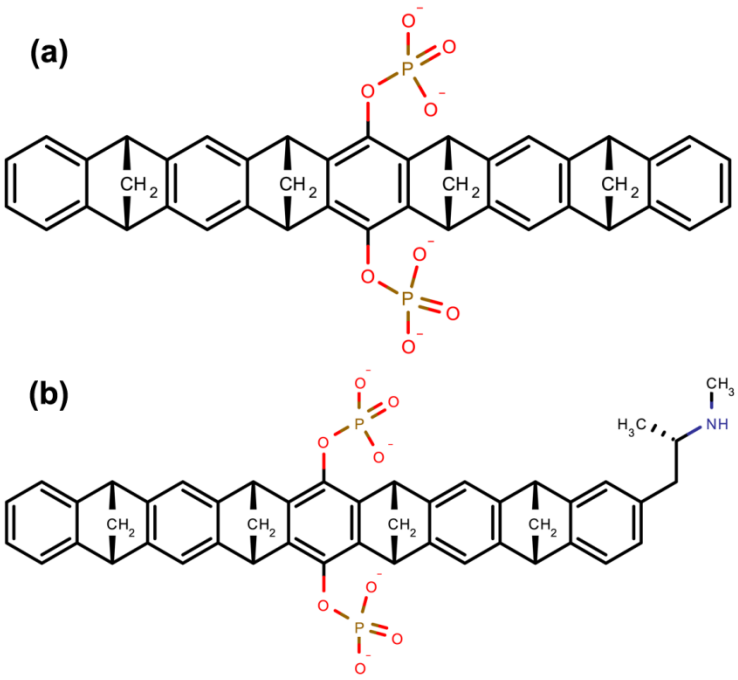

Figure 4.10 Structure of CLR01 (a) and CLR01 with a (l)-N-methyl-propan-2-amine moiety attached to one of the side benzyl rings (b)

From the above discussion it would appear that many lead compounds are available and that a suitable drug with high affinity and specificity will be available soon. Nanopore analysis will undoubtedly prove useful in evaluating the interactions of these drugs with AS.

5 References

Abe, K., Kobayashi, N., Sode, K., and Ikebukuro, K. (2007). Peptide ligand screening of alpha-synuclein aggregation modulators by in silico panning. BMC Bioinformatics *8*, 451.

Abramov, A.Y., Gegg, M., Grunewald, A., Wood, N.W., Klein, C., and Schapira, A.H. (2011). Bioenergetic consequences of PINK1 mutations in Parkinson disease. PLoS One *6*, e25622.

Acharya, S., Safaie, B.M., Wongkongkathep, P., Ivanova, M.I., Attar, A., Klärner, F.-G., Schrader, T., Loo, J.A., Bitan, G., and Lapidus, L.J. (2014). Molecular Basis for Preventing α-Synuclein Aggregation by a Molecular Tweezer. J. Biol. Chem. *289*, 10727-10737.

Ahmad, B., and Lapidus, L.J. (2012). Curcumin Prevents Aggregation in α-Synuclein by Increasing Reconfiguration Rate. J. Biol. Chem. *287*, 9193-9199.

Ajjimaporn, A., Phansuwan-Pujito, P., Ebadi, M., and Govitrapong, P. (2007). Zinc protects SK-N-SH cells from methamphetamine-induced alpha-synuclein expression. Neurosci. Lett. *419*, 59-63.

Alderson, T.R., and Markley, J.L. (2013). Biophysical characterization of alpha-synuclein and its controversial structure. Intrinsic. Disord. Prot. *1*, 18-39.

Altman, R.D., Lang, A.E., and Postuma, R.B. (2011). Caffeine in Parkinson's disease: A pilot open-label, dose-escalation study. Mov. Disord. *26*, 2427-2431.

Alves, G., Kurz, M., Lie, S.A., and Larsen, J.P. (2004). Cigarette smoking in Parkinson's disease: Influence on disease progression. Mov. Disord. *19*, 1087-1092.

Amer, D.A., Irvine, G.B., and El-Agnaf, O.M. (2006). Inhibitors of alpha-synuclein oligomerization and toxicity: a future therapeutic strategy for Parkinson's disease and related disorders. Exp. Brain Res. *173*, 223-233.

Andén, N.-E., Fuxe, K., Hamberoer, B., and Hökfelt, T. (1966). A Quantitative Study on the Nigro-Neostriatal Dopamine Neuron System in the Rat. Acta Physiol. Scand. *67*, 306-312.

Anderson, V.L., Ramlall, T.F., Rospigliosi, C.C., Webb, W.W., and Eliezer, D. (2010). Identification of a helical intermediate in trifluoroethanol-induced alpha-synuclein aggregation. Proc. Natl. Acad. Sci. U.S.A. *107*, 18850-18855.

Andres-Mateos, E., Perier, C., Zhang, L., Blanchard-Fillion, B., Greco, T.M., Thomas, B., Ko, H.S., Sasaki, M., Ischiropoulos, H., Przedborski, S., *et al.* (2007). DJ-1 gene deletion reveals that DJ-1 is an atypical peroxiredoxin-like peroxidase. Proc. Natl. Acad. Sci. U.S.A. *104*, 14807-14812.

Anglin, M.D., Burke, C., Perrochet, B., Stamper, E., and Dawud-Noursi, S. (2000). History of the methamphetamine problem. J. Psychoactive Drugs *32*, 137-141.

Angot, E., Steiner, J.A., Lema Tome, C.M., Ekstrom, P., Mattsson, B., Bjorklund, A., and Brundin, P. (2012). Alpha-synuclein cell-to-cell transfer and seeding in grafted dopaminergic neurons in vivo. PLoS One *7*, e39465.

Antony, T., Hoyer, W., Cherny, D., Heim, G., Jovin, T.M., and Subramaniam, V. (2003). Cellular Polyamines Promote the Aggregation of α-Synuclein. J. Biol. Chem. *278*, 3235-3240.

Apetri, M.M., Maiti, N.C., Zagorski, M.G., Carey, P.R., and Anderson, V.E. (2006). Secondary Structure of α-Synuclein Oligomers: Characterization by Raman and Atomic Force Microscopy. J. Mol. Biol. *355*, 63-71.

Arduino, D.M., Esteves, A.R., and Cardoso, S.M. (2011). Mitochondrial fusion/fission, transport and autophagy in Parkinson's disease: when mitochondria get nasty. Parkinsons Dis. *2011*, 1-13.

Arnaut, V., Langecker, M., and Simmel, Friedrich C. Nanopore Force Spectroscopy of Aptamer–Ligand Complexes. Biophys. J. *105*, 1199-1207.

Asandei, A., Schiopu, I., Iftemi, S., Mereuta, L., and Luchian, T. (2013). Investigation of Cu2+ Binding to Human and Rat Amyloid Fragments Aβ (1–16) with a Protein Nanopore. Langmuir *29*, 15634-15642.

Ascherio, A., and Chen, H. (2003). Caffeinated clues from epidemiology of Parkinson's disease. Neurology *61*, S51-S54.

Attar, A., and Bitan, G. (2014). Disrupting self-assembly and toxicity of amyloidogenic protein oligomers by "molecular tweezers" - from the test tube to animal models. Curr. Pharm. Des. *20*, 2469-2483.

Attar, A., Chan, W.T., Klarner, F.G., Schrader, T., and Bitan, G. (2014). Safety and pharmacological characterization of the molecular tweezer CLR01 - a broad-spectrum inhibitor of amyloid proteins' toxicity. BMC Pharmacol. Toxicol. *15*, 1-14.

Attar, A., Ripoli, C., Riccardi, E., Maiti, P., Li Puma, D.D., Liu, T., Hayes, J., Jones, M.R., Lichti-Kaiser, K., Yang, F., *et al.* (2012). Protection of primary neurons and mouse brain from Alzheimer's pathology by molecular tweezers. Brain *135*, 3735-3748.

Auluck, P.K., Caraveo, G., and Lindquist, S. (2010). α-Synuclein: Membrane Interactions and Toxicity in Parkinson's Disease. Annu. Rev. Cell Dev. Biol. *26*, 211-233.

Babu, M.M., van der Lee, R., de Groot, N.S., and Gsponer, J. (2011). Intrinsically disordered proteins: regulation and disease. Curr. Opin. Struct. Biol. *21*, 432-440.

Banerjee, J., and Nilsen-Hamilton, M. (2013). Aptamers: multifunctional molecules for biomedical research. J. Mol. Med. *91*, 1333-1342.

Banerjee, K., Sinha, M., Pham, C.L.L., Jana, S., Chanda, D., Cappai, R., and Chakrabarti, S. (2010). α-Synuclein induced membrane depolarization and loss of phosphorylation capacity of isolated rat brain mitochondria: Implications in Parkinson's disease. FEBS Lett. *584*, 1571-1576.

Baptista, M.J., O'Farrell, C., Daya, S., Ahmad, R., Miller, D.W., Hardy, J., Farrer, M.J., and Cookson, M.R. (2003). Co-ordinate transcriptional regulation of dopamine synthesis genes by α-synuclein in human neuroblastoma cell lines. J. Neurochem. *85*, 957-968.

Baran, C., Smith, G.S.T., Bamm, V.V., Harauz, G., and Lee, J.S. (2010). Divalent cations induce a compaction of intrinsically disordered myelin basic protein. Biochem. Biophys. Res. Commun. *391*, 224-229.

Barbar, E. (1999). NMR characterization of partially folded and unfolded conformational ensembles of proteins. Pept. Sci. *51*, 191-207.

Barber, T.W., Brockway, J.A., and Higgins, L.S. (1970). The density of tissues in and about the head. Acta Neurol. Scand. *46*, 85-92.

Barsoum, M.J., Yuan, H., Gerencser, A.A., Liot, G., Kushnareva, Y., Gräber, S., Kovacs, I., Lee, W.D., Waggoner, J., Cui, J., *et al.* (2006). Nitric oxide-induced mitochondrial fission is regulated by dynamin-related GTPases in neurons. EMBO J. *25*, 3900-3911.

Bartels, T., Choi, J.G., and Selkoe, D.J. (2011). alpha-Synuclein occurs physiologically as a helically folded tetramer that resists aggregation. Nature *477*, 107-110.

Bekris, L.M., Mata, I.F., and Zabetian, C.P. (2010). The Genetics of Parkinson Disease. J. Geriatr. Psychiatry Neurol. *23*, 228-242.

Bellucci, A., Navarria, L., Zaltieri, M., Falarti, E., Bodei, S., Sigala, S., Battistin, L., Spillantini, M., Missale, C., and Spano, P. (2011). Induction of the unfolded protein response by α-synuclein in experimental models of Parkinson's disease. J. Neurochem. *116*, 588-605.

Benowitz, N.L., Kuyt, F., and Jacob, P., III (1982). Circadian blood nicotine concentrations during cigarette smoking. Clin. Pharm. Ther. *32*, 758-764.

Bernales, S., Soto, M.M., and McCullagh, E. (2012). Unfolded protein stress in the endoplasmic reticulum and mitochondria: a role in neurodegeneration. Front. Aging Neurosci. *4*, 1-13.

Berry, C., La Vecchia, C., and Nicotera, P. (2010). Paraquat and Parkinson's disease. Cell Death Differ. *17*, 1115-1125.

Berube, B.J., and Bubeck Wardenburg, J. (2013). Staphylococcus aureus alpha-toxin: nearly a century of intrigue. Toxins (Basel) *5*, 1140-1166.

Bharathi, and Rao, K.S.J. (2008). Molecular Understanding of Copper and Iron Interaction with α-Synuclein by Fluorescence Analysis. J. Mol. Neurosci. *35*, 273-281.

Binolfi, A., Quintanar, L., Bertoncini, C.W., Griesinger, C., and Fernández, C.O. (2012). Bioinorganic chemistry of copper coordination to alpha-synuclein: Relevance to Parkinson's disease. Coord. Chem. Rev. *256*, 2188-2201.

Binolfi, A., Rasia, R.M., Bertoncini, C.W., Ceolin, M., Zweckstetter, M., Griesinger, C., Jovin, T.M., and Fernandez, C.O. (2006). Interaction of alpha-synuclein with divalent metal ions reveals key differences: a link between structure, binding specificity and fibrillation enhancement. J. Am. Chem. Soc. *128*, 9893-9901.

Bisaglia, M., Tessari, I., Mammi, S., and Bubacco, L. (2009). Interaction between alpha-synuclein and metal ions, still looking for a role in the pathogenesis of Parkinson's disease. Neuromolecular Med. *11*, 239-251.

Blake, C.I., Spitz, E., Leehey, M., Hoffer, B.J., and Boyson, S.J. (1997). Platelet mitochondrial respiratory chain function in Parkinson's disease. Mov. Disord. *12*, 3-8.

Bohic, S., Murphy, K., Paulus, W., Cloetens, P., Salomé, M., Susini, J., and Double, K. (2008). Intracellular Chemical Imaging of the Developmental Phases of Human Neuromelanin Using Synchrotron X-ray Microspectroscopy. Anal. Chem. *80*, 9557-9566.

Boll, M.-C., Alcaraz-Zubeldia, M., Montes, S., and Rios, C. (2008). Free Copper, Ferroxidase and SOD1 Activities, Lipid Peroxidation and NO x Content in the CSF. A Different Marker Profile in Four Neurodegenerative Diseases. Neurochem. Res. *33*, 1717-1723.

Bonini, N.M., and Giasson, B.I. (2005). Snaring the Function of α-Synuclein. Cell *123*, 359-361.

Bortolus, M., Tombolato, F., Tessari, I., Bisaglia, M., Mammi, S., Bubacco, L., Ferrarini, A., and Maniero, A.L. (2008). Broken Helix in Vesicle and Micelle-Bound α-Synuclein: Insights from Site-Directed Spin Labeling-EPR Experiments and MD Simulations. J. Am. Chem. Soc. *130*, 6690-6691.

Bové, J., Prou, D., Perier, C., and Przedborski, S. (2005). Toxin-induced models of Parkinson’s disease. NeuroRx *2*, 484-494.

Braak, H., Tredici, K.D., Rüb, U., de Vos, R.A.I., Jansen Steur, E.N.H., and Braak, E. (2003). Staging of brain pathology related to sporadic Parkinson’s disease. Neurobiol. Aging *24*, 197-211.

Braga, C.A., Follmer, C., Palhano, F.L., Khattar, E., Freitas, M.S., Romao, L., Di Giovanni, S., Lashuel, H.A., Silva, J.L., and Foguel, D. (2011). The anti-Parkinsonian drug selegiline delays the nucleation phase of alpha-synuclein aggregation leading to the formation of nontoxic species. J. Mol. Biol. *405*, 254-273.

Branton, D., Deamer, D.W., Marziali, A., Bayley, H., Benner, S.A., Butler, T., Di Ventra, M., Garaj, S., Hibbs, A., Huang, X., *et al.* (2008). The potential and challenges of nanopore sequencing. Nat. Biotechnol. *26*, 1146-1153.

Bridges, H.R., Birrell, J.A., and Hirst, J. (2011). The mitochondrial-encoded subunits of respiratory complex I (NADH:ubiquinone oxidoreductase): identifying residues important in mechanism and disease. Biochem. Soc. Trans. *39*, 799-806.

Brody, A.L., Mandelkern, M.A., London, E.D., Olmstead, R.E., Farahi, J., Scheibal, D., Jou, J., Allen, V., Tiongson, E., Chefer, S.I., *et al.* (2006). Cigarette smoking saturates brain alpha 4 beta 2 nicotinic acetylcholine receptors. Arch. Gen. Psychiatry *63*, 907-915.

Brorsson, A.C., Kumita, J.R., MacLeod, I., Bolognesi, B., Speretta, E., Luheshi, L.M., Knowles, T.P., Dobson, C.M., and Crowther, D.C. (2010). Methods and models in neurodegenerative and systemic protein aggregation diseases. Front Biosci. (Landmark Ed) *15*, 373-396.

Brown, D.R. (2013). alpha-Synuclein as a ferrireductase. Biochem. Soc. Trans. *41*, 1513-1517.

Brucale, M., Sandal, M., Di Maio, S., Rampioni, A., Tessari, I., Tosatto, L., Bisaglia, M., Bubacco, L., and Samori, B. (2009). Pathogenic mutations shift the equilibria of alpha-synuclein single molecules towards structured conformers. ChemBioChem *10*, 176-183.

Brucale, M., Schuler, B., and Samorì, B. (2014). Single-Molecule Studies of Intrinsically Disordered Proteins. Chem. Rev. *114*, 3281-3317.

Burré, J., Sharma, M., and Südhof, T.C. (2012). Systematic Mutagenesis of α-Synuclein Reveals Distinct Sequence Requirements for Physiological and Pathological Activities. J. Neurosci. *32*, 15227-15242.

Burre, J., Vivona, S., Diao, J., Sharma, M., Brunger, A.T., and Sudhof, T.C. (2013). Properties of native brain [agr]-synuclein. Nature *498*, E4-E6.

Butler, B., Saha, K., and Khoshbouei, H. (2012). α-synuclein regulation of dopamine transporter. Transl. Neurosci. *3*, 249-257.

Cagalinec, M., Safiulina, D., Liiv, M., Liiv, J., Choubey, V., Wareski, P., Veksler, V., and Kaasik, A. (2013). Principles of the mitochondrial fusion and fission cycle in neurons. J. Cell Sci.

Calì, T., Ottolini, D., and Brini, M. (2011). Mitochondria, calcium, and endoplasmic reticulum stress in Parkinson's disease. Biofactors *37*, 228-240.

Callaghan, R.C., Cunningham, J.K., Sajeev, G., and Kish, S.J. (2010). Incidence of Parkinson's disease among hospital patients with methamphetamine-use disorders. Mov. Disord. *25*, 2333-2339.

Callaghan, R.C., Cunningham, J.K., Sykes, J., and Kish, S.J. (2012). Increased risk of Parkinson's disease in individuals hospitalized with conditions related to the use of methamphetamine or other amphetamine-type drugs. Drug Alcohol Depend. *120*, 35-40.

Cappai, R., Leck, S.L., Tew, D.J., Williamson, N.A., Smith, D.P., Galatis, D., Sharples, R.A., Curtain, C.C., Ali, F.E., Cherny, R.A., *et al.* (2005). Dopamine promotes alpha-synuclein aggregation into SDS-resistant soluble oligomers via a distinct folding pathway. FASEB J. *19*, 1377-1379.

Carlsen, A.T., Zahid, O.K., Ruzicka, J.A., Taylor, E.W., and Hall, A.R. (2014). Selective Detection and Quantification of Modified DNA with Solid-State Nanopores. Nano Lett.

Chan, D.C. (2012). Fusion and Fission: Interlinked Processes Critical for Mitochondrial Health. Annu. Rev. Genet. *46*, 265-287.

Chan, P., DeLanney, L.E., Irwin, I., Langston, J.W., and Di Monte, D. (1991). Rapid ATP Loss Caused by 1-Methyl-4-Phenyl-1,2,3,6-Tetrahydropyridine in Mouse Brain. J. Neurochem. *57*, 348-351.

Chandra, S., Chen, X., Rizo, J., Jahn, R., and Südhof, T.C. (2003). A Broken α-Helix in Folded α-Synuclein. J. Biol. Chem. *278*, 15313-15318.

Chandra, S., Gallardo, G., Fernandez-Chacon, R., Schluter, O.M., and Sudhof, T.C. (2005). Alpha-synuclein cooperates with CSPalpha in preventing neurodegeneration. Cell *123*, 383-396.

Chatterjee, A., Kumar, A., Chugh, J., Srivastava, S., Bhavesh, N., and Hosur, R. (2005). NMR of unfolded proteins. J. Chem. Sci. *117*, 3-21.

Checkoway, H., Powers, K., Smith-Weller, T., Franklin, G.M., Longstreth, W.T., and Swanson, P.D. (2002). Parkinson's Disease Risks Associated with Cigarette Smoking, Alcohol Consumption, and Caffeine Intake. Am. J. Epidemiol. *155*, 732-738.

Chen, J.F., Xu, K., Petzer, J.P., Staal, R., Xu, Y.H., Beilstein, M., Sonsalla, P.K., Castagnoli, K., Castagnoli, N., Jr., and Schwarzschild, M.A. (2001). Neuroprotection by caffeine and A(2A) adenosine receptor inactivation in a model of Parkinson's disease. J. Neurosci. *21*, RC143.

Chen, L., Huang, E., Wang, H., Qiu, P., and Liu, C. (2013). RNA interference targeting α-synuclein attenuates methamphetamine-induced neurotoxicity in SH-SY5Y cells. Brain Res. *1521*, 59-67.

Chen, Y., and Dorn, G.W. (2013). PINK1-Phosphorylated Mitofusin 2 Is a Parkin Receptor for Culling Damaged Mitochondria. Science *340*, 471-475.

Chinta, S.J., Mallajosyula, J.K., Rane, A., and Andersen, J.K. (2010). Mitochondrial alpha-synuclein accumulation impairs complex I function in dopaminergic neurons and results in increased mitophagy in vivo. Neurosci. Lett. *486*, 235-239.

Chiti, F., and Dobson, C.M. (2006). Protein misfolding, functional amyloid, and human disease. Annu. Rev. Biochem. *75*, 333-366.

Cho, A.K., and Melega, W.P. (2002). Patterns of methamphetamine abuse and their consequences. J. Addict. Dis. *21*, 21-34.

Choi, M.Y., Kim, Y.S., Lim, D., Kang, S.J., Kim, Y.H., Lee, K., and Im, H. (2011). The hexapeptide PGVTAV suppresses neurotoxicity of human alpha-synuclein aggregates. Biochem. Biophys. Res. Commun. *408*, 334-338.

Christensen, C., Baran, C., Krasniqi, B., Stefureac, R.I., Nokhrin, S., and Lee, J.S. (2011). Effect of charge, topology and orientation of the electric field on the interaction of peptides with the alpha-hemolysin pore. J. Pept. Sci. *17*, 726-734.

Clarke, J., Wu, H.C., Jayasinghe, L., Patel, A., Reid, S., and Bayley, H. (2009). Continuous base identification for single-molecule nanopore DNA sequencing. Nat. Nanotechnol. *4*, 265-270.

Colla, E., Coune, P., Liu, Y., Pletnikova, O., Troncoso, J.C., Iwatsubo, T., Schneider, B.L., and Lee, M.K. (2012a). Endoplasmic Reticulum Stress Is Important for the Manifestations of α-Synucleinopathy In Vivo. J. Neurosci. *32*, 3306-3320.

Colla, E., Jensen, P.H., Pletnikova, O., Troncoso, J.C., Glabe, C., and Lee, M.K. (2012b). Accumulation of Toxic α-Synuclein Oligomer within Endoplasmic Reticulum Occurs in α-Synucleinopathy In Vivo. J. Neurosci. *32*, 3301-3305.

Conway, K.A., Lee, S.-J., Rochet, J.-C., Ding, T.T., Williamson, R.E., and Lansbury, P.T. (2000). Acceleration of oligomerization, not fibrillization, is a shared property of both α-synuclein mutations linked to early-onset Parkinson's disease: Implications for pathogenesis and therapy. Proc. Natl. Acad. Sci. U.S.A. *97*, 571-576.

Conway, K.A., Rochet, J.C., Bieganski, R.M., and Lansbury, P.T., Jr. (2001). Kinetic stabilization of the alpha-synuclein protofibril by a dopamine-alpha-synuclein adduct. Science *294*, 1346-1349.

Cooper, A.A., Gitler, A.D., Cashikar, A., Haynes, C.M., Hill, K.J., Bhullar, B., Liu, K., Xu, K., Strathearn, K.E., Liu, F., *et al.* (2006). Alpha-synuclein blocks ER-Golgi traffic and Rab1 rescues neuron loss in Parkinson's models. Science *313*, 324-328.

Cremades, N., Cohen, Samuel I.A., Deas, E., Abramov, Andrey Y., Chen, Allen Y., Orte, A., Sandal, M., Clarke, Richard W., Dunne, P., Aprile, Francesco A., *et al.* (2012). Direct Observation of the Interconversion of Normal and Toxic Forms of α-Synuclein. Cell *149*, 1048-1059.

Cui, M., Tang, X., Christian, W.V., Yoon, Y., and Tieu, K. (2010). Perturbations in Mitochondrial Dynamics Induced by Human Mutant PINK1 Can Be Rescued by the Mitochondrial Division Inhibitor mdivi-1. J. Biol. Chem. *285*, 11740-11752.

da Silva, F.L., Coelho Cerqueira, E., de Freitas, M.S., Gonçalves, D.L., Costa, L.T., and Follmer, C. (2013). Vitamins K interact with N-terminus α-synuclein and modulate the protein fibrillization in vitro. Exploring the interaction between quinones and α-synuclein. Neurochem. Int. *62*, 103-112.

Danzer, K.M., Kranich, L.R., Ruf, W.P., Cagsal-Getkin, O., Winslow, A.R., Zhu, L., Vanderburg, C.R., and McLean, P.J. (2012). Exosomal cell-to-cell transmission of alpha synuclein oligomers. Mol. Neurodegener. *7*, 1-18.

Darvesh, A.S., Carroll, R.T., Bishayee, A., Novotny, N.A., Geldenhuys, W.J., and Van der Schyf, C.J. (2012). Curcumin and neurodegenerative diseases: a perspective. Expert Opin. Invest. Drugs *21*, 1123-1140.

Dauer, W., and Przedborski, S. (2003). Parkinson's Disease: mechanisms and models. Neuron *39*, 889-909.

Davidson, W.S., Jonas, A., Clayton, D.F., and George, J.M. (1998). Stabilization of α-Synuclein Secondary Structure upon Binding to Synthetic Membranes. J. Biol. Chem. *273*, 9443-9449.

Davies, K.M., Bohic, S., Carmona, A., Ortega, R., Cottam, V., Hare, D.J., Finberg, J.P.M., Reyes, S., Halliday, G.M., Mercer, J.F.B., *et al.* (2014). Copper pathology in vulnerable brain regions in Parkinson's disease. Neurobiol. Aging *35*, 858-866.

Davies, P., Moualla, D., and Brown, D.R. (2011). Alpha-synuclein is a cellular ferrireductase. PLoS One *6*, e15814.

Dawson, T.M., and Dawson, V.L. (2003). Molecular Pathways of Neurodegeneration in Parkinson's Disease. Science *302*, 819-822.

Deas, E., Wood, N.W., and Plun-Favreau, H. (2011). Mitophagy and Parkinson's disease: The PINK1–parkin link. Biochim. Biophys. Acta *1813*, 623-633.

DeGuzman, V.S., Lee, C.C., Deamer, D.W., and Vercoutere, W.A. (2006). Sequence-dependent gating of an ion channel by DNA hairpin molecules. Nucleic Acids Res. *34*, 6425-6437.

Delaglio, F., Grzesiek, S., Vuister, G., Zhu, G., Pfeifer, J., and Bax, A. (1995). NMRPipe: A multidimensional spectral processing system based on UNIX pipes. J. Biomol. NMR *6*, 277-293.

Deng, H., Dodson, M.W., Huang, H., and Guo, M. (2008). The Parkinson's disease genes pink1 and parkin promote mitochondrial fission and/or inhibit fusion in Drosophila. Proc. Natl. Acad. Sci. U.S.A. *105*, 14503-14508.

Derrington, I.M., Butler, T.Z., Collins, M.D., Manrao, E., Pavlenok, M., Niederweis, M., and Gundlach, J.H. (2010). Nanopore DNA sequencing with MspA. Proc. Natl. Acad. Sci. *107*, 16060-16065.

Desplats, P., Lee, H.-J., Bae, E.-J., Patrick, C., Rockenstein, E., Crews, L., Spencer, B., Masliah, E., and Lee, S.-J. (2009). Inclusion formation and neuronal cell death through neuron-to-neuron transmission of α-synuclein. Proc. Natl. Acad. Sci. U.S.A. *106*, 13010-13015.

Devi, L., Raghavendran, V., Prabhu, B.M., Avadhani, N.G., and Anandatheerthavarada, H.K. (2008). Mitochondrial Import and Accumulation of α-Synuclein Impair Complex I in Human Dopaminergic Neuronal Cultures and Parkinson Disease Brain. J. Biol. Chem. *283*, 9089-9100.

Dexter, D.T., Wells, F.R., Lees, A.J., Agid, F., Agid, Y., Jenner, P., and Marsden, C.D. (1989). Increased nigral iron content and alterations in other metal ions occurring in brain in Parkinson's disease. J. Neurochem. *52*, 1830-1836.

Di Giovanni, S., Eleuteri, S., Paleologou, K.E., Yin, G., Zweckstetter, M., Carrupt, P.A., and Lashuel, H.A. (2010). Entacapone and tolcapone, two catechol O-methyltransferase inhibitors, block fibril formation of alpha-synuclein and beta-amyloid and protect against amyloid-induced toxicity. J. Biol. Chem. *285*, 14941-14954.

Dieteren, C.E.J., Willems, P.H.G.M., Vogel, R.O., Swarts, H.G., Fransen, J., Roepman, R., Crienen, G., Smeitink, J.A.M., Nijtmans, L.G.J., and Koopman, W.J.H. (2008). Subunits of Mitochondrial Complex I Exist as Part of Matrix- and Membrane-associated Subcomplexes in Living Cells. J. Biol. Chem. *283*, 34753-34761.

Dikiy, I., and Eliezer, D. (2012). Folding and misfolding of alpha-synuclein on membranes. Biochim. Biophys. Acta *1818*, 1013-1018.

DiMauro, S., and Schon, E.A. (2003). Mitochondrial Respiratory-Chain Diseases. N. Engl. J. Med. *348*, 2656-2668.

Douna, H., Bavelaar, B.M., Pellikaan, H., Olivier, B., and Pieters, T. (2012). Neuroprotection in Parkinson's Disease: A Systematic Review of the Preclinical Data. Open Pharmacol. J. *6*, 12-26.

Doyle, K.M., Kennedy, D., Gorman, A.M., Gupta, S., Healy, S.J.M., and Samali, A. (2011). Unfolded proteins and endoplasmic reticulum stress in neurodegenerative disorders. J. Cell. Mol. Med. *15*, 2025-2039.

Dyson, H.J., and Wright, P.E. (2004). Unfolded Proteins and Protein Folding Studied by NMR. Chem. Rev. *104*, 3607-3622.

Dyson, H.J., and Wright, P.E. (2005). Intrinsically unstructured proteins and their functions. Nat. Rev. Mol. Cell Biol. *6*, 197-208.

El-Agnaf, O.M., Paleologou, K.E., Greer, B., Abogrein, A.M., King, J.E., Salem, S.A., Fullwood, N.J., Benson, F.E., Hewitt, R., Ford, K.J., *et al.* (2004). A strategy for designing inhibitors of alpha-synuclein aggregation and toxicity as a novel treatment for Parkinson's disease and related disorders. FASEB J. *18*, 1315-1317.

Exner, N., Lutz, A.K., Haass, C., and Winklhofer, K.F. (2012). Mitochondrial dysfunction in Parkinson's disease: molecular mechanisms and pathophysiological consequences. EMBO J. *31*, 3038-3062.

Ferreira, N., Pereira-Henriques, A., Attar, A., Klärner, F.-G., Schrader, T., Bitan, G., Gales, L., Saraiva, M., and Almeida, M. (2014). Molecular Tweezers Targeting Transthyretin Amyloidosis. Neurotherapeutics *11*, 450-461.

Ferreon, A.C.M., Moosa, M.M., Gambin, Y., and Deniz, A.A. (2012). Counteracting chemical chaperone effects on the single-molecule α-synuclein structural landscape. Proc. Natl. Acad. Sci. U.S.A. *109*, 17826-17831.

Ferri, K.F., and Kroemer, G. (2001). Organelle-specific initiation of cell death pathways. Nat. Cell Biol. *3*, E255-E263.

Finder, V.H., and Glockshuber, R. (2007). Amyloid-β Aggregation. Neurodegener. Dis. *4*, 13-27.

Fink, A.L. (2006). The Aggregation and Fibrillation of α-Synuclein. Acc. Chem. Res. *39*, 628-634.

Fokkens, M., Schrader, T., and Klärner, F.-G. (2005). A Molecular Tweezer for Lysine and Arginine. J. Am. Chem. Soc. *127*, 14415-14421.

Follmer, C., Romão, L., Einsiedler, C.M., Porto, T.C.R., Lara, F.A., Moncores, M., Weissmüller, G., Lashuel, H.A., Lansbury, P., Neto, V.M., *et al.* (2006). Dopamine Affects the Stability, Hydration, and Packing of Protofibrils and Fibrils of the Wild Type and Variants of α-Synuclein. Biochemistry *46*, 472-482.

Fornai, F., Lenzi, P., Ferrucci, M., Lazzeri, G., Poggio, A.B.d., Natale, G., Busceti, C.L., Biagioni, F., Giusiani, M., Ruggieri, S., *et al.* (2005). Occurrence of neuronal inclusions combined with increased nigral expression of α-synuclein within dopaminergic neurons following treatment with amphetamine derivatives in mice. Brain Res. Bull. *65*, 405-413.

Franco, R., Li, S., Rodriguez-Rocha, H., Burns, M., and Panayiotidis, M.I. (2010). Molecular mechanisms of pesticide-induced neurotoxicity: Relevance to Parkinson's disease. Chem. Biol. Interact. *188*, 289-300.

Franssens, V., Boelen, E., Anandhakumar, J., Vanhelmont, T., Buttner, S., and Winderickx, J. (2010). Yeast unfolds the road map toward [alpha]-synuclein-induced cell death. Cell Death Differ. *17*, 746-753.

Frid, P., Anisimov, S.V., and Popovic, N. (2007). Congo red and protein aggregation in neurodegenerative diseases. Brain Res. Rev. *53*, 135-160.

Fujita, M., Ichise, M., Zoghbi, S.S., Liow, J.-S., Ghose, S., Vines, D.C., Sangare, J., Lu, J.-Q., Cropley, V.L., Iida, H., *et al.* (2006). Widespread decrease of nicotinic acetylcholine receptors in Parkinson's disease. Ann. Neurol. *59*, 174-177.

Gautier, C.A., Kitada, T., and Shen, J. (2008). Loss of PINK1 causes mitochondrial functional defects and increased sensitivity to oxidative stress. Proc. Natl. Acad. Sci. U.S.A. *105*, 11364-11369.

Georgieva, E.R., Ramlall, T.F., Borbat, P.P., Freed, J.H., and Eliezer, D. (2008). Membrane-Bound α-Synuclein Forms an Extended Helix: Long-Distance Pulsed ESR Measurements Using Vesicles, Bicelles, and Rodlike Micelles. J. Am. Chem. Soc. *130*, 12856-12857.

Georgieva, E.R., Ramlall, T.F., Borbat, P.P., Freed, J.H., and Eliezer, D. (2010). The Lipid-binding Domain of Wild Type and Mutant α-Synuclein: Compactness and interconversion between the broken and extended helix forms. J. Biol. Chem. *285*, 28261-28274.

Goers, J., Uversky, V.N., and Fink, A.L. (2003). Polycation-induced oligomerization and accelerated fibrillation of human α-synuclein in vitro. Prot. Sci. *12*, 702-707.

Srandaert, D.G., and Walsh R.R. (2007). Pharmacology of dopaminergic neurotransmission. In Principles of Pharmacology: The Pathophysiologic Basis of Drug Therapy, Golan, D.E., Tashjian, A.H., Armstrong, E.J., and Armstrong, A.W., eds. (Lippincott Williams & Wilkins), pp. 186-207.

Gomez-Lazaro, M., Bonekamp, N.A., Galindo, M.F., Jordán, J., and Schrader, M. (2008). 6-Hydroxydopamine (6-OHDA) induces Drp1-dependent mitochondrial fragmentation in SH-SY5Y cells. Free Radic. Biol. Med. *44*, 1960-1969.

Gorbatyuk, M.S., Shabashvili, A., Chen, W., Meyers, C., Sullivan, L.F., Salganik, M., Lin, J.H., Lewin, A.S., Muzyczka, N., and Gorbatyuk, O.S. (2012). Glucose regulated protein 78 diminishes alpha-synuclein neurotoxicity in a rat model of Parkinson disease. Mol. Ther. *20*, 1327-1337.

Gorell, J.M., Ordidge, R.J., Brown, G.G., Deniau, J.-C., Buderer, N.M., and Helpern, J.A. (1995). Increased iron-related MRI contrast in the substantia nigra in Parkinson's disease. Neurology *45*, 1138-1143.

Granado, N., Ares-Santos, S., and Moratalla, R. (2013). Methamphetamine and Parkinson's disease. Parkinsons Dis. *2013*, 1-10.

Grenier, K., McLelland, G.-L., and Fon, E.A. (2013). Parkin- and PINK1-dependent mitophagy in neurons: Will the real pathway please stand up? Front. Neurol. *4*. 1-8.

Griffiths, P.D., Dobson, B.R., Jones, G.R., and Clarke, D.T. (1999). Iron in the basal ganglia in Parkinson's disease: An in vitro study using extended X-ray absorption fine structure and cryo-electron microscopy. Brain *122*, 667-673.

Gritz, E.R., Baer-Weiss, V., Benowitz, N.L., Van Vunakis, H., and Jarvik, M.E. (1981). Plasma nicotine and cotinine concentrations in habitual smokeless tobacco users. Clin. Pharmacol. Ther. *30*, 201-209.

Grosset, D.G., Grosset, K.A., Okun, M.S., and Fernandez, H.H. (2009). Drug treatment of Parkinson’s disease. In Parkinson's Disease : Clinician's Desk Reference, Grosset, D.G., Grosset, K.A., Okun, M.S., and Fernandez, H.H., eds. (London: Manson Publishing Ltd), pp. 59-68.

Gurnev, Philip A., Yap, Thai L., Pfefferkorn, Candace M., Rostovtseva, Tatiana K., Berezhkovskii, Alexander M., Lee, Jennifer C., Parsegian, V.A., and Bezrukov, Sergey M. (2014). Alpha-Synuclein Lipid-Dependent Membrane Binding and Translocation through the α-Hemolysin Channel. Biophys. J. *106*, 556-565.

Hajduk, P.J., and Greer, J. (2007). A decade of fragment-based drug design: strategic advances and lessons learned. Nat. Rev. Drug Discov. *6*, 211-219.

Hansen, C., Angot, E., Bergstrom, A.L., Steiner, J.A., Pieri, L., Paul, G., Outeiro, T.F., Melki, R., Kallunki, P., Fog, K., *et al.* (2011). alpha-Synuclein propagates from mouse brain to grafted dopaminergic neurons and seeds aggregation in cultured human cells. J. Clin. Invest. *121*, 715-725.

Hansen, C., and Li, J.-Y. (2012). Beyond α-synuclein transfer: pathology propagation in Parkinson's disease. Trends Mol. Med. *18*, 248-255.

Hartmann, R., Stangler, T., König, B.W., Willbold, D., and Musil, D. (2008). Structural Proteomics. In Proteomics Sample Preparation, von Hagen, J., eds. (Wiley-VCH Verlag GmbH & Co. KGaA), pp. 273-293.

Henchcliffe, C., and Beal, M.F. (2008). Mitochondrial biology and oxidative stress in Parkinson disease pathogenesis. Nat. Clin. Pract. Neuro. *4*, 600-609.

Henley, B.M., Williams, B.A., Srinivasan, R., Cohen, B.N., Xiao, C., Mackey, E.D., Wold, B.J., and Lester, H.A. (2013). Transcriptional regulation by nicotine in dopaminergic neurons. Biochem. Pharmacol. *86*, 1074-1083.

Hernán, M.A., Takkouche, B., Caamaño-Isorna, F., and Gestal-Otero, J.J. (2002). A meta-analysis of coffee drinking, cigarette smoking, and the risk of Parkinson's disease. Ann. Neurol. *52*, 276-284.

Herrera, F.E., Chesi, A., Paleologou, K.E., Schmid, A., Munoz, A., Vendruscolo, M., Gustincich, S., Lashuel, H.A., and Carloni, P. (2008). Inhibition of alpha-synuclein fibrillization by dopamine is mediated by interactions with five C-terminal residues and with E83 in the NAC region. PLoS One *3*, e3394.

Hoffmann, A., Neupane, K., and Woodside, M.T. (2013). Single-molecule assays for investigating protein misfolding and aggregation. Phys. Chem. Chem. Phys. *15*, 7934-7948.

Hong, D.-P., Fink, A.L., and Uversky, V.N. (2009). Smoking and Parkinson's disease: Does nicotine affect α-synuclein fibrillation? Biochim. Biophys. Acta *1794*, 282-290.

Hoyer, W., Cherny, D., Subramaniam, V., and Jovin, T.M. (2004). Impact of the acidic C-terminal region comprising amino acids 109-140 on alpha-synuclein aggregation in vitro. Biochemistry *43*, 16233-16242.

Hozumi, I., Hasegawa, T., Honda, A., Ozawa, K., Hayashi, Y., Hashimoto, K., Yamada, M., Koumura, A., Sakurai, T., Kimura, A., *et al.* (2011). Patterns of levels of biological metals in CSF differ among neurodegenerative diseases. J. Neurol. Sci. *303*, 95-99.

Hsu, L.J., Sagara, Y., Arroyo, A., Rockenstein, E., Sisk, A., Mallory, M., Wong, J., Takenouchi, T., Hashimoto, M., and Masliah, E. (2000). α-Synuclein Promotes Mitochondrial Deficit and Oxidative Stress. Am. J. Pathol. *157*, 401-410.

Iliuk, A.B., Hu, L., and Tao, W.A. (2011). Aptamer in Bioanalytical Applications. Anal. Chem. *83*, 4440-4452.

Imai, Y., and Lu, B. (2011). Mitochondrial dynamics and mitophagy in Parkinson's disease: disordered cellular power plant becomes a big deal in a major movement disorder. Curr. Opin. Neurobiol. *21*, 935-941.

Imai, Y., Soda, M., and Takahashi, R. (2000). Parkin suppresses unfolded protein stress-induced cell death through its E3 ubiquitin-protein ligase activity. J. Biol. Chem. *275*, 35661-35664.

Venkatesan, B.M., and Bashir, R. (2011). Solid state nanopore sensors for nucleic acid analysis. In Nanopores: Sensing and Fundamental Biological Interactions, Iqbal, S.M., and Bashir, R., eds. (Springer), pp. 1-7.

Ivatt, R.M., and Whitworth, A.J. (2014). The many faces of mitophagy. EMBO Rep. *15*. 5-6.

Iwai, A., Masliah, E., Yoshimoto, M., Ge, N., Flanagan, L., Rohan de Silva, H.A., Kittel, A., and Saitoh, T. (1995). The precursor protein of non-Aβ component of Alzheimer's disease amyloid is a presynaptic protein of the central nervous system. Neuron *14*, 467-475.

Jackson, K., Barisone, G.A., Diaz, E., Jin, L.-w., DeCarli, C., and Despa, F. (2013). Amylin deposition in the brain: A second amyloid in Alzheimer disease? Ann. Neurol. *74*, 517-526.

Jaikaran, E.T.A.S., and Clark, A. (2001). Islet amyloid and type 2 diabetes: from molecular misfolding to islet pathophysiology. Biochim. Biophys. Acta *1537*, 179-203.

Janson, J., Laedtke, T., Parisi, J.E., O'Brien, P., Petersen, R.C., and Butler, P.C. (2004). Increased Risk of Type 2 Diabetes in Alzheimer Disease. Diabetes *53*, 474-481.

Jao, C.C., Hegde, B.G., Chen, J., Haworth, I.S., and Langen, R. (2008). Structure of membrane-bound α-synuclein from site-directed spin labeling and computational refinement. Proc. Natl. Acad. Sci. U.S.A. *105*, 19666-19671.

Jetha, N.N., Semenchenko, V., Wishart, D.S., Cashman, N.R., and Marziali, A. (2013). Nanopore analysis of wild-type and mutant prion protein (PrP(C)): single molecule discrimination and PrP(C) kinetics. PLoS One *8*, e54982.

Jethva, P.N., Kardani, J.R., and Roy, I. (2011). Modulation of alpha-synuclein aggregation by dopamine in the presence of MPTP and its metabolite. FEBS J. *278*, 1688-1698.

Jiang, T.-F., Zhang, Y.-J., Zhou, H.-Y., Wang, H.-M., Tian, L.-P., Liu, J., Ding, J.-Q., and Chen, S.-D. (2013). Curcumin Ameliorates the Neurodegenerative Pathology in A53T α-synuclein Cell Model of Parkinson's Disease Through the Downregulation of mTOR/p70S6K Signaling and the Recovery of Macroautophagy. J. Neuroimmune Pharmacol. *8*, 356-369.

Jin, S.M., and Youle, R.J. (2012). PINK1- and Parkin-mediated mitophagy at a glance. J. Cell Sci. *125*, 795-799.

Jo, E., McLaurin, J., Yip, C.M., St. George-Hyslop, P., and Fraser, P.E. (2000). α-Synuclein Membrane Interactions and Lipid Specificity. J. Biol. Chem. *275*, 34328-34334.

Johnson, B., and Blevins, R. (1994). NMR View: A computer program for the visualization and analysis of NMR data. J. Biomol. NMR *4*, 603-614.

Joseph-McCarthy, D., Campbell, A.J., Kern, G., and Moustakas, D. (2014). Fragment-Based Lead Discovery and Design. J. Chem. Inf. Model. *54*, 693-704.

Kanaan, N.M., and Manfredsson, F.P. (2012). Loss of Functional Alpha-Synuclein: A Toxic Event in Parkinson's Disease? J. Parkinsons Dis. *2*, 249-267.

Kanda, S., Bishop, J.F., Eglitis, M.A., Yang, Y., and Mouradian, M.M. (2000). Enhanced vulnerability to oxidative stress by α-synuclein mutations and C-terminal truncation. Neurosci. *97*, 279-284.

Kasianowicz, J.J., Brandin, E., Branton, D., and Deamer, D.W. (1996). Characterization of individual polynucleotide molecules using a membrane channel. Proc. Natl. Acad. Sci. U.S.A. *93*, 13770-13773.

Kasianowicz, J.J., Robertson, J.W.F., Chan, E.R., Reiner, J.E., and Stanford, V.M. (2008). Nanoscopic Porous Sensors. Annu. Rev. Anal. Chem. *1*, 737-766.

Kawano, R., Osaki, T., Sasaki, H., Takinoue, M., Yoshizawa, S., and Takeuchi, S. (2011). Rapid Detection of a Cocaine-Binding Aptamer Using Biological Nanopores on a Chip. J. Am. Chem. Soc. *133*, 8474-8477.

Kaylor, J., Bodner, N., Edridge, S., Yamin, G., Hong, D.-P., and Fink, A.L. (2005). Characterization of Oligomeric Intermediates in α-Synuclein Fibrillation: FRET Studies of Y125W/Y133F/Y136F α-Synuclein. J. Mol. Biol. *353*, 357-372.

Keane, P.C., Kurzawa, M., Blain, P.G., and Morris, C.M. (2011). Mitochondrial dysfunction in Parkinson's disease. Parkinsons Dis. *2011*, 716871.

Keeney, P.M., Xie, J., Capaldi, R.A., and Bennett, J.P. (2006). Parkinson's Disease Brain Mitochondrial Complex I Has Oxidatively Damaged Subunits and Is Functionally Impaired and Misassembled. J. Neurosci. *26*, 5256-5264.

Kessler, I.I., and Diamond, E.L. (1971). Epidemiologic studies of parkinson's disease: i. Smoking and parkinson's disease: a survey and explanatory hypothesis. Am. J. Epidemiol. *94*, 16-25.

Khurana, R., Ionescu-Zanetti, C., Pope, M., Li, J., Nielson, L., Ramírez-Alvarado, M., Regan, L., Fink, A.L., and Carter, S.A. (2003). A General Model for Amyloid Fibril Assembly Based on Morphological Studies Using Atomic Force Microscopy. Biophys. J. *85*, 1135-1144.

Kim, Y.S., Lim, D., Kim, J.Y., Kang, S.J., Kim, Y.H., and Im, H. (2009). beta-Sheet-breaking peptides inhibit the fibrillation of human alpha-synuclein. Biochem. Biophys. Res. Commun. *387*, 682-687.

Kish, S.J. (2008). Pharmacologic mechanisms of crystal meth. Can. Med. Assoc. J. *178*, 1679-1682.

Klärner, F.-G., Benkhoff, J., Boese, R., Burkert, U., Kamieth, M., and Naatz, U. (1996). Molecular Tweezers as Synthetic Receptors in Host—Guest Chemistry: Inclusion of Cyclohexane and Self-Assembly of Aliphatic Side Chains. Angew. Chem. Int. Ed. Engl. *35*, 1130-1133.

Konrat, R. (2014). NMR contributions to structural dynamics studies of intrinsically disordered proteins. J. Magn. Reson. *241*, 74-85.

Koo, H.J., Choi, M.Y., and Im, H. (2009). Aggregation-defective alpha-synuclein mutants inhibit the fibrillation of Parkinson's disease-linked alpha-synuclein variants. Biochem. Biophys. Res. Commun. *386*, 165-169.

Kordower, J.H., Chu, Y., Hauser, R.A., Freeman, T.B., and Olanow, C.W. (2008). Lewy body-like pathology in long-term embryonic nigral transplants in Parkinson's disease. Nat. Med. *14*, 504-506.

Kosol, S., Contreras-Martos, S., Cedeno, C., and Tompa, P. (2013). Structural characterization of intrinsically disordered proteins by NMR spectroscopy. Molecules *18*, 10802-10828.

Krasniqi, B., and Lee, J.S. (2012). The importance of adding EDTA for the nanopore analysis of proteins. Metallomics *4*, 539-544.

Krasniqi, B., and Lee, J.S. (2014). RNase A does not translocate the alpha-hemolysin pore. PLoS One *9*, e88004.

Krasniqi, B., Scruten, E., Piller, J., Lee, J., and Napper, S. (2012). Stability, toxicity and biological activity of retro, inversed and retro-inversed glucagon isomers. J. Pept. Sci. *18*, 519-526.

Kritzer, J.A., Hamamichi, S., McCaffery, J.M., Santagata, S., Naumann, T.A., Caldwell, K.A., Caldwell, G.A., and Lindquist, S. (2009). Rapid selection of cyclic peptides that reduce [alpha]-synuclein toxicity in yeast and animal models. Nat. Chem. Biol. *5*, 655-663.

Ku, C.-S., and Roukos, D.H. (2013). From next-generation sequencing to nanopore sequencing technology: paving the way to personalized genomic medicine. Expert Rev. Med. Devices *10*, 1-6.

Kurowska, Z., Englund, E., Widner, H., Lindvall, O., Li, J.-Y., and Brundin, P. (2011). Signs of Degeneration in 12–22-Year Old Grafts of Mesencephalic Dopamine Neurons in Patients with Parkinson's Disease. J. Parkinsons Dis. *1*, 83-92.

Kwan, A.H., Mobli, M., Gooley, P.R., King, G.F., and Mackay, J.P. (2011). Macromolecular NMR spectroscopy for the non-spectroscopist. FEBS J. *278*, 687-703.

Larkin, J., Carson, S., Stoloff, D.H., and Wanunu, M. (2013). Nanopore-Based Analysis of Chemically Modified DNA and Nucleic Acid Drug Targets. Isr. J. Chem. *53*, 431-441.

Lashuel, H.A., Overk, C.R., Oueslati, A., and Masliah, E. (2013). The many faces of [alpha]-synuclein: from structure and toxicity to therapeutic target. Nat. Rev. Neurosci. *14*, 38-48.

Lashuel, H.A., Petre, B.M., Wall, J., Simon, M., Nowak, R.J., Walz, T., and Lansbury Jr, P.T. (2002). α-Synuclein, Especially the Parkinson's Disease-associated Mutants, Forms Pore-like Annular and Tubular Protofibrils. J. Mol. Biol. *322*, 1089-1102.

Ledesma, M.D., Galvan, C., Hellias, B., Dotti, C., and Jensen, P.H. (2002). Astrocytic but not neuronal increased expression and redistribution of parkin during unfolded protein stress. J. Neurochem. *83*, 1431-1440.

Lee, F.J.S., LIU, F., PRISTUPA, Z.B., and NIZNIK, H.B. (2001). Direct binding and functional coupling of α-synuclein to the dopamine transporters accelerate dopamine-induced apoptosis. FASEB J. *15*, 916-926.

Lee, H.-J., Baek, S.M., Ho, D.-H., Suk, J.-E., Cho, E.-D., and Lee, S.-J. (2011). Dopamine promotes formation and secretion of non-fibrillar alpha-synuclein oligomers. Exp. Mol. Med. *43*, 216-222.

Lee, J.S. (2014). Nanopore analysis of the effect of metal ions on the folding of peptides and proteins. Prot. Pept. Lett. *21*, 247-255.

Lee, V.M.Y., and Trojanowski, J.Q. (2006). Mechanisms of Parkinson's Disease Linked to Pathological α-Synuclein: New Targets for Drug Discovery. Neuron *52*, 33-38.

Lendel, C., Bertoncini, C.W., Cremades, N., Waudby, C.A., Vendruscolo, M., Dobson, C.M., Schenk, D., Christodoulou, J., and Toth, G. (2009). On the mechanism of nonspecific inhibitors of protein aggregation: dissecting the interactions of alpha-synuclein with Congo red and Lacmoid. Biochemistry *48*, 8322-8334.

Leonard, B.E. (2002). Neuropsychopharmacology—The fifth generation of progress. Edited by K. L. Davis, D. Charney, J. T. Coyle, C. Nemeroff. Lippincott, Williams and Wilkins: Philadelphia, 2002. ISBN: 0-7817-2837-1. Pages: 2080. Hum. Psychopharmacol. Clin. Exp. *17*, 433-433.

Leong, S.L., Cappai, R., Barnham, K.J., and Pham, C.L. (2009). Modulation of alpha-synuclein aggregation by dopamine: a review. Neurochem. Res. *34*, 1838-1846.

Li, H.-T., Lin, D.-H., Luo, X.-Y., Zhang, F., Ji, L.-N., Du, H.-N., Song, G.-Q., Hu, J., Zhou, J.-W., and Hu, H.-Y. (2005). Inhibition of α-synuclein fibrillization by dopamine analogs via reaction with the amino groups of α-synuclein. FEBS J. *272*, 3661-3672.

Li, J.-Y., Englund, E., Holton, J.L., Soulet, D., Hagell, P., Lees, A.J., Lashley, T., Quinn, N.P., Rehncrona, S., Bjorklund, A., *et al.* (2008). Lewy bodies in grafted neurons in subjects with Parkinson's disease suggest host-to-graft disease propagation. Nat. Med. *14*, 501-503.

Li, J., Uversky, V.N., and Fink, A.L. (2001). Effect of Familial Parkinson's Disease Point Mutations A30P and A53T on the Structural Properties, Aggregation, and Fibrillation of Human α-Synuclein. Biochemistry *40*, 11604-11613.

Li, J., Zhu, M., Manning-Bog, A.B., Di Monte, D.A., and Fink, A.L. (2004). Dopamine and L-dopa disaggregate amyloid fibrils: implications for Parkinson's and Alzheimer's disease. FASEB J. *18*, 962-964.

Li, N., Ragheb, K., Lawler, G., Sturgis, J., Rajwa, B., Melendez, J.A., and Robinson, J.P. (2003). Mitochondrial Complex I Inhibitor Rotenone Induces Apoptosis through Enhancing Mitochondrial Reactive Oxygen Species Production. J. Biol. Chem. *278*, 8516-8525.

Lin, C.-H., Tsai Pei, I., Wu, R.-M., and Chien, C.-T. (2011). LRRK2 Parkinson's disease: from animal models to cellular mechanisms. Rev. Neurosci. 22, 411-418.

Liu, G., Zhang, C., Yin, J., Li, X., Cheng, F., Li, Y., Yang, H., Uéda, K., Chan, P., and Yu, S. (2009). α-Synuclein is differentially expressed in mitochondria from different rat brain regions and dose-dependently down-regulates complex I activity. Neurosci. Lett. *454*, 187-192.

Liu, Z., Yu, Y., Li, X., Ross, C.A., and Smith, W.W. (2011). Curcumin protects against A53T alpha-synuclein-induced toxicity in a PC12 inducible cell model for Parkinsonism. Pharmacol. Res. *63*, 439-444.

Loeb, V., Yakunin, E., Saada, A., and Sharon, R. (2010). The Transgenic Overexpression of α-Synuclein and Not Its Related Pathology Associates with Complex I Inhibition. J. Biol. Chem. *285*, 7334-7343.

Loeffler, D.A., LeWitt, P.A., Juneau, P.L., Sima, A.A.F., Nguyen, H.U., DeMaggio, A.J., Brickman, C.M., Brewer, G.J., Dick, R.D., Troyer, M.D., *et al.* (1996). Increased regional brain concentrations of ceruloplasmin in neurodegenerative disorders. Brain Res. *738*, 265-274.

Lokappa, S.B., and Ulmer, T.S. (2011). α-Synuclein Populates Both Elongated and Broken Helix States on Small Unilamellar Vesicles. J. Biol. Chem. *286*, 21450-21457.

Lombardo, M.F., Ciriolo, M.R., Rotilio, G., and Rossi, L. (2003). Prolonged copper depletion induces expression of antioxidants and triggers apoptosis in SH-SY5Y neuroblastoma cells. Cell. Mol. Life Sci. *60*, 1733-1743.

Lotharius, J., and Brundin, P. (2002a). Impaired dopamine storage resulting from α-synuclein mutations may contribute to the pathogenesis of Parkinson's disease. Hum. Mol. Genet. *11*, 2395-2407.

Lotharius, J., and Brundin, P. (2002b). Pathogenesis of parkinson's disease: dopamine, vesicles and [alpha]-synuclein. Nat. Rev. Neurosci. *3*, 932-942.

Luk, K.C., Kehm, V.M., Zhang, B., O'Brien, P., Trojanowski, J.Q., and Lee, V.M. (2012). Intracerebral inoculation of pathological alpha-synuclein initiates a rapidly progressive neurodegenerative alpha-synucleinopathy in mice. J. Exp. Med. *209*, 975-986.

Lutsenko, S., Bhattacharjee, A., and Hubbard, A.L. (2010). Copper handling machinery of the brain. Metallomics *2*, 596-608.

Lutz, A.K., Exner, N., Fett, M.E., Schlehe, J.S., Kloos, K., Lämmermann, K., Brunner, B., Kurz-Drexler, A., Vogel, F., Reichert, A.S., *et al.* (2009). Loss of Parkin or PINK1 Function Increases Drp1-dependent Mitochondrial Fragmentation. J. Biol. Chem. *284*, 22938-22951.

Ma, L., and Cockroft, S.L. (2010). Biological nanopores for single-molecule biophysics. ChemBioChem *11*, 25-34.

Machado-Filho, J.A., Correia, A.O., Montenegro, A.B.A., Nobre, M.E.P., Cerqueira, G.S., Neves, K.R.T., Naffah-Mazzacoratti, M.d.G., Cavalheiro, E.A., de Castro Brito, G.A., and de Barros Viana, G.S. (2014). Caffeine neuroprotective effects on 6-OHDA-lesioned rats are mediated by several factors, including pro-inflammatory cytokines and histone deacetylase inhibitions. Behav. Brain Res. *264*, 116-125.

Madampage, C., Tavassoly, O., Christensen, C., Kumari, M., and Lee, J.S. (2012). Nanopore analysis: An emerging technique for studying the folding and misfolding of proteins. Prion *6*, 116-123.

Madampage, C.A., Andrievskaia, O., and Lee, J.S. (2010). Nanopore detection of antibody prion interactions. Anal. Biochem. *396*, 36-41.

Madampage, C.A., Määttänen, P., Marciniuk, K., Brownlie, R., Andrievskaia, O., Potter, A., Cashman, N.R., Lee, J.S., and Napper, S. (2013a). Binding of bovine T194A PrP(C) by PrP(Sc)-specific antibodies: Potential implications for immunotherapy of familial prion diseases. Prion *7*, 301-311.

Madampage, C.A., Marciniuk, K., Määttänen, P., Cashman, N.R., Potter, A., Lee, J.S., and Napper, S. (2013b). Nanopore analysis reveals differences in structural stability of ovine PrP(C) proteins corresponding to scrapie susceptible (VRQ) and resistance (ARR) genotypes. Prion *7*, 511-519.

Maitra, R.D., Kim, J., and Dunbar, W.B. (2012). Recent advances in nanopore sequencing. Electrophoresis *33*, 3418-3428.

Maltsev, A.S., Grishaev, A., and Bax, A. (2011). Monomeric α-Synuclein Binds Congo Red Micelles in a Disordered Manner. Biochemistry *51*, 631-642.

Maltsev, A.S., Ying, J., and Bax, A. (2012). Impact of N-Terminal Acetylation of α-Synuclein on Its Random Coil and Lipid Binding Properties. Biochemistry *51*, 5004-5013.

Mann, V.M., Cooper, J.M., Daniel, S.E., Srai, K., Jenner, P., Marsden, C.D., and Schapira, A.H.V. (1994). Complex I, Iron, and ferritin in Parkinson's disease substantia nigra. Ann. Neurol. *36*, 876-881.

Martin, L.J., Pan, Y., Price, A.C., Sterling, W., Copeland, N.G., Jenkins, N.A., Price, D.L., and Lee, M.K. (2006). Parkinson's Disease α-Synuclein Transgenic Mice Develop Neuronal Mitochondrial Degeneration and Cell Death. J. Neurosci. *26*, 41-50.

Masuda-Suzukake, M., Nonaka, T., Hosokawa, M., Oikawa, T., Arai, T., Akiyama, H., Mann, D.M.A., and Hasegawa, M. (2013). Prion-like spreading of pathological α-synuclein in brain. Brain *136*, 1128-1138.

Masuda, M., Suzuki, N., Taniguchi, S., Oikawa, T., Nonaka, T., Iwatsubo, T., Hisanaga, S., Goedert, M., and Hasegawa, M. (2006). Small molecule inhibitors of alpha-synuclein filament assembly. Biochemistry *45*, 6085-6094.

Mata, I.F., Wedemeyer, W.J., Farrer, M.J., Taylor, J.P., and Gallo, K.A. (2006). LRRK2 in Parkinson's disease: protein domains and functional insights. Trends Neurosci. *29*, 286-293.

Matsuda, S., Kitagishi, Y., and Kobayashi, M. (2013). Function and characteristics of PINK1 in mitochondria. Oxid. Med. Cell. Longev. *2013*, 1-6.

Mauceli, G., Busceti, C.I., Pellegrini, A., Soldani, P., Lenzi, P., Paparelli, A., and Fornai, F. (2006). Overexpression of α-Synuclein following Methamphetamine. Ann. N. Y. Acad. Sci. *1074*, 191-197.

May, B.C.H., Govaerts, C., and Cohen, F.E. (2006). Developing therapeutics for the diseases of protein misfolding. Neurology *66*, S118-S122.

McClendon, S., Rospigliosi, C.C., and Eliezer, D. (2009). Charge neutralization and collapse of the C-terminal tail of alpha-synuclein at low pH. Prot. Sci. *18*, 1531-1540.

Mendelson, J., Uemura, N., Harris, D., Nath, R.P., Fernandez, E., Jacob, P., 3rd, Everhart, E.T., and Jones, R.T. (2006). Human pharmacology of the methamphetamine stereoisomers. Clin. Pharmacol. Ther. *80*, 403-420.

Menestrina, G., Dalla Serra, M., and Prévost, G. (2001). Mode of action of β-barrel pore-forming toxins of the staphylococcal α-hemolysin family. Toxicon *39*, 1661-1672.

Meng, H., Detillieux, D., Baran, C., Krasniqi, B., Christensen, C., Madampage, C., Stefureac, R.I., and Lee, J.S. (2010a). Nanopore analysis of tethered peptides. J. Pept. Sci. *16*, 701-708.

Meng, X., Munishkina, L.A., Fink, A.L., and Uversky, V.N. (2010b). Effects of Various Flavonoids on the alpha-Synuclein Fibrillation Process. Parkinsons Dis. *2010*, 1-16.

Mercado, G., Valdes, P., and Hetz, C. (2013). An ERcentric view of Parkinson's disease. Trends Mol. Med. *19*, 165-175.

Mereuta, L., Schiopu, I., Asandei, A., Park, Y., Hahm, K.-S., and Luchian, T. (2012). Protein Nanopore-Based, Single-Molecule Exploration of Copper Binding to an Antimicrobial-Derived, Histidine-Containing Chimera Peptide. Langmuir *28*, 17079-17091.

Merstorf, C., Cressiot, B., Pastoriza-Gallego, M., Oukhaled, A., Bacri, L., Gierak, J., Pelta, J., Auvray, L., and Mathé, J. (2012). DNA Unzipping and Protein Unfolding Using Nanopores. In Nanopore-Based Technology, M.E. Gracheva, ed. (Humana Press), pp. 55-75.

Meuer, K., Suppanz, I.E., Lingor, P., Planchamp, V., Goricke, B., Fichtner, L., Braus, G.H., Dietz, G.P.H., Jakobs, S., Bahr, M., *et al.* (2007). Cyclin-dependent kinase 5 is an upstream regulator of mitochondrial fission during neuronal apoptosis. Cell Death Differ. *14*, 651-661.

Minati, L., Grisoli, M., Carella, F., De Simone, T., Bruzzone, M.G., and Savoiardo, M. (2007). Imaging Degeneration of the Substantia Nigra in Parkinson Disease with Inversion-Recovery MR Imaging. Am. J. Neuroradiol. *28*, 309-313.

Montes, S., Rivera-Mancia, S., Diaz-Ruiz, A., Tristan-Lopez, L., and Rios, C. (2014). Copper and copper proteins in Parkinson's disease. Oxid. Med. Cell. Longev. *2014*, 1-15.

Moore, D.J., West, A.B., Dawson, V.L., and Dawson, T.M. (2005). MOLECULAR PATHOPHYSIOLOGY OF PARKINSON'S DISEASE. Annu. Rev. Neurosci. *28*, 57-87.

Moore, S.A., Huckerby, T.N., Gibson, G.L., Fullwood, N.J., Turnbull, S., Tabner, B.J., El-Agnaf, O.M.A., and Allsop, D. (2003). Both the d-(+) and l-(−) Enantiomers of Nicotine Inhibit Aβ Aggregation and Cytotoxicity. Biochemistry *43*, 819-826.

Morais, V.A., Haddad, D., Craessaerts, K., De Bock, P.-J., Swerts, J., Vilain, S., Aerts, L., Overbergh, L., Grünewald, A., Seibler, P., *et al.* (2014). PINK1 Loss-of-Function Mutations Affect Mitochondrial Complex I Activity via NdufA10 Ubiquinone Uncoupling. Science *344*, 203-207.

Morais, V.A., Verstreken, P., Roethig, A., Smet, J., Snellinx, A., Vanbrabant, M., Haddad, D., Frezza, C., Mandemakers, W., Vogt-Weisenhorn, D., *et al.* (2009). Parkinson's disease mutations in PINK1 result in decreased Complex I activity and deficient synaptic function. EMBO Mol. Med. *1*, 99-111.

Moszczynska, A., Fitzmaurice, P., Ang, L., Kalasinsky, K.S., Schmunk, G.A., Peretti, F.J., Aiken, S.S., Wickham, D.J., and Kish, S.J. (2004). Why is parkinsonism not a feature of human methamphetamine users? Brain *127*, 363-370.

Mpofana, T., Daniels, W.M.U., and Mabandla, M.V. (2014). Neuroprotective Effects of Caffeine on a Maternally Separated Parkinsonian Rat Model. J. Behav. Brain Sci. *4*, 84-91.

Mulero, R., Prabhu, A.S., Freedman, K.J., and Kim, M.J. (2010). Nanopore-Based Devices for Bioanalytical Applications. J. Assoc. Lab. Automa. *15*, 243-252.

Mythri, R.B., and Bharath, M.M. (2012). Curcumin: a potential neuroprotective agent in Parkinson's disease. Curr. Pharm. Des. *18*, 91-99.

Nasica-Labouze, J., and Mousseau, N. (2012). Kinetics of amyloid aggregation: a study of the GNNQQNY prion sequence. PLoS Comput. Biol. *8*, e1002782.

Nielsen, S.S., Franklin, G.M., Longstreth, W.T., Swanson, P.D., and Checkoway, H. (2013). Nicotine from edible Solanaceae and risk of Parkinson disease. Ann. Neurol. *74*, 472-477.

Norris, E.H., Giasson, B.I., Hodara, R., Xu, S., Trojanowski, J.Q., Ischiropoulos, H., and Lee, V.M. (2005). Reversible inhibition of alpha-synuclein fibrillization by dopaminochrome-mediated conformational alterations. J. Biol. Chem. *280*, 21212-21219.

Olanow, C.W., and Tatton, W.G. (1999). ETIOLOGY AND PATHOGENESIS OF PARKINSON'S DISEASE. Annu. Rev. Neurosci. *22*, 123-144.

Oldfield, C.J., and Dunker, A.K. (2014). Intrinsically Disordered Proteins and Intrinsically Disordered Protein Regions. Annu. Rev. Biochem. *83*, 553-584.

Olefirowicz, T.M., and Ewing, A.G. (1990). Dopamine concentration in the cytoplasmic compartment of single neurons determined by capillary electrophoresis. J. Neurosci. Methods *34*, 11-15.

Olivares, D., Huang, X., Branden, L., Greig, N.H., and Rogers, J.T. (2009). Physiological and pathological role of alpha-synuclein in Parkinson's disease through iron mediated oxidative stress; The role of a putative iron-responsive element. Int. J. Mol. Sci. *10*, 1226-1260.

Ono, K., Hirohata, M., and Yamada, M. (2007a). Anti-fibrillogenic and fibril-destabilizing activities of anti-Parkinsonian agents for alpha-synuclein fibrils in vitro. J. Neurosci. Res. *85*, 1547-1557.

Ono, K., Hirohata, M., and Yamada, M. (2007b). Anti-fibrillogenic and fibril-destabilizing activity of nicotine in vitro: Implications for the prevention and therapeutics of Lewy body diseases. Exp. Neurol. *205*, 414-424.

Ottolini, D., Calì, T., and Brini, M. (2013). Etiology and pathogenesis of Parkinson’s disease: role of mitochondrial pathology. Res. Rep. Biochem. *2013*, 55 - 70.

Outeiro, T.F., Klucken, J., Bercury, K., Tetzlaff, J., Putcha, P., Oliveira, L.M., Quintas, A., McLean, P.J., and Hyman, B.T. (2009). Dopamine-induced conformational changes in alpha-synuclein. PLoS One *4*, e6906.

Jankovic, J. (2007). Pathophysiology and Clinical Assessment. In Handbook of Parkinson’s Disease, Pahwa, R., and Lyons, K.E., eds. (New York: Informa Healthcare USA Inc), pp. 49-77.

Pall, H.S., Blake, D.R., Gutteridge, J.M., Williams, A.C., Lunec, J., Hall, M., and Taylor, A. (1987). Raised cerebrospinal-fluid copper concentration in Parkinson's disease. The Lancet *330*, 238-241.

Pandey, N., Schmidt, R.E., and Galvin, J.E. (2006). The alpha-synuclein mutation E46K promotes aggregation in cultured cells. Exp. Neurol. *197*, 515-520.

Pandey, N., Strider, J., Nolan, W.C., Yan, S.X., and Galvin, J.E. (2008). Curcumin inhibits aggregation of alpha-synuclein. Acta Neuropathol. *115*, 479-489.

Parker, W.D., Jr., and Swerdlow, R.H. (1998). Mitochondrial Dysfunction in Idiopathic Parkinson Disease. Am. J. Hum. Genet. *62*, 758-762.

Pastoriza-Gallego, M., Oukhaled, G., Mathé, J., Thiebot, B., Betton, J.-M., Auvray, L.c., and Pelta, J. (2007). Urea denaturation of α-hemolysin pore inserted in planar lipid bilayer detected by single nanopore recording: Loss of structural asymmetry. FEBS Lett. *581*, 3371-3376.

Patrick, G.L. (2009). Pharmacokinetics and related topics. In An Introduction to Medicinal Chemistry, Patrick, G.L., ed. (Oxford University Press), pp. 153-174.

Perier, C., Tieu, K., Guégan, C., Caspersen, C., Jackson-Lewis, V., Carelli, V., Martinuzzi, A., Hirano, M., Przedborski, S., and Vila, M. (2005). Complex I deficiency primes Bax-dependent neuronal apoptosis through mitochondrial oxidative damage. Proc. Natl. Acad. Sci. U. S. A. *102*, 19126-19131.

Perier, C., and Vila, M. (2012). Mitochondrial Biology and Parkinson's Disease. Cold Spring Harb. Perspect. Med. *2*, 1-19.

Perlman, R.L., and Sheard, B.E. (1982). Estimation of the cytoplasmic catecholamine concentrations in pheochromocytoma cells. Biochim. Biophys. Acta *719*, 334-340.

Perrin, R.J., Woods, W.S., Clayton, D.F., and George, J.M. (2000). Interaction of Human α-Synuclein and Parkinson's Disease Variants with Phospholipids: structural analysis using site-directed mutagenesis. J. Biol. Chem. *275*, 34393-34398.

Pham, C.L., and Cappai, R. (2013). The interplay between lipids and dopamine on alpha-synuclein oligomerization and membrane binding. Biosci. Rep. *33*, 807-814.

Plun-Favreau, H., and Hardy, J. (2008). PINK1 in mitochondrial function. Proc. Natl. Acad. Sci. U.S.A. *105*, 11041-11042.

Postuma, R.B., Lang, A.E., Munhoz, R.P., Charland, K., Pelletier, A., Moscovich, M., Filla, L., Zanatta, D., Romenets, S.R., Altman, R., *et al.* (2012). Caffeine for treatment of Parkinson disease: A randomized controlled trial. Neurology *79*, 651-658.

Prabhudesai, S., Sinha, S., Attar, A., Kotagiri, A., Fitzmaurice, A., Lakshmanan, R., Ivanova, M., Loo, J., Klärner, F.-G., Schrader, T., *et al.* (2012). A Novel "Molecular Tweezer" Inhibitor of α-Synuclein Neurotoxicity in Vitro and in Vivo. Neurotherapeutics *9*, 464-476.

Prusiner, S.B. (2001). Neurodegenerative Diseases and Prions. N. Engl. J. Med. *344*, 1516-1526.

Qualls, Z., Brown, D., Ramlochansingh, C., Hurley, L., and Tizabi, Y. (2014). Protective Effects of Curcumin Against Rotenone and Salsolinol-Induced Toxicity: Implications for Parkinson's Disease. Neurotox. Res. *25*, 81-89.

Quik, M. (2004). Smoking, nicotine and Parkinson's disease. Trends Neurosci. *27*, 561-568.

Quik, M., Huang, L.Z., Parameswaran, N., Bordia, T., Campos, C., and Perez, X.A. (2009). Multiple roles for nicotine in Parkinson's disease. Biochem. Pharmacol. *78*, 677-685.

Quik, M., Mallela, A., Ly, J., and Zhang, D. (2013). Nicotine reduces established levodopa-induced dyskinesias in a monkey model of Parkinson's disease. Mov. Disord. *28*, 1398-1406.

Radom, F., Jurek, P.M., Mazurek, M.P., Otlewski, J., and Jeleń, F. (2013). Aptamers: Molecules of great potential. Biotechnol. Adv. *31*, 1260-1274.

Ramsay, R.R., Kowal, A.T., Johnson, M.K., Salach, J.I., and Singer, T.P. (1987). The inhibition site of MPP+, the neurotoxic bioactivation product of 1-methyl-4-phenyl-1,2,3, 6-tetrahydropyridine is near the Q-binding site of NADH dehydrogenase. Arch. Biochem. Biophys. *259*, 645-649.

Rao, J.N., Dua, V., and Ulmer, T.S. (2008). Characterization of α-Synuclein Interactions with Selected Aggregation-Inhibiting Small Molecules. Biochemistry *47*, 4651-4656.

Rao, J.N., Jao, C.C., Hegde, B.G., Langen, R., and Ulmer, T.S. (2010). A Combinatorial NMR and EPR Approach for Evaluating the Structural Ensemble of Partially Folded Proteins. J. Am. Chem. Soc. *132*, 8657-8668.

Rapier, C., Lunt, G.G., and Wonnacott, S. (1988). Stereoselective nicotine-induced release of dopamine from striatal synaptosomes: concentration dependence and repetitive stimulation. J. Neurochem. *50*, 1123-1130.

Rasia, R.M., Bertoncini, C.W., Marsh, D., Hoyer, W., Cherny, D., Zweckstetter, M., Griesinger, C., Jovin, T.M., and Fernandez, C.O. (2005). Structural characterization of copper(II) binding to alpha-synuclein: Insights into the bioinorganic chemistry of Parkinson's disease. Proc. Natl. Acad. Sci. U. S. A. *102*, 4294-4299.

Riederer, P., Sofic, E., Rausch, W.D., Schmidt, B., Reynolds, G.P., Jellinger, K., and Youdim, M.B. (1989). Transition metals, ferritin, glutathione, and ascorbic acid in parkinsonian brains. J. Neurochem. *52*, 515-520.

Rijal Upadhaya, A., Kosterin, I., Kumar, S., von Arnim, C.A.F., Yamaguchi, H., Fändrich, M., Walter, J., and Thal, D.R. (2014). Biochemical stages of amyloid-β peptide aggregation and accumulation in the human brain and their association with symptomatic and pathologically preclinical Alzheimer’s disease. Brain *137*, 887-903.

Rivera-Oliver, M., and Díaz-Ríos, M. (2014). Using caffeine and other adenosine receptor antagonists and agonists as therapeutic tools against neurodegenerative diseases: A review. Life Sci. *101*, 1-9.

Rochet, J.-C. (2007). Novel therapeutic strategies for the treatment of protein-misfolding diseases. Expert Rev. Mol. Med. *9*, 1-34.

Rongzhu, L., Suhua, W., Guangwei, X., Chunlan, R., Fangan, H., Junjie, J., and Aschner, M. (2009). Zinc, Copper, Iron, and Selenium Levels in Brain and Liver of Mice Exposed to Acrylonitrile. Biol. Trace Elem. Res. *130*, 39-47.

Rose, F., Hodak, M., and Bernholc, J. (2011). Mechanism of copper(II)-induced misfolding of Parkinson's disease protein. Sci. Rep. *1*, 1-5.

Rose, J.E., Behm, F.M., Westman, E.C., and Coleman, R.E. (1999). Arterial nicotine kinetics during cigarette smoking and intravenous nicotine administration: implications for addiction. Drug Alcohol Depend. *56*, 99-107.

Rose, J.E., Mukhin, A.G., Lokitz, S.J., Turkington, T.G., Herskovic, J., Behm, F.M., Garg, S., and Garg, P.K. (2010). Kinetics of brain nicotine accumulation in dependent and nondependent smokers assessed with PET and cigarettes containing 11C-nicotine. Proc. Natl. Acad. Sci. U.S.A. *107*, 5190-5195.

Ross, G., Abbott, R.D., Petrovitch, H., and et al. (2000). ASsociation of coffee and caffeine intake with the risk of parkinson disease. JAMA *283*, 2674-2679.

Ross, G.W., and Petrovitch, H. (2001). Current evidence for neuroprotective effects of nicotine and caffeine against Parkinson's disease. Drugs Aging *18*, 797-806.

Russell, M.A., Jarvis, M., Iyer, R., and Feyerabend, C. (1980). Relation of nicotine yield of cigarettes to blood nicotine concentrations in smokers. Br. Med. J. *280*, 972-976.

Sandal, M., Valle, F., Tessari, I., Mammi, S., Bergantino, E., Musiani, F., Brucale, M., Bubacco, L., and Samori, B. (2008). Conformational equilibria in monomeric alpha-synuclein at the single-molecule level. PLoS Biol. *6*, e6.

Schapira, A.H.V., Bezard, E., Brotchie, J., Calon, F., Collingridge, G.L., Ferger, B., Hengerer, B., Hirsch, E., Jenner, P., Novere, N.L., *et al.* (2006). Novel pharmacological targets for the treatment of Parkinson's disease. Nat. Rev. Drug Discov. *5*, 845-854.

Scheicher, R., Grigoriev, A., and Ahuja, R. (2012). DNA sequencing with nanopores from an ab initio perspective. J. Mater. Sci. *47*, 7439-7446.

Schneider, J.S., Pope-Coleman, A., Van Velson, M., Menzaghi, F., and Kenneth Lloyd, G. (1998). Effects of SIB-1508Y, a novel neuronal nicotinic acetylcholine receptor agonist, on motor behavior in parkinsonian monkeys. Mov. Disord. *13*, 637-642.

Schonthal, A.H. (2012). Endoplasmic reticulum stress: its role in disease and novel prospects for therapy. Scientifica (Cairo) *2012*, 857516.

Schröder, M., and Kaufman, R.J. (2005). ER stress and the unfolded protein response. Mut. Res./Fundament. Mol. Mech. Mutagen. *569*, 29-63.

Schwarzschild, M.A., Xu, K., Oztas, E., Petzer, J.P., Castagnoli, K., Castagnoli, N., and Chen, J.-F. (2003). Neuroprotection by caffeine and more specific A2A receptor antagonists in animal models of Parkinson's disease. Neurology *61*, S55-S61.

Scotcher, K.P., Irwin, I., DeLanney, L.E., Langston, J.W., and Di Monte, D. (1990). Effects of 1-Methyl-4-Phenyl- 1,2,3,6-Tetrahydropyridine and 1 -Methyl-4-Phenylpyridinium Ion on ATP Levels of Mouse Brain Synaptosomes. J. Neurochem. *54*, 1295-1301.

Selkoe, D.J. (2004). Cell biology of protein misfolding: The examples of Alzheimer's and Parkinson's diseases. Nat. Cell Biol. *6*, 1054-1061.

Serpell, L.C., Berriman, J., Jakes, R., Goedert, M., and Crowther, R.A. (2000). Fiber diffraction of synthetic α-synuclein filaments shows amyloid-like cross-β conformation. Proc. Natl. Acad. Sci. U.S.A. *97*, 4897-4902.

Padma Srivastava, M.V., Garg, J., and Seth, V. (2009). Drug therapy for neurodegenerative disorders. In Textbook of Pharmacology, Seth, S.D., and Seth, V., eds. (Elsevier), pp. III_71-87.

Shaltiel-Karyo, R., Frenkel-Pinter, M., Egoz-Matia, N., Frydman-Marom, A., Shalev, D.E., Segal, D., and Gazit, E. (2010). Inhibiting alpha-synuclein oligomerization by stable cell-penetrating beta-synuclein fragments recovers phenotype of Parkinson's disease model flies. PLoS One *5*, e13863.

Sharma, M., Burre, J., and Sudhof, T.C. (2011). CSP[alpha] promotes SNARE-complex assembly by chaperoning SNAP-25 during synaptic activity. Nat. Cell Biol. *13*, 30-39.

Shimizu, K., Ohtaki, K., Matsubara, K., Aoyama, K., Uezono, T., Saito, O., Suno, M., Ogawa, K., Hayase, N., Kimura, K., *et al.* (2001). Carrier-mediated processes in blood–brain barrier penetration and neural uptake of paraquat. Brain Res. *906*, 135-142.

Shimura, H., Hattori, N., Kubo, S.-i., Mizuno, Y., Asakawa, S., Minoshima, S., Shimizu, N., Iwai, K., Chiba, T., Tanaka, K., *et al.* (2000). Familial Parkinson disease gene product, parkin, is a ubiquitin-protein ligase. Nat. Genet. *25*, 302-305.

Shulman, J.M., De Jager, P.L., and Feany, M.B. (2011). Parkinson's Disease: Genetics and Pathogenesis. Annu. Rev. Pathol. *6*, 193-222.

Siddique, Y.H., Naz, F., and Jyoti, S. (2014). Effect of curcumin on lifespan, activity pattern, oxidative stress, and apoptosis in the brains of transgenic Drosophila model of Parkinson's disease. Biomed. Res. Int. *2014*, 1-6.

Silva, B.A., Einarsdottir, O., Fink, A.L., and Uversky, V.N. (2013). Biophysical Characterization of alpha-Synuclein and Rotenone Interaction. Biomolecules *3*, 703-732.

Singh, P.K., Kotia, V., Ghosh, D., Mohite, G.M., Kumar, A., and Maji, S.K. (2012). Curcumin Modulates α-Synuclein Aggregation and Toxicity. ACS Chem. Neurosci. *4*, 393-407.

Sinha, S., Du, Z., Maiti, P., Klärner, F.-G., Schrader, T., Wang, C., and Bitan, G. (2012a). Comparison of Three Amyloid Assembly Inhibitors: The Sugar scyllo-Inositol, the Polyphenol Epigallocatechin Gallate, and the Molecular Tweezer CLR01. ACS Chem. Neurosci. *3*, 451-458.

Sinha, S., Lopes, D.H., Du, Z., Pang, E.S., Shanmugam, A., Lomakin, A., Talbiersky, P., Tennstaedt, A., McDaniel, K., Bakshi, R., *et al.* (2011a). Lysine-specific molecular tweezers are broad-spectrum inhibitors of assembly and toxicity of amyloid proteins. J. Am. Chem. Soc. *133*, 16958-16969.

Sinha, S., Lopes, D.H.J., and Bitan, G. (2012b). A Key Role for Lysine Residues in Amyloid β-Protein Folding, Assembly, and Toxicity. ACS Chem. Neurosci. *3*, 473-481.

Sinha, S., Lopes, D.H.J., Du, Z., Pang, E.S., Shanmugam, A., Lomakin, A., Talbiersky, P., Tennstaedt, A., McDaniel, K., Bakshi, R., *et al.* (2011b). Lysine-Specific Molecular Tweezers Are Broad-Spectrum Inhibitors of Assembly and Toxicity of Amyloid Proteins. J. Am. Chem. Soc. *133*, 16958-16969.

Skjørringe, T., Møller, L.B., and Moos, T. (2012). Impairment of interrelated iron- and copper homeostatic mechanisms in brain contributes to the pathogenesis of neurodegenerative disorders. Front. Pharmacol. *3*, 1-14.

Smith, W.W., Jiang, H., Pei, Z., Tanaka, Y., Morita, H., Sawa, A., Dawson, V.L., Dawson, T.M., and Ross, C.A. (2005). Endoplasmic reticulum stress and mitochondrial cell death pathways mediate A53T mutant alpha-synuclein-induced toxicity. Hum. Mol. Genet. *14*, 3801-3811.

Smith, W.W., Pei, Z., Jiang, H., Dawson, V.L., Dawson, T.M., and Ross, C.A. (2006). Kinase activity of mutant LRRK2 mediates neuronal toxicity. Nat. Neurosci. *9*, 1231-1233.

Song, L., Hobaugh, M.R., Shustak, C., Cheley, S., Bayley, H., and Gouaux, J.E. (1996). Structure of Staphylococcal α-Hemolysin, a Heptameric Transmembrane Pore. Science *274*, 1859-1865.

Soto, C. (2003). Unfolding the role of protein misfolding in neurodegenerative diseases. Nat. Rev. Neurosci. *4*, 49-60.

Spencer, J.P.E., Jenner, A., Butler, J., Aruoma, O.I., Dexter, D.T., Jenner, P., and Halliwell, B. (1996). Evaluation of the Pro-Oxidant and Antioxidant Actions of L-DOPA and Dopamine in Vitro: Implications for Parkinson's Disease. Free Radic. Res. *24*, 95-105.

Spinelli, K.J., Taylor, J.K., Osterberg, V.R., Churchill, M.J., Pollock, E., Moore, C., Meshul, C.K., and Unni, V.K. (2014). Presynaptic Alpha-Synuclein Aggregation in a Mouse Model of Parkinson's Disease. J. Neurosci. *34*, 2037-2050.

Springer, W., and Kahle, P.J. (2011). Regulation of PINK1-Parkin-mediated mitophagy. Autophagy *7*, 266-278.

Moreau, D. (2008). Neurological and neuromuscular drugs. In Clinical Pharmacology Made Incredibly Easy, Moreau, D., ed. (Lippincott Williams & Wilkins), pp. 49-70.

Stefanis, L. (2012). α-Synuclein in Parkinson's Disease. Cold Spring Harb. Perspect. Med. *2*, 1-23.

Stefureac, R., Waldner, L., Howard, P., and Lee, J.S. (2008). Nanopore analysis of a small 86-residue protein. Small *4*, 59-63.

Stefureac, R.I., and Lee, J.S. (2008). Nanopore analysis of the folding of zinc fingers. Small *4*, 1646-1650.

Stefureac, R.I., Madampage, C.A., Andrievskaia, O., and Lee, J.S. (2010). Nanopore analysis of the interaction of metal ions with prion proteins and peptides. Biochem. Cell Biol. *88*, 347-358.

Steiner, J.A., Angot, E., and Brundin, P. (2011). A deadly spread: cellular mechanisms of [alpha]-synuclein transfer. Cell Death Differ. *18*, 1425-1433.

Sudhof, T.C. (2013). A molecular machine for neurotransmitter release: synaptotagmin and beyond. Nat. Med. *19*, 1227-1231.

Sung, Y.-h., and Eliezer, D. (2007). Residual Structure, Backbone Dynamics, and Interactions within the Synuclein Family. J. Mol. Biol. *372*, 689-707.

Sutherland, T.C., Long, Y.-T., Stefureac, R.-I., Bediako-Amoa, I., Kraatz, H.-B., and Lee, J.S. (2004). Structure of Peptides Investigated by Nanopore Analysis. Nano Lett. *4*, 1273-1277.

Talbiersky, P., Bastkowski, F., Klärner, F.-G., and Schrader, T. (2008). Molecular Clip and Tweezer Introduce New Mechanisms of Enzyme Inhibition. J. Am. Chem. Soc. *130*, 9824-9828.

Tan, Y.-Y., Zhou, H.-Y., Wang, Z.-Q., and Chen, S.-D. (2008). Endoplasmic reticulum stress contributes to the cell death induced by UCH-L1 inhibitor. Mol. Cell. Biochem. *318*, 109-115.

Tanaka, Y., Hirano, N., Kaneko, J., Kamio, Y., Yao, M., and Tanaka, I. (2011). 2-Methyl-2,4-pentanediol induces spontaneous assembly of staphylococcal α-hemolysin into heptameric pore structure. Prot. Sci. *20*, 448-456.

Theillet, F.-X., Kalmar, L., Tompa, P., Han, K.-H., Selenko, P., Dunker, A.K., Daughdrill, G.W., and Uversky, V.N. (2013). The alphabet of intrinsic disorder: I. Act like a Pro: On the abundance and roles of proline residues in intrinsically disordered proteins. Intrinsic. Disord. Prot. *1*, 5-17.

Thrash, B., Thiruchelvan, K., Ahuja, M., Suppiramaniam, V., and Dhanasekaran, M. (2009). Methamphetamine-induced neurotoxicity: the road to Parkinson's disease. Pharmacol. Rep. *61*, 966-977.

Tirmenstein, M.A., Hu, C.X., Scicchitano, M.S., Narayanan, P.K., McFarland, D.C., Thomas, H.C., and Schwartz, L.W. (2005). Effects of 6-hydroxydopamine on mitochondrial function and glutathione status in SH-SY5Y human neuroblastoma cells. Toxicol. In Vitro *19*, 471-479.

Tompa, P. (2012). Intrinsically disordered proteins: a 10-year recap. Trends Biochem. Sci. *37*, 509-516.

Toth, G., Gardai, S.J., Zago, W., Bertoncini, C.W., Cremades, N., Roy, S.L., Tambe, M.A., Rochet, J.C., Galvagnion, C., Skibinski, G., *et al.* (2014). Targeting the intrinsically disordered structural ensemble of alpha-synuclein by small molecules as a potential therapeutic strategy for Parkinson's disease. PLoS One *9*, e87133.

Trempe, J.-F., Sauvé, V., Grenier, K., Seirafi, M., Tang, M.Y., Ménade, M., Al-Abdul-Wahid, S., Krett, J., Wong, K., Kozlov, G., *et al.* (2013). Structure of Parkin Reveals Mechanisms for Ubiquitin Ligase Activation. Science *340*, 1451-1455.

Trexler, A.J., and Rhoades, E. (2010a). Single molecule characterization of alpha-synuclein in aggregation-prone states. Biophys. J. *99*, 3048-3055.

Trexler, A.J., and Rhoades, E. (2010b). Single Molecule Characterization of α-Synuclein in Aggregation-Prone States. Biophys. J. *99*, 3048-3055.

Tsai, Y.C., Fishman, P.S., Thakor, N.V., and Oyler, G.A. (2003). Parkin facilitates the elimination of expanded polyglutamine proteins and leads to preservation of proteasome function. J. Biol. Chem. *278*, 22044-22055.

Ulmer, T.S., Bax, A., Cole, N.B., and Nussbaum, R.L. (2005a). Structure and dynamics of micelle-bound human alpha-synuclein. J. Biol. Chem. *280*, 9595-9603.

Ulmer, T.S., Bax, A., Cole, N.B., and Nussbaum, R.L. (2005b). Structure and Dynamics of Micelle-bound Human α-Synuclein. J. Biol. Chem. *280*, 9595-9603.

Uversky, V.N. (2007). Neuropathology, biochemistry, and biophysics of alpha-synuclein aggregation. J. Neurochem. *103*, 17-37.

Uversky, V.N. (2008). Alpha-synuclein misfolding and neurodegenerative diseases. Curr. Protein Pept. Sci. *9*, 507-540.

Uversky, V.N. (2011). Intrinsically disordered proteins from A to Z. Int. J. Biochem. Cell Biol. *43*, 1090-1103.

Uversky, V.N. (2013a). The alphabet of intrinsic disorder: II. Various roles of glutamic acid in ordered and intrinsically disordered proteins. Intrinsic. Disord. Prot. *1*, 18-40.

Uversky, V.N. (2013b). Unusual biophysics of intrinsically disordered proteins. Biochim. Biophys. Acta *1834*, 932-951.

Uversky, V.N., and Eliezer, D. (2009). Biophysics of Parkinson's disease: structure and aggregation of alpha-synuclein. Curr. Protein Pept. Sci. *10*, 483-499.

Uversky, V.N., Lee, H.-J., Li, J., Fink, A.L., and Lee, S.-J. (2001a). Stabilization of Partially Folded Conformation during α-Synuclein Oligomerization in Both Purified and Cytosolic Preparations. J. Biol. Chem. *276*, 43495-43498.

Uversky, V.N., Li, J., Bower, K., and Fink, A.L. (2002). Synergistic Effects of Pesticides and Metals on the Fibrillation of α-Synuclein: Implications for Parkinson's Disease. Neurotoxicology *23*, 527-536.

Uversky, V.N., Li, J., and Fink, A.L. (2001b). Evidence for a partially folded intermediate in alpha-synuclein fibril formation. J. Biol. Chem. *276*, 10737-10744.

Uversky, V.N., Li, J., and Fink, A.L. (2001c). Metal-triggered structural transformations, aggregation, and fibrillation of human alpha-synuclein. A possible molecular NK between Parkinson's disease and heavy metal exposure. J. Biol. Chem. *276*, 44284-44296.

Uversky, V.N., Li, J., and Fink, A.L. (2001d). Pesticides directly accelerate the rate of α-synuclein fibril formation: a possible factor in Parkinson's disease. FEBS Lett. *500*, 105-108.

Uversky, V.N., Oldfield, C.J., and Dunker, A.K. (2008). Intrinsically Disordered Proteins in Human Diseases: Introducing the D2 Concept. Annu. Rev. Biophys. *37*, 215-246.

Valentine, J.S., Doucette, P.A., and Zittin Potter, S. (2005). Copper-zinc superoxide dismutase and amyotrophic lateral sclerosis. Annu. Rev. Biochem. *74*, 563-593.

van der Bliek, A.M., Shen, Q., and Kawajiri, S. (2013). Mechanisms of mitochondrial fission and fusion. Cold Spring Harb. Perspect. Biol. *5*, 1-16.

Venkatesan, B.M., and Bashir, R. (2011). Nanopore sensors for nucleic acid analysis. Nat. Nano *6*, 615-624.

Vigneswara, V., Cass, S., Wayne, D., Bolt, E.L., Ray, D.E., and Carter, W.G. (2013). Molecular ageing of alpha- and Beta-synucleins: protein damage and repair mechanisms. PLoS One *8*, e61442.

Villafane, G., Cesaro, P., Rialland, A., Baloul, S., Azimi, S., Bourdet, C., Le Houezec, J., Macquin-Mavier, I., and Maison, P. (2007). Chronic high dose transdermal nicotine in Parkinson's disease: an open trial. Eur. J. Neurol. *14*, 1313-1316.

Vincow, E.S., Merrihew, G., Thomas, R.E., Shulman, N.J., Beyer, R.P., MacCoss, M.J., and Pallanck, L.J. (2013). The PINK1–Parkin pathway promotes both mitophagy and selective respiratory chain turnover in vivo. Proc. Natl. Acad. Sci. U.S.A. *110*, 6400-6405.

Volkow, N.D., Chang, L., Wang, G.-J., Fowler, J.S., Franceschi, D., Sedler, M., Gatley, S.J., Miller, E., Hitzemann, R., Ding, Y.-S., *et al.* (2001a). Loss of Dopamine Transporters in Methamphetamine Abusers Recovers with Protracted Abstinence. J. Neurosci. *21*, 9414-9418.

Volkow, N.D., Chang, L., Wang, G.J., Fowler, J.S., Leonido-Yee, M., Franceschi, D., Sedler, M.J., Gatley, S.J., Hitzemann, R., Ding, Y.S., *et al.* (2001b). Association of dopamine transporter reduction with psychomotor impairment in methamphetamine abusers. Am. J. Psychiatry *158*, 377-382.

Volkow, N.D., Fowler, J.S., Wang, G.J., Shumay, E., Telang, F., Thanos, P.K., and Alexoff, D. (2010). Distribution and pharmacokinetics of methamphetamine in the human body: clinical implications. PLoS One *5*, e15269.

Volles, M.J., and Lansbury, P.T. (2002). Vesicle Permeabilization by Protofibrillar α-Synuclein Is Sensitive to Parkinson's Disease-Linked Mutations and Occurs by a Pore-like Mechanism†. Biochemistry *41*, 4595-4602.

Volles, M.J., Lee, S.-J., Rochet, J.-C., Shtilerman, M.D., Ding, T.T., Kessler, J.C., and Lansbury, P.T. (2001). Vesicle Permeabilization by Protofibrillar α-Synuclein: Implications for the Pathogenesis and Treatment of Parkinson's Disease. Biochemistry *40*, 7812-7819.

Volpicelli-Daley, Laura A., Luk, Kelvin C., Patel, Tapan P., Tanik, Selcuk A., Riddle, Dawn M., Stieber, A., Meaney, David F., Trojanowski, John Q., and Lee, Virginia M.Y. (2011). Exogenous α-Synuclein Fibrils Induce Lewy Body Pathology Leading to Synaptic Dysfunction and Neuron Death. Neuron *72*, 57-71.

Wan, O.W., and Chung, K.K. (2012). The role of alpha-synuclein oligomerization and aggregation in cellular and animal models of Parkinson's disease. PLoS One *7*, e38545.

Wang, H.-Y., Gu, Z., Cao, C., Wang, J., and Long, Y.-T. (2013). Analysis of a Single α-Synuclein Fibrillation by the Interaction with a Protein Nanopore. Anal. Chem. *85*, 8254-8261.

Wang, H.Y., Ying, Y.L., Li, Y., Kraatz, H.B., and Long, Y.T. (2011a). Nanopore Analysis of beta-Amyloid Peptide Aggregation Transition Induced by Small Molecules. Anal. Chem. *83*, 1746–1752.

Wang, H.Y., Ying, Y.L., Li, Y., and Long, Y.T. (2010a). Peering into biological nanopore: a practical technology to single-molecule analysis. Chem. Asian J. *5*, 1952-1961.

Wang, M.S., Boddapati, S., Emadi, S., and Sierks, M.R. (2010b). Curcumin reduces alpha-synuclein induced cytotoxicity in Parkinson's disease cell model. BMC Neurosci. *11*, 1-10.

Wang, W., Perovic, I., Chittuluru, J., Kaganovich, A., Nguyen, L.T.T., Liao, J., Auclair, J.R., Johnson, D., Landeru, A., Simorellis, A.K., *et al.* (2011b). A soluble α-synuclein construct forms a dynamic tetramer. Proc. Natl. Acad. Sci. U.S.A. *108*, 17797-17802.

Wanunu, M., Bhattacharya, S., Xie, Y., Tor, Y., Aksimentiev, A., and Drndic, M. (2011). Nanopore Analysis of Individual RNA/Antibiotic Complexes. ACS Nano *5*, 9345-9353.

Watanabe, M., Dykes-Hoberg, M., Cizewski Culotta, V., Price, D.L., Wong, P.C., and Rothstein, J.D. (2001). Histological Evidence of Protein Aggregation in Mutant SOD1 Transgenic Mice and in Amyotrophic Lateral Sclerosis Neural Tissues. Neurobiol. Dis. *8*, 933-941.

Wauer, T., and Komander, D. (2013). Structure of the human Parkin ligase domain in an autoinhibited state. EMBO J. *32*, 2099-2112.

Weinreb, P.H., Zhen, W., Poon, A.W., Conway, K.A., and Lansbury, P.T. (1996). NACP, A Protein Implicated in Alzheimer's Disease and Learning, Is Natively Unfolded. Biochemistry *35*, 13709-13715.

Welch, B.D., VanDemark, A.P., Heroux, A., Hill, C.P., and Kay, M.S. (2007). Potent D-peptide inhibitors of HIV-1 entry. Proc. Natl. Acad. Sci. U.S.A. *104*, 16828-16833.

Welter, C., Moreno, R.M., Streiff, S., and Helmchen, G. (2005). Enantioselective synthesis of (+)(R)- and (-)(S)-nicotine based on Ir-catalysed allylic amination. Org. Biomol. Chem. *3*, 3266-3268.

Winner, B., Jappelli, R., Maji, S.K., Desplats, P.A., Boyer, L., Aigner, S., Hetzer, C., Loher, T., Vilar, M., Campioni, S., *et al.* (2011). In vivo demonstration that α-synuclein oligomers are toxic. Proc. Natl. Acad. Sci. U.S.A. *108*, 4194-4199.

Wood, S.J., Wypych, J., Steavenson, S., Louis, J.C., Citron, M., and Biere, A.L. (1999). alpha-synuclein fibrillogenesis is nucleation-dependent. Implications for the pathogenesis of Parkinson's disease. J. Biol. Chem. *274*, 19509-19512.

Wu, K.-P., Kim, S., Fela, D.A., and Baum, J. (2008). Characterization of Conformational and Dynamic Properties of Natively Unfolded Human and Mouse α-Synuclein Ensembles by NMR: Implication for Aggregation. J. Mol. Biol. *378*, 1104-1115.

Xiong, N., Long, X., Xiong, J., Jia, M., Chen, C., Huang, J., Ghoorah, D., Kong, X., Lin, Z., and Wang, T. (2012). Mitochondrial complex I inhibitor rotenone-induced toxicity and its potential mechanisms in Parkinson’s disease models. Crit. Rev. Toxicol. *42*, 613-632.

Yamaguchi, Y., Masuda, M., Sasakawa, H., Nonaka, T., Hanashima, S., Hisanaga, S.-i., Kato, K., and Hasegawa, M. (2010). Characterization of Inhibitor-Bound α-Synuclein Dimer: Role of α-Synuclein N-Terminal Region in Dimerization and Inhibitor Binding. J. Mol. Biol. *395*, 445-456.

Yang, J., Song, S., Li, J., and Liang, T. (2014). Neuroprotective effect of curcumin on hippocampal injury in 6-OHDA-induced Parkinson's disease rat. Pathol. Res. Pract. *210*, 357-362.

Ying, Y.-L., Wang, H.-Y., Sutherland, T.C., and Long, Y.-T. (2011). Monitoring of an ATP-Binding Aptamer and its Conformational Changes Using an α-Hemolysin Nanopore. Small *7*, 87-94.

Youle, R.J., and van der Bliek, A.M. (2012). Mitochondrial Fission, Fusion, and Stress. Science *337*, 1062-1065.

Yu, S., Uéda, K., and Chan, P. (2005). α-Synuclein and dopamine metabolism. Mol. Neurobiol. *31*, 243-254.

Yu, W.-B., Jiang, T., Lan, D.-M., Lu, J.-H., Yue, Z.-Y., Wang, J., and Zhou, P. (2012). Trehalose inhibits fibrillation of A53T mutant alpha-synuclein and disaggregates existing fibrils. Arch. Biochem. Biophys. *523*, 144-150.

Yu, W., Sun, Y., Guo, S., and Lu, B. (2011). The PINK1/Parkin pathway regulates mitochondrial dynamics and function in mammalian hippocampal and dopaminergic neurons. Hum. Mol. Genet. *20*, 3227-3240.

Yusko, E.C., Johnson, J.M., Majd, S., Prangkio, P., Rollings, R.C., Li, J., Yang, J., and Mayer, M. (2011). Controlling protein translocation through nanopores with bio-inspired fluid walls. Nat. Nano *6*, 253-260.

Zheng, G., Chen, J., and Zheng, W. (2012). Relative contribution of CTR1 and DMT1 in copper transport by the blood–CSF barrier: Implication in manganese-induced neurotoxicity. Toxicol. Appl. Pharmacol. *260*, 285-293.

Zheng, J.-S., Tang, S., Qi, Y.-K., Wang, Z.-P., and Liu, L. (2013). Chemical synthesis of proteins using peptide hydrazides as thioester surrogates. Nat. Protocols *8*, 2483-2495.

Zigmond, M.J., and Burke, R.E. (2002). Pathophysiology Of Parkinson's Disease. In Neuropsychopharmacology, K.L. Davis, D. Charney, J.T. Coyle, and C. Nemeroff, eds. (Philadelphia, Pennsylvania: Lippincott, Williams, & Wilkins), pp. 1781-1793.